Strength and Fatigue Resistance of Clustered Shear Stud Connectors in Composite Steel Girders

PUBLICATION NO. FHWA-HRT-20-005

NOVEMBER 2019

U.S. Department of Transportation
Federal Highway Administration

Research, Development, and Technology
Turner-Fairbank Highway Research Center
6300 Georgetown Pike
McLean, VA 22101-2296

FOREWORD

This report documents fatigue and static testing of shear stud composite connections between steel girders and precast (PC) concrete decks. The purpose of the testing was to assess American Association of State Highway and Transportation Officials (AASHTO) shear stud–fatigue, strength, and spacing design provisions and how they relate to using PC concrete decks on top of steel girders as a means of accelerated bridge construction (ABC).[(1)] The static test results suggest current AASHTO shear stud–strength design provisions are unconservative. However, this is balanced by fatigue test results suggesting current AASHTO shear stud–fatigue provisions are probably too conservative, which explains why there have not been widespread in-service performance problems. The results from the testing regime also showed current AASHTO minimum and maximum spacing limits for shear studs could be relaxed in both the longitudinal and transverse directions. Relaxing these spacing requirements would greatly benefit the constructability of the full-depth PC concrete deck panels needed in some ABC construction techniques for steel superstructures.

This report will benefit those interested in the design, fabrication, and construction of steel bridges and PC concrete decks, including State transportation departments, bridge design consultants, and PC concrete facilities.

Cheryl Allen Richter, Ph.D., P.E.
Director, Office of Infrastructure
Research and Development

TECHNICAL REPORT DOCUMENTATION PAGE

1. Report No. FHWA-HRT-20-005	2. Government Accession No.	3. Recipient's Catalog No.
4. Title and Subtitle Strength and Fatigue Resistance of Clustered Shear Stud Connectors in Composite Steel Girders		5. Report Date November 2019 6. Performing Organization Code
7. Author(s) Jason T. Provines, Justin M. Ocel (ORCID 0000-0002-0176-7276), and Kevin Zmetra (ORCID 0000-0002-1329-7443)		8. Performing Organization Report No.
9. Performing Organization Name and Address Professional Service Industries, Inc. 13873 Park Center Rd., Suite 315 Herndon, VA 20171 Rao Research and Consultants, LLC 1775 Tysons Blvd., Fifth Floor Tysons Corner, VA 22102		10. Work Unit No. 11. Contract or Grant No. DTFH61-10-D-00017, DTFH61-17P-00006, and DTFH61-D-17-00015
12. Sponsoring Agency Name and Address Office of Infrastructure Research and Development Federal Highway Administration 6300 Georgetown Pike McLean, VA 22101-2296		13. Type of Report and Period Covered Final Report; January 2012–May 2018 14. Sponsoring Agency Code HRDI-40

15. Supplementary Notes
The work reported herein was conducted in the Turner-Fairbank Highway Research Center Structures Laboratory under various support service contractors. Justin Ocel (HRDI-40) of the Federal Highway Administration provided technical oversight and assistance to the contractors. The Contracting Officer's Representative was Fassil Beshah (HRDI-40), Mark Swanlund (HRDI-1), or Justin Ocel (HRDI-40), depending on the contract.

16. Abstract
Accelerated bridge construction (ABC) is a technique in which large bridge elements are fabricated offsite or next to the site and are then connected onsite to complete the bridge. One such ABC method is the use of full-depth precast (PC) concrete deck panels, which are placed on top of steel girders connected via shear studs. The PC concrete deck panels typically have pockets cast into them so that they fit around the shear studs. These pockets are then filled with grout to form the composite connection with the girder. When using PC deck panels, it is beneficial to place the shear studs in clusters (i.e., close together longitudinally and transversely). The clusters of studs can then be spaced at greater distances apart. By reducing the number and size of the pockets in the PC concrete deck panels, panel fabrication and constructability can be simplified.
Large- and small-scale fatigue and static tests were conducted in this study to evaluate the American Association of State Highway and Transportation Officials (AASHTO) fatigue, strength, and spacing design provisions for shear studs. The large-scale tests in this study were constructed with PC concrete deck panels and steel beams. Twelve shear studs were used in each shear span but were spaced at intervals of 1, 2, 3, and 4 ft between specimens. The small-scale tests were similar to historical tests and served as a comparison between the historical small-scale test data and the current large-scale tests. Results of the study showed that the AASHTO shear stud–fatigue design provisions can be overly conservative, requiring more studs than are necessary. Testing also showed that the AASHTO shear stud–strength design provisions overpredict a shear stud's strength, making them unconservative. The results also demonstrated that the AASHTO shear stud–spacing requirements can be relaxed to allow for details more conducive to using PC concrete deck panels. Proposed alternative design provisions for the fatigue, strength, and spacing of shear studs are included.

17. Key Words	18. Distribution Statement
Shear studs, fatigue testing, static testing, steel bridges, accelerated bridge construction, ABC	No restrictions. This document is available through the National Technical Information Service, Springfield, VA 22161. http://www.ntis.gov

19. Security Classif. (of this report)	20. Security Classif. (of this page)	21. No. of Pages	22. Price
Unclassified	Unclassified	250	N/A

Form DOT F 1700.7 (8-72) Reproduction of completed page authorized.

SI* (MODERN METRIC) CONVERSION FACTORS

APPROXIMATE CONVERSIONS TO SI UNITS

Symbol	When You Know	Multiply By	To Find	Symbol
		LENGTH		
in	inches	25.4	millimeters	mm
ft	feet	0.305	meters	m
yd	yards	0.914	meters	m
mi	miles	1.61	kilometers	km
		AREA		
in^2	square inches	645.2	square millimeters	mm^2
ft^2	square feet	0.093	square meters	m^2
yd^2	square yard	0.836	square meters	m^2
ac	acres	0.405	hectares	ha
mi^2	square miles	2.59	square kilometers	km^2
		VOLUME		
fl oz	fluid ounces	29.57	milliliters	mL
gal	gallons	3.785	liters	L
ft^3	cubic feet	0.028	cubic meters	m^3
yd^3	cubic yards	0.765	cubic meters	m^3
	NOTE: volumes greater than 1000 L shall be shown in m^3			
		MASS		
oz	ounces	28.35	grams	g
lb	pounds	0.454	kilograms	kg
T	short tons (2000 lb)	0.907	megagrams (or "metric ton")	Mg (or "t")
		TEMPERATURE (exact degrees)		
^oF	Fahrenheit	5 (F-32)/9 or (F-32)/1.8	Celsius	^oC
		ILLUMINATION		
fc	foot-candles	10.76	lux	lx
fl	foot-Lamberts	3.426	$candela/m^2$	cd/m^2
		FORCE and PRESSURE or STRESS		
lbf	poundforce	4.45	newtons	N
lbf/in^2	poundforce per square inch	6.89	kilopascals	kPa

APPROXIMATE CONVERSIONS FROM SI UNITS

Symbol	When You Know	Multiply By	To Find	Symbol
		LENGTH		
mm	millimeters	0.039	inches	in
m	meters	3.28	feet	ft
m	meters	1.09	yards	yd
km	kilometers	0.621	miles	mi
		AREA		
mm^2	square millimeters	0.0016	square inches	in^2
m^2	square meters	10.764	square feet	ft^2
m^2	square meters	1.195	square yards	yd^2
ha	hectares	2.47	acres	ac
km^2	square kilometers	0.386	square miles	mi^2
		VOLUME		
mL	milliliters	0.034	fluid ounces	fl oz
L	liters	0.264	gallons	gal
m^3	cubic meters	35.314	cubic feet	ft^3
m^3	cubic meters	1.307	cubic yards	yd^3
		MASS		
g	grams	0.035	ounces	oz
kg	kilograms	2.202	pounds	lb
Mg (or "t")	megagrams (or "metric ton")	1.103	short tons (2000 lb)	T
		TEMPERATURE (exact degrees)		
^oC	Celsius	1.8C+32	Fahrenheit	^oF
		ILLUMINATION		
lx	lux	0.0929	foot-candles	fc
cd/m^2	$candela/m^2$	0.2919	foot-Lamberts	fl
		FORCE and PRESSURE or STRESS		
N	newtons	0.225	poundforce	lbf
kPa	kilopascals	0.145	poundforce per square inch	lbf/in^2

*SI is the symbol for the International System of Units. Appropriate rounding should be made to comply with Section 4 of ASTM E380.
(Revised March 2003)

TABLE OF CONTENTS

LIST OF FIGURES

LIST OF TABLES

LIST OF ABBREVIATIONS AND SYMBOLS

Abbreviations

AASHO	American Association of State Highway Officials
AASHTO	American Association of State Highway and Transportation Officials
ABC	accelerated bridge construction
AISC	American Institute of Steel Construction
AWS	American Welding Society
CAFT	constant-amplitude fatigue threshold
CIP	cast-in-place
CL	confidence limit
FHWA	Federal Highway Administration
JSCE	Japan Society of Civil Engineers
LVDT	linear variable differential transducer
LRFD BDS	*Load and Resistance Factor Design Bridge Design Specifications*
MLE	maximum likelihood estimation
NA	neutral axis
PC	precast
PCI	Precast Concrete Institute
PT	post-tensioning
S-N	stress versus number of cycles
SSRC	Structural Stability Research Council
TFHRC	Turner-Fairbank Highway Research Center

Symbols

A	fatigue detail constant
A_{sc}	cross-sectional area of a shear stud
d	diameter of shear stud
E_c	modulus of elasticity of concrete

F_u	tensile strength of shear stud
f'_c	concrete design compressive strength
h_s	height of shear stud
M_n	calculated moment capacity
N	number of cycles
Q_n	shear resistance of a shear connector
$S_{r,HLS,95}$	shear stress range based on lower 95 percent confidence limit using the historical large-scale fatigue tests
$S_{r,HSS,95}$	shear stress range based on lower 95 percent confidence limit using the historical small-scale fatigue tests
$S_{r,LS,95}$	shear stress range based on lower 95 percent confidence limit using this study's large-scale specimen data
$S_{r,SS,95}$	shear stress range based on lower 95 percent confidence limit using this study's small-scale specimen data
t_s	thickness of concrete slab
Z_r	shear force range
$(\Delta F)_n$	nominal fatigue resistance

Schematic Abbreviations

C/L	centerline
CLR	clear
DIC	digital image correlation
HSS	hollow structural section
NC	national course
OC	on center
P	applied force
SYM	symmetric
TYP	typical
SPA	space

INTRODUCTION

BACKGROUND

One increasingly common accelerated bridge construction (ABC) technique is the use of large modular bridge components, which are fabricated offsite and then connected together onsite to construct the bridge. One such method of this practice is the use of full-depth precast (PC) concrete deck panels placed on top of steel girders and connected via shear studs. In this case, the concrete panels have pockets cast into them so that they fit around the shear studs. Once the deck panels have been placed on top of the steel girders, these pockets are filled with grout to form a composite connection between the deck and the girders. Aside from the benefit of ABC, using PC concrete deck panels can also provide better quality concrete since they are fabricated at a PC plant rather than in the field.

On a typical bridge using a conventional cast-in-place (CIP) concrete deck, shear studs are regularly spaced along the length of the girder top flange and have a maximum longitudinal spacing of 24 inches per the current American Association of State Highway and Transportation Officials (AASHTO) *Load and Resistance Factor Design Bridge Design Specifications* (LRFD BDS).[(1)] When PC concrete deck panels are used, it is beneficial to cluster individual shear studs to minimize the number of pockets that must be formed into the PC panel. This clustering simplifies panel construction and increases constructability (e.g., fewer interference possibilities during field fit-up).

To provide full composite action between the concrete deck and steel girder, the shear studs must be designed for the fatigue and strength limit states while meeting minimum and maximum spacing limits.[(1)] For short spans, such as 120 ft or less, and near the supports, the fatigue limit state can govern the number of shear studs and lead to a significantly larger number of shear studs than required for the strength limit state. In some cases, the number of shear studs required along the length of a girder leads to a very small longitudinal spacing between shear studs.

Using shear studs spaced at close distances complicates the use of PC concrete deck panels because it is not feasible to form pockets into a deck panel at such a small spacing. This study was undertaken to investigate if improvements can be made to the current AASHTO shear stud design provisions to better facilitate the use of PC deck panels. As such, a brief discussion follows on the current AASHTO shear stud design provisions for the fatigue and strength limit states, as well as the maximum and minimum spacing limits. When applicable, comparisons will also be made to international shear stud design provisions.

Shear Stud–Fatigue Design Provisions

When this project began in 2012, the most recent version of the AASHTO LRFD BDS was the sixth edition.[(2)] In 2014, AASHTO published the seventh edition of the AASHTO LRFD BDS.[(1)] Between these two editions, there were no changes in the shear stud design provisions. Although an eighth edition has now been published, most of this research project was conducted when the seventh edition was the current version of the AASHTO LRFD BDS; therefore, it will be referenced as the "current" version of the AASHTO LRFD BDS throughout this report.[(1,3)]

The current AASHTO shear stud–fatigue design provisions are based on results from 44 small-scale tests conducted in 1966.[4] These tests, called push-out tests, are a common alternative to large-scale tests conducted on shear studs. A schematic of these push-out test specimens is shown in figure 1.

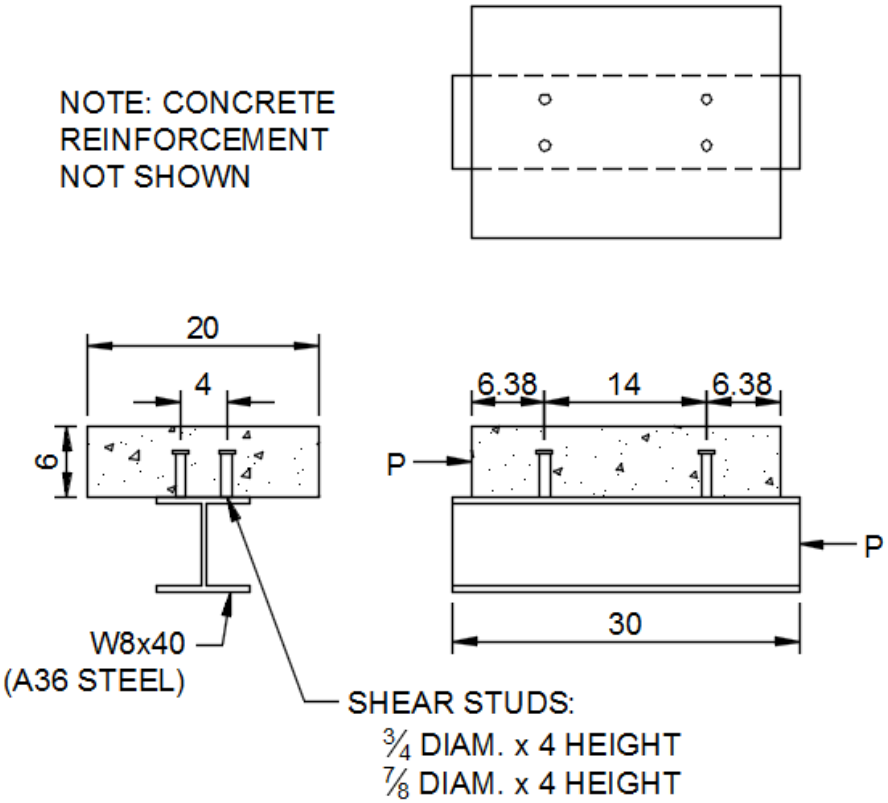

Source: FHWA.
Note: Measurements are in inches.

Figure 1. Schematic. Test specimens used to develop AASHTO shear stud–fatigue provisions.[4]

For these tests, both ¾- and ⅞-inch-diameter shear studs were used. Studs were welded to one side of the short steel beam and concrete was cast around the shear studs, resulting in a one-sided push-out test. Once the specimens were completely constructed, cyclic load was applied to the steel beam and concrete slab until the shear studs failed from fatigue. The small-scale test results were compared to beam tests conducted at the same time. The lower limit of dispersion of the beam tests (taken as twice the standard error of the estimate) was approximately equal to the mean results of the push-out tests.[5,6] Therefore, the mean results from the push-out tests were used to develop shear stud–fatigue design equations.

A constant-amplitude fatigue threshold (CAFT) of 7.0 ksi was later added to the AASHTO *Interim Specifications for Highway Bridges* in 1977, though no test results were cited for this addition.[7] The addition of the CAFT produced the provisions that are currently in use. The AASHTO fatigue design resistance of a single shear stud is expressed in terms of a shear force range rather than a stress range (which is typically used for the other AASHTO fatigue details) and is determined using the equations in figure 2 and figure 3.

$$Z_r = 5.5d^2$$

Figure 2. Equation. Current AASHTO infinite life shear stud design equation.[1]

$$Z_r = (34.5 - 4.28 \log N)d^2$$

Figure 3. Equation. Current AASHTO finite life shear stud design equation.[1]

Where:
Z_r = shear force range (kips).
d = diameter of a shear stud (inches).
N = number of cycles.

When compared to some international shear stud–fatigue design provisions, the AASHTO equations are quite different. Figure 4 shows the shear stud–fatigue design curves according to AASHTO, the Eurocode 4, the Australian Standard, and the Japan Society of Civil Engineers (JSCE).[1,8–10] The AASHTO category C fatigue detail is included in the figure for reference. The JSCE design equation depends on various geometric and material properties, so the following were assumed: shear stud diameter of ⅞ inch, shear stud height of 6 inches, and concrete compressive design strength of 4.0 ksi.

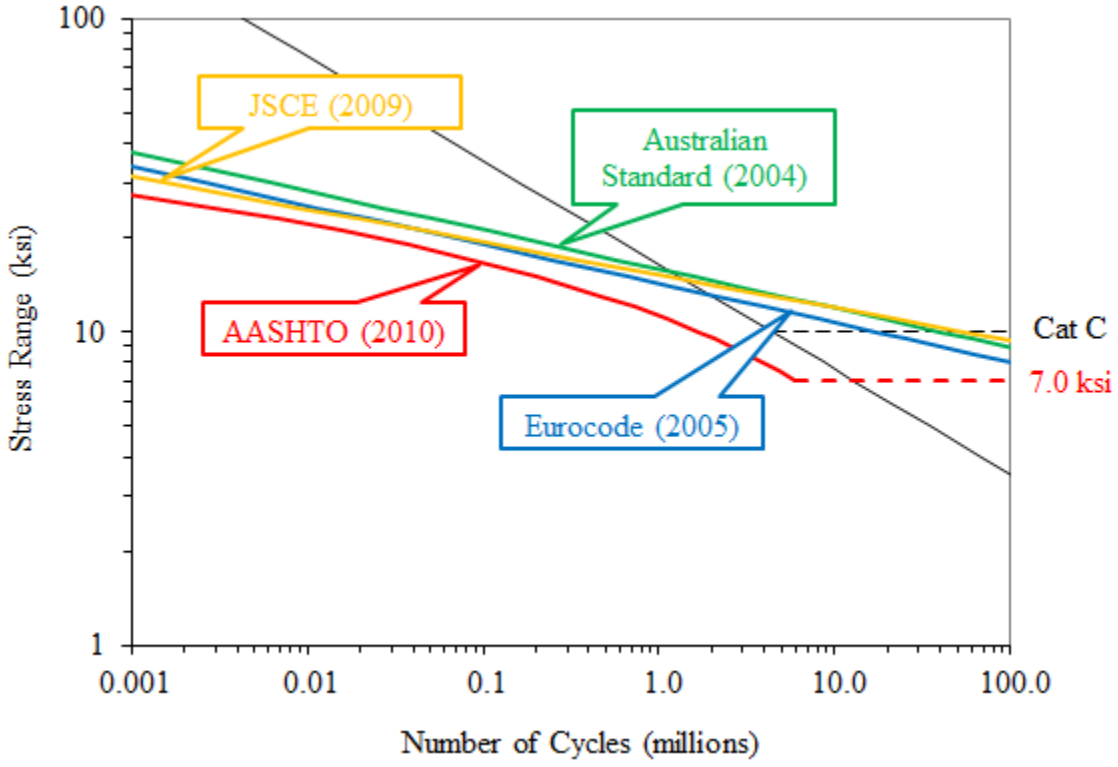

Source: FHWA.

Figure 4. Graph. Shear stud–fatigue design provisions from AASHTO and international codes.

As shown in figure 4, the AASHTO fatigue design curve follows a semi-log format (i.e., it is curved in the log-log space). The other international provisions follow a log-log format, with slopes ranging from −8 to −9.5.[8–10] These slopes are much shallower than the −3 slope for the other AASHTO fatigue details. This difference in slope is because of the difference in mode of cracking. Shear studs develop fatigue cracks because of shear stresses, whereas the other AASHTO details develop cracks because of tensile stresses. Since the AASHTO shear stud–fatigue design curve is semi-log, the design stress range reduces more drastically as the number of design cycles increases. This is especially evident at approximately 6.0 million cycles, where the infinite fatigue life equation begins to govern. At this point, the AASHTO design stress range is approximately 1.6–1.8 times less than the international provisions shown, requiring a greater number of shear studs. The AASHTO shear stud CAFT of 7.0 ksi also appears somewhat conservative since the international provisions do not include CAFTs.

Push-out tests conducted at the University of Auburn also suggest that the actual fatigue behavior of shear studs may be closer to the international provisions than the current AASHTO LRFD BDS.[11] These tests were conducted on both ⅞- and 1¼-inch-diameter shear studs, though only the results of the ⅞-inch-diameter shear studs are discussed herein. The tests were cycled at stress ranges of 18, 22, and 26 ksi. All of the fatigue tests produced fatigue failures, and no runout tests were reported. A linear regression analysis was performed on the fatigue data, and the slope of the regression line was found to be −8.7. This slope and the location of the lower 97.5 percent confidence-limit equation on the stress cycle (S-N) curve were shown to be very similar to the three international shear stud–fatigue provisions.[8–10]

Additional push-out testing and analysis was conducted at the University of Arkansas; this testing program consisted of six small-scale tests at relatively small stress ranges between 4.4 and 8.7 ksi.[12] One of these tests produced a fatigue failure, while the remaining five tests were declared runouts after more than 12 million cycles. The S-N test results were analyzed using a statistical method called maximum likelihood estimation (MLE). In a typical linear regression analysis of fatigue data, runout tests are ignored in the analysis, and CAFT is determined through a combination of the analysis and engineering judgement. Using MLE allows for runouts to be included in the test data since they indicate the absence of a failure. The MLE method was used to analyze historical shear stud–fatigue data and determined that a CAFT of 6.5 ksi was likely, which is similar to the current AASHTO value of 7.0 ksi.[1] The analysis also showed that a slope of −4 appropriately fit the existing shear stud–fatigue data.

Shear Stud–Strength Design Provisions

The strength of a shear stud embedded in concrete depends on two factors: the resistance of the concrete around the shear stud and the resistance of the steel stud itself. The current AASHTO shear stud–strength design provisions were developed based on 48 two-sided push-out tests conducted in 1971.[13] The specimens used in that study were constructed using ⅝- and ¾-inch-diameter shear studs and both normal and lightweight concrete mixes. An example of the specimens used in the study is shown in figure 5.

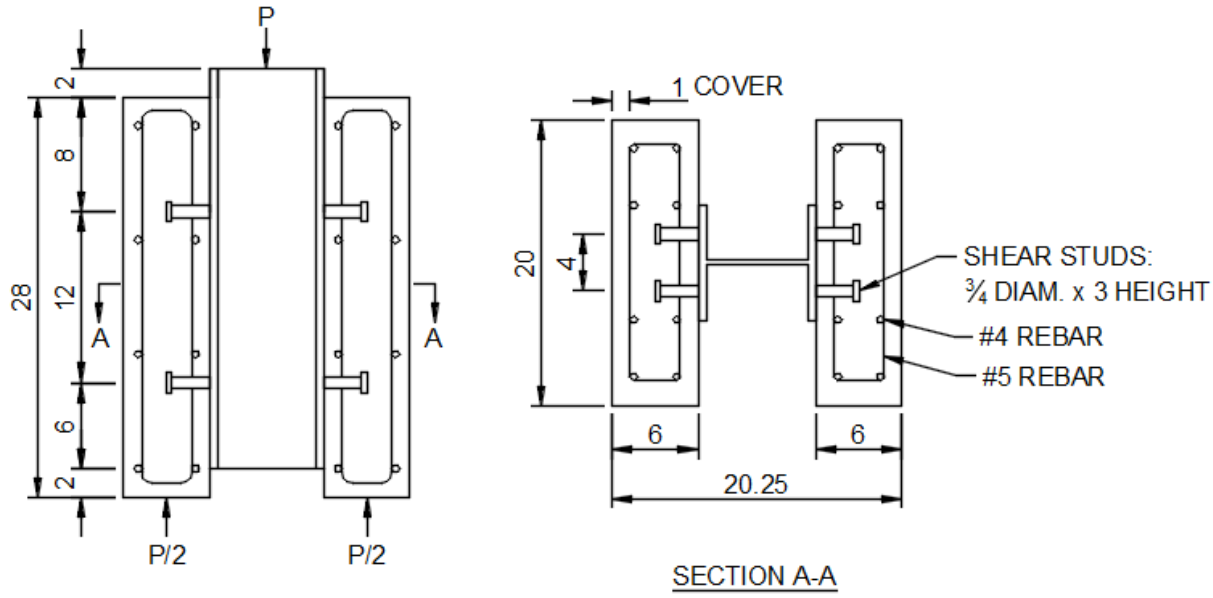

Source: FHWA.
Note: Measurements are in inches.

Figure 5. Schematic. Test specimens used to develop AASHTO shear stud–strength provisions.[13]

Figure 6 shows the current AASHTO LRFD BDS provisions for predicting a shear stud's strength.[1] The left side of this equation represents the strength of the concrete surrounding the stud, while the right side represents the strength of the steel shear stud itself. The aforementioned small-scale test results were used to develop resistance equations for the strength of the concrete surrounding a shear stud (left side of equation), but no recommendations were made regarding the strength of the shear stud itself (right side of equation) until 1994. The resistance of a steel shear stud was incorporated into the AASHTO LRFD BDS in its first edition in 1994 and into the *Standard Specifications for Highway Bridges* in the 2000 interim revisions to the 16th edition.[14,15] No test results were cited as the basis for this addition in either specification. Those provisions were the same as those currently in use and are shown in figure 6.

$$Q_n = 0.5\, A_{SC}\sqrt{f_c' E_c} \leq A_{SC} F_u$$

Figure 6. Equation. Current AASHTO shear stud–strength design provisions.[1]

Where:
Q_n = shear resistance of a shear connector (kips).
A_{sc} = cross sectional area of a shear stud (inch^2).
f_c' = concrete design compressive strength (ksi).
E_c = modulus of elasticity of concrete (ksi).
F_u = Tensile strength of steel shear stud (ksi).

Since the shear stud's strength (right side of equation) is written in terms of its tensile strength, the equation implies that a shear stud resists pure tension force rather than shear force, which

seems unlikely. When other structural members, such as beams, are designed for shear, a 0.58 factor is multiplied by the member's tensile strength to reflect shear strength via the von Mises failure criteria. No such factor is included in the AASHTO shear stud–strength design equation. However, both the Eurocode and Australian provisions include a 0.80 factor in the portion of the equation concerning the resistance of the shear stud.[8,9] This factor would imply that shear studs fail somewhere in between pure shear and pure tension. Since the AASHTO shear stud–strength equation does not include any such factor, a shear stud's strength could be overpredicted, making the current AASHTO LRFD BDS provisions unconservative.[1] This has probably not resulted in any performance issues because the fatigue provisions are overly conservative, such that they compensate for the unconservative strength provisions.

When shear studs are placed closely together in clusters, as they would be when used with PC concrete deck panels, the strength of the surrounding concrete (left side of equation) also has the potential to be unconservative. In this case, it is likely that the surrounding concrete would experience overlapping stresses, thereby reducing its overall resistance. Since the tests used to develop the surrounding concrete strength of a shear stud connection did not include closely spaced shear studs, it is not known if the current strength provisions would be applicable to clustered shear studs.

Research conducted at Auburn University also indicated that the AASHTO LRFD BDS shear stud–strength design provisions may be unconservative.[16] Their comparison between AASHTO LRFD BDS, the Eurocode, JSCE, and British Standards showed that AASHTO provisions predicted the greatest shear stud capacity. Large-scale tests were conducted on steel beams with concrete decks using ⅞-inch-diameter shear studs to provide composite action. The test results showed that none of the beams tested reached their theoretical moment capacity as calculated using the AASHTO LRFD BDS design provisions. The conclusions reached in the study included that the AASHTO shear stud provisions were inconsistent with their international counterparts and that AASHTO overestimates the static capacity of shear studs, making the strength design limit state unconservative.

Shear Stud–Spacing Design Provisions

The current AASHTO LRFD BDS shear stud provisions provide limitations on the minimum and maximum spacing between shear studs in both the longitudinal and transverse directions.[1] The longitudinal spacing, or pitch, of shear studs is limited to a minimum value of 6*d*. The maximum allowable pitch of shear studs is 24 inches. No commentary is provided for the basis of these values.[17,18]

The transverse spacing of shear studs is limited to a value of 4*d*; no maximum transverse spacing is provided. No basis for either the minimum longitudinal or transverse spacing provisions is provided in the commentary of the AASHTO LRFD BDS.[1] A recent study on the use of shear stud details in PC concrete decks provided a brief history of shear stud–spacing limitations, mostly focused on the longitudinal spacing; a brief summary of that history is provided herein.[18]

The first composite bridge beam in the United States was constructed in the 1930s in Iowa, with a concrete slab placed on a steel I-beam.[18] Newmark and Seiss created a composite bridge design example in 1943, which indicated that the spacing of shear connectors should not be more

than three to four times the depth of the slab.[19] The design example was based on channel-type shear connectors, which were common at that time. Though the design example was written in accordance with the 1941 American Association of State Highway Officials (AASHO) *Standard Specifications for Highway Bridges*, this spacing limitation does not appear in those specifications.[20] It appears that this limit was based more on a rule of thumb at the time rather than a provision. However, the 24-inch maximum longitudinal spacing limit did appear for the first time in the fourth edition of the AASHO *Standard Specifications for Highway Bridges* in 1944, though without commentary.[21]

In 1954, Viest and Seiss published a paper detailing results of some experimental testing on component and composite beam tests, both constructed with channel-type shear connectors.[22] Tests were conducted on beams with spacings of 18 and 36 inches. The beams with 18-inch spacing performed adequately, but the beams with 36-inch spacing experienced uplift between the concrete deck and steel beam. This motivated the authors to recommend a maximum spacing of no greater than four times the thickness of the slab, or 24 inches. The slabs tested in the study were 6 inches thick, which could explain where the recommendation of 24 inches came from.

Minimum shear stud–spacing limits did not appear in AASHTO publications until the 1990 interim revisions to the *Standard Specifications for Highway Bridges* adopted a minimum shear stud spacing of 4*d*, both longitudinally and transversely.[23] The current minimum pitch of 6*d* first appeared in the 1994 interim revisions to the *Standard Specifications for Highway Bridges*.[24] No commentary was included in these versions of the *Standard Specifications for Highway Bridges,* so there was no medium in which to provide rationale for these additions to the code.

Each of the international specifications discussed previously also provides minimum and maximum limitations for both the longitudinal and transverse spacing. These specifications, along with those from AASHTO, are provided in the following tables. Table 1 provides limitations on the longitudinal shear stud spacing, while table 2 is focused on transverse spacing. Where spacing limitations were originally provided in metric units in the international provisions, these values have been converted to U.S. units and rounded to the nearest inch for ease in quickly comparing values.

Table 1. Minimum and maximum longitudinal shear stud–spacing provisions.

Specification	Minimum Longitudinal Spacing	Maximum Longitudinal Spacing
AASHTO LRFD BDS, seventh edition[1]	6*d*	24 inches
Eurocode[8]	5*d*	Lesser of 32 inches or 4t_s
Australian Standard[9]	Lesser of 5*d*, 3 inches, or h_s	Lesser of 24 inches, 3t_s, or 4h_s
JSCE[10]	Greater of 5*d* or 4 inches	Lesser of 24 inches or 3t_s

t_s = thickness of concrete slab (inches); h_s = height of shear stud (inches).

Table 2. Minimum and maximum transverse shear stud–spacing provisions.

Specification	Minimum Transverse Spacing	Maximum Transverse Spacing
AASHTO LRFD BDS, seventh edition[1]	4*d*	None
Eurocode[8]	2.5*d* in solid slabs or 4*d* in other cases	None
Australian Standard[9]	3 inches	None
JSCE[10]	Greater of 5*d* or 4 inches	None

In general, the AASHTO provisions are similar to the international provisions; however, there are some interesting observations when comparing the spacing limits between codes. The Eurocode has the greatest limit on longitudinal spacing at 32 inches, while each of the other three specifications limit it to 24 inches.[1,8–10] AASHTO has the greatest minimum longitudinal spacing limit at 6*d*, while the others require at least a 5*d* spacing.[1,8–10] The minimum transverse spacing varies between 2.5*d* and 5*d* among the codes.[1,8–10] None of the specifications provide a limit on the maximum transverse spacing, though this would probably only become applicable on bridges with extremely wide top flanges.[1,8–10]

These spacing limitations are relevant when employing the use of PC concrete deck panels. In order to more easily facilitate the use of deck panels, shear studs can be clustered closely together in both longitudinal and transverse directions, and clusters of shear studs can be placed at greater distances between one another. This means fewer and smaller pockets need to be formed in the deck panels during fabrication. It also allows for easier fit-up when placing deck panels on top of steel girders at a job site. Currently, the AASHTO LRFD BDS does not provide any guidance for grouping clusters of shear studs close together.[1] However, the three international specifications do include guidance on this topic.[8–10] Summaries of these specifications are provided in table 3.

Table 3. Comparison of shear stud–clustering provisions.

Specification	Shear Stud–Clustering Provisions
AASHTO LRFD BDS, seventh edition[1]	None
Eurocode[8]	Provided that spacing between groups is greater than for individual connectors, connectors may be placed in groups if consideration is given to the following: • Nonuniform longitudinal shear flow. • Greater possibility of slip and uplift between slab and beam. • Buckling of steel flange. • Local resistance of slab owing to concentrated force from connectors (could require additional reinforcement in slab)
Australian Standard[9]	Provided that spacing between groups is greater than for individual connectors, connectors may be placed in groups if consideration is given to the following: • Nonuniform longitudinal shear flow. • Greater possibility of slip and uplift between slab and beam.
JSCE[10]	When shear studs are placed in grouped arrangements, consideration should be given to the following: • Nonuniform longitudinal shear flow. • Greater possibility of slip and uplift between slab and beam. • Buckling of steel flange. • Local resistance of slab owing to concentrated force from connectors. • Shape of the pocket in a PC deck. • Distance between face of pocket and shank of shear stud. When shear studs are arranged close together, reduction of the strength of a shear stud should be considered because of the overlap of concrete stress near the shear studs.

Each of the three international specifications provides similar clustering provisions, and all mention that nonuniform longitudinal shear flow and the increased possibility of slip and uplift should be considered.[8–10] As noted, these provisions include design considerations for clustered shear studs but do not contain specifics on how to mitigate the considerations. Although Eurocode and the Australian Standard do not provide citations for the basis of their clustering provisions, the JSCE references a study in Japan in which experimental and analytical tests were used to estimate the concrete strength reduction when clustering shear studs in both the transverse and longitudinal directions.[25] Another study conducted in Korea provided similar recommendations; if shear studs are grouped close together longitudinally, a concrete strength reduction factor must be applied.[26] One study in the United States noted that, when more shear studs are placed in a cluster, the concrete strength increases but not proportional to the number of shear studs added.[27]

OBJECTIVE

The objective of this project was to evaluate the current AASHTO LRFD BDS shear stud–fatigue and strength design provisions, primarily as they relate to the use of PC concrete decks placed on top of steel girders and connected via grouted shear studs.[1] There are limited test data on the use of shear studs placed at a longitudinal spacing greater than 24 inches and even fewer data on composite beams tested with shear studs placed closely together in clusters. Testing composite beams with shear studs placed in clusters at extended spacings will determine if the current AASHTO LRFD BDS shear stud–fatigue and strength design provisions are applicable or if revisions are warranted.[1] Topics the experimental testing will address include the overly conservative nature of the fatigue limit, the appropriateness of the current CAFT, and the unconservative nature of the strength limit.

APPROACH

In the Background section discussion on the fatigue and strength of shear studs, it was apparent that the majority of historical test data were based on push-out tests, including those used to develop the current shear stud provisions. While push-out tests have been shown to be a cost-effective means of testing shear studs, questions still exist about how they simulate large-scale behavior. This study focused on large-scale testing to address a gap in the literature. Large-scale testing allows tests to be conducted on shear stud spacings greater than the current maximum limit of 24 inches; conducting push-out tests with such large spacings would be difficult. Push-out tests were also conducted to increase the sample size of tests. Although channels have been used historically as shear connectors in bridges and in the research used to develop the current AASHTO LRFD BDS provisions, this study will focus on the use of shear stud connectors because that is the typical current practice.[1] Shear studs with a diameter of ⅞ inch were chosen for this study since this is the common size used in U.S. bridges.

EXPERIMENTAL DESIGN AND TESTING

SPECIMEN DESIGN AND CONSTRUCTION

Large-Scale Fatigue and Static Tests

This study tested 17 large-scale composite beams. The fatigue and static tests were constructed in the same fashion and are thus discussed together. Each beam consisted of a 30-foot-long W27x84 rolled steel beam and two concrete deck panels fabricated by a Precast Concrete Institute (PCI)-certified precaster. To ease in storage and handling of the panels, two deck panels were placed end to end longitudinally with a grouted closure pour at the midspan rather than using a single deck panel. The rebar in the deck panels was designed using the empirical deck design in AASHTO LRFD BDS, and the concrete was a typical bridge deck mix with a compressive design strength of 6.0 ksi.[(1)] Shear pockets were cast into the deck panels and sized depending on the number of shear studs in each cluster and the spacing between clusters. Detailed drawings of the deck panels can be found in appendix A. The shear stud–cluster spacing and corresponding number of studs per cluster varied between sets of beams to evaluate how the different spacings affect both the strength and fatigue resistance of the shear studs. Table 4 presents the experimental test matrix for the large-scale fatigue and static tests.

Table 4. Large-scale experimental test matrix.

Stud Cluster Spacing (Inches)	Number of Clusters per Shear Span	Number of Longitudinal Studs per Cluster	Number of Transverse Studs per Cluster	Total Number of Studs per Shear Span	Number of Fatigue Tests	Number of Static Tests
12	12	1	2	24	0	1
12	12	1	1	12	3	1
24	6	2	1	12	3	1
36	4	3	1	12	3	1
48	3	4	1	12	3	1

The first column of the table shows the shear stud–cluster spacings selected for testing: 12, 24, 36, and 48 inches. The 12-inch spacing was chosen to represent a typical shear stud configuration, with shear studs placed at regular intervals (i.e., no clustering) over the length of a shear span. The 24-inch spacing beams had groups of two shear studs clustered in the longitudinal direction with 24 inches between clusters, which satisfies the current AASHTO shear stud maximum spacing limit. The 36- and 48-inch spacing specimens were selected to determine how the strength and fatigue resistance of the beams changed when the maximum spacing limit was exceeded.

Of the 17 large-scale tests, 12 were tested under fatigue loads, while the remaining 5 were tested statically. For each cluster spacing, a total of three replicate fatigue specimens were tested. The naming convention for the large-scale fatigue test specimens is shown in table 5.

Table 5. Large-scale fatigue test naming convention.

Specimen Name	Stud Cluster Spacing (Inches)	Replicate Number
1F1	12	1
1F2	12	2
1F3	12	3
2F1	24	1
2F2	24	2
2F3	24	3
3F1	36	1
3F2	36	2
3F3	36	3
4F1	48	1
4F2	48	2
4F3	48	3

Of the five static test specimens, two were tested at a shear stud spacing of 12 inches, while the remaining three specimens were tested at spacings of 24, 36, and 48 inches. The difference between the two 12-inch spacing specimens was that one beam had two shear studs placed transversely across the flange for each shear stud cluster, while the other beam had a single shear stud per cluster. The naming convention for the large-scale static test specimens can be found in table 6.

Table 6. Large-scale static test naming convention.

Specimen Name	Stud Cluster Spacing (Inches)	Number of Transverse Studs per Cluster
1S2	12	2
1S1	12	1
2S1	24	1
3S1	36	1
4S1	48	1

Beam 1S2 (first row of both table 4 and table 6) contained 24 shear studs per shear span, whereas all of the other beams contained 12 shear studs per shear span. This beam was constructed and tested prior to constructing any of the other beams; its purpose was to serve as a trial to evaluate the horizontal shear force needed to cause a horizontal shear failure in the shear studs. As is discussed in the Large-Scale Static Test Results section of this report, the beam failed because of

concrete crushing at the midspan, and thus the number of shear studs for the rest of the beams was reduced in the rest of the testing program to ensure shear failure of the shear studs.

The remaining beams in table 4 all contained 12 shear studs per shear span, which corresponds to approximately 38 percent composite action. At each of the four cluster spacings, one static test and three fatigue tests were conducted. Since AASHTO does not encourage partially composite beams, the American Institute of Steel Construction (AISC) specifications were used to determine the flexural resistance and rigidity of the beams.[28] As stated previously, partially composite beams were needed to produce the desired horizontal shear failure in the shear studs.

Each of the shear studs on the beams had a diameter of ⅞ inch and a height of 6 inches; this size was selected because of its use in typical bridge construction. The shear studs were detailed to penetrate 5 inches into the concrete deck and maintain a cover of at least 3 inches, which satisfies AASHTO LRFD BDS.[1] When shear studs were clustered longitudinally, they were spaced at a pitch of 3.5 inches, or 4*d*, which is less than the minimum AASHTO spacing of 6*d*. The research team chose the smaller pitch to minimize the length of the pockets as desired when using PC concrete decks. The Texas Department of Transportation specified this minimum spacing of 4*d* in their bridge design manual when the test matrix was conceived.[29] The team welded shear studs onto the steel beams in accordance with AASHTO/American Welding Society (AWS) D1.5 *Bridge Welding Code*.[30]

Before placing the PC deck panels on the steel beams, the top flange of each beam was coated with a thin layer of grease; this was done to drive all horizontal shear force into the shear studs by eliminating any bond between the top flange and the grouted haunch. The research used to develop the current AASHTO shear stud–fatigue provisions also used this process of greasing the top flange.[4] Once the deck panels were set in place on top of the steel beams, the team used leveling bolts to form a 1-inch haunch. Formwork was then constructed to form the haunch and the midspan transverse joint between the two deck panels. Prebagged, nonshrink grout was then mixed with enough water to create a flowable mixture per the manufacturer's recommendations. Researchers used a grout pump to transport the grout and fill the pockets, haunch, and transverse joint, starting from one end of the beam and ending at the opposite end. After grouting was complete, wet burlap was placed over the grout pockets to aid in the curing process.

Figure 7 through figure 12 show plan and elevation views for each of the large-scale beams tested in this study. Typical sections for each of the beams, except for beam 2S1, are also shown in figure 12. Beam 2S1 has the same sections, except rather than a single shear stud across the width of the flange, there are two shear studs spaced at 4⅜ inches apart, symmetrically located about the center of the beam web, as shown in figure 8.

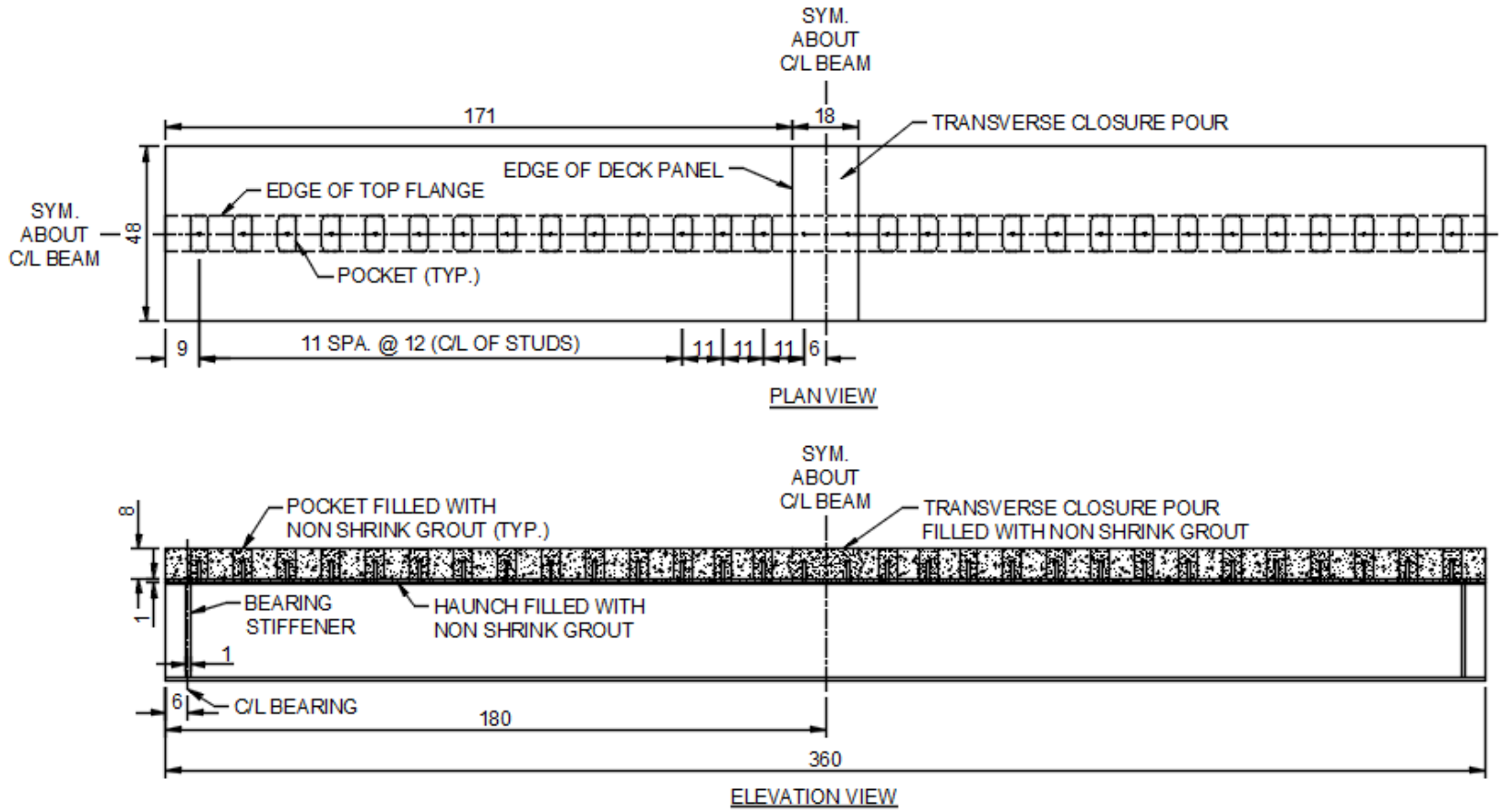

Source: FHWA.
Note: Measurements are in inches.

Figure 7. Schematic. Plan and elevation view for all 12-inch spacing beams except 1S2.

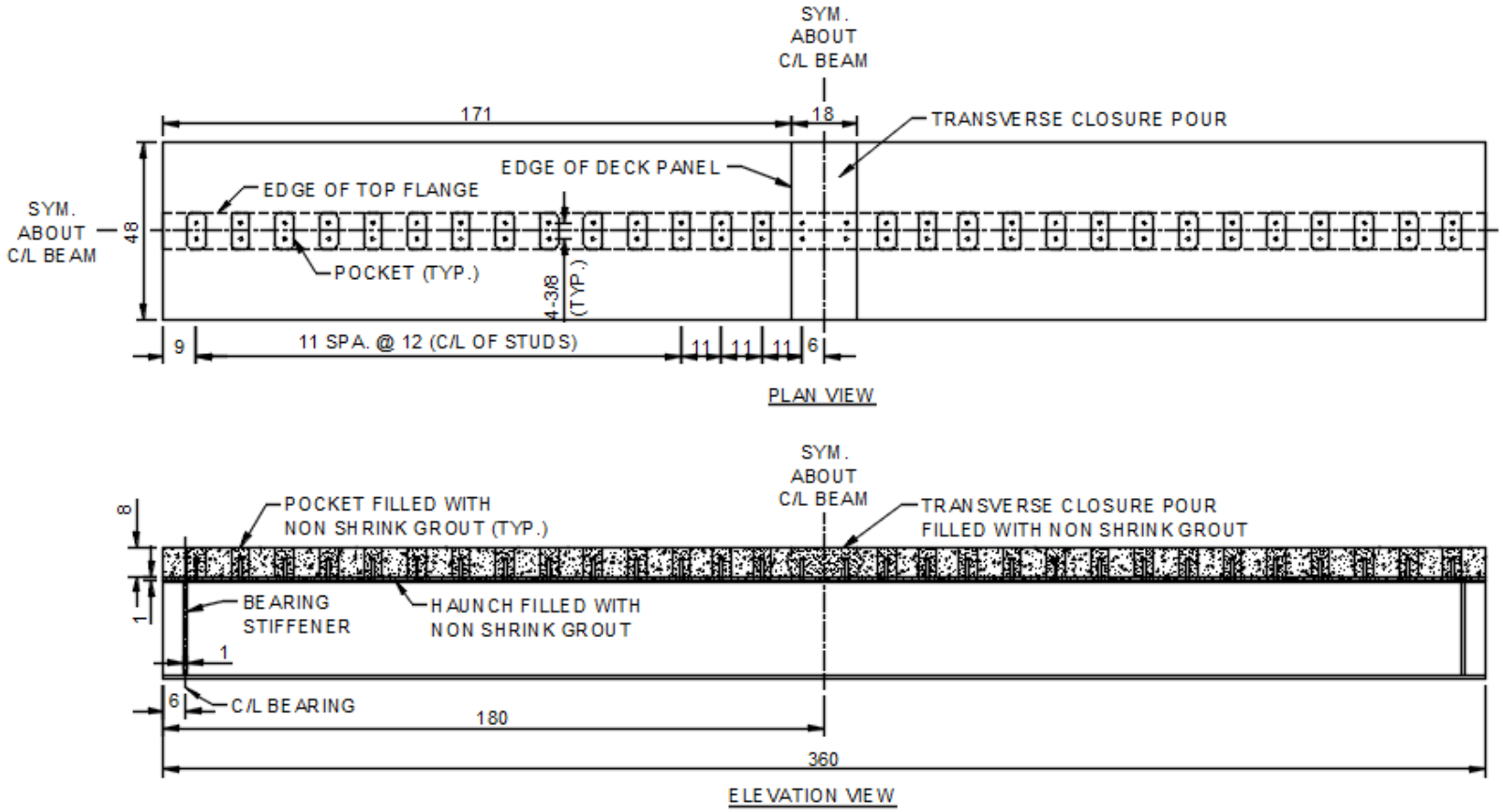

Source: FHWA.
Note: Measurements are in inches.

Figure 8. Schematic. Plan and elevation view for 1S2 beam.

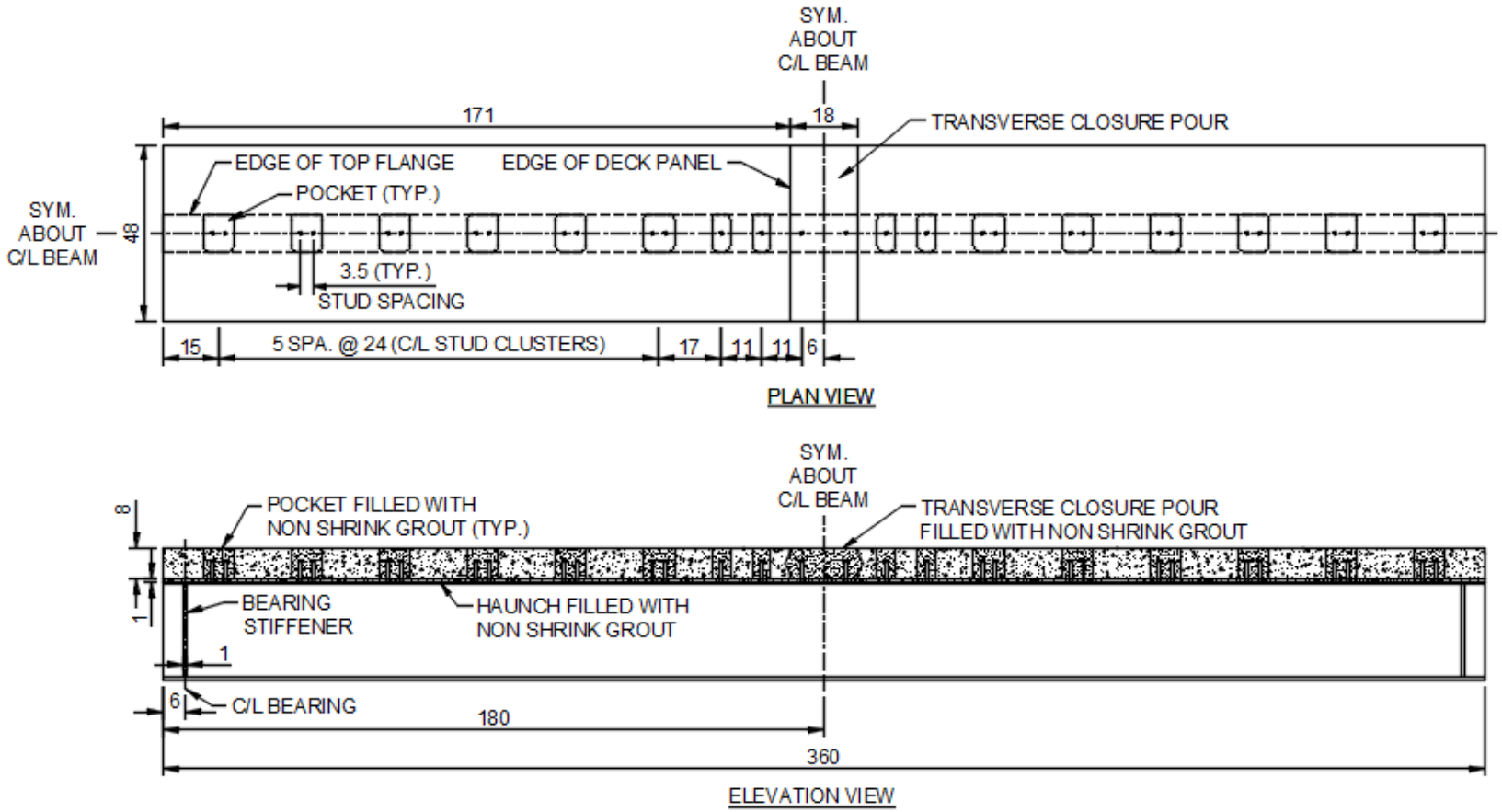

Source: FHWA.
Note: Measurements are in inches.

Figure 9. Schematic. Plan and elevation view for all 24-inch shear stud–cluster spacing beams.

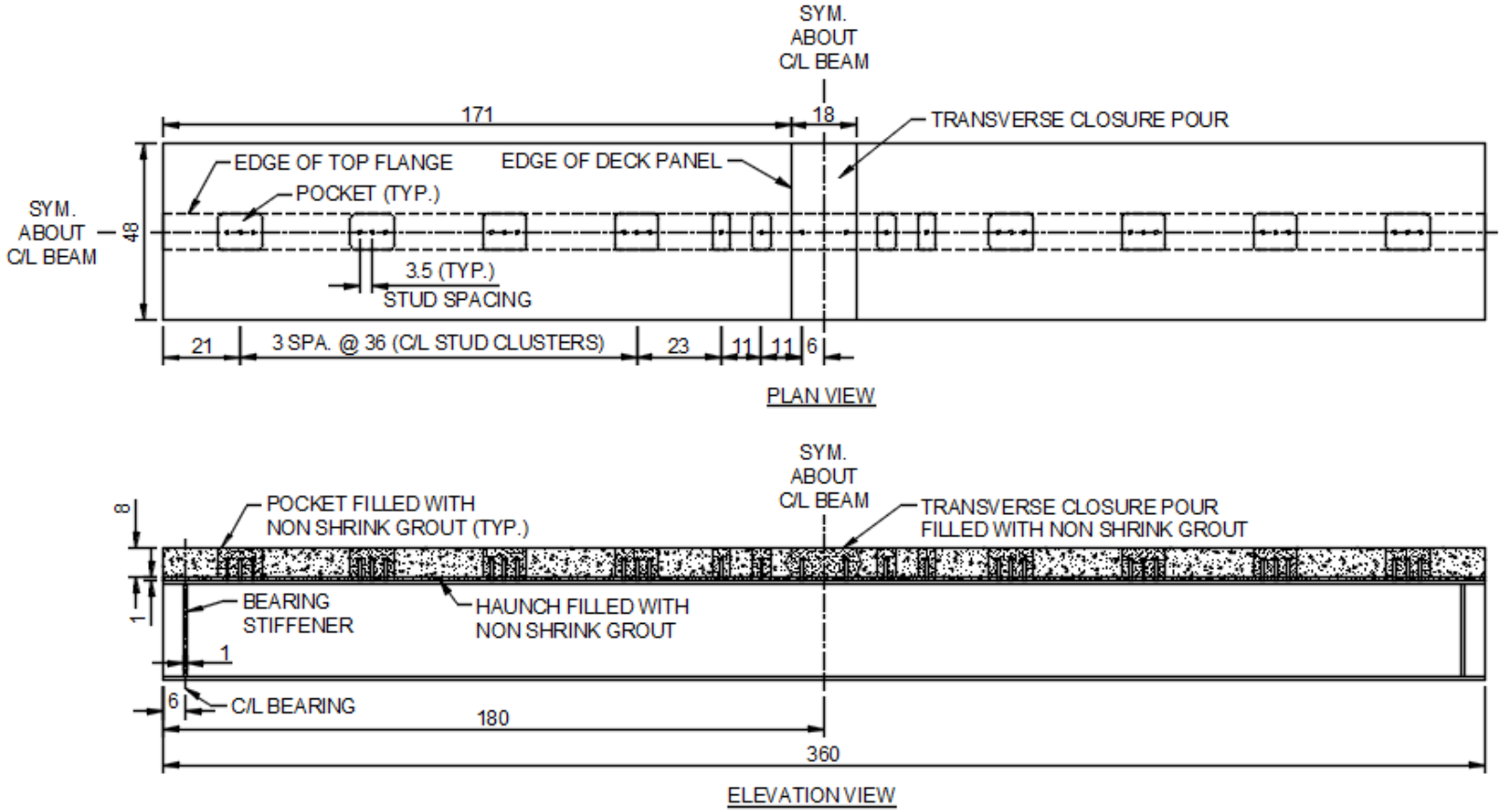

Source: FHWA.
Note: Measurements are in inches.

Figure 10. Schematic. Plan and elevation view for all 36-inch shear stud–cluster spacing beams.

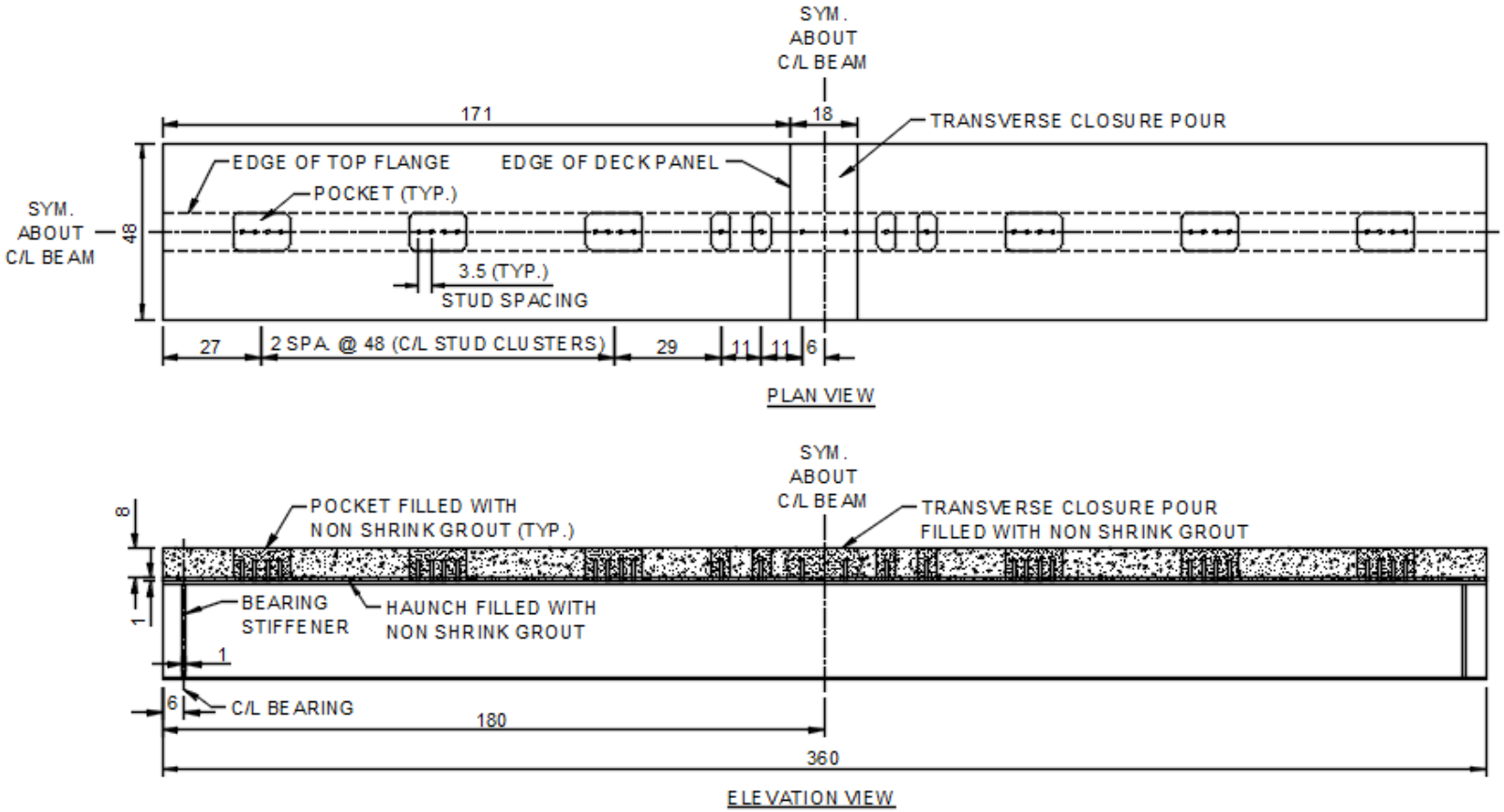

Source: FHWA.
Note: Measurements are in inches.

Figure 11. Schematic. Plan and elevation view for all 48-inch shear stud–cluster spacing beams.

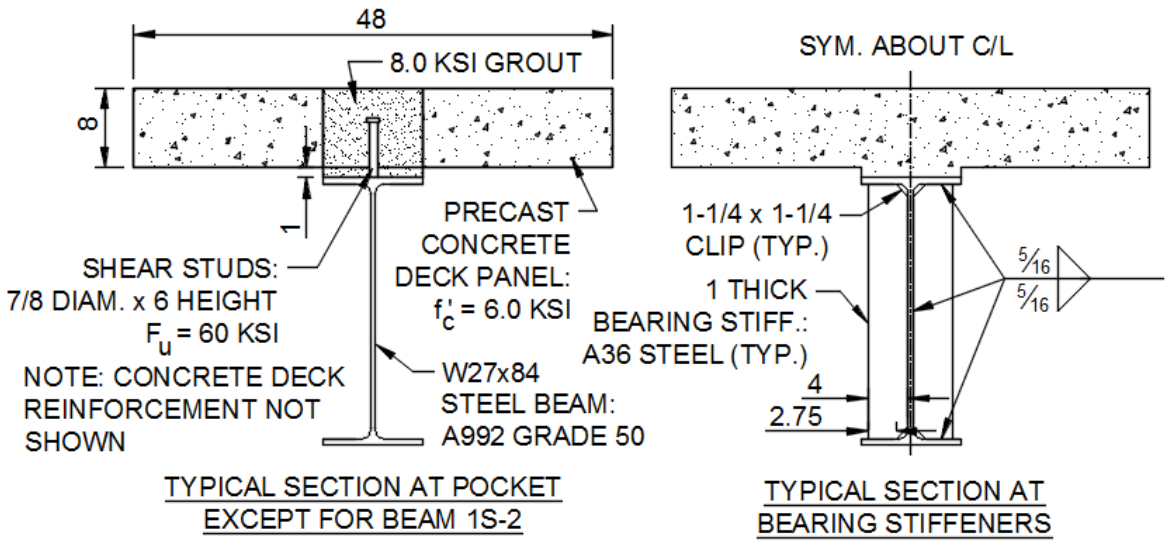

Source: FHWA.
Note: Measurements are in inches.

Figure 12. Schematic. Typical sections for large-scale beams.

Figure 13 shows a photo of beam 4F1 before the deck panels were grouted in place on top of the steel beams, and figure 14 shows a photo after this has taken place.

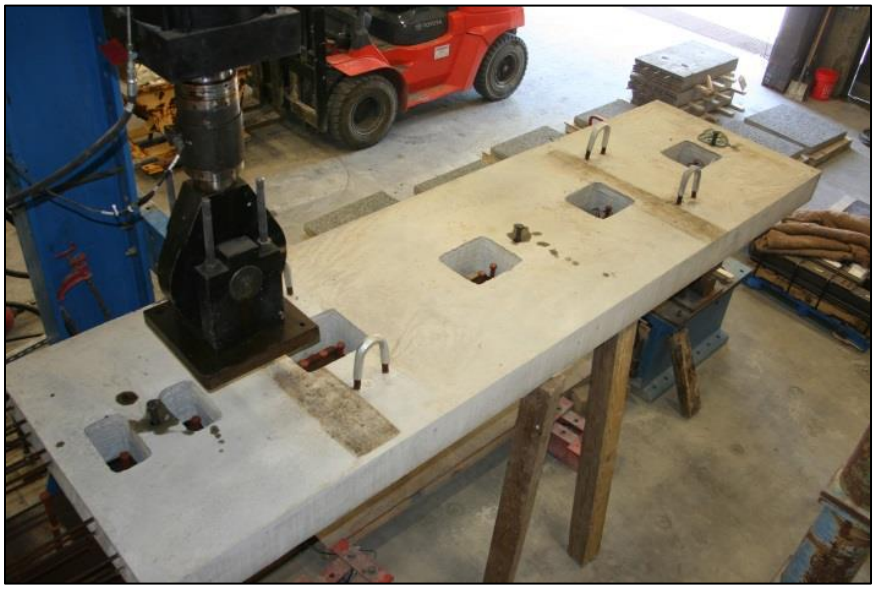

Source: FHWA.

Figure 13. Photo. Before grouting large-scale beam specimen 4F1.

Source: FHWA.

Figure 14. Photo. After grouting large-scale beam specimen 4F1.

Small-Scale Fatigue Tests

There were 14 small-scale fatigue specimens in this study. Each of the specimens was constructed using the same design; the test variable between specimens was the stress range that was cyclically applied during testing. For this reason, no test matrix is presented. The specimen naming convention was in the form of PO-Fx, where PO-F represents "push-out fatigue" and the letter "x" represents a number between 1 and 14 for all of the replicates.

Each of the small-scale fatigue tests was constructed with a 24-inch long W10x60 steel beam with a small PC concrete deck panel on each side. All of these PC deck panels were constructed and cast in the Federal Highway Administration's (FHWA's) Turner-Fairbank Highway Research Center (TFHRC) Structures Laboratory by laboratory staff. This included forming the shear pockets and placing the No. 4 reinforcing steel bars. All reinforcement was placed such that it would not interfere with the shear pockets.

A single shear stud was welded to each flange, and the PC decks were connected to the shear studs via a grouted pocket. The team constructed the specimens by laying the steel beam on its side and setting one of the PC concrete deck panels in place. The same prebagged grout that was used in the large-scale tests was then placed in the pocket to connect the beam and concrete deck. To aid in the curing process, the researchers placed wet burlap on the grout. After 3 days, the grout was sufficiently hardened. The specimens were flipped over and the process was repeated, placing the second deck panel on the opposite flange. Figure 15 shows a drawing of the test specimens after construction.

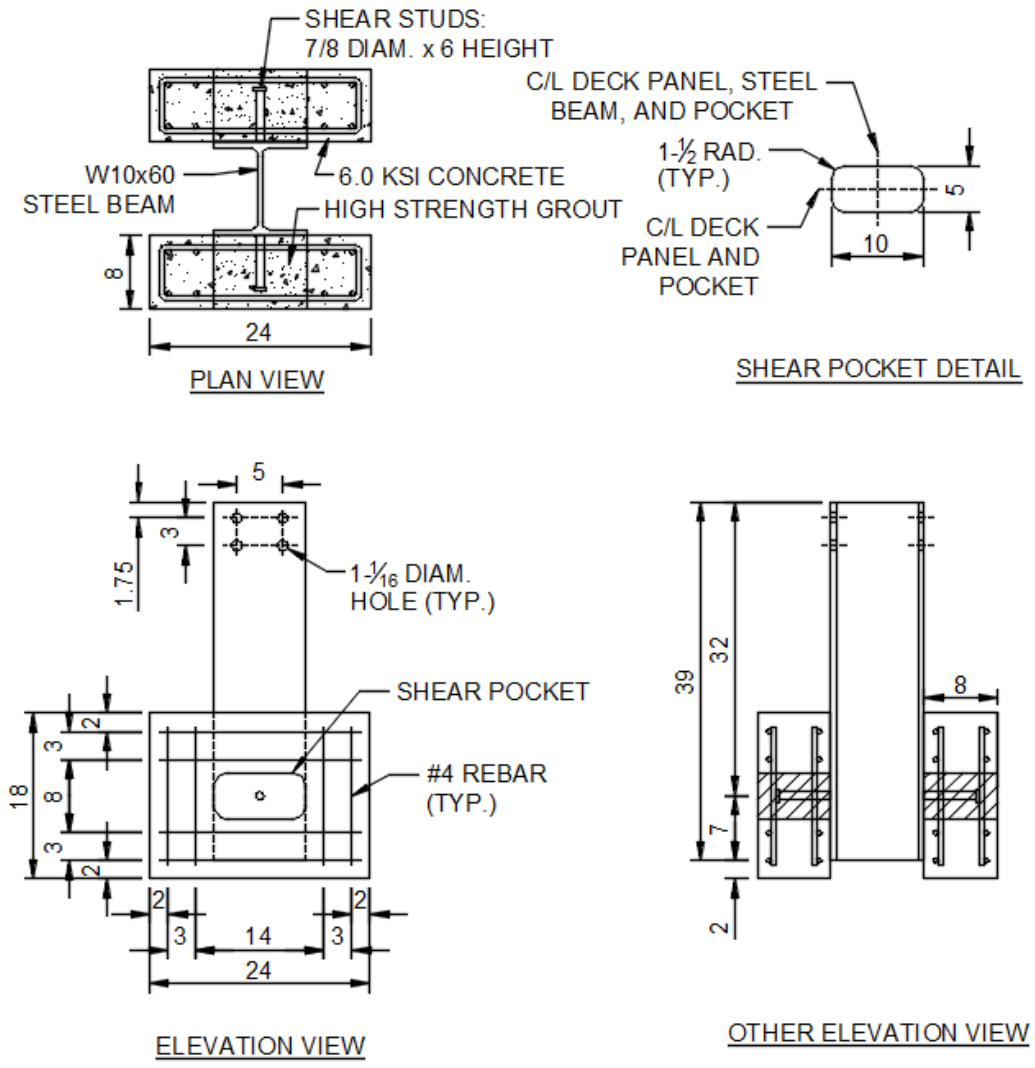

Source: FHWA.
Note: Measurements are in inches.

Figure 15. Schematic. Plan and elevation views for small-scale fatigue test specimens.

The small-scale fatigue specimens used in this study were similar to historical push-out tests but with a few differences. Firstly, this study used PC concrete slabs with grouted pockets rather than CIP concrete decks; there have been studies that used PC decks, but the majority of them have utilized CIP concrete.[18,27] Since the use of ABC was a large focus of this study, PC decks were used for these tests. No large difference in the fatigue performance of the shear studs was expected, whether they were embedded in CIP concrete decks or in PC concrete decks with grouted shear pockets. Also, the large-scale tests were all constructed with PC concrete decks; utilizing the same strategy for the small-scale fatigue tests would allow for a simple comparison between the two scales of testing.

A second difference between the small-scale fatigue tests in this project and those used to develop the current AASHTO provisions was the presence of shear studs welded to both sides of the steel beam. Although the majority of historical push-out tests were constructed with shear

studs welded to both flanges of a steel beam, those referenced in the development of the AASHTO shear stud–fatigue provisions only had shear studs welded to one flange. An analytical study showed that conducting push-out fatigue tests in such a fashion can induce up to 20 percent more tensile forces in the shear studs, causing a reduction in the fatigue life.[31] For this reason, the team decided to construct small-scale fatigue tests with shear studs and concrete deck panels connected to each flange of the steel beam.

The third difference in the small-scale fatigue tests in this study is that only one shear stud was welded to each side of the steel beam. In most push-out tests, there are either two or four shear studs per side. For those tests, failure is typically defined as the time at which one of two slabs becomes completely separated from the steel beam, which means either two or four shear studs have failed. For this study, only one shear stud was welded to each flange so that the failure of a specimen would represent the fatigue life of a single shear stud.

Small-Scale Static Tests

A total of 24 small-scale static tests were conducted in this study. The primary motivation for the small-scale static tests was to evaluate how closely shear studs can be placed together, both longitudinally and transversely, and determine how these different spacings affect the strength of the connection. These specimens were designed and constructed in a similar fashion to historical push-out tests. All specimens were constructed with a 24-inch-long W10x60 steel beam. Each of the specimens had a total of four shear studs. The team welded two shear studs onto each flange, oriented either longitudinally or transversely at variable spacings. Of the 24 small-scale static tests, 12 were constructed with CIP concrete decks, and 12 were constructed with PC decks with grouted pockets; both types of deck connections were tested to determine if there was a difference between them.

The longitudinal spacing static tests were designed to determine if concrete or grout can develop its full strength when shear studs are placed closely together. As shown in table 7, the longitudinal shear stud spacing varied between 3*d* and 6*d*. The upper limit of 6*d* was chosen because it is the current AASHTO maximum spacing limit and could serve as a baseline for comparison to the lesser spacings. The lower limit of 3*d* was selected because, for practical purposes, it is probably the smallest possible pitch. At a center-to-center spacing of 3*d*, the clear distance between the shanks of ⅞-inch-diameter shear studs is 1¾ inch, which is probably larger than the vast majority of aggregates used in a typical concrete mix. If the spacing of shear studs is decreased to 2*d*, the clear distance between shanks becomes ⅞ inch, which would make it difficult for larger aggregates to fit between the shear studs. A ⅞-inch-diameter shear stud also typically has a 1⅜-inch head. At a pitch of 2*d*, the clear distance between adjacent shear stud heads is only ⅜ inches; such a small clearance could pose problems when welding shear studs.

The purpose of the transverse spacing static tests was to determine if the concrete failure zones overlap when shear studs are spaced closer together. The transverse shear stud spacing of the tests varied from 3*d* to 4*d*. The rationale for these limits was similar to that for determining longitudinal spacing limits. The upper limit of 4*d* is the current minimum transverse spacing allowed by AASHTO. The lower limit of 3*d* is probably the smallest possible transverse spacing for the same practical reasons discussed for the longitudinal spacing limits. The test matrix and naming convention for the small-scale static tests are shown in table 7.

Table 7. Small-scale static test matrix and naming convention.

Specimen Name	Replicate Number	Stud Spacing Orientation	Stud Spacing	Deck Type
PO-S1-L3D-CIP	1	Longitudinal	3*d*	CIP
PO-S2-L3D-CIP	2	Longitudinal	3*d*	CIP
PO-S1-L3D-PC	1	Longitudinal	3*d*	PC
PO-S2-L3D-PC	2	Longitudinal	3*d*	PC
PO-S1-L4D-CIP	1	Longitudinal	4*d*	CIP
PO-S2-L4D-CIP	2	Longitudinal	4*d*	CIP
PO-S1-L4D-PC	1	Longitudinal	4*d*	PC
PO-S2-L4D-PC	2	Longitudinal	4*d*	PC
PO-S1-L5D-CIP	1	Longitudinal	5*d*	CIP
PO-S2-L5D-CIP	2	Longitudinal	5*d*	CIP
PO-S1-L5D-PC	1	Longitudinal	5*d*	PC
PO-S2-L5D-PC	2	Longitudinal	5*d*	PC
PO-S1-L6D-CIP	1	Longitudinal	6*d*	CIP
PO-S2-L6D-CIP	2	Longitudinal	6*d*	CIP
PO-S1-L6D-PC	1	Longitudinal	6*d*	PC
PO-S2-L6D-PC	2	Longitudinal	6*d*	PC
PO-S1-T3D-CIP	1	Transverse	3*d*	CIP
PO-S2-T3D-CIP	2	Transverse	3*d*	CIP
PO-S1-T3D-PC	1	Transverse	3*d*	PC
PO-S2-T3D-PC	2	Transverse	3*d*	PC
PO-S1-T4D-CIP	1	Transverse	4*d*	CIP
PO-S2-T4D-CIP	2	Transverse	4*d*	CIP
PO-S1-L4D-PC	1	Transverse	4*d*	PC
PO-S2-L4D-PC	2	Transverse	4*d*	PC

Both the CIP and PC deck specimens were constructed in the Structures Laboratory at TFHRC. For the CIP specimens, the team built a formwork and placed rebar so that both concrete decks for a given specimen could be cast at the same time in the vertical direction. The team constructed the PC deck specimens in a similar way as for the small-scale fatigue tests by first constructing the PC slabs and then connecting them to the steel beam one at a time via prebagged, nonshrink grout. Researchers used the same rebar layout for both the CIP and PC specimens, with No. 4 rebar oriented such that it would not interfere with the shear pockets. Figure 16 shows a drawing of the small-scale static test specimens.

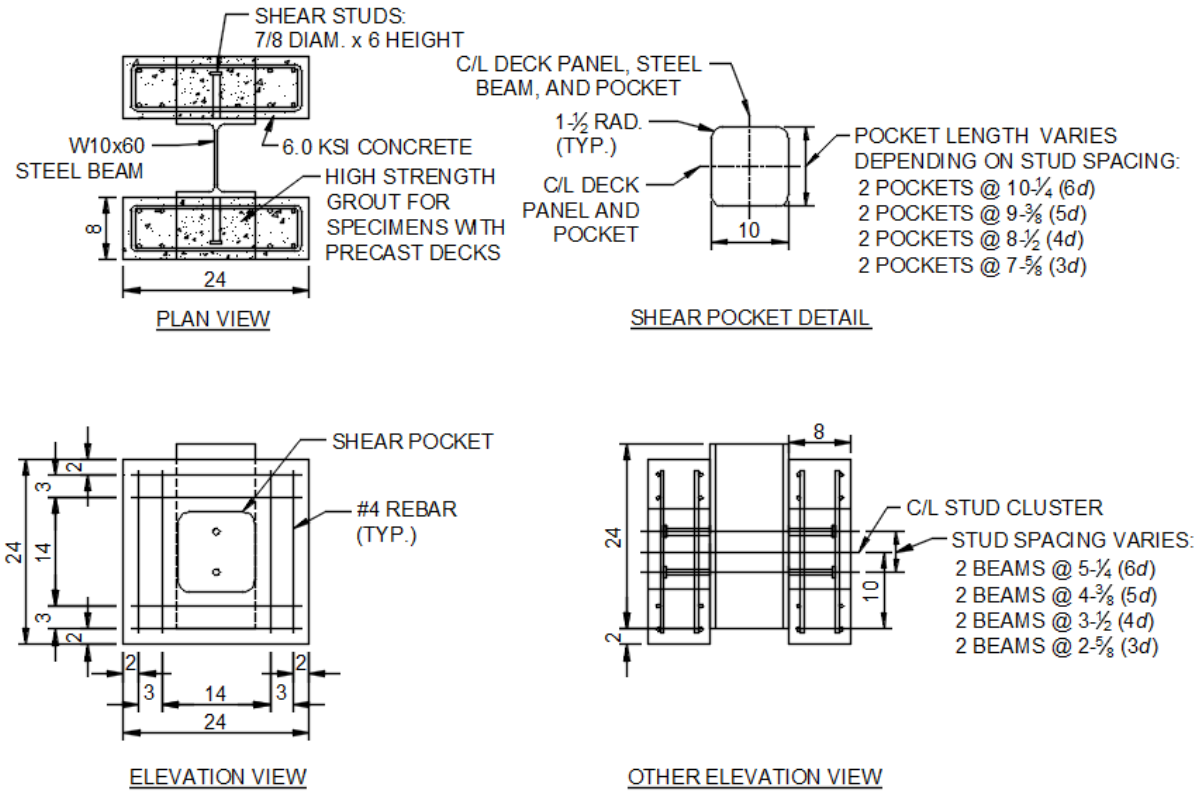

Source: FHWA.
Note: Measurements are in inches.

Figure 16. Schematic. Plan and elevation views for small-scale static test specimens.

INSTRUMENTATION AND LOADING

All of the large- and small-scale tests were conducted in the Structures Laboratory at TFHRC. The following subsections describe the experimental test setup and testing procedure for each of the tests conducted.

Large-Scale Fatigue Tests

All 12 large-scale fatigue tests were loaded in four-point bending, with the load points placed to form an 11.5-foot shear span on each end of the beam. The researchers chose four-point bending to create a constant shear force in the shear span because it should create uniform shear stress ranges in the shear studs. To maximize the length of each shear span, the load points were placed as close together as the load frame allowed. Load was applied at each load point using a 220-kip servo-hydraulic actuator, as shown in figure 17. Figure 18 and figure 19 show the test setup.

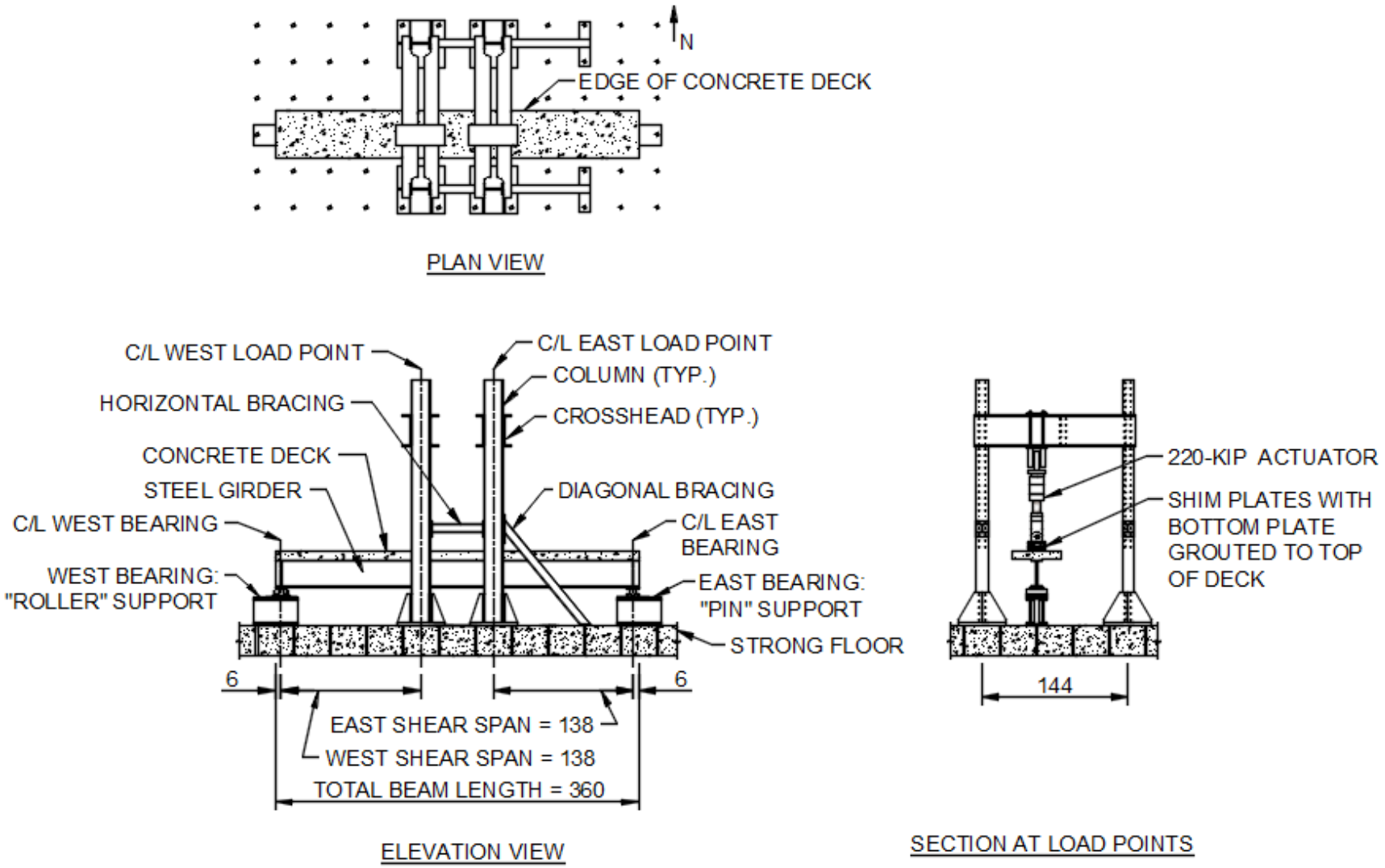

Source: FHWA.
Note: Measurements are in inches.

Figure 17. Schematic. Plan and elevation views for large-scale fatigue loading.

Source: FHWA.

Figure 18. Photo. Southwest view of large-scale fatigue test setup.

Source: FHWA.

Figure 19. Photo. East view of large-scale fatigue test setup.

To produce the desired average stress range at the base of all shear studs in each shear span while still maintaining elastic behavior in the composite beam, the actuators were cycled under a constant load range for each test. Load was applied cyclically until it was apparent that at least one of the PC concrete decks had completely separated from the beam. The research team recorded load and displacement readings from both actuators during testing, along with various other types of data.

A total of 54 strain gauges were installed on the south side of the steel beam and concrete deck for each test. Six strain gauges were used at each of the four cross sections on each shear span and one cross section at the midspan. Each of these cross sections contained three strain gauges installed on the steel beam and three gauges on the concrete deck. Of the four cross sections within each shear span, two were located at a shear stud cluster, and two were located halfway between clusters.

An additional 32 strain gauges were used for 8 of the 12 large-scale fatigue tests; for these tests, the team installed the additional strain gauges on all 12 of the shear studs in the east shear span and the 4 shear studs closest to the west end of the beam in the west shear span. Strain gauges were only installed on four of the shear studs in the west shear span, owing to a lack of channel availability in the data acquisition system. Rather than evenly split up the remaining available data channels between the east and west shear spans, the team decided to record data from all of the shear studs in the east shear span in hopes of extrapolating behavior to the limited number of gauges in the west shear span. For each of these shear studs, the team installed strain gauges on the east and west sides near the base of the shear stud. Since the strains should decrease as fatigue cracks grow, these strain gauges were installed in hopes of determining the order in which shear studs failed in fatigue during testing.

A total of 12 linear variable differential transducers (LVDTs) were also used on each beam. Nine were used to measure the relative horizontal slip between the top flange of the steel beam and the bottom of the concrete deck panel. Two LVDTs were used to measure the relative vertical uplift between the steel beam and the deck. These two LVDTs were located at the midpoint of each shear span. The remaining LVDT was used to measure vertical deflection of the beam at the midspan.

Detailed instrumentation plan drawings for each of the specimen types are shown in figure 20 through figure 29.

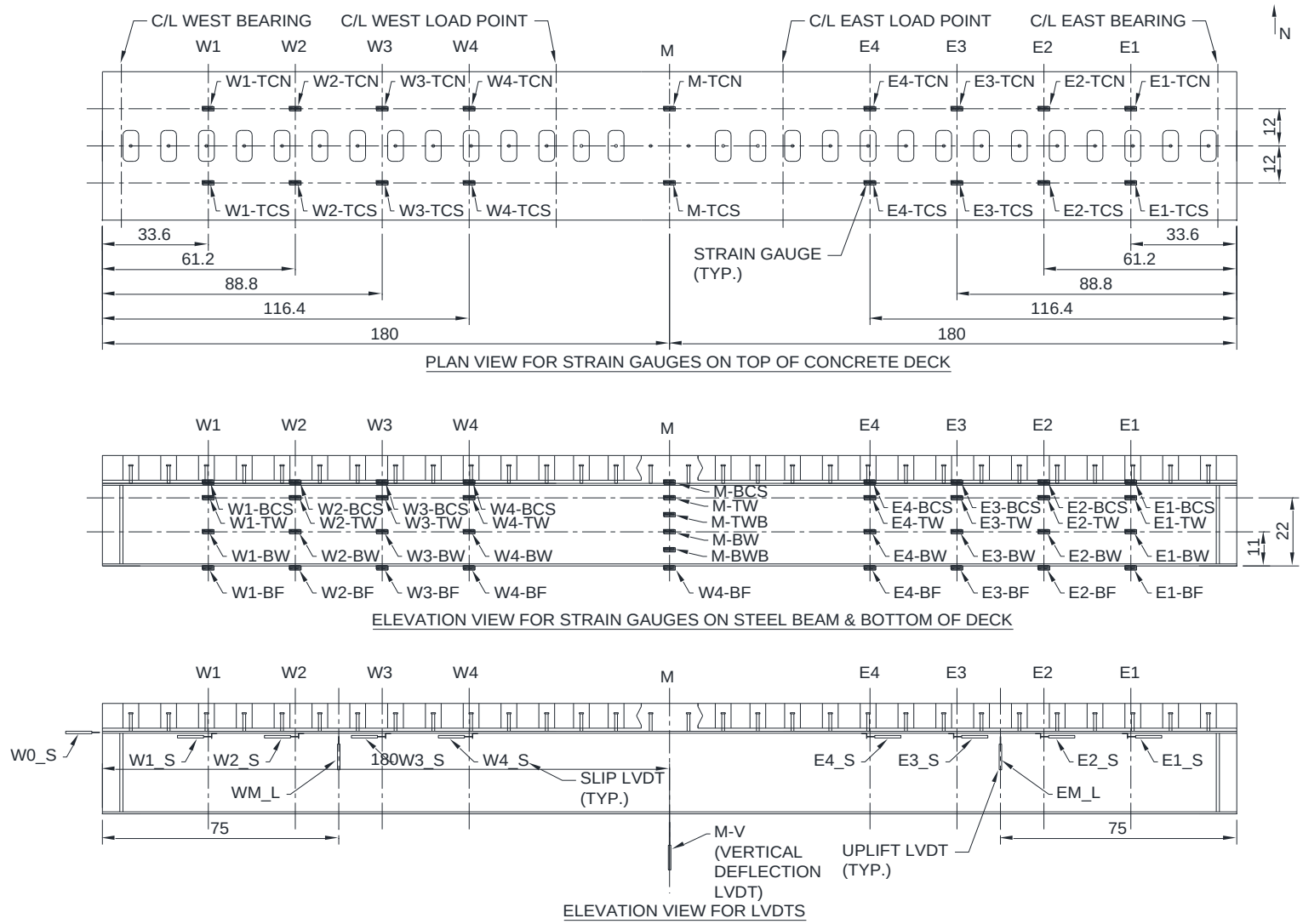

Source: FHWA.
Note: Measurements are in inches.

Figure 20. Schematic. Plan and elevation views for instrumentation on a large-scale specimen with 12-inch shear stud spacing.

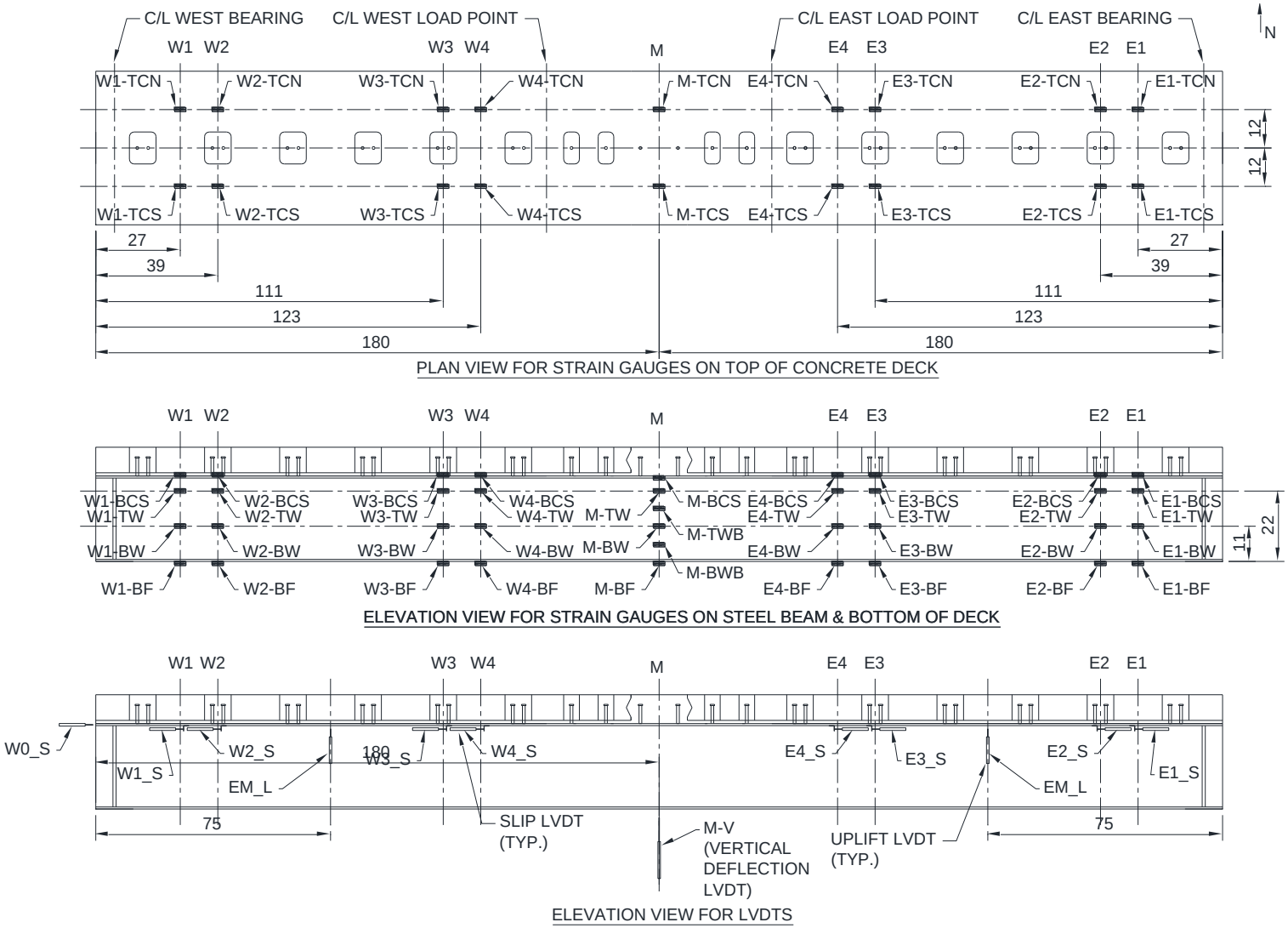

Source: FHWA.
Note: Measurements are in inches.

Figure 21. Schematic. Plan and elevation views for instrumentation on a large-scale specimen with 24-inch shear stud spacing.

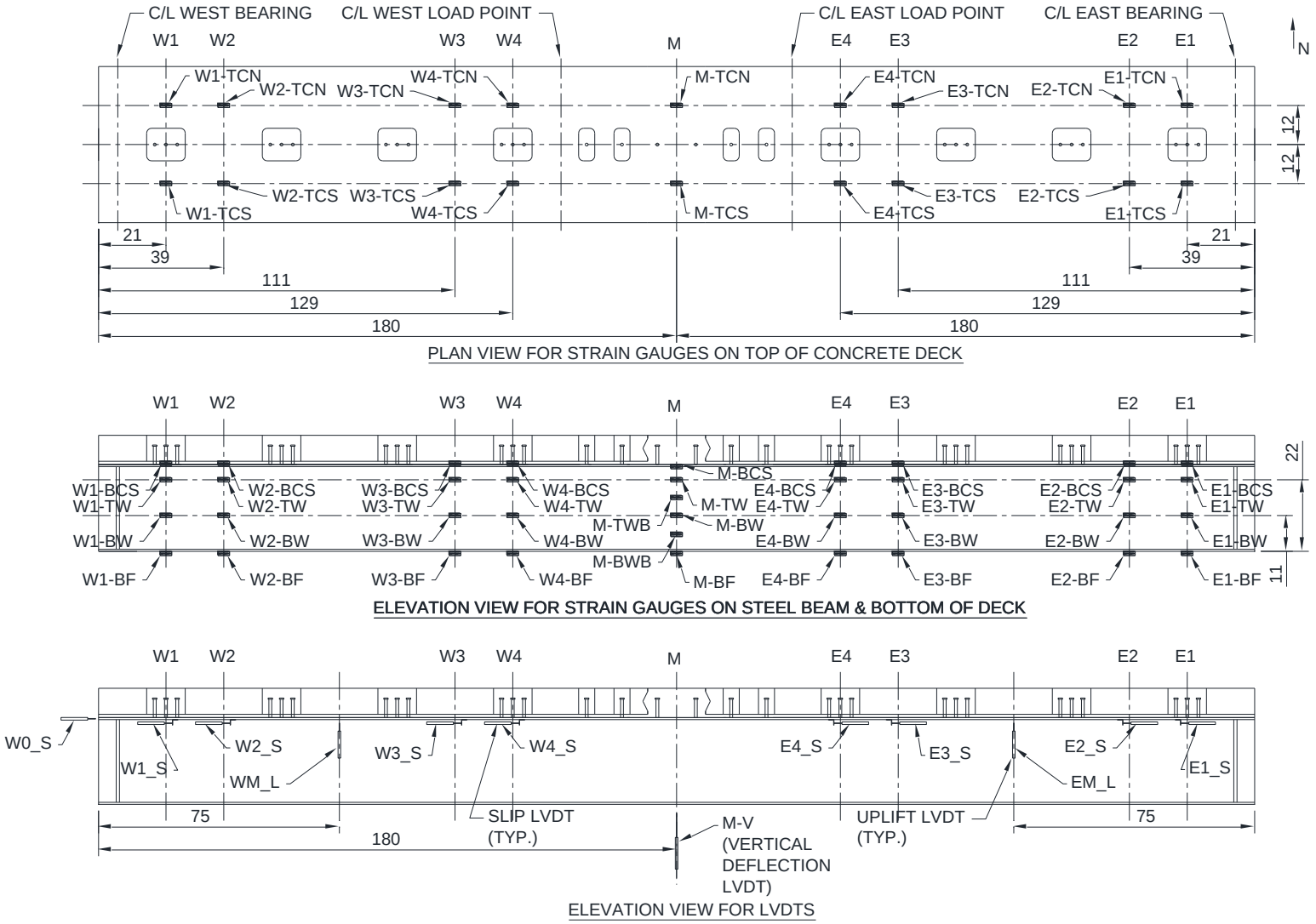

Source: FHWA.
Note: Measurements are in inches.

Figure 22. Schematic. Plan and elevation views for instrumentation on a large-scale specimen with 36-inch shear stud spacing.

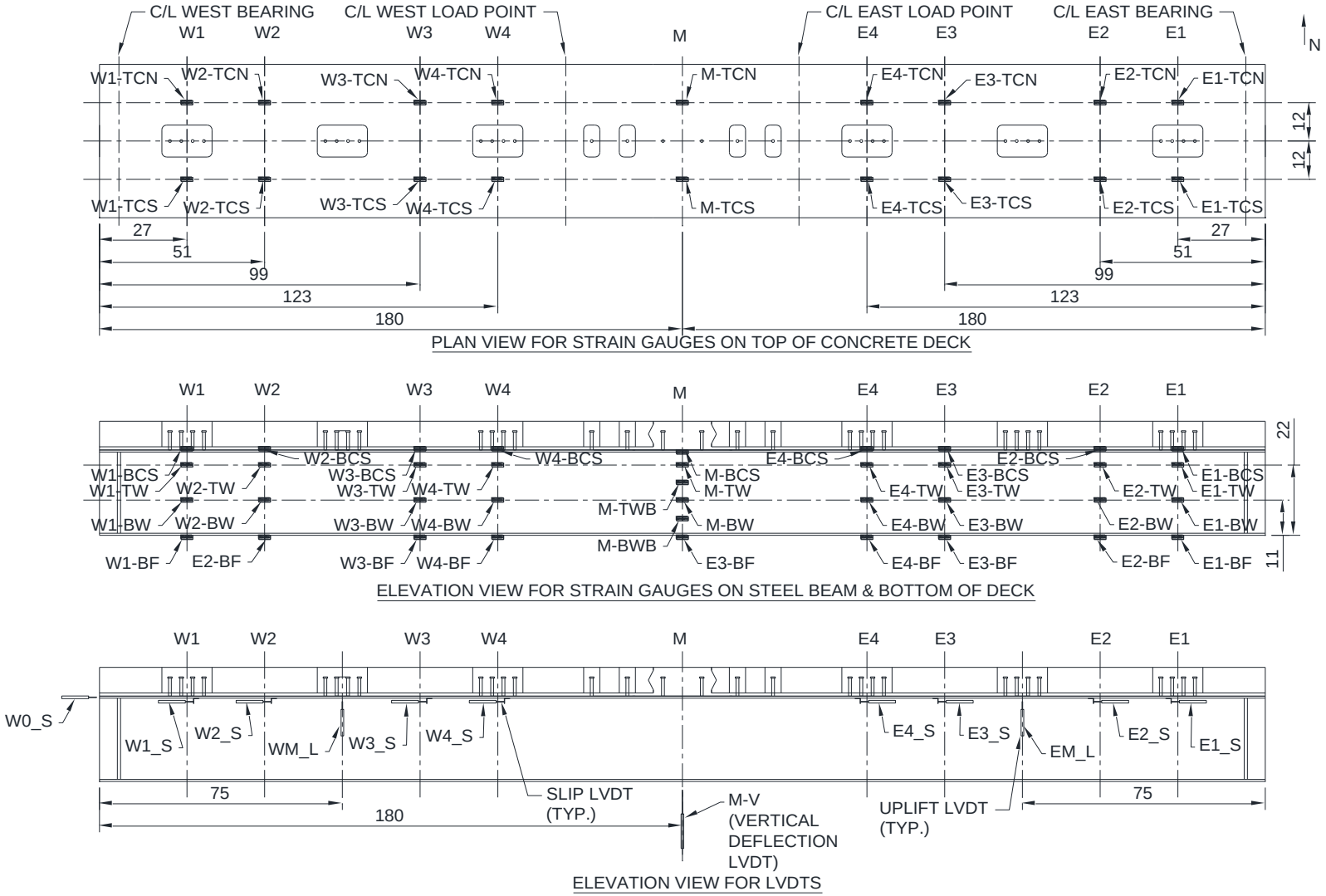

Source: FHWA.
Note: Measurements are in inches.

Figure 23. Schematic. Plan and elevation views for instrumentation on a large-scale specimen with 48-inch shear stud spacing.

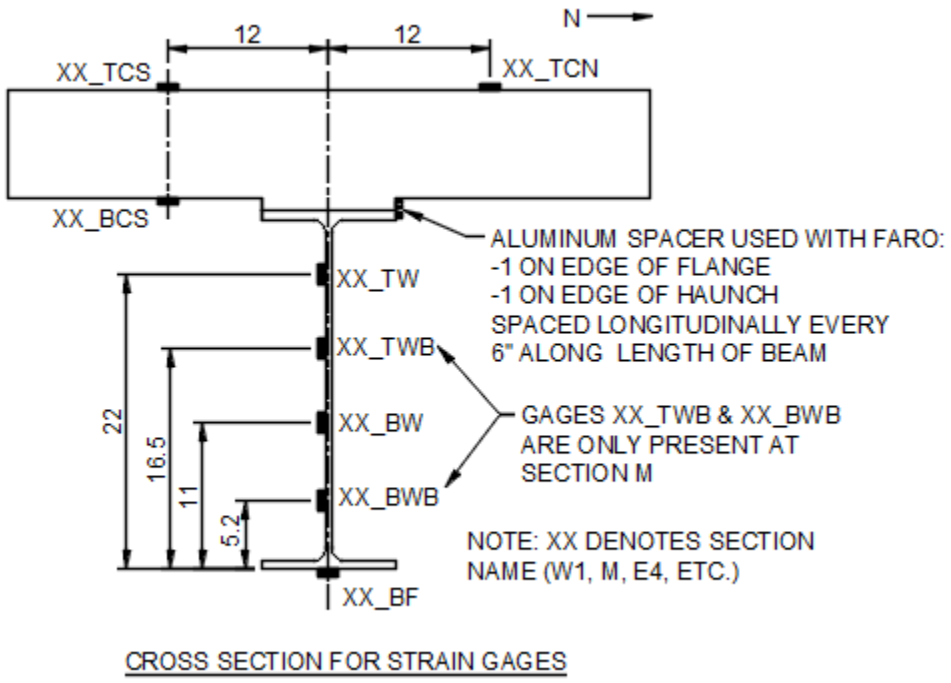

Source: FHWA.
Note: Measurements are in inches.

Figure 24. Schematic. Typical section for instrumentation on all large-scale specimens.

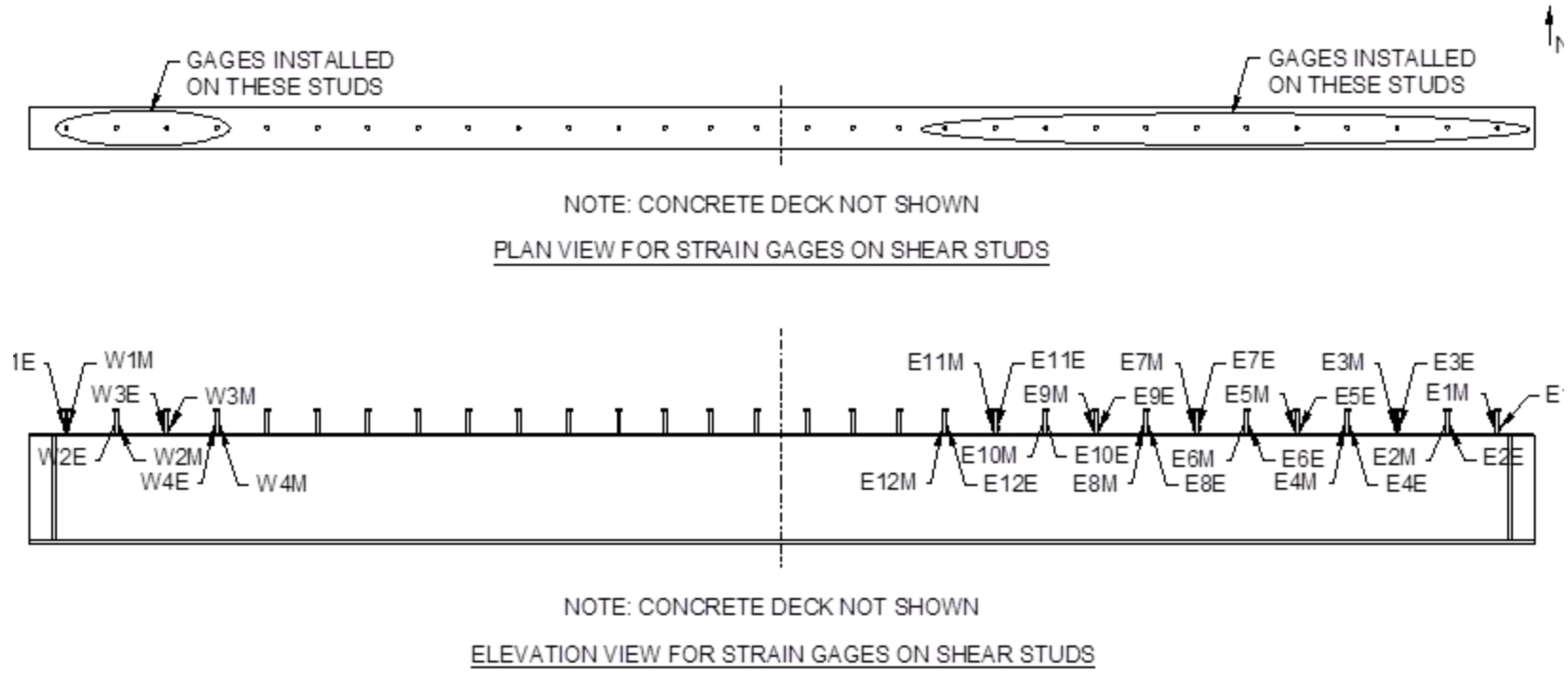

Source: FHWA.

Figure 25. Schematic. Plan and elevation views of shear stud strain gauges for beams 1F2 and 1F3.

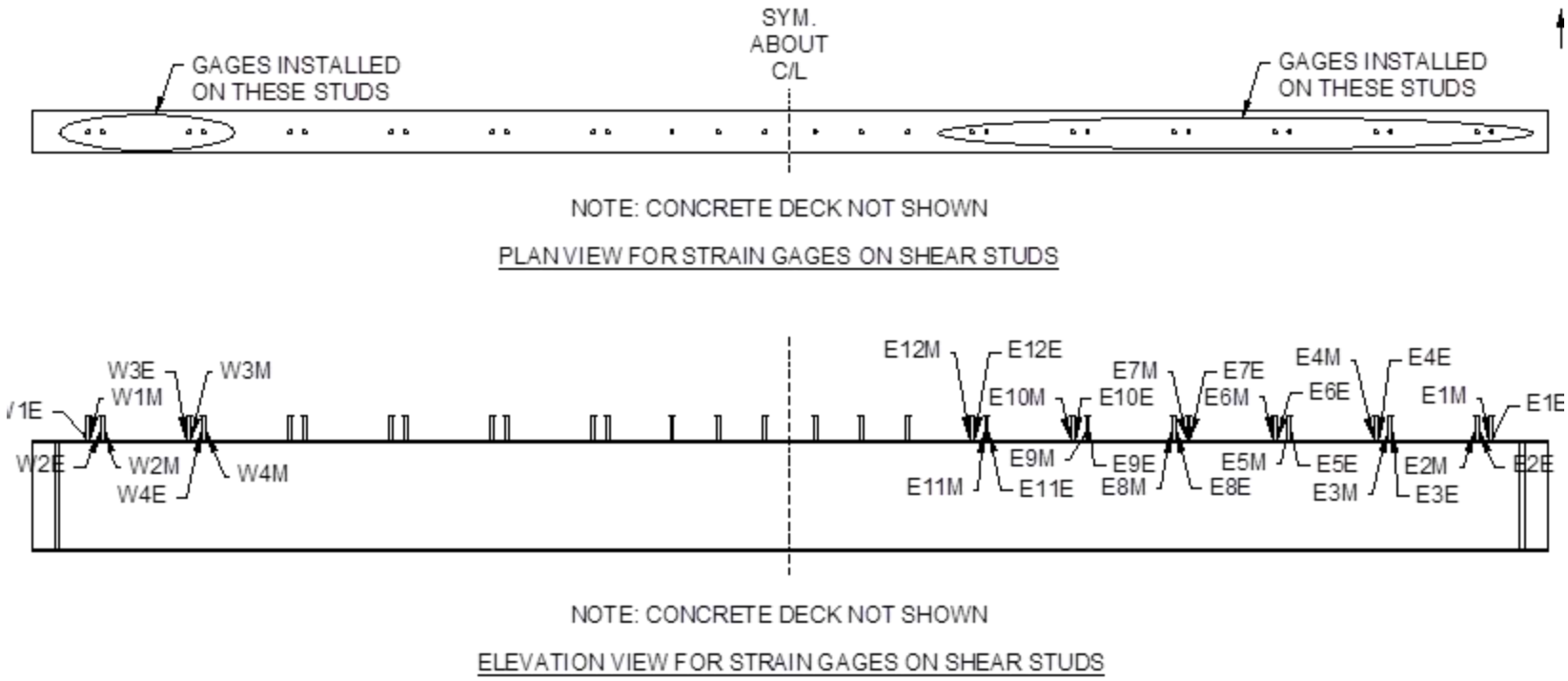

Source: FHWA.

Figure 26. Schematic. Plan and elevation views of shear stud strain gauges for beams 2F2 and 2F3.

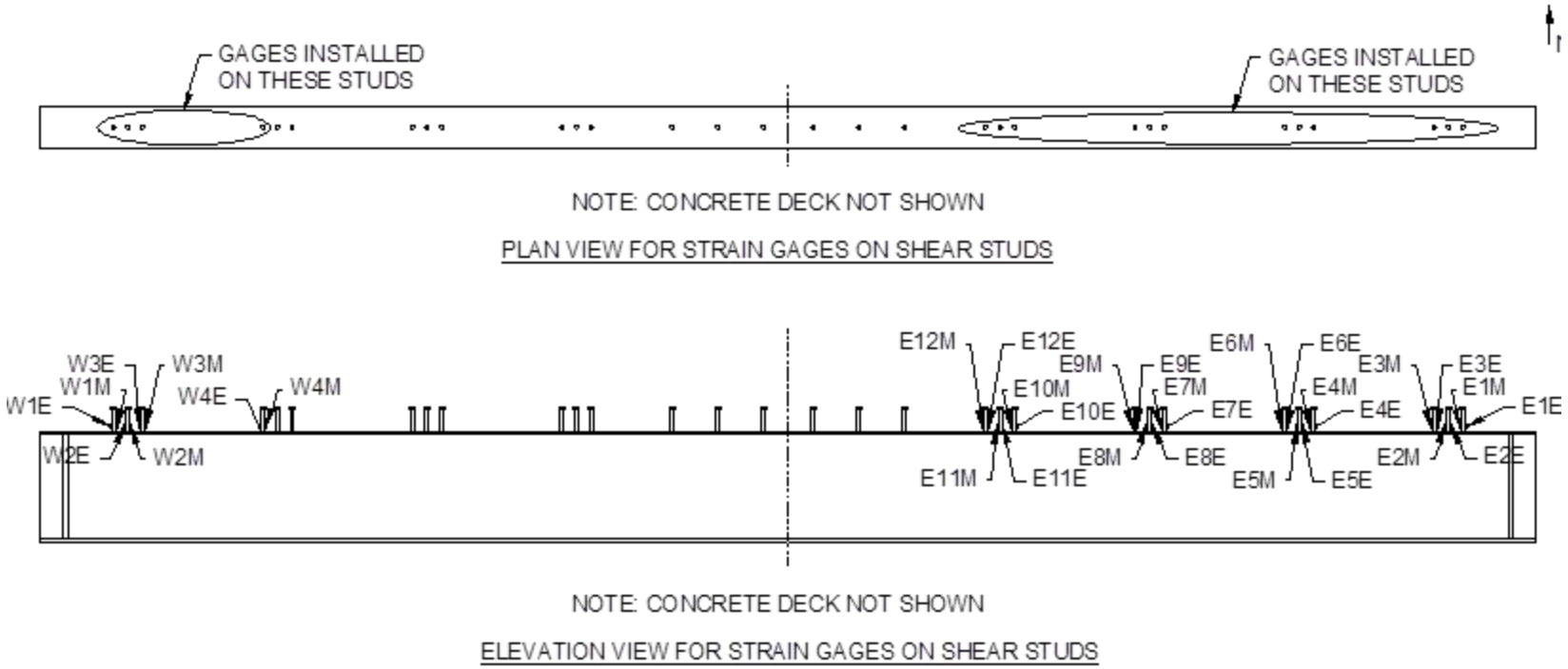

Source: FHWA.

Figure 27. Schematic. Plan and elevation views of shear stud strain gauges for beams 3F2 and 3F3.

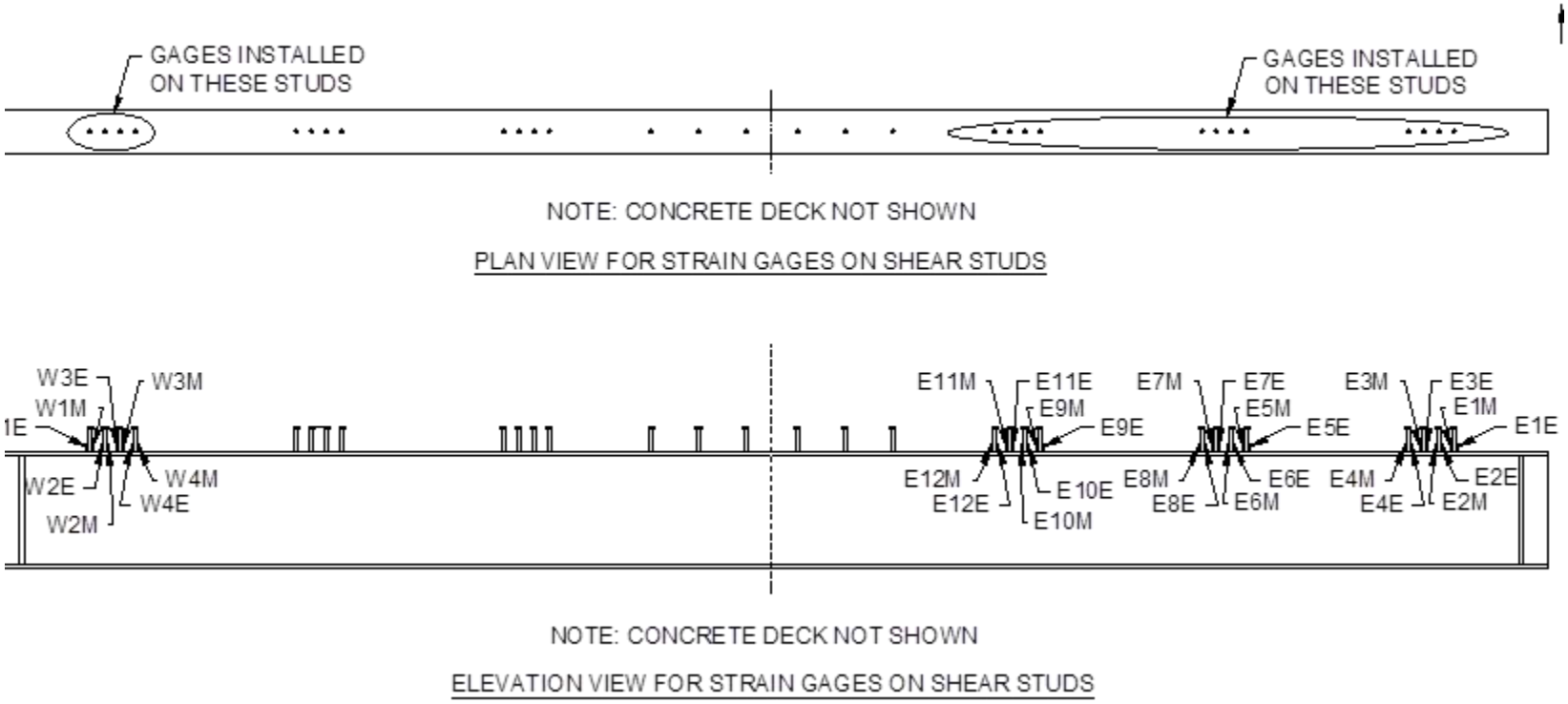

Source: FHWA.

Figure 28. Schematic. Plan and elevation views of shear stud strain gauges for beams 4F2 and 4F3.

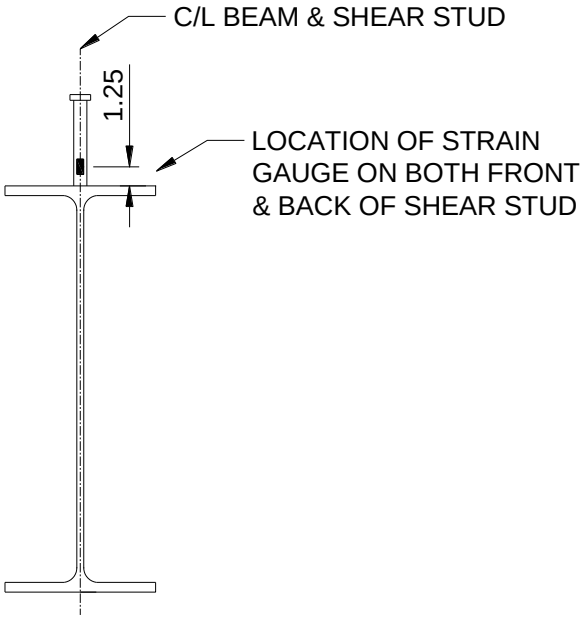

Source: FHWA.
Note: Measurements are in inches.

Figure 29. Schematic. Typical section of shear stud strain gauges on large-scale tests.

One unique instrumentation technique used on these tests was taking slip and uplift measurements using a laser tracker. This system uses a centralized head unit on a tripod. The head has two encoders to measure horizontal and vertical angles and an absolute distance measurement laser, which, together, are able to provide highly accurate three-dimensional coordinates of a spherically mounted reflector moved through space by the user. Slip and uplift measurements were recorded by first mounting aluminum spacers, which acted as reference points, to the edges of the haunch and top flange every 6 inches along the entire length of the beam. All of the spacers were mounted to the north side of the beam using hot glue so that the instrumentation cables would not be disturbed when laser tracker measurements were taken. Measurements were recorded by stopping the fatigue tests at predetermined cyclic intervals, depending on the expected life of the fatigue tests, and applying a static load equal to the maximum fatigue load. The spherically mounted reflector was nested into each aluminum spacer, and the team recorded the measurements. Using these measurements, researchers calculated relative slip and uplift between the haunch and the top flange from the baseline measurement. Figure 30 shows a photo of the laser tracker head unit, and figure 31 shows a photo of the method of nesting the prism into the aluminum spacers to record data.

Source: FHWA.

Figure 30. Photo. Laser tracker system head unit.

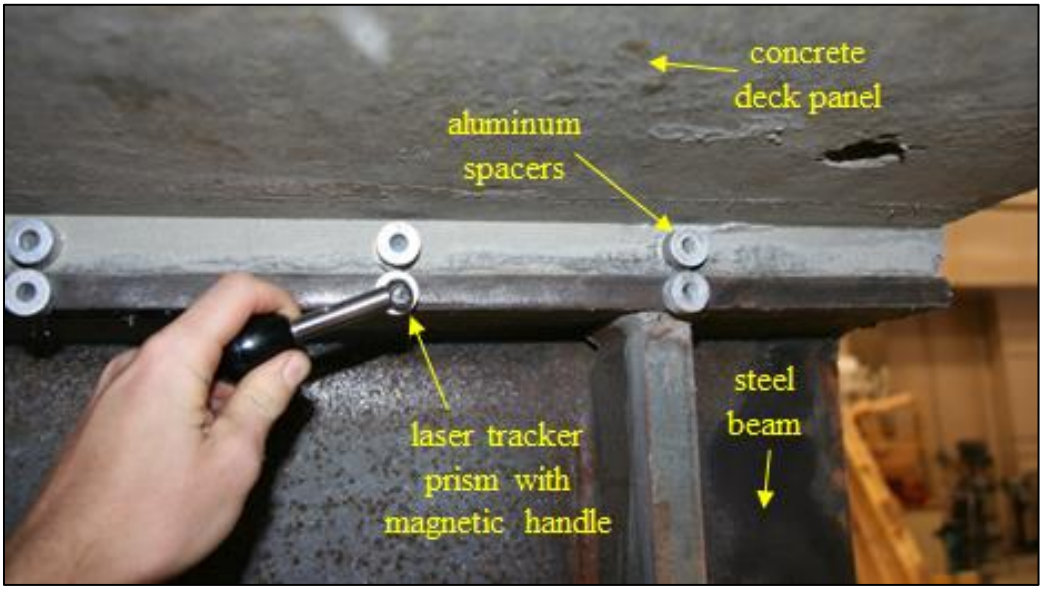

Source: FHWA.

Figure 31. Photo. Method of nesting laser tracker prism into aluminum spacers on large-scale tests.

Large-Scale Static Tests

Similar to the large-scale fatigue tests, the static tests were loaded in four-point bending to produce two 11.5-foot-long shear spans. This was done to produce a constant shear force applied to each shear stud in both shear spans. The team loaded the static tests using a spreader beam placed transversely across the width of the concrete deck at both load points. During the loading process, the spreader beam was pulled downward using a post-tensioning (PT) rod on either side of the beam. Each PT rod was loaded by a pair of hollow core jacks reacting against the bottom of the concrete strong floor of the Structures Laboratory. The two jacks, each having a capacity of 100 T and maximum stroke of 6 inches, were placed in series on each PT rod to provide a maximum travel distance of 12 inches to accommodate the expected vertical deflection of the beam during loading. Load cells were placed on spherical bearings between the spreader beams and concrete deck of the specimen to record the applied load during testing. A passive lateral bracing system was used to prevent movement throughout testing. Figure 32 shows a drawing and figure 33 shows a photo of the loading setup for each of the static tests.

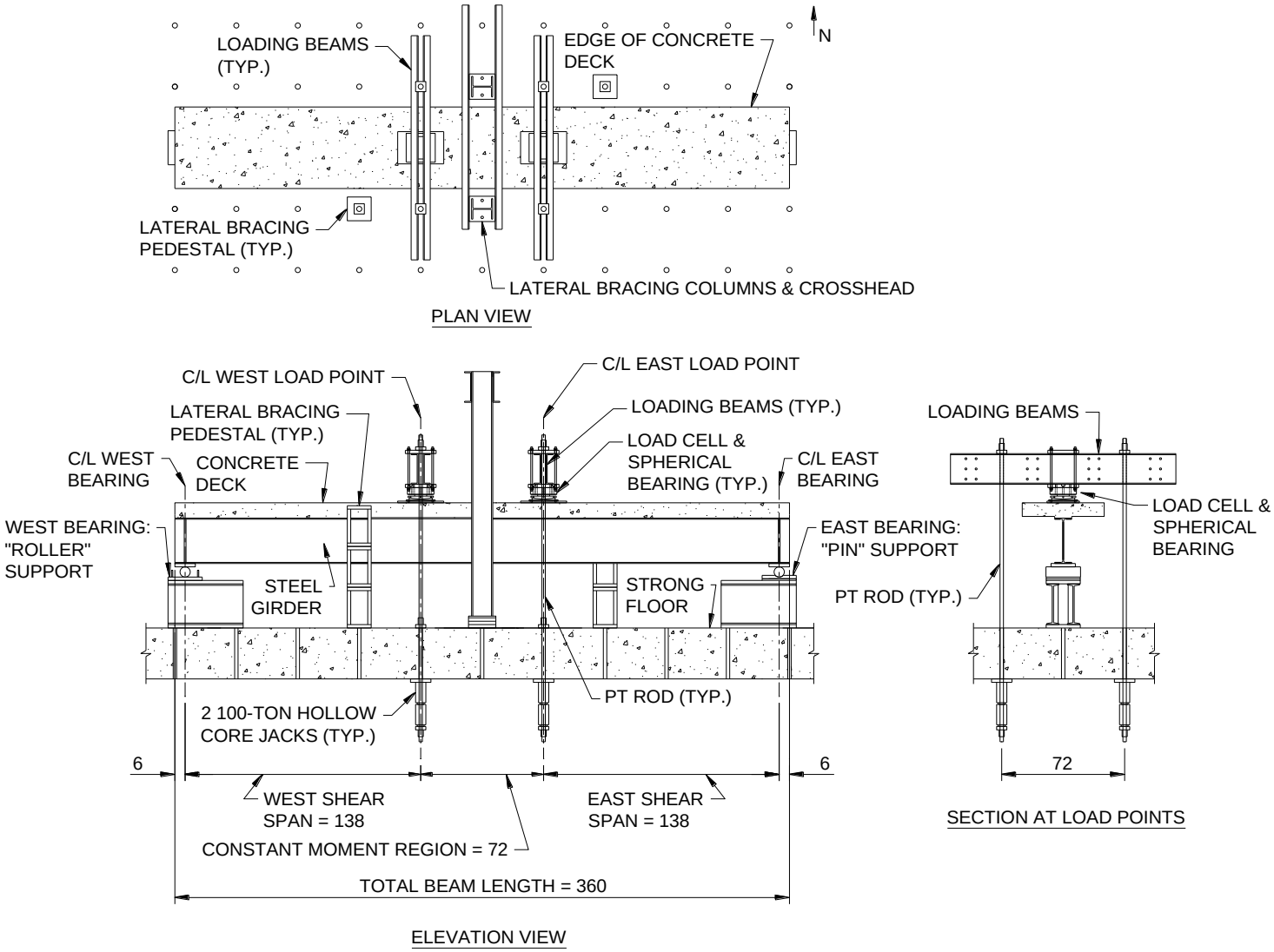

Source: FHWA.
Note: Measurements are in inches.

Figure 32. Schematic. Plan and elevation views of large-scale static loading.

Source: FHWA.

Figure 33. Photo. Southwest view of large-scale static testing setup.

The team used an open-loop controlled hydraulic pump to apply load at a slow rate throughout each test. The operator manually controlled the speed of loading by releasing a valve, which slowly allowed hydraulic pressure to be applied to the loading jacks. Loading was paused at applied moments of 0; 460; 860; 1,270; 1,380; and 1,500 kip-ft for approximately 30 min to take measurements with the laser tracker laser system. After the last set of laser tracker measurements were taken, the load was increased slowly until the beam reached a maximum moment and then failed, either because of grout crushing at the midspan or a shear failure of the shear studs in one of the two shear spans. After the beam reached failure, loading continued until the beam could not support any additional load. After this point, the team slowly unloaded the beam, and the test was considered complete.

The instrumentation used on the large-scale static tests was similar to the large-scale fatigue tests. Researchers took strain gauge, LVDT, and laser tracker data from the same locations as were used in the large-scale fatigue tests.

Small-Scale Fatigue Tests

All 14 of the push-out fatigue tests were loaded in tension rather than in compression like many of the historical tests. Because of the single-stud configuration, researchers were concerned that the concrete slabs would rotate about the shear studs because of small misalignments when loaded in compression. Loading the specimens in tension allowed the concrete slabs to essentially “self-level” to prevent any unwanted rotation. The specimens were loaded using a

55-kip servo-hydraulic actuator. The team constructed reaction fixtures out of channels and placed them on top of the concrete slabs. Then, they grouted steel plates in place on top of both concrete slabs to ensure that load was applied evenly between the two slabs. A diagram of the loading setup for these small-scale fatigue tests is shown in figure 34, and a photo is shown in figure 35.

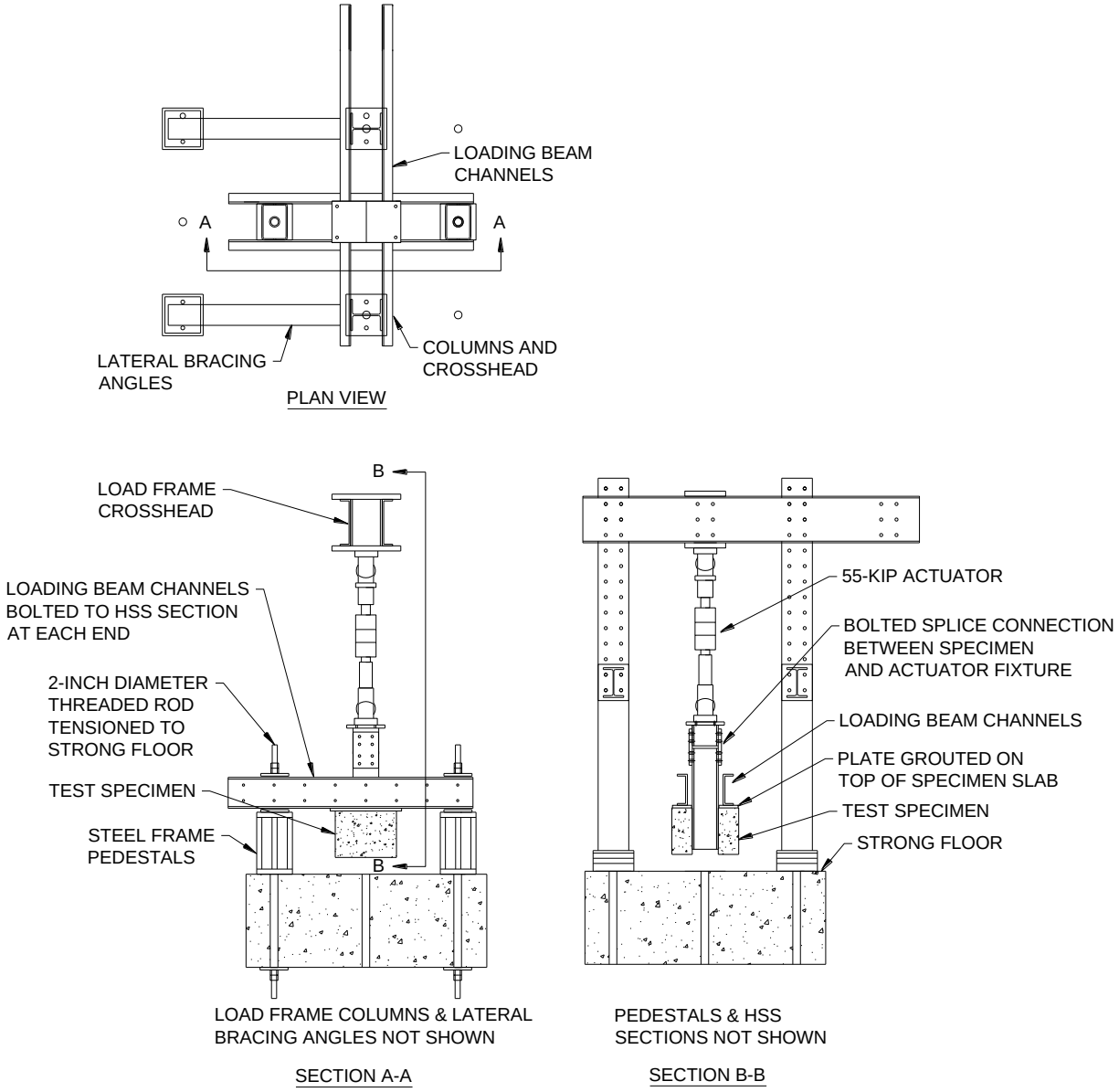

Source: FHWA.

Figure 34. Schematic. Plan and elevation views of small-scale fatigue loading.

Source: FHWA.

Figure 35. Photo. Small-scale fatigue test setup.

The actuator was cycled at a constant load range to produce the desired stress range at the base of both shear studs while maintaining elastic behavior throughout the test. Cyclic loading was continued until one or both of the slabs had completely separated from the steel beam. Generally, one slab separated first because one of the shear studs failed in fatigue before the other. There were cases, however, in which both shear studs failed in fatigue at approximately the same cycle count.

A total of four strain gauges and two LVDTs were used in each small-scale fatigue test. The team placed strain gauges on the top and bottom of each shear stud in the direction of force and as close to the base of the shear stud as possible without interfering with the shear stud weld flash. Similarly placed strain gauges were used on the large-scale fatigue tests; the gauges on the small-scale tests provided a means of comparison. Researchers installed one LVDT on each deck panel to measure the relative slip between concrete deck and steel beam. They also mounted an aluminum angle to the inside of the flange of the beam to facilitate measuring the relative slip. The instrumentation plan for the small-scale fatigue tests is shown in figure 36.

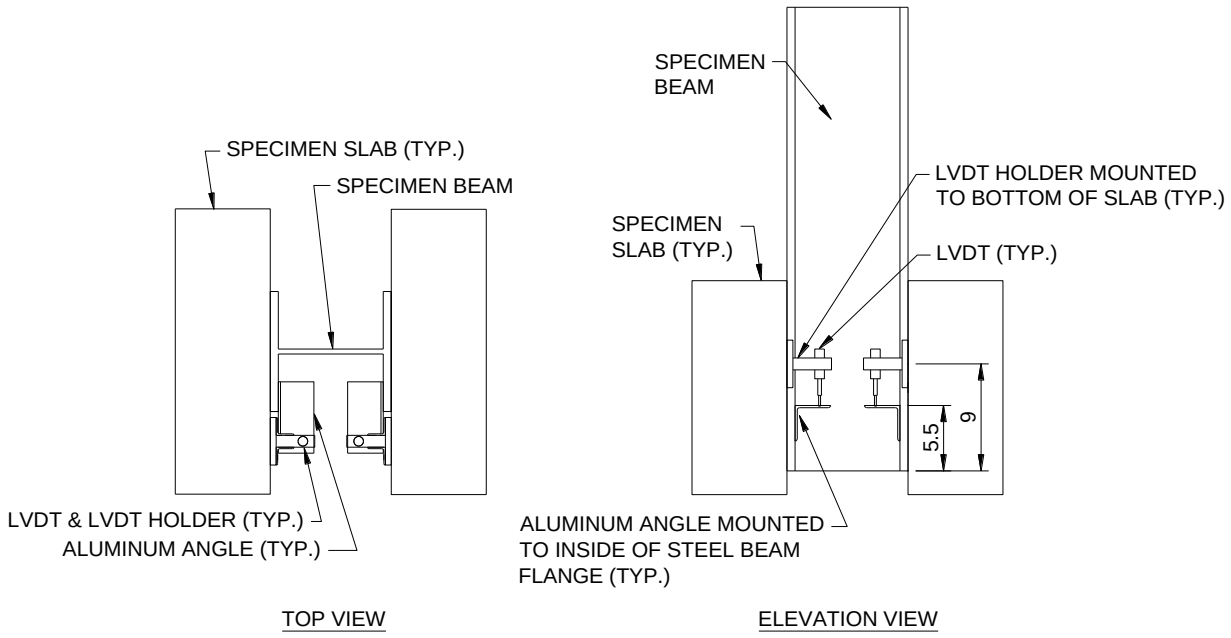

Source: FHWA.
Note: Measurements are in inches.

Figure 36. Schematic. Instrumentation plan for small-scale fatigue tests.

Small-Scale Static Tests

All 24 small-scale static tests were loaded in compression, similar to historical push-out tests. The loading was conducted using a servo-hydraulic controlled jack with a capacity of 300 kips. The team recorded the load and displacement during testing with a load cell and LVDT, respectively. They grouted a large concrete reaction block into place under the jack to spread out the compressive load on the strong floor during testing. Then, each specimen was leveled and grouted into place between the concrete reaction block and the jack. Figure 37 and figure 38 show a diagram and a photo of the loading setup, respectively.

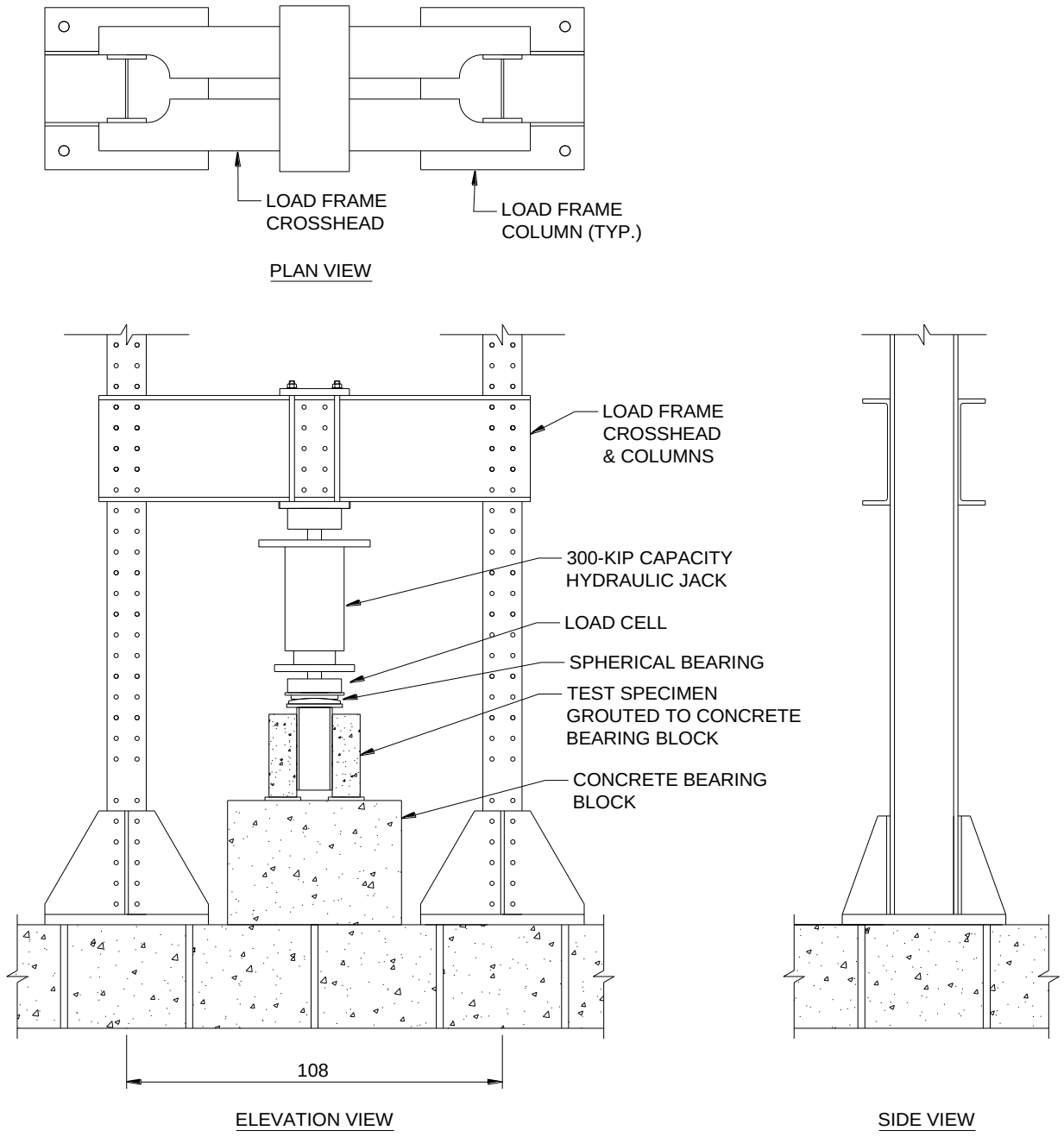

Source: FHWA.
Note: Measurements are in inches.

Figure 37. Schematic. Plan and elevation views of small-scale static loading.

Source: FHWA.

Figure 38. Photo. Small-scale static test setup.

Load was applied in displacement control at a constant rate of approximately 0.0005 inch/min throughout each test. Loading continued until the specimen could no longer support additional load. At that point, it was clear that one or both slabs had completely separated from the steel beam. Load was then removed from the specimen, and the test concluded.

Two types of instrumentation were used to measure the relative slip between the slabs and the steel beam. The team installed LVDTs in a similar way as for the small-scale fatigue tests, with the LVDT mounted to the concrete slabs and the aluminum angles mounted to the steel beam flange. A video extensometer recorded video data during testing that could be postprocessed into relative slip data. LVDTs were used to measure data on both the concrete and steel beam in the same way as in the small-scale fatigue tests. Data were recorded using LVDTs and the video extensometer so that the results from each could be compared after testing was complete. Figure 39 shows the instrumentation plan for the LVDTs on the small-scale static tests.

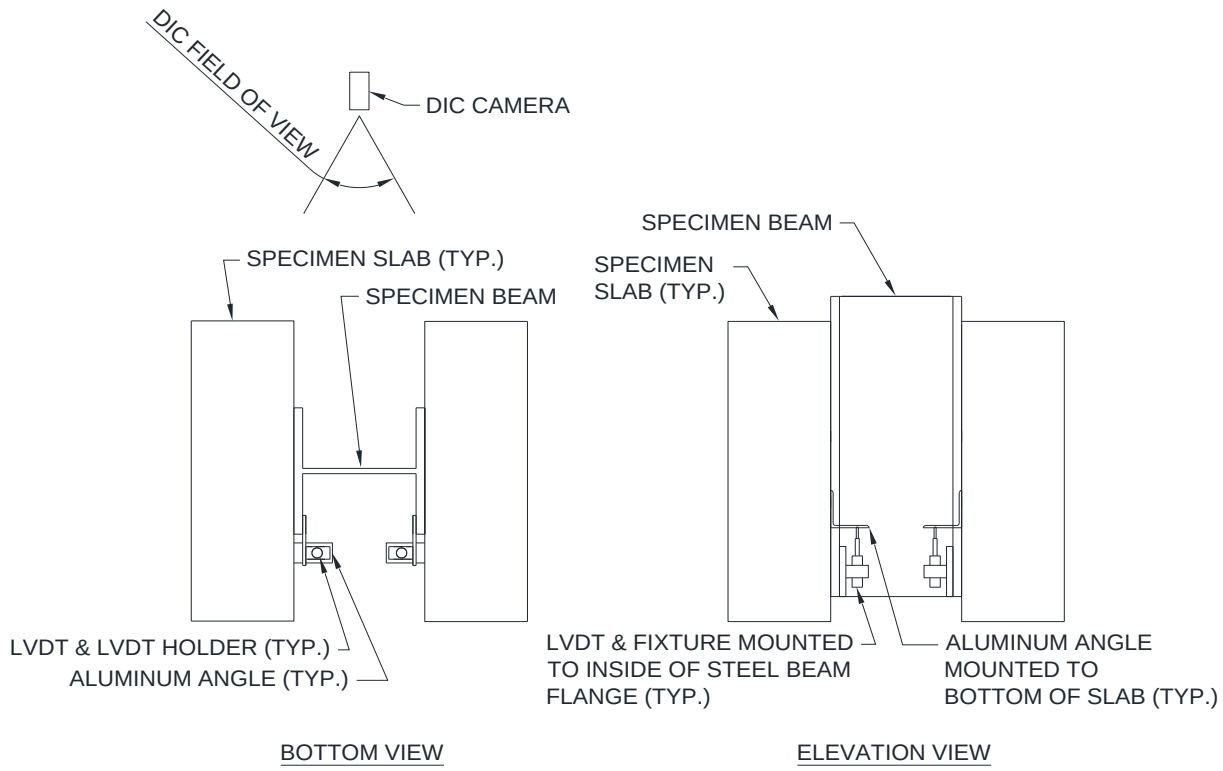

Source: FHWA.

Figure 39. Schematic. LVDT instrumentation plan for small-scale static tests.

EXPERIMENTAL RESULTS AND DISCUSSION

MATERIAL TEST RESULTS

A thorough description of all steel, concrete, and grout material testing results can be found in appendix B. The average results are shown in table 8 for the steel material properties and table 9 for the concrete and grout strengths.

Table 8. Summary of steel strength properties.

Steel Tested	Average Yield Stress (ksi)	Average Tensile Strength (ksi)	Average Elongation at Fracture (Percent)
W27x84	56.4	72.9	25
W10x60	54.7	73.0	24
Shear studs	56.4	73.5	24

Table 9. Summary of concrete and grout strength properties.

Specimen	Average Concrete Cylinder Strength (ksi)	Average Grout Cube Strength (ksi)
1S2	8.0	7.6
1S1	9.1	6.9
1F1	7.3	9.4
1F2	10.1	5.4
1F3	8.4	5.7
2S1	10.0	7.0
2F1	10.8	8.7
2F2	7.0	7.5
2F3	8.5	10.1
3S1	9.2	6.7
3F1	9.4	7.7
3F2	9.7	6.8
3F3	9.9	6.6
4S1	8.5	7.6
4F1	8.8	8.6
4F2	11.0	7.0
4F3	10.2	8.6
Small-scale static CIP	9.6	—
Small-scale static PC	7.5	7.8
Small-scale fatigue	5.3	10.1

—No data to report since CIP specimens do not use grout.

LARGE-SCALE FATIGUE TEST RESULTS

The following subsections describe the results of the large-scale fatigue tests. Since a large amount of data was generated in these tests, only tests that resulted in relevant, meaningful findings are presented. The strain gauges installed on the shear studs showed unusually large strain values, with behavior that was difficult to interpret or draw any meaningful conclusions from. For this reason, data from these strain gauges are not included.

Visual Observations

The large-scale beams were cyclically loaded until it was clear that one of the concrete decks had separated from the steel beam. At this point, the test was considered complete. The concrete decks were then removed from the steel beam. This was somewhat challenging for two reasons. Typically, the shear studs in only one shear span had completely failed, and the shear studs in the constant-moment region were still intact. This necessitated the use of a jackhammer to remove the grout in the shear pockets to separate the concrete decks from the steel beam. In some instances, the team drilled cores into the grout around the shear studs to assist with removal of the concrete deck and to allow for examination of the grout directly around the shear studs. When this was done, the beam flange and web were flame-cut so that the entire shear stud and grout core assembly could be examined.

Once the concrete decks had been successfully removed from the steel beam, researchers examined the fracture surfaces of the shear studs. Figure 40 shows a closeup photo of two typical fracture surfaces from the large-scale tests. These specific fracture surfaces came from beam 3F2 and were the second and third shear studs from west end of the beam, as indicated by the “W2” and “W3” in the photo.

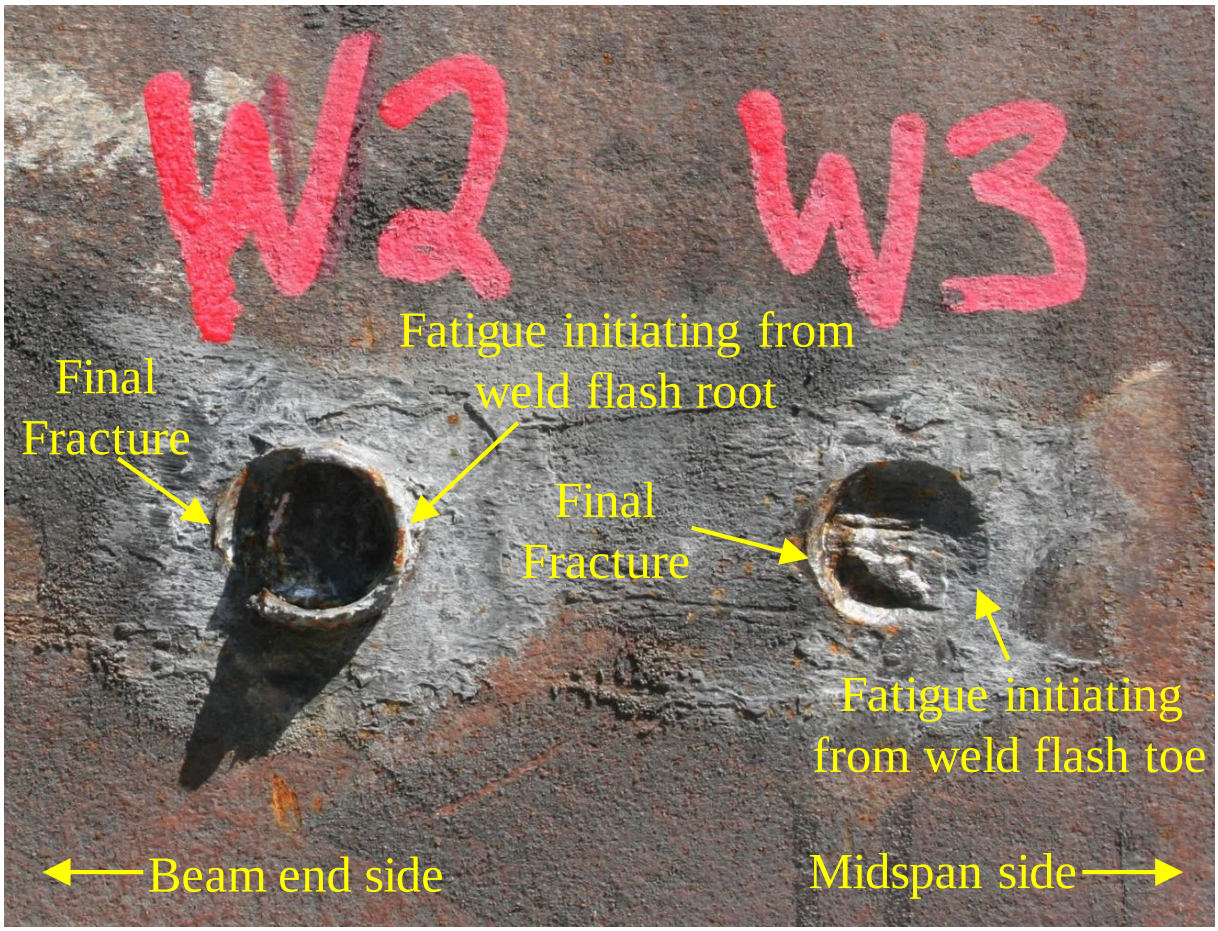

Source: FHWA.

Figure 40. Photo. Typical shear stud fracture surfaces from large-scale fatigue tests.

Nearly all of the shear stud fracture surfaces looked like those in figure 40, with the W3 fracture surface the most prevalent. This fracture surface demonstrated a fatigue crack initiating on the midspan side of the shear stud at the weld toe on the beam flange and propagating into the flange base metal following the heat-affected zone. Fracture then occurred on the beam-end side of the shear stud, leaving a distinct divot in the top flange base metal. The remaining fracture surfaces looked like the W2 fracture surface. In this case, the fatigue crack initiated from the weld flash on the shear stud before propagating into the base metal along the heat-affected zone. Again, the fracture occurred on the beam-end side of the shear stud, leaving most of the weld flash in place but removing a divot of beam flange base metal. There were also a few instances in which the fatigue crack initiated from the top of the weld flash and propagated through the shear stud base metal on a plane even with the top of the weld flash. In these cases, the portion of the shear stud above the top of the weld flash completely separated from the beam, but the remainder of the shear stud and weld flash remained in place.

After examining the shear stud fracture surfaces, the research team investigated the cores with the grout and intact shear studs to determine the behavior of the grout during testing. They began this process by carefully cutting the grout core open with a concrete saw. Once the grout core was separated into two halves, the two sample pieces were photographed using a macrostand;

figure 41 shows a typical photo. This specific grout core was taken from the sixth easternmost shear stud in beam 4F3. Note that this shear stud had a strain gauge installed on it; the protective coating system applied to this strain gauge is seen on the shear stud.

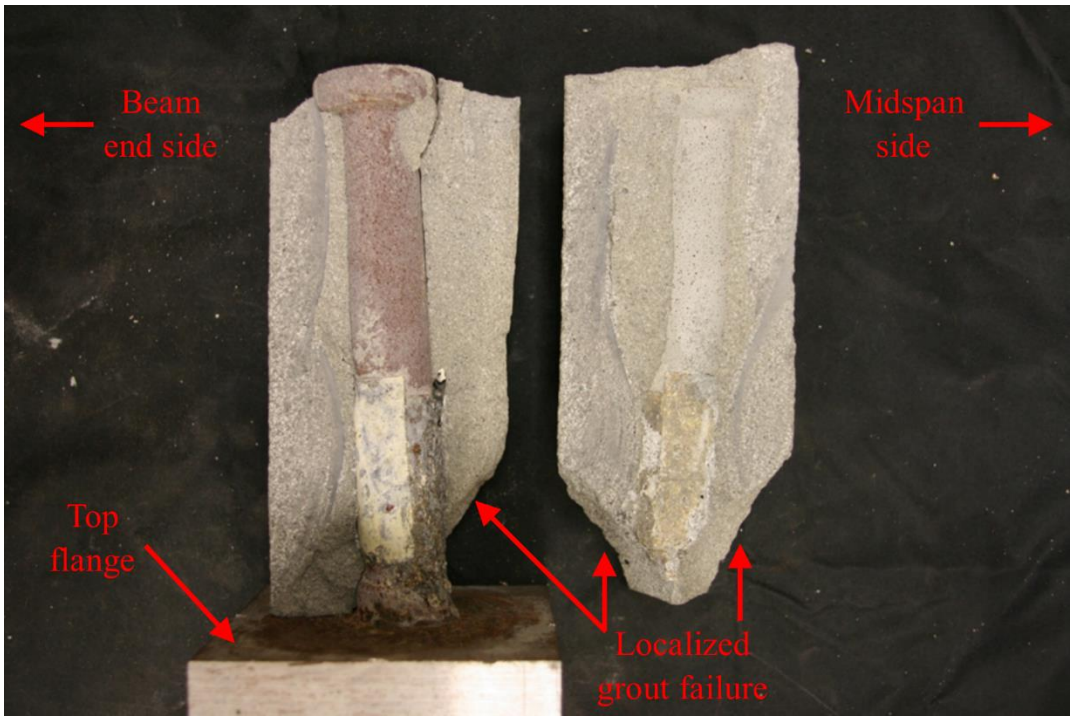

Source: FHWA.

Figure 41. Photo. Typical large-scale fatigue test core showing shear failure in grout.

In figure 41, it is clear that the grout crushed locally near the base of the shear stud since no large pieces were retained in that area. This is evident by the diagonal fracture plane on both the midspan and beam-end side of the shear stud. These localized grout failures were common among the intact shear studs. In some cases, the localized grout failures occurred only on the beam-end side, only on the midspan side, or, as shown in the photo, on both sides of the shear stud. The beam-end side and the midspan side of the same grout core are shown in figure 42 and figure 43, respectively. For both of these photos, the two halves of the grout core were placed together to clearly show the entire core.

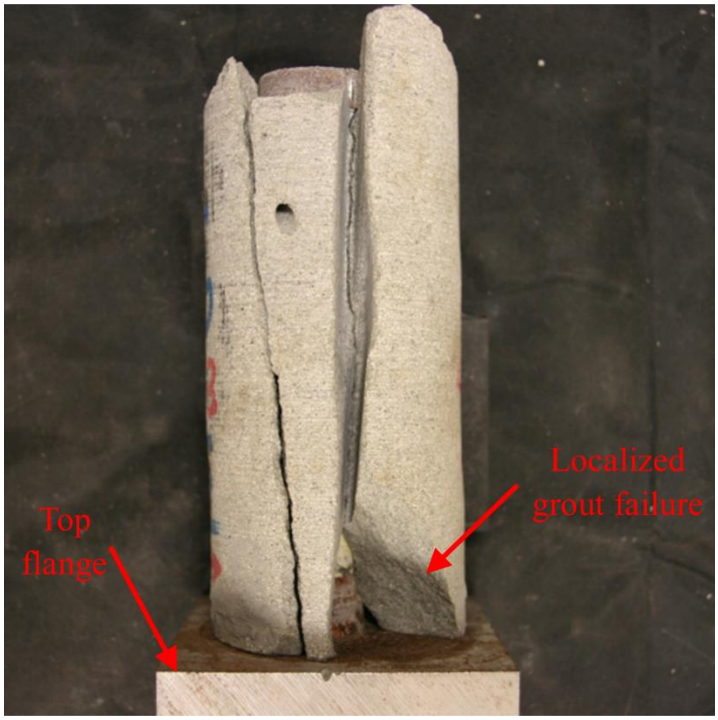

Source: FHWA.

Figure 42. Photo. Typical shear failure in grout on beam-end side of shear stud in large-scale fatigue test.

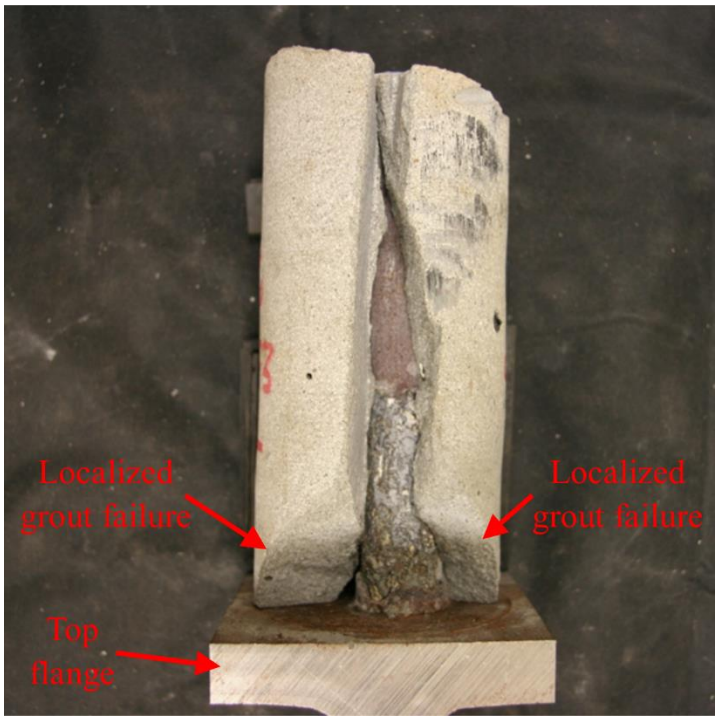

Source: FHWA.

Figure 43. Photo. Typical shear failure in grout on midspan side of shear stud in large-scale fatigue test.

Strain Gauge and LVDT Results

During the fatigue loading of each large-scale beam test, the team recorded strain gauge measurements intermittently throughout the testing process. These measurements were used to determine the location of the neutral axis (NA) at various cross sections over the fatigue life of each test. The location of the NA could then be used as a measure of fatigue damage sustained in the shear studs. When shear studs are completely intact, the steel beam and concrete deck should act as one composite section; thus, the measured location of the NA should be similar to the theoretical composite section NA. Once the shear studs have completely failed from fatigue, the location of the NA measured in the steel beam should be similar to the theoretical NA of the bare steel beam. Since the NA plots are based on a curve fit of numerous strain gauges mounted to both the beam and deck, they can be subject to variation based on errant readings from a particular gauge. Therefore, the NA plots should only be inspected from a high level, and the reader should not focus on local aberrations of the NA depth. The point of the NA plots is merely to observe when the NA plateaus to a depth approximately that of the steel beam itself.

Figure 44 shows a plot of the NA versus the number of cycles for beam 1F1. The location of the NA was measured from the bottom of the bottom flange of the steel beam. It is shown for three different cross sections along the length of the beam: W4, which is on the west shear span nearest to the west load point; M, which is at the midspan; and E4, which is on the east shear span nearest to the east load point. For reference, the plot includes dashed lines to show the location of the NAs for the bare steel beam and the composite section. Included in the figure is a diagram of beam 1F1 to illustrate the locations of the cross sections where the NAs were determined from the strain gauge data.

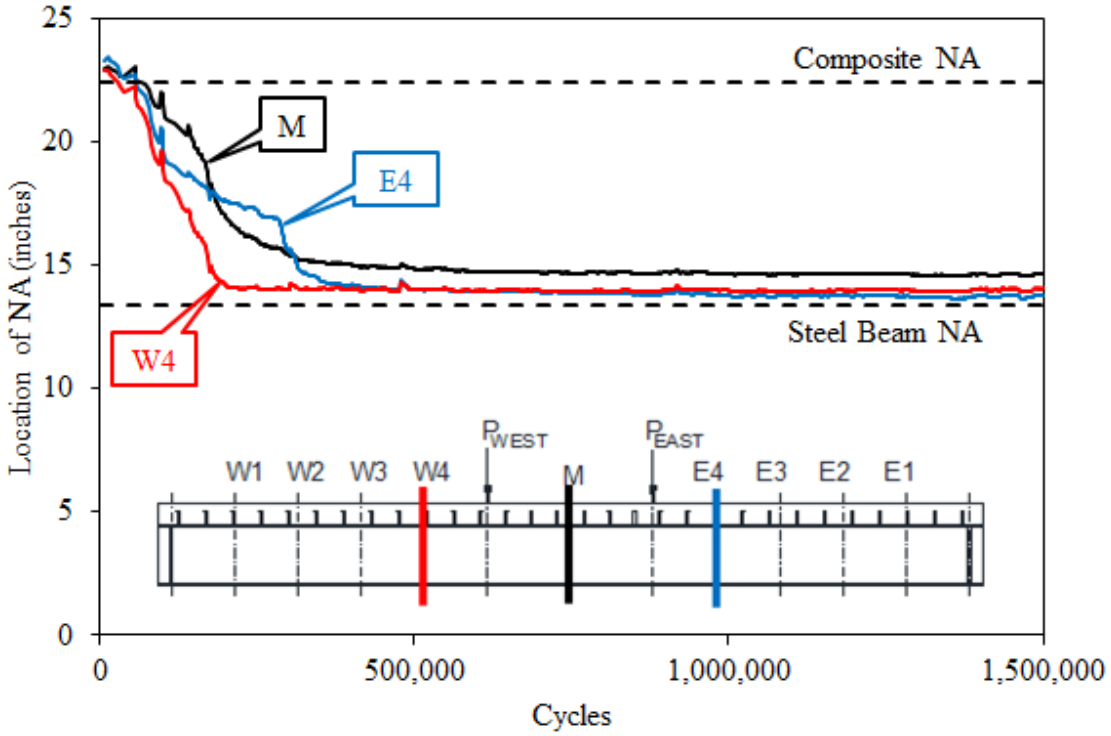

Source: FHWA.

Figure 44. Graph. Location of NA for both shear spans of 1F1.

In figure 44, the NA for all three sections began approximately at the composite section NA. As the beam was loaded and fatigue damage accumulated, the location of the NA dropped down into the steel beam for each section. This happened faster for section W4. In this cross section, the NA leveled off and reached the steel beam NA at approximately 200,000 cycles. This shows that composite action was completely lost for this section at this point in time. The NA in section E4 behaved somewhat similarly. The drop in the NA began gradually but became more sudden at approximately 275,000 cycles until leveling off and reaching the steel beam NA at 400,000 cycles. This clearly illustrates that the west shear span lost composite action before the east shear span. To examine the west shear span more closely, figure 45 shows the location of the NA for all four sections in just the west shear span.

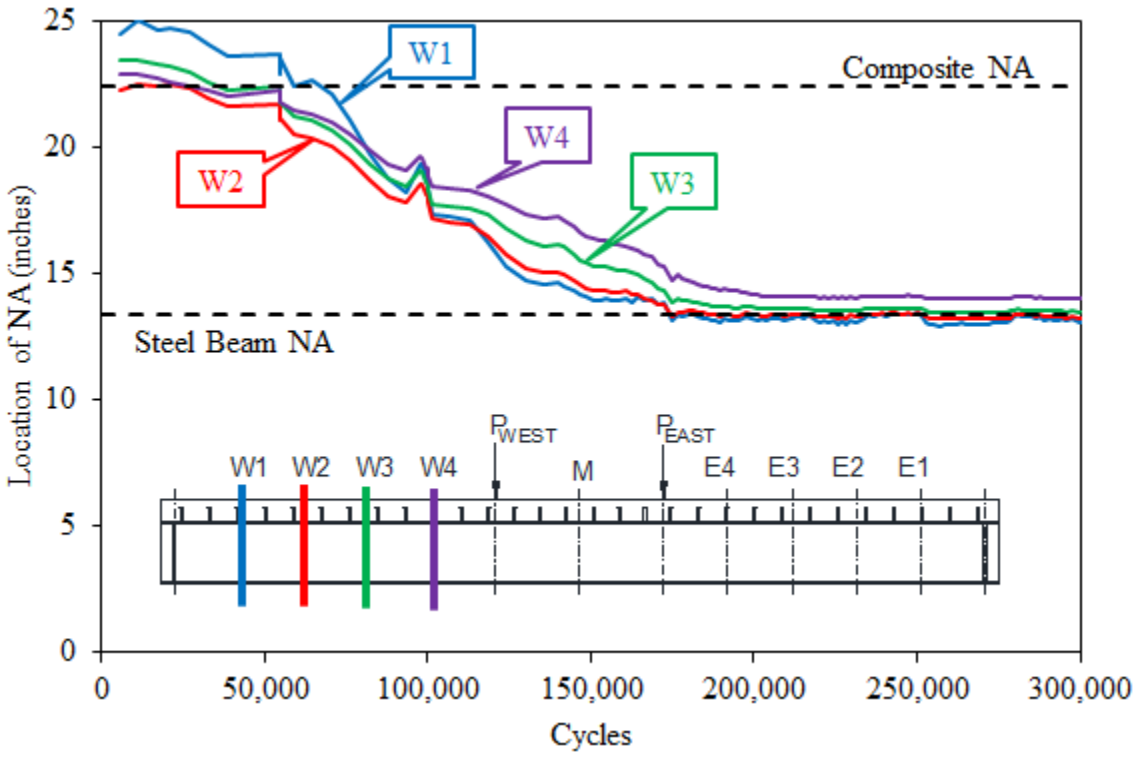

Source: FHWA.

Figure 45. Graph. Location of NA for west shear span of 1F1.

This plot shows that the locations of all the NAs in the west span cross sections follow a similar trend. All sections began with their NAs near the composite section, and then they decreased until gradually leveling off at the steel beam NA. The NA of section W1 began slightly above the composite NA; since that section is nearest to the west end of the beam, this is probably because of the smaller stresses in that section. One notable observation is the rate at which the NA in each section drops seemed to increase from the west end of the beam to the west load point. From approximately 50,000 to 175,000 cycles, the W1 NA plot experienced a faster drop than the other sections with its NA reaching the steel beam NA prior to any of the other west span sections. In examining all the sections, it appears that composite action was lost at a faster rate for sections closer to the end of the beam. This is a reasonable trend since the shear studs closer to the end of the beam resist a larger horizontal slip to maintain compatibility than those closer to

midspan. However, all sections within the entire shear span seemed to reach a point of noncomposite action at approximately the same cycle count.

The research team developed a failure definition for the fatigue tests based on the strain gauge data and the location of the NA. A beam has reached failure when one or more of the cross sections experience a complete loss of composite action. In examining figure 45, beam 1F1 reached failure at 175,000 cycles since this is when the NA for sections W1 and W2 reached the steel beam NA. Since beam 1F1 was the first beam subject to fatigue testing, the definition of failure had not yet been developed when the beam was tested. This is why figure 44 shows that the beam was cycled for 1.5 million cycles when the test data showed that the beam failed at 175,000 cycles. Subsequent testing showed that the failure definition agreed with the physical observations that the concrete deck had separated from the steel beam. The authors of this report have also discussed the development of this failure definition and testing results in previous publications.[32,33]

This definition of failure is similar to that used in prior research of large-scale tests to evaluate shear stud fatigue. Toprac defined failure as the point at which the rate of loss in composite action increases considerably.[6] That definition of failure is similar to the one proposed in this study since the rate at which composite action is lost remains fairly constant until failure occurs. Although the definition of failure presented in this study has some subjectivity, the authors believe it is a much less subjective definition than trying to estimate when a rate of loss of composite action increases "considerably."

In addition to the location of the NA, the relative slip between the concrete deck and the steel beam can show an accumulation of fatigue damage in the shear studs. Figure 46 shows the relative horizontal slip of the deck and steel beam (measured with LVDTs) versus the number of cycles for specimen 1F1. Positive slip in a section refers to movement of the concrete slab in a direction toward the end of the beam. The slip at two cross sections is shown in this figure: E1 is near the east end of the beam, and W1 is near the west end of the beam. The slip is shown for sections near the end of the beam since the horizontal slip is maximized near the beam ends. There was another section, W0, at the far west end of the beam, but figure 46 shows W1 because W1 and E1 are roughly equidistant from either end of the beam. Thus, W1 and E1 provide a more direct comparison of the slip in each shear span.

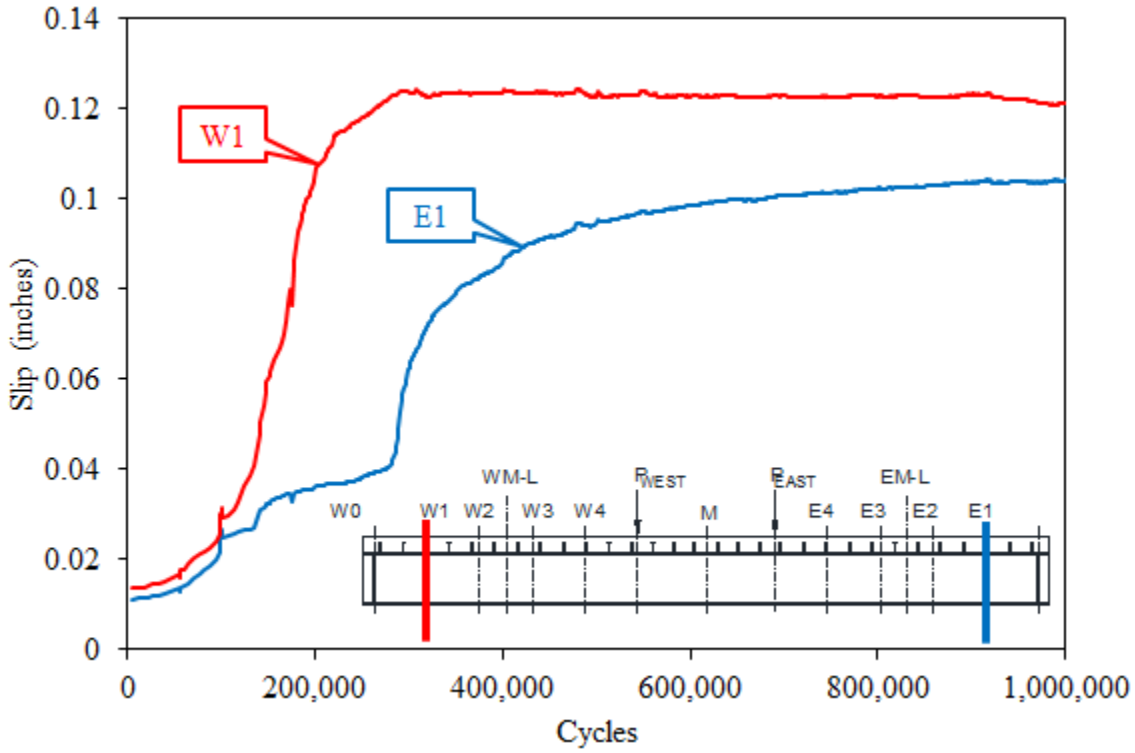

Source: FHWA.

Figure 46. Graph. Horizontal slip in both shear spans of 1F1.

In general, the slip behavior followed a similar trend to the NA data. The west shear span experienced slip that was far greater and increased at a much faster rate than the east shear span. The slip for the west shear span increased at a constant rate until leveling off at approximately 300,000 cycles. In comparing this figure with figure 44, the leveling off of the slip came at a later point in the fatigue loading than the leveling off of the NA, which occurred at approximately 200,000 cycles.

The east shear span also experienced a gradual increase in slip until approximately 300,000 cycles, when the rate of slip drastically increased before becoming more gradual and leveling off near 1 million cycles. This sudden change in the rate of slip increase at 300,000 cycles coincided with the west shear span slip leveling off, which suggests that some load originally applied to the west shear span was shed to the east shear span once the shear studs began to fail. The cycle count also coincided with the sudden change in the rate of NA shown in figure 44. Since it was also clear from the slip data that the west span lost composite action first, figure 47 shows the horizontal slip for all of the cross sections on the west shear span.

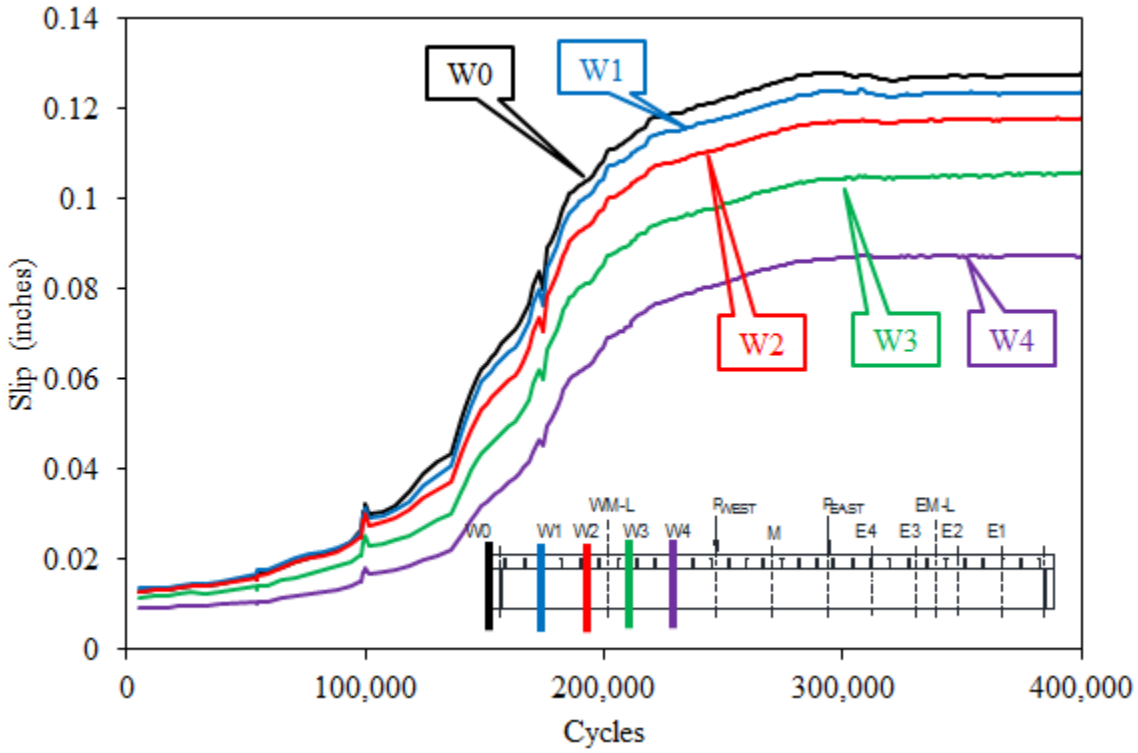

Source: FHWA.

Figure 47. Graph. Horizontal slip in west shear span of 1F1.

When examining figure 47, it is clear that the slip in all five cross sections follows the same general trend: continuously increasing until leveling off at approximately 300,000 cycles. The plots in the graph also indicate that fatigue was uniform throughout the shear span because all sections have approximately the same slope. The slip leveled off at a later point in time than the NA did in figure 45, which occurred at 175,000 cycles. This confirms that while an increase in slip can indicate a decrease in composite action, the qualitative slip behavior cannot be used to determine whether the shear studs failed in fatigue. It is likely that the slip continued to increase after the studs failed because of continued crushing of the grout surrounding the studs. The slip then stabilized once the fatigue loading was no longer driving additional grout crushing.

Figure 48 shows a similar plot but contains the uplift LVDT data from the midpoint of each shear span. EM-L represents the uplift at the midspan of the east shear span, while WM-L represents the same for the west shear span. Positive values indicate an upward displacement of the concrete deck relative to the steel beam.

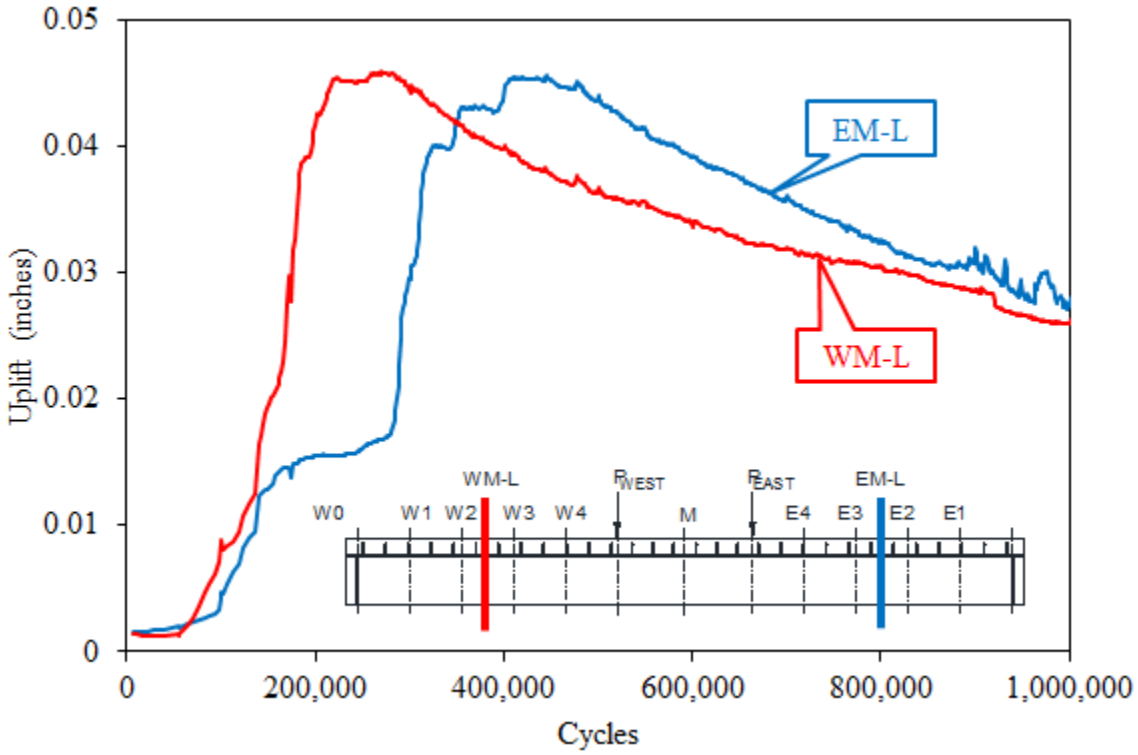

Source: FHWA.

Figure 48. Graph. Vertical uplift in both shear spans of 1F1.

Like with slip and NA data for beam 1F1, the uplift data show that the west shear span experienced more damage before the east shear span. The west shear span uplift reached a maximum value at approximately 250,000 cycles and then gradually decreased for the remainder of loading. Once the uplift in the west shear span reached a maximum value, the uplift in the east shear span began to increase at a much more drastic rate before reaching its maximum value at approximately 425,000 cycles. From that point forward, the uplift decreased gradually in a similar fashion to the west shear span. The uplift probably continued to decrease throughout testing because the grout in the haunch was wearing down as it slid back and forth over the top flange. Similar to the slip behavior, the uplift response indicates a measure of composite action in the beam, but once again, the location of the NA provides a better correlation to the physical failure of the studs.

Overall, the NA, slip, and uplift response for the other beams exhibited relatively similar behavior to that presented for beam 1F1. To provide a comparison between the minimum and maximum shear stud–cluster spacing, data from beam 4F1 are also presented. This beam was selected since both beams 1F1 and 4F1 were tested under a 20-ksi stress range. Figure 49 shows the location of the NA for one section at the midspan and one section on each shear span.

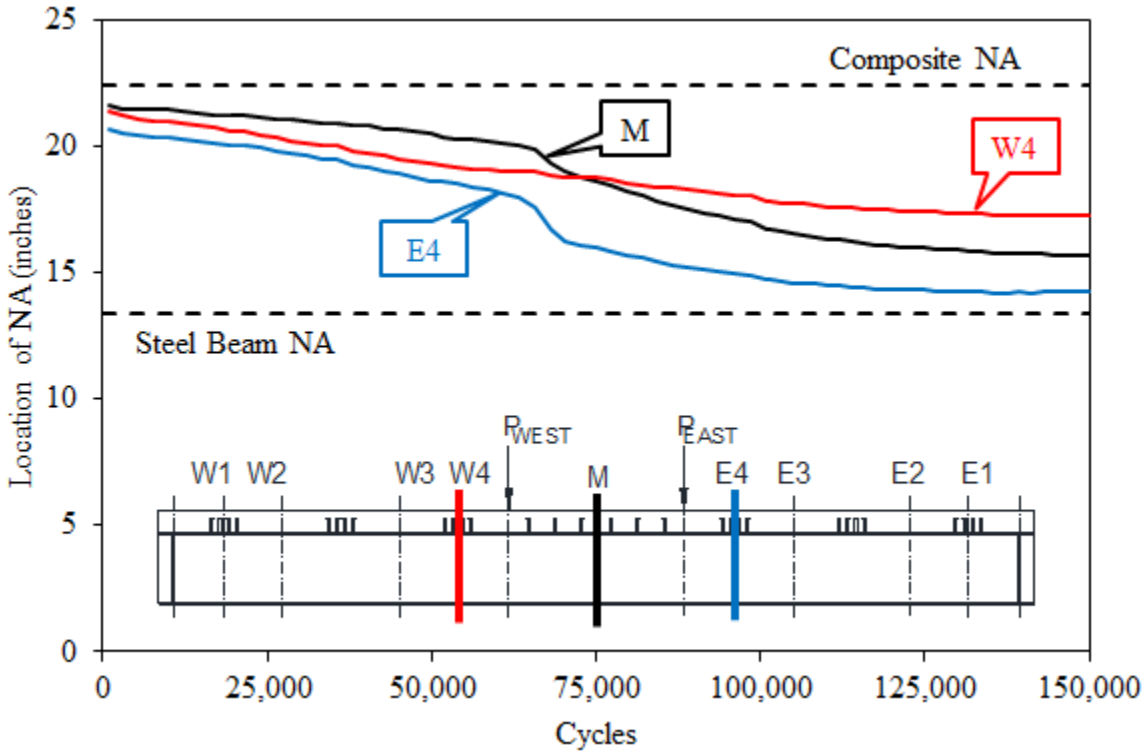

Source: FHWA.

Figure 49. Graph. Location of NA for both shear spans of 4F1.

Similar to figure 44, all three cross sections gradually lost composite action from the start of the fatigue loading. After approximately 60,000 cycles, the NA began to drop more rapidly in the east shear span than in the other two sections. At approximately 120,000 cycles, the location of the E4 section began to level out at a value similar to the steel beam NA. Sections M and W4 leveled out at approximately 135,000 cycles. Since it is clear from these data that the east shear span failed first, figure 50 shows all four cross sections in the east shear span.

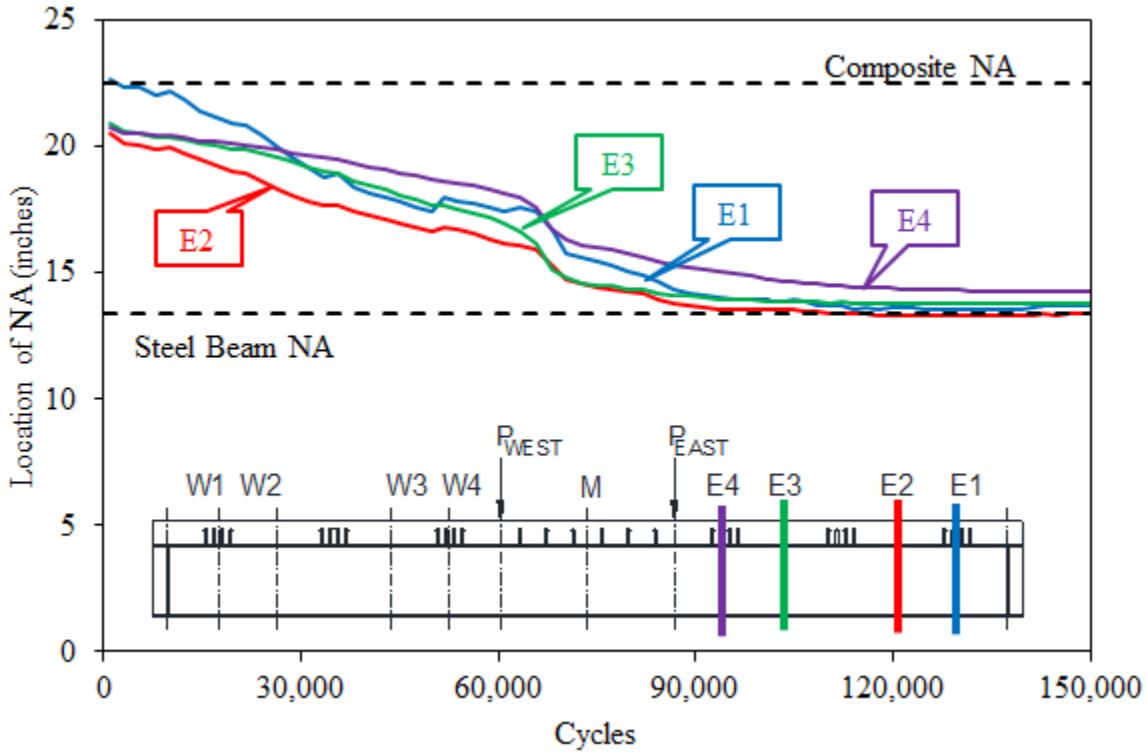

Source: FHWA.

Figure 50. Graph. Location of NA for east shear span of 4F1.

Similar to previous plots, this figure shows that sections closer to the end of the beam lose composite action at a faster rate than sections closer to midspan. It is also interesting to note that although beam 4F1 had a much greater shear stud–cluster spacing (4 ft) than beam 1F1 (1 ft), the NA behavior between the beams was not significantly different. That is, the extended shear stud–cluster spacing did not seem to affect the fatigue performance of the shear studs. The effect of the shear stud clusters can also be examined by comparing the NA behavior of similarly located cross sections, one of which is located within a shear stud cluster (e.g., E1) and one that is located between clusters (e.g., E2). When E1 and E2 are compared, the two sections appear to behave in a similar fashion. Although section E2 was located halfway between shear stud clusters, the section still experienced a loss of composite action as though there were shear studs at that location. This shows that there was no significant effect on the fatigue performance of clustering shear studs at spacings beyond 24 inches. All of the sections of beam 4F1 reached a point of no composite action at a cycle count of approximately 91,000 cycles. This is considered the point at which beam 4F1 failed in fatigue according to this study's definition of failure.

Figure 51 shows the horizontal slip behavior of beam 4F1. The east shear span sustained the most horizontal slip damage on the beam. Both shear spans experienced minimal slip damage until approximately 60,000 cycles. At this point, the slip damage in the east shear span increased rapidly until the beam eventually failed. As the damage began to increase in the east shear span, the slip in the west shear span remained relatively constant. The slip in the west shear span did not increase after the east shear span failed, because the test was stopped.

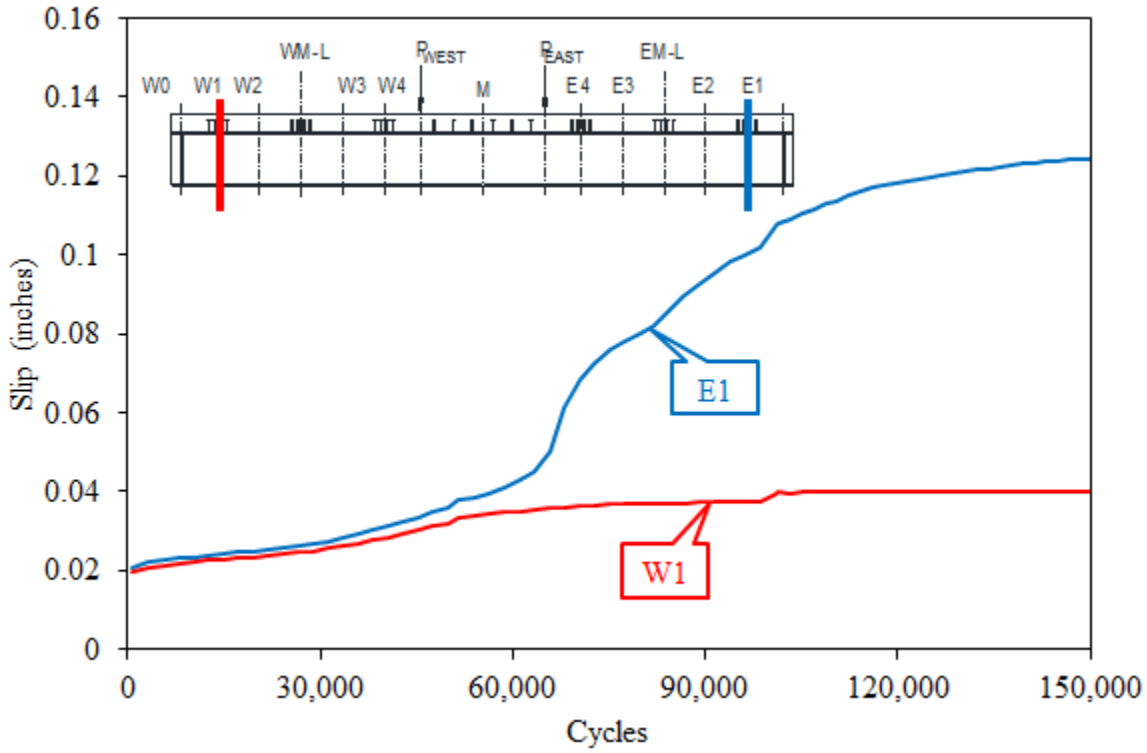

Source: FHWA.

Figure 51. Graph. Horizontal slip in both shear spans of 4F1.

Since it was clear that the east shear span experienced the most slip damage, figure 52 shows the horizontal slip in each of the instrumented sections in the east shear span. As expected, sections closer to the end of the beam experienced more slip damage than those closer to midspan. There was no apparent difference in the slip behavior of the failing shear span between this beam and beam 1F1 (shown in figure 47). This provides evidence that the extended shear stud–cluster spacing of 48 inches did not have a significant impact on the fatigue slip behavior.

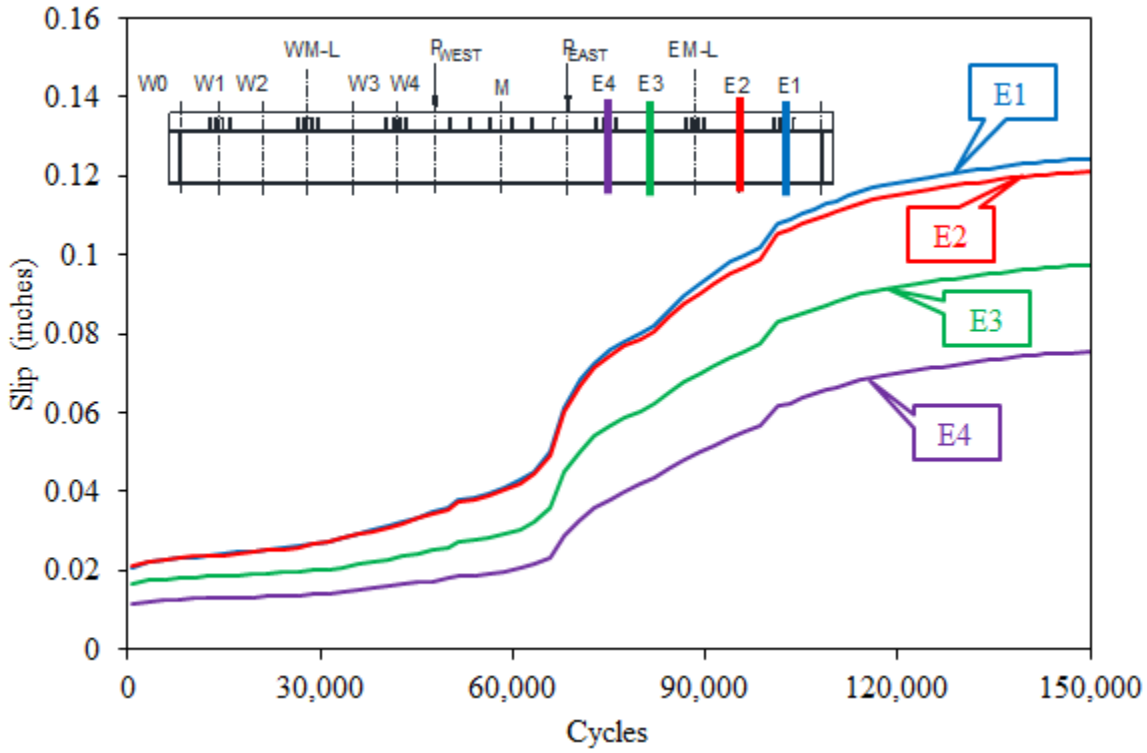

Source: FHWA.

Figure 52. Graph. Horizontal slip in east shear span of 4F1.

Figure 53 shows the uplift behavior in both shear spans of beam 4F1. Similar to figure 49 through figure 51, it is clear that the east shear span sustained the most damage. Both shear spans sustained minor uplift damage until about 50,000 cycles, but at this point, the uplift in the east shear span increased at a much greater rate. The uplift in the east shear span reached a maximum value at approximately 105,000 cycles, which was after the point of failure according to the NA data. As with the NA and slip behavior, there are no signs that the extended shear stud spacing in this beam had an effect on the fatigue uplift behavior.

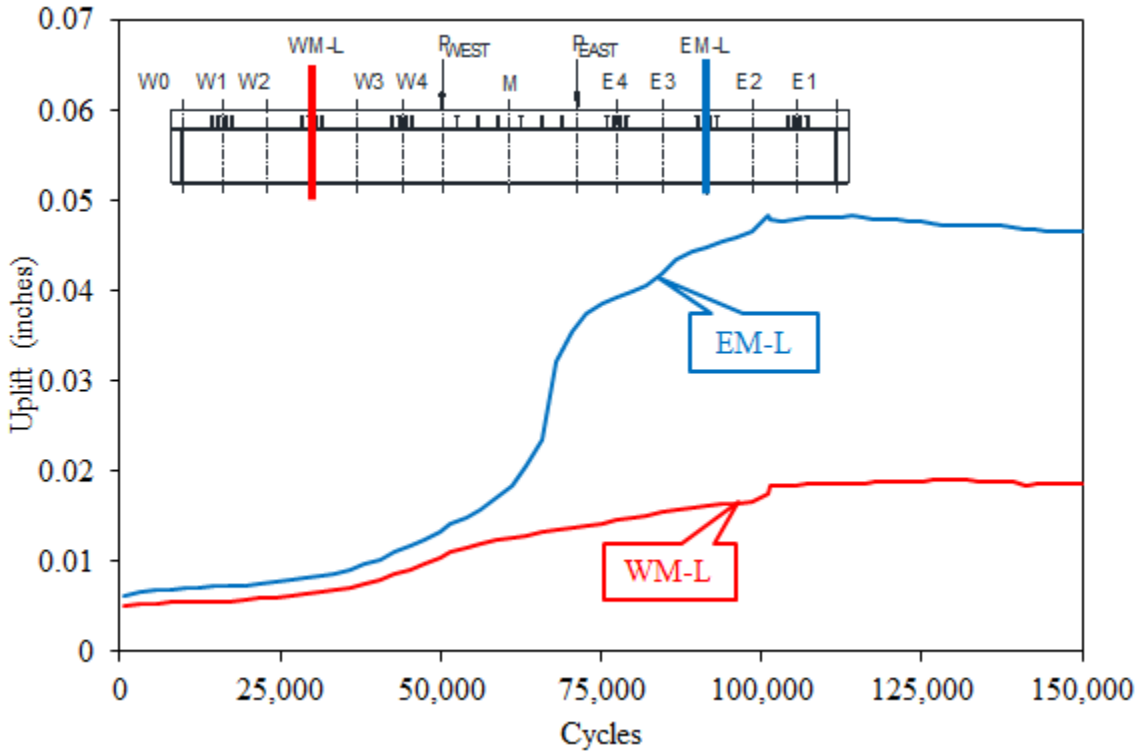

Source: FHWA.

Figure 53. Graph. Vertical uplift in both shear spans of 4F1.

All of the beams showed similar NA, slip, and uplift behavior to beams 1F1 and 4F1. Data for the remaining beams can be found in appendix C. All beams were considered failed in fatigue when at least one of the cross sections experienced a complete loss of composite action according to the location of the NA. There was no apparent difference in the behavior of the beams with the extended shear stud–cluster spacings of 36 and 48 inches.

One of the concerns for composite beams with extended shear stud spacings is the potential for an increase in the initial relative uplift between the steel girder and concrete deck panel owing to the greater distance between shear studs. This increased initial uplift could provide an opening for moisture or salt to penetrate between the girder and concrete deck and thus accelerate corrosion. However, when comparing the initial uplift values, all of the large-scale fatigue tests, regardless of shear stud–cluster spacing, had initial uplift values less than 0.01 inch. At an opening of such small magnitude, no accelerated corrosion would be expected to occur.

Laser Tracker Slip Results

During the large-scale fatigue tests, loading was paused at predetermined cycle counts to record displacement data using the laser tracker system. The team recorded data at discrete points on the side of the top flange and haunch every 6 inches along the length of each beam. Researchers determined the relative slip and uplift between the haunch and top flange by resolving the displacement data along two axes: one along the length of the beam for slip and one oriented orthogonal to the length of the beam for uplift. The slip data from selected large-scale fatigue tests beams are presented in this subsection.

Figure 54 shows the laser tracker slip data along the length of beam 1F1. The vertical axis shows the relative slip between the haunch and top flange of the beam. The horizontal axis shows the length of the beam starting from the east end. Slip data were typically recorded every 100,000 cycles, and data from notable cycle counts are shown in the figure. Positive values indicate that slip occurred in a direction moving away from midspan and toward each respective end of the beam. The shear stud clusters are shown in the figure as vertical lines in each shear span. Both load points and the midspan of the beam are also noted in the figure.

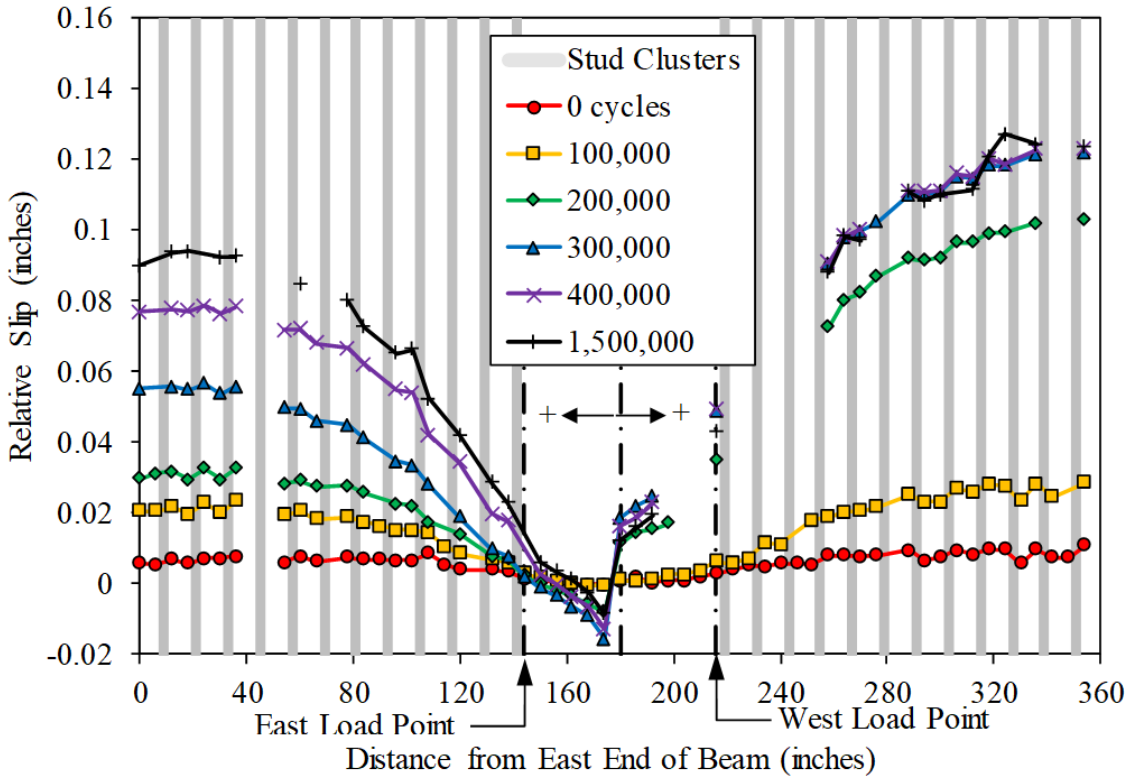

Source: FHWA.

Figure 54. Graph. Laser tracker slip results for beam 1F1.

It is clear that there are a large number of data points missing since data should have been collected every 6 inches along the length of the beam. Faulty installation of the spacers mounted to the side of the top flange of the beam caused many of the spacers to fall off during testing. The installation procedure was improved for later tests, which resulted in much better adhesion of the spacers to the top flange, as shown in graphs for other beams in appendix D.

Figure 54 shows that a significant amount of damage occurred in the west shear span between 100,000 and 200,000 cycles. Between the recorded measurements at these two cycle counts, the slip increased significantly. This corresponds well with the failure definition, which determined that beam 1F1 failed at 175,000 cycles on the west shear span. It is also noteworthy that the slip seemed to remain relatively constant in the west shear span after approximately 300,000 cycles, which shows very close agreement with the LVDT data for beam 1F1 shown in figure 46 and figure 47.

From all of the measurements taken at 200,000 cycles and after, figure 54 shows negative slip values between the centerline of the beam and the east load point. These values are negative because the west shear span failed before the east shear span. After the studs in the west shear span failed in fatigue, shear stresses were distributed to the studs in the constant-moment region on the east side of the beam. The negative slip values in this region show that the studs experienced a horizontal slip toward the west end of the beam.

In general, the plots in figure 54 all increase from the load point to the end of the beam in each shear span and have a smooth concave shape. This smooth behavior contrasts with that seen in figure 55, which shows the laser tracker slip measurements taken from beam 4F1; that beam was also tested at a 20-ksi stress range but had a 48-inch shear stud–cluster spacing.

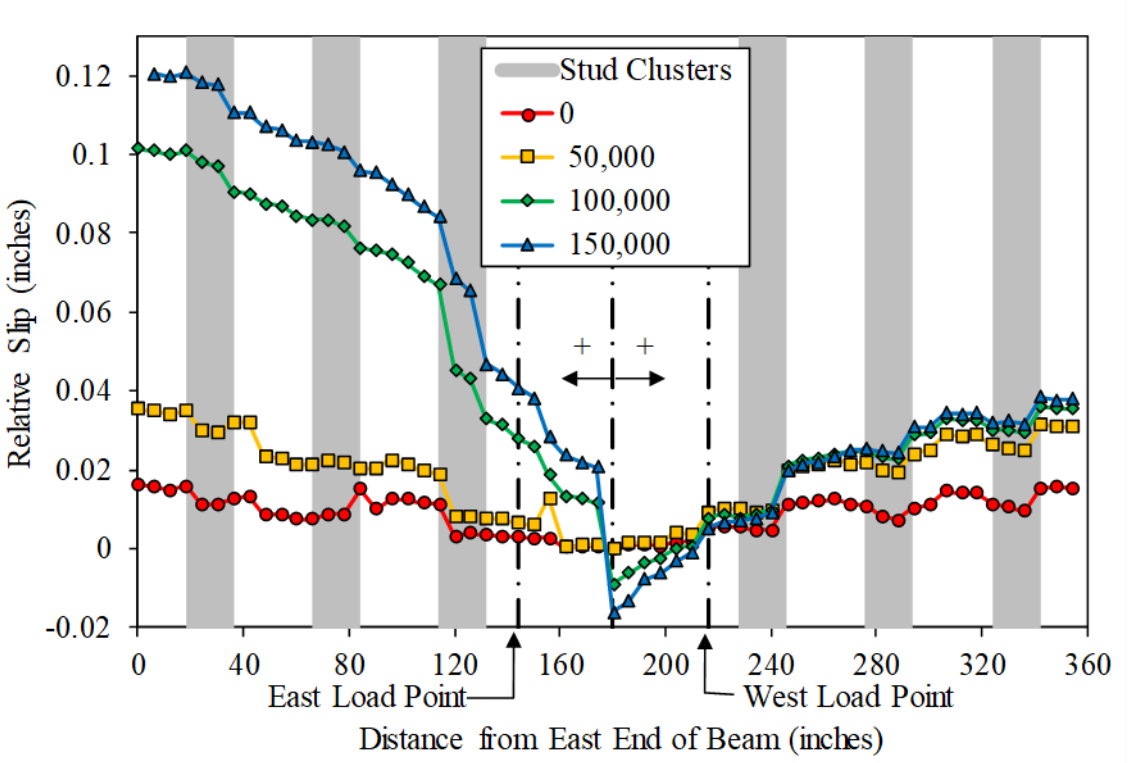

Source: FHWA.

Figure 55. Graph. Laser tracker slip results for beam 4F1.

In the figure, the horizontal slip increased significantly between 50,000 and 100,000 cycles. This agrees with the failure definition, which determined that the west shear span of this beam failed at 91,000 cycles. For the east shear span, the slip plots exhibit a concave shape but, rather than the gradual behavior seen in beam 1F1, beam 4F1 shows slip increasing in steps. In general, at any particular cycle count, the slip remained relatively constant between the shear stud clusters but increased suddenly on the beam-end side of each shear stud cluster within the west shear span. This behavior suggests that some shear lag occurred within each shear stud cluster; this is reasonable since the shear stud closest to the beam end within each cluster would be expected to carry slightly more horizontal shear load.

This stairlike slip behavior was generally present in each of the 36- and 48-inch spacing beams, while the 12- and 24-inch spacing beams exhibited the more continuous behavior shown in figure 54. Although this shear lag was observed in the shear stud clusters with extended spacings, it did not appear to have a negative effect. When comparing the various shear stud–cluster spacings, there were no noticeable differences in the overall fatigue performance of the beams.

Of the 12 large-scale fatigue tests, 2 were considered runouts. Figure 56 shows the slip results of one of these runouts, beam 4F2. In the figure, during the 25 million cycles, there was no significant increase in the horizontal slip between any two cycle counts. The slip damage appeared to occur at a relatively slow rate, especially after 7 million cycles.

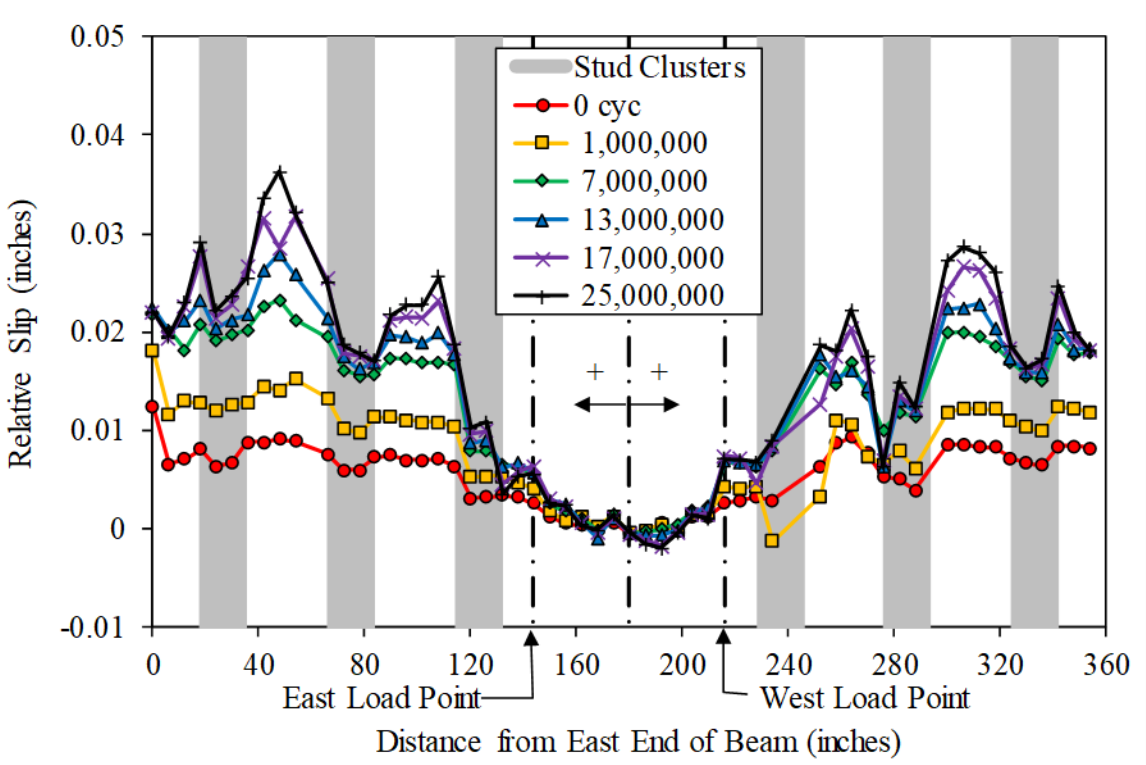

Source: FHWA.

Figure 56. Graph. Laser tracker slip results for beam 4F3.

One interesting feature to note is the shape of the slip plots. Some local peaks of slip damage are present between the shear stud clusters. This is expected behavior since the studs act to maintain horizontal compatibility between the deck and beam. Some of this behavior is also attributable to the larger spacing between the shear stud clusters. The local peaks of slip damage were also present in the other runout beam, 2F3. For beam 2F3, the local peaks were not generally as pronounced as those seen in 4F3, because of the smaller shear stud spacing of 24 inches.

The remaining beams showed similar behavior to those discussed previously in this subsection. The beams that experienced fatigue failure showed a significant increase in slip for the failed shear span at approximately the same cycle count determined using the failure definition. The slip smoothly increased from a load point to one end of the beam for the smaller shear stud

spacings of 12 and 24 inches, while the increase was more stairlike for the 36- and 48-inch spacing beams. For the runout tests, slip damage was more pronounced between the shear stud clusters, resulting in local peaks of damage. Overall, the laser tracker slip data provided good agreement with the LVDT data. Laser tracker slip plots for all of the remaining beams are shown in appendix D.

Laser Tracker Uplift Results

As with the slip data, researchers also used the laser tracker laser system to measure and plot uplift data. In these plots, the vertical axis represents uplift, with positive values indicating separation of the concrete deck away from the steel beam. Figure 57 shows the uplift behavior for beam 1F1.

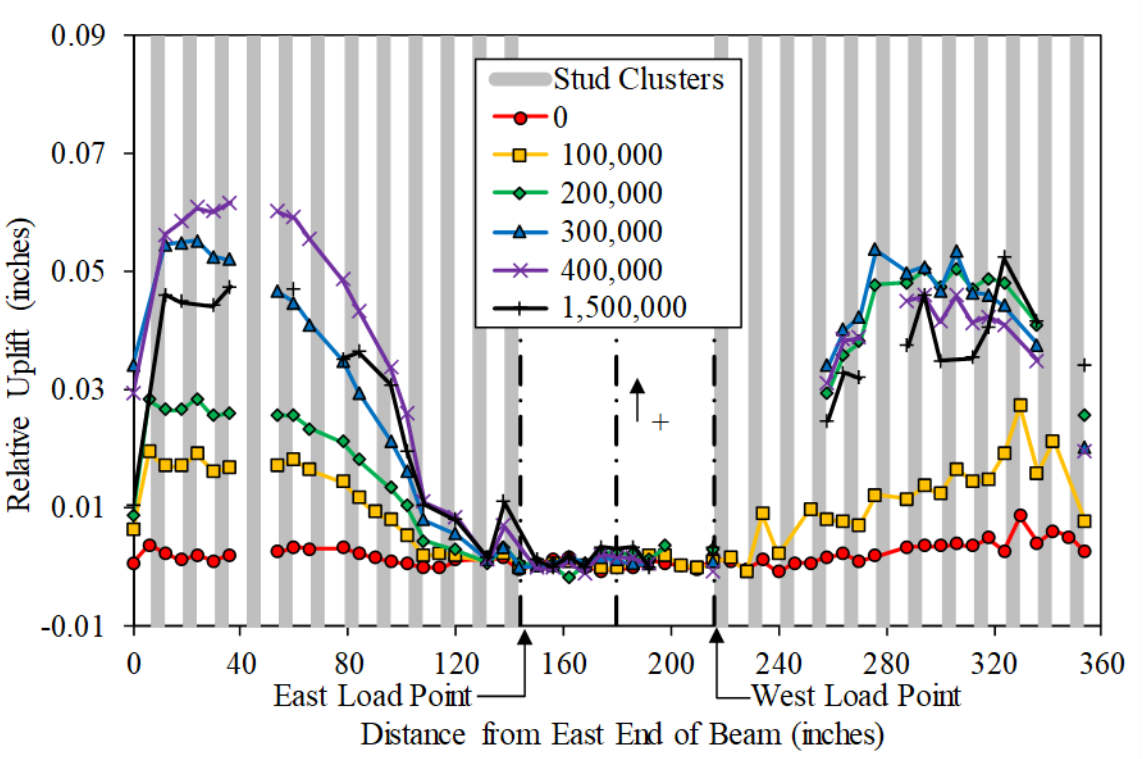

Source: FHWA.

Figure 57. Graph. Laser tracker uplift results for beam 1F1.

The figure shows a significant increase in the uplift in the west shear span between 100,000 and 200,000 cycles; this matches the failure definition, which considered the west shear span failed in fatigue at 175,000 cycles. From that point on, the uplift remained relatively constant until it began to decrease at 300,000 cycles. That behavior also matches the LVDT uplift data presented in figure 48.

The east shear span provides some insight into the overall uplift behavior. In general, uplift increased somewhat steadily going from the load points to the ends of the beam. It reached a maximum value at a length approximately one-quarter of the shear span away from the end of the beam. From this point, the uplift decreased until it reached a value of approximately 0 at the

end of the beam. This behavior indicates the deck was arching upward over the steel beam along the shear spans. This arching behavior was generally present in all of the beams but was more uniform in the 12- and 24-inch spacing beams. To show the behavior of a beam with larger shear stud–cluster spacing, figure 58 shows the uplift for beam 4F1.

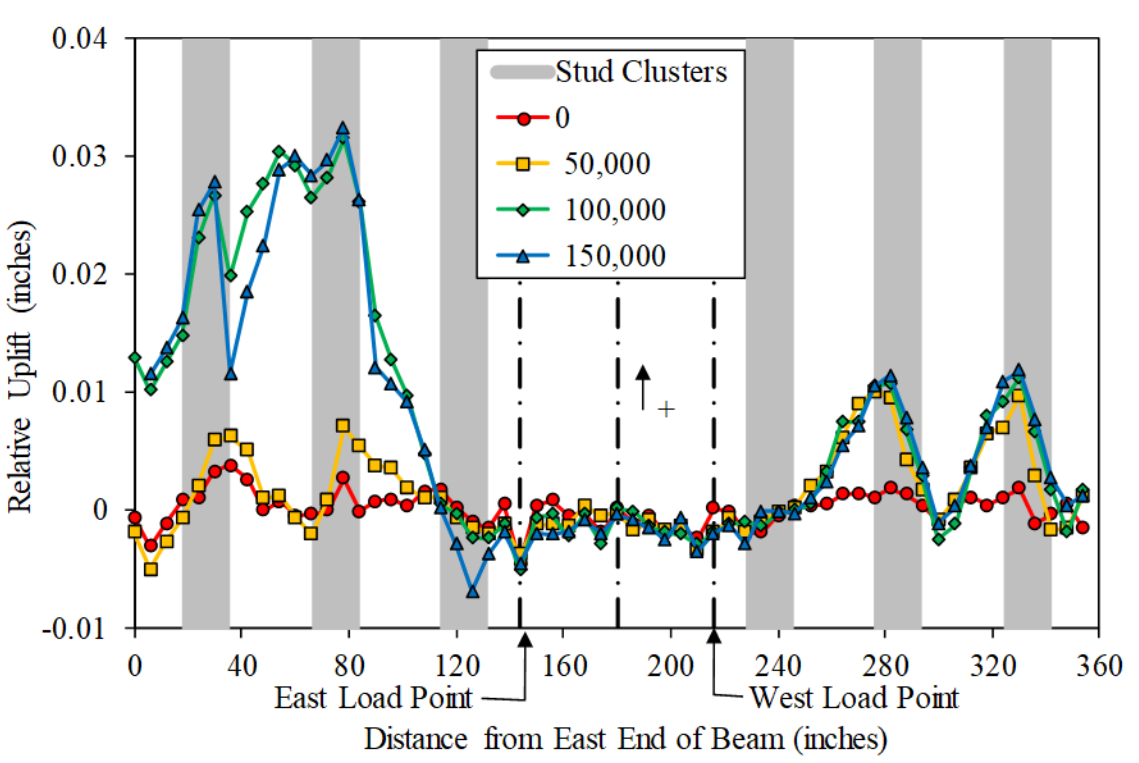

Source: FHWA.

Figure 58. Graph. Laser tracker uplift results for beam 4F1.

This figure shows that a significant increase in uplift was observed in the east shear span between 50,000 and 100,000 cycles. This agrees with the proposed failure definition, which determined this shear span failed at 91,000 cycles. Note that some negative uplift values were observed in this beam test and in most of the other tests, likely because of degradation of the grout during fatigue loading. There was still an overall arching upward in the east shear span, maximizing at approximately the midpoint of the shear span. It is also interesting to note the effect of the extended spacing of shear stud clusters in the west shear span. Here, local peaks of uplift damage can be seen on the midspan side of the two westernmost shear stud clusters. On the beam-end side of these two shear stud clusters, the uplift returned to approximately 0. This occurred because the shear studs were attempting to maintain vertical compatibility between the deck and beam. These local peaks of uplift were generally observed in the extended spacing clusters of 36 and 48 inches.

To illustrate the uplift behavior of a runout large-scale test, figure 59 shows the results from beam 4F3. This beam did not sustain any significant increases in uplift like those in beams that failed in fatigue. The arch shape of the uplift is barely apparent, and uplift increases from the midspan to the end of the beam with localized peaks in the middle of the shear stud clusters.

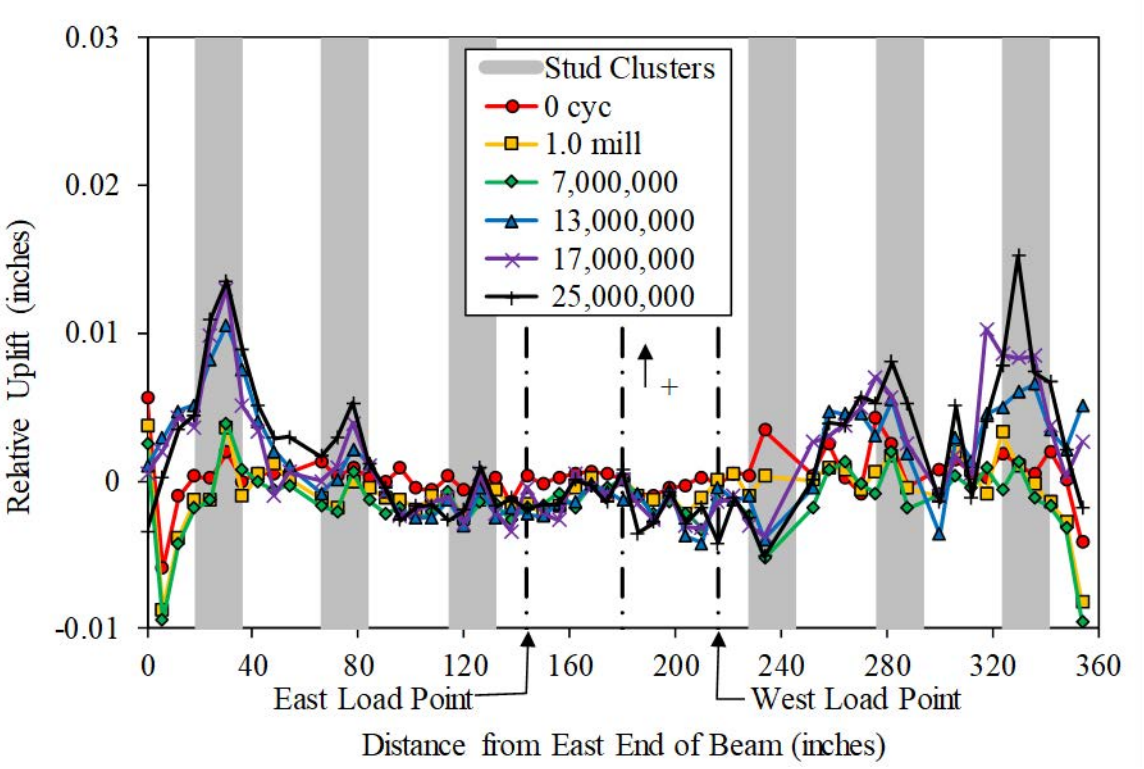

Source: FHWA.

Figure 59. Graph. Laser tracker uplift results for beam 4F3.

The uplift behavior presented in this section is characteristic of the remaining large-scale fatigue tests. For the beams that failed in fatigue, a significant increase in uplift was present in the measurements taken before and after failure. On the beams that failed, the uplift typically reached a maximum value at approximately one-quarter to one-half the length of the shear span from the end of the beam. Uplift behavior varied smoothly for the closer shear stud–cluster spacings of 12 and 24 inches, while local peaks of uplift damage were seen in the larger spacings of 36 and 48 inches. Overall, the laser tracker uplift data provided good agreement with the LVDT data. Laser tracker uplift plots for all of the remaining beams are shown in appendix D.

S-N Results

Researchers used the failure definition based on NA data to determine a cycle count at failure for each large-scale beam. These values are shown in table 10, along with an indication of which shear span failed first. For beams 2F3 and 4F3, the fatigue loading was stopped at 25 million cycles, and the tests were considered runouts since neither beam had reached failure according to this study's definition. After loading was stopped on these two beams, the team removed the concrete slabs, but not the studs, from both of the beams. Although the shear studs were cracked, they had not yet been completely separated from the top flange. Pictures of these studs can be found in appendix E. It is unclear exactly why these cracked studs were able to continue providing composite behavior for 25 million cycles. It is speculated that the applied stress range was low enough, and that the formed cracks introduced enough compliance in the partially composite system that the stress intensity at the crack tips was below the threshold for

crack growth. Using the data in table 10, the researchers developed a S-N plot of the large-scale test data (figure 60).

Table 10. S-N results for large-scale fatigue tests.

Specimen	Shear Span Failed	Actuator Minimum Load (kips)	Actuator Maximum Load (kips)	Shear Stress Range (ksi)[a]	Cycles to Failure
1F1	West	8.4	41.9	20.0	175,000
1F2	East	8.4	35.2	16.0	130,000
1F3	East	8.4	28.5	12.0	2,800,000
2F1	West	8.4	41.9	20.0	174,000
2F2	East	8.4	35.2	16.0	260,000
2F3	[b]	8.4	28.5	12.0	25,000,000[b]
3F1	West	8.4	35.2	16.0	747,000
3F2	East	8.4	41.9	20.0	51,000
3F3	West	8.4	28.5	12.0	3,800,000
4F1	East	8.4	41.9	20.0	91,000
4F2	West	8.4	35.2	16.0	680,000
4F3	[b]	8.4	25.2	10.0	25,000,000[b]

[a]Calculated assuming uniform shear flow from bending through all studs in the shear span.
[b]Test was declared a runout without failing.

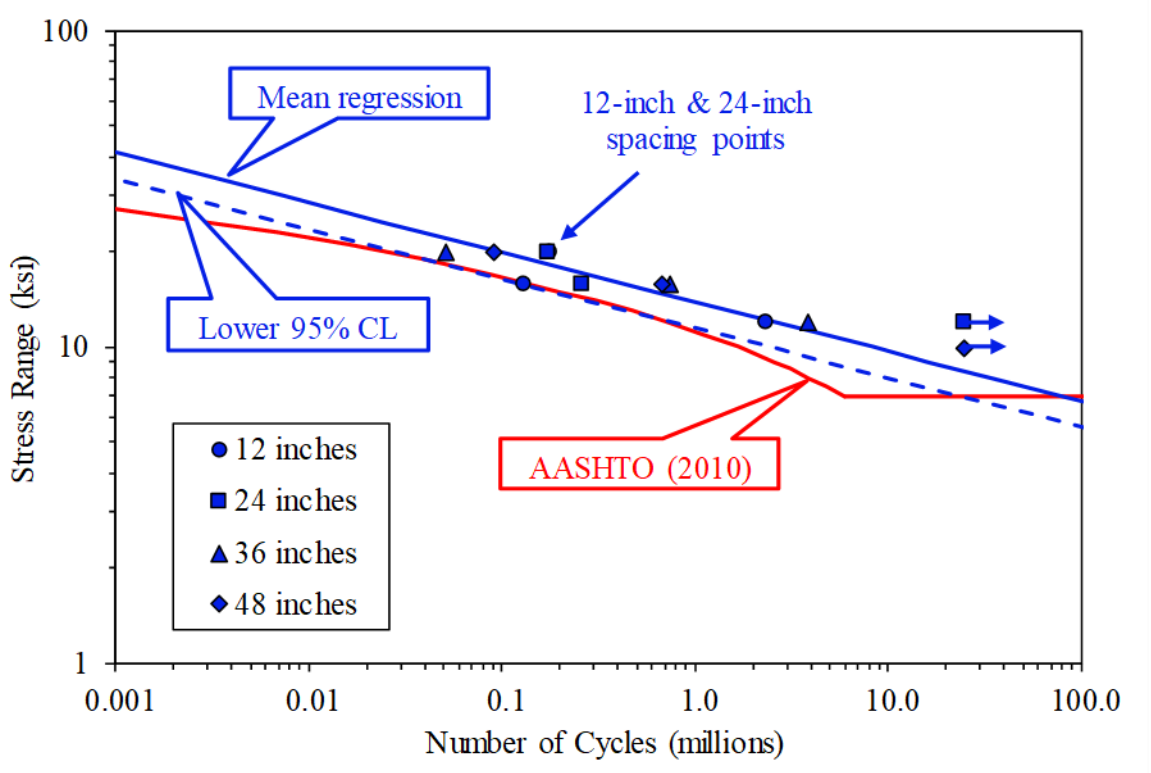

Source: FHWA.
CL = confidence limit.

Figure 60. Graph. S-N data for large-scale fatigue tests.

In addition to the large-scale test data, figure 60 also includes the AASHTO LRFD BDS shear stud–fatigue design curve.[(1)] In comparing the test data to the AASHTO shear stud–fatigue design curve, it is clear that all of the data points fall above the fatigue design curve. Researchers determined a mean regression by performing a linear regression of the test data (omitting runouts), which is also shown in the figure. The team chose a log-log line for this regression, rather than the semi-log shape of the current AASHTO provisions, for simplicity and to more closely match the shape of typical AASHTO categories. The lower 95 percent CL of the test data, which represents two standard deviations from the mean, is also shown in the graph. The lower 95 percent CL is represented by the equation in figure 61.

$$S_{r,\,LS,\,95} = \left(\frac{577{,}000 \times 10^8}{N}\right)^{\frac{1}{6.4}}$$

Figure 61. Equation. Equation of lower 95 percent CL through large-scale fatigue test data.

Where $S_{r,LS,95}$ is the shear stress range acting on studs for large-scale tests using a lower 95 percent CL (ksi).

The form of this equation also matches that of the AASHTO fatigue design equation. One notable difference between this equation and AASHTO is the slope of the fatigue design curve.

The typical fatigue design curve follows a slope of −3, whereas the slope of the lower 95 percent CL line is −6.4. This is because shear studs are loaded in a combination of shear and tension rather than pure tension as is the case for other fatigue details.

In figure 60, the lower 95 percent CL line follows the AASHTO shear stud–fatigue design curve very closely from approximately 10,000 to 2 million cycles. In this cycle range, the AASHTO equation appears to accurately represent the S-N test data. However, after 2 million cycles, the lines diverge because of the semi-log nature of the current AASHTO fatigue design curve and because the design provisions underestimate the fatigue life of the large-scale test specimens, especially at the CAFT of 7.0 ksi. This is especially notable since two tests were declared runouts at 25 million cycles (beam 2F3 cycled at a stress range of 12 ksi, and beam 4F3 cycled at 10 ksi).

Another clear observation from the S-N plot in figure 60 is a lack of correlation between the shear stud–cluster spacing and fatigue life. In particular, the extended shear stud–cluster spacings of 36 and 48 inches did not seem to have a negative impact on the shear studs' fatigue performance. If there was a difference, it fell within the typical scatter of fatigue data.

Summary of Large-Scale Fatigue Tests

A total of 12 large-scale fatigue tests were conducted with 4 different shear stud–cluster spacings: 12, 24, 36, and 48 inches. This study's failure definition considered a beam to have failed when it reached a complete loss of composite action, as indicated by the location of the NA in the steel beam. Using this definition of failure, researchers developed S-N data for the large-scale tests.

A regression analysis revealed that a log-log line with a slope of −6.4 (figure 60) represented the test data. The lower 95 percent CL of this regression line closely followed the AASHTO shear stud–fatigue design curve from approximately 10,000 to 2 million cycles. At cycle counts greater than this, the AASHTO provisions appear overly conservative compared to the test data because of the semi-log shape of the fatigue design curve. The extended spacing of shear stud clusters did not produce any negative effect on the fatigue performance of the large-scale beams tested.

Strain gauge, LVDT, and laser tracker test data indicated that, as expected, composite action was lost at a faster rate near the ends of the beams. However, the entire shear span seemed to reach a point of no composite action at approximately the same time. The laser tracker test data did illustrate that the extended shear stud–cluster spacings of 36 and 48 inches exhibited slightly different slip and uplift behavior than the closer shear stud spacings, and some shear lag was observed in these larger spacings. However, this slight difference in behavior did not affect the fatigue performance of the beams.

LARGE-SCALE STATIC TEST RESULTS

The following subsections detail the results of the large-scale static tests. Only data that resulted in relevant, meaningful findings are presented.

Visual Observations

After the large-scale static tests were complete, researchers visually examined the beams in their damaged states. This included examining the steel beam and identifying the failure mechanism. Figure 62 shows an overall photo of beam 3S1 after completion of the static test. Figure 63 shows a closeup view of the opposite side of beam 3S1. This view shows the grout and concrete crushing on one side of the grouted transverse joint and also shows the yield lines visible in the whitewash that was applied to the steel beam. Both photos represent typical observations seen in the large-scale static tests.

Source: FHWA.

Figure 62. Photo. Overall view of beam 3S1 after completion of large-scale static test.

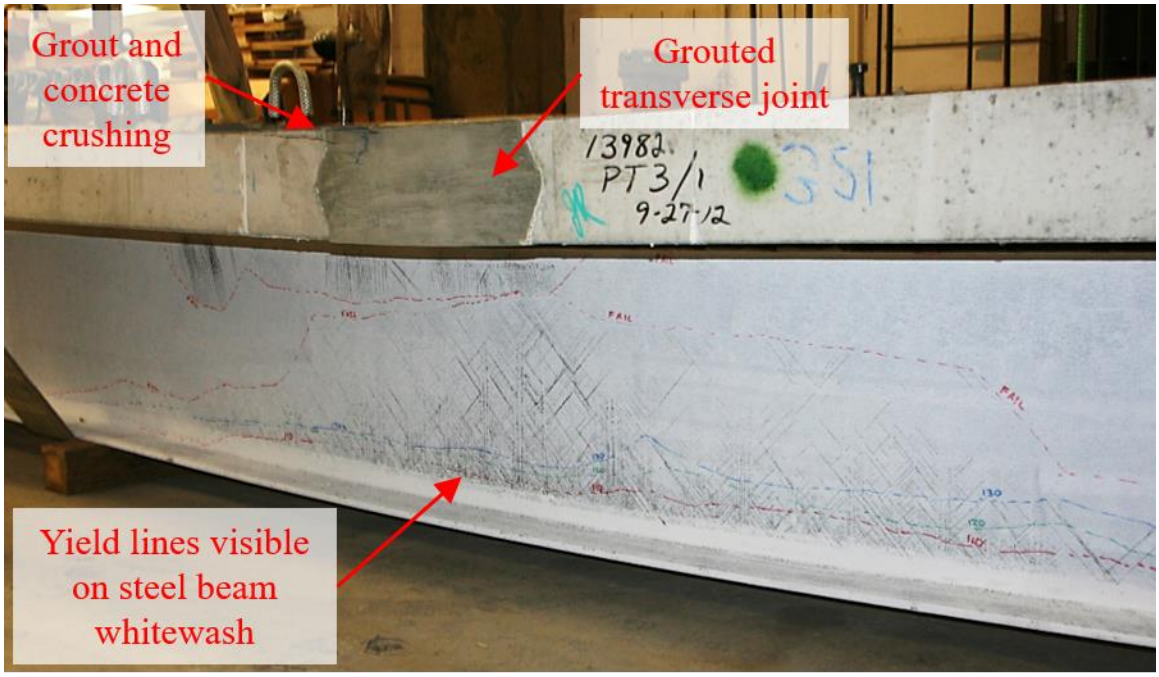

Source: FHWA.

Figure 63. Photo. View of concrete crushing and steel yielding on beam 3S1 after testing.

All of the static test beams initially failed because of grout or concrete crushing at the midspan with the exception of beam 1S1. Researchers determined that this beam failed because of a horizontal shear stud failure in the east shear span. This was determined from the sounds of the studs fracturing during testing as well as the significant amount of slip and uplift seen at the east end of the beam, as shown in figure 64.

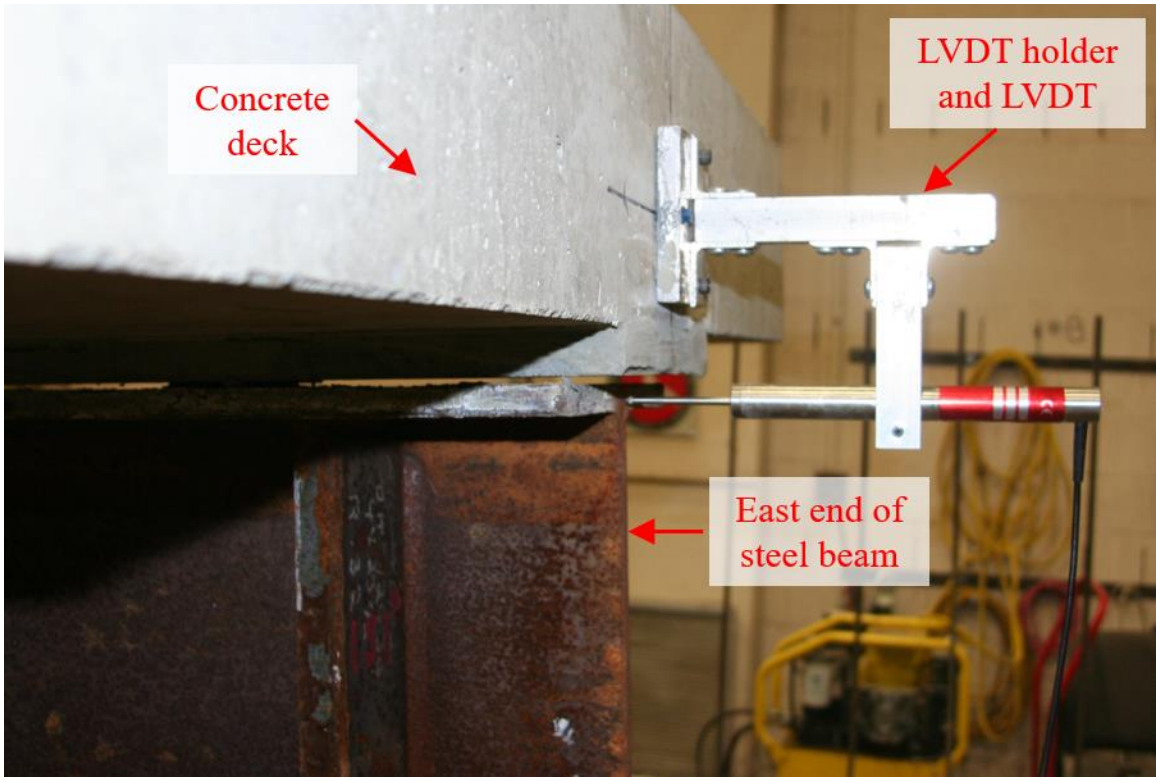

Source: FHWA.

Figure 64. Photo. Significant amount of slip and uplift in east end of beam 1S1 after testing.

Once visual observations were complete, the team removed the concrete decks from the steel beams, as was done for the large-scale fatigue tests. Researchers took care to remove the concrete decks without further damaging the shear studs. Cores of the concrete surrounding the shear studs were not obtained for the static tests. Once the decks were removed, the team further examined the shear studs. For specimens other than beam 1S1, the shear studs appeared to have bent in double curvature, as shown in figure 65, which shows the first and second shear studs from the west end (indicated by W1 and W2) of beam 2S1. The double curvature bending shown is representative of the damage in all of the beams tested. The curvature took place in the bottom 1–2 inches of the shear studs in all cases. This double curvature indicates that shear studs were loaded in a combination of bending and shear. If the studs were loaded primarily in tension, as the current AASHTO provision implies, the studs would have bent toward the end of the beam and behaved like a tension member. No tension member behavior was observed on any of the shear studs on any of the tests.

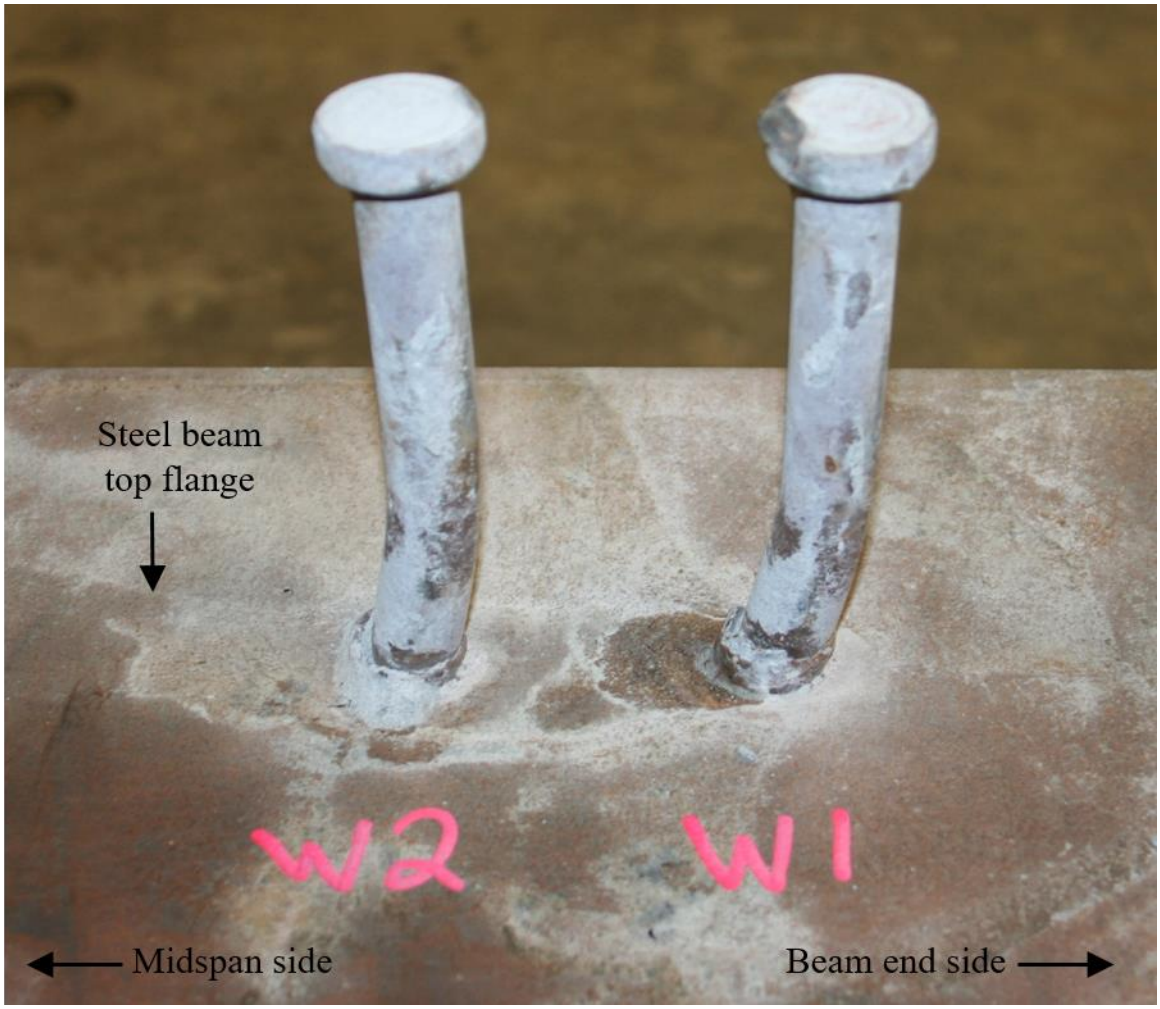

Source: FHWA.

Figure 65. Photo. Double curvature in shear studs after large-scale static testing.

Because beam 1S1 initially failed owing to a shear stud failure, it displayed somewhat different behavior. Once the team removed the concrete decks from this beam, the failed shear studs were examined. They saw two apparent modes of failure, both similar to what was seen in the fatigue tests. The first was a horizontal shear failure in the shear stud across a plane even with the top of the weld flash. An example of this failure on beam 1S1 is shown in figure 66. This specific failure was from the easternmost shear stud, indicated by the label E1. For this failure mode, the weld flash and the portion of the shear stud within the flash remained attached to the beam.

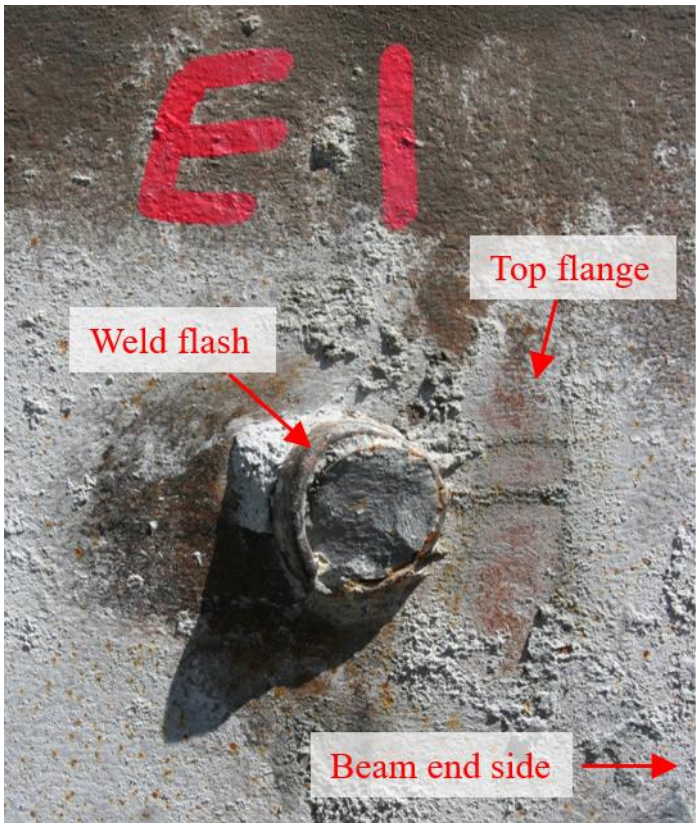

Source: FHWA.

Figure 66. Photo. Shear stud failure at plane above weld flash in beam 1S1.

The second mode of failure was a horizontal shear failure in the shear stud across a plane even with the top flange of the steel beam. An example on beam 1S1 is shown in figure 67. This specific failure was from the second easternmost shear stud, labeled E2. There was no apparent correlation between the location of the shear stud on the beam and the mode of failure.

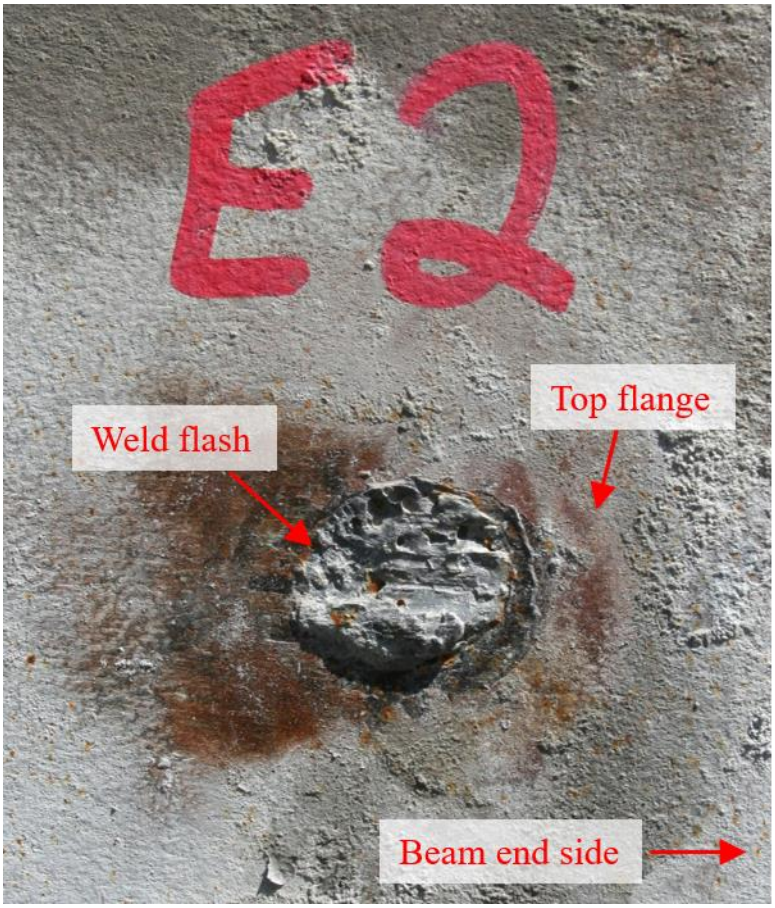

Source: FHWA.

Figure 67. Photo. Shear stud failure at plane even with top flange in beam 1S1.

Moment–Displacement Data

During the static loading, data from the load cells and midspan LVDTs were used to develop a moment–displacement curve for each of the five beams tested. Figure 68 shows these moment–displacement data for each beam. Recall that one beam (1S2) had two shear studs placed transversely across the flange in each shear stud cluster. The remaining four beams had a single shear stud placed transversely in each cluster. Researchers calculated the nominal moment capacity for both of these cases and subtracted the dead load moments to determine the calculated moment capacity (M_n). For beam 1S2, with two transverse studs, the calculated M_n was 2,157 kip-ft. For the remaining beams with a single transverse stud, it was 1,831 kip-ft. Note that this calculation is an average moment capacity for the beams with one transverse stud. The exact values differed slightly because of differences in concrete strength. Both values are represented in figure 68 by a dashed line. In both cases, the strength of the shear stud connection was governed by the strength of the steel shear studs (right side of equation in figure 6). Also, the horizontal shear force in the shear studs determined the M_n of the composite beams for both beam designs. This was probably because the beams were designed as partially composite. Thus, the M_n of the beams was governed by the strength of the steel shear studs. As previously mentioned, because partial-composite beam design was used, AISC specifications were used to calculate the moment capacity since AASHTO does not provide calculations for a

partial-composite beam design.[28] It is important to note that the two design procedures are essentially identical; the only difference is that AISC allows for partial-composite action, while AASHTO does not. The AISC shear stud–strength design provisions have additional factors that apply to ribbed steel decking, but since it was not used in construction of the beams, these factors were not applicable. Note that actual material properties from the mechanical test results were used in the moment capacity calculations rather than design values.

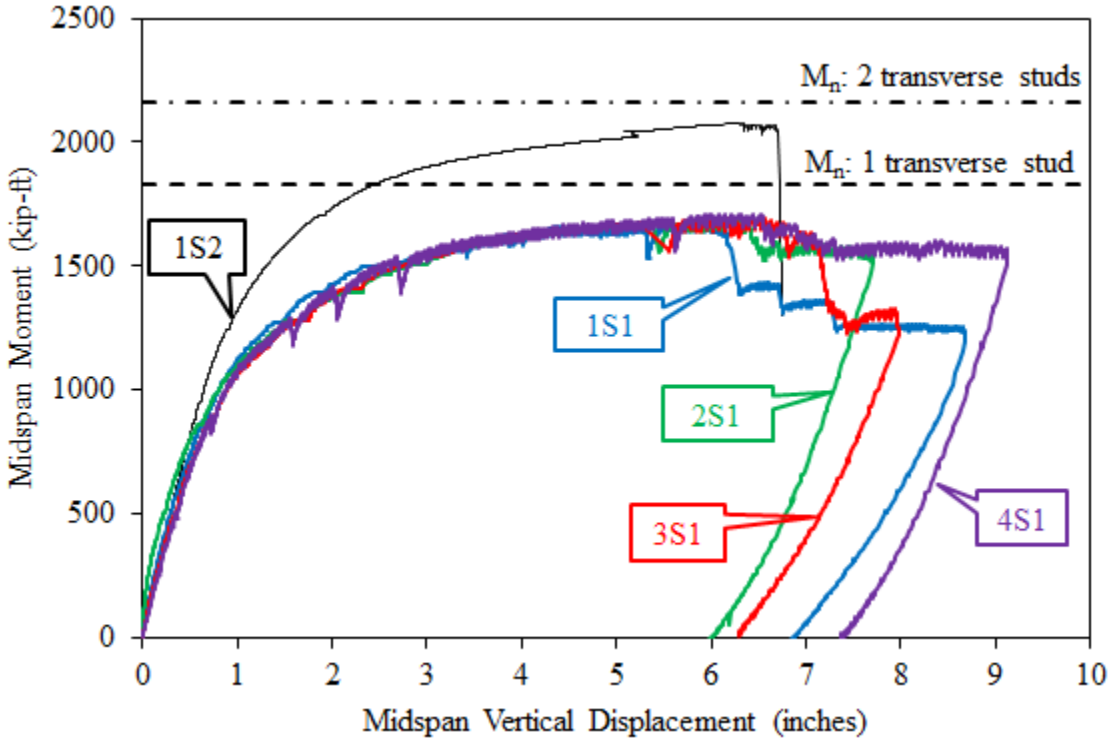

Source: FHWA.

Figure 68. Graph. Moment–displacement plot for large-scale static tests.

Beam 1S2 was the first beam tested. This beam failed because of grout crushing at the midspan of the beam rather any of the shear studs in either shear span failing. Though the beam nearly reached its M_n, because it did not fail in the desired fashion, other beams were designed differently. All other beams had only one transversely spaced shear stud.

Figure 68 shows moment–displacement data for the four beams with a single transverse shear stud (1S1, 2S1, 3S1, and 4S1). All four beams exhibited similar global behavior throughout the test until they reached failure. The small reductions in moment during the loading portion of the test (e.g., at a moment value of 1,380 kip-ft) occurred when the loading was paused to record displacement data using the laser tracker. They do not reflect a loss of load from any localized failures. These loading pauses were much more apparent in the four beams with one transverse shear stud than in beam 1S2. Clearly none of these four beams reached their M_n.

Table 11 provides a summary of the moment–displacement results. Of the four beams with one transverse stud, 1S1 was the only beam to experience a failure because of horizontal shear on the shear studs. The other beams failed initially because of grout crushing at the midspan. The point

at which the shear studs failed in beam 1S1 illustrates the most noticeable difference in the four beams' behavior. The shear stud failure in beam 1S1 occurred at a vertical displacement of approximately 6 inches. When the shear studs failed, 1S1 experienced a drop in load because of a drastic reduction in composite action. A similar drop in load is also shown in 3S1 at a vertical deflection of approximately 7 inches. This beam also experienced shear stud failures at this point, though from visual observation, it was clear that the beam had already failed because of the grout crushing at the midspan prior to any shear stud failures.

Table 11. Summary of moment–displacement data for large-scale static tests.

Specimen	M_n (kip-ft)	Maximum Midspan Moment (kip-ft)	Shear Factor	Initial Failure Mode
1S2	2,157	2,077	0.86[a]	Grout crushing at the midspan
1S1	1,831	1,667	0.71	Horizontal shear stud failure in east shear span
2S1	1,834	1,692	0.75[a]	Grout crushing at the midspan
3S1	1,831	1,693	0.75[a]	Grout crushing at the midspan
4S1	1,829	1,711	0.78[a]	Grout crushing at the midspan

[a]Represents a minimum value since horizontal shear stud failure did not occur.

The second column of the table shows the M_n for each beam. For each of the beams with one transverse shear stud, the capacities differed slightly because of the difference in concrete strength. The third column shows the maximum moment during testing. Among the four beams with the same number of shear studs, this value varied by approximately 2 percent. Since the maximum moment and the beams showed similar moment–displacement behavior, shear stud–cluster spacing (up to 48 inches) did not appear to have any influence on the global flexural performance of the beams. The fourth column shows a shear factor. This is the factor that would need to be applied to a shear stud's resistance (right side of the equation shown in figure 6) to make the calculated moment match the moment capacity. Note that in each case (except for beam 1S1), these shear factors are minimum values since the beams did not fail because of horizontal shear failure of the studs. Thus, these values could be greater since the beam did not reach the calculated moment to cause failure of the studs. However, the shear factor shown for beam 1S1 is accurate since this beam did fail in horizontal shear at the shear studs. It is also important to note that these factors are average values applied equally to each shear stud within a given shear span.

As shown in table 11, none of the five beams reached their M_n; therefore, all of the shear factors were less than 1.00. Currently, the AASHTO shear stud–strength design equation in figure 6 contains an implied shear factor of 1.00. Since the strength of the steel shear studs determined the M_n, it is evident that the AASHTO equation overpredicted the strength of the shear studs, leading to an unconservative estimate of the beam's M_n. This is especially true for beam 1S1, which failed in horizontal shear at the base of the shear studs, and for beam 3S1, which experienced shear stud failures after an initial beam failure of grout crushing.

The shear factors for the beams tested ranged from 0.71 to 0.86. Although the shear factors for four of the beams represent minimum values since the beams did not experience an initial shear stud failure, the shear factor for beam 1S1 was the lowest value and occurred with a shear stud failure. Based on the large-scale static test data, a shear factor of 0.70 should be applied to the AASHTO shear stud–strength design equation. This value is similar to the shear factor of 0.80 that is used in the Australian shear stud–strength design provisions.[9] Having a shear factor between 0.60 and 1.00 would imply that shear studs are loaded in a combination of pure shear and pure tension, which seems reasonable based on the test results.

LVDT Data

Data from the LVDTs were collected continuously throughout the static testing. Figure 69 and figure 70 show the LVDT slip data for the west and east shear spans, respectively, of beam 1S1.

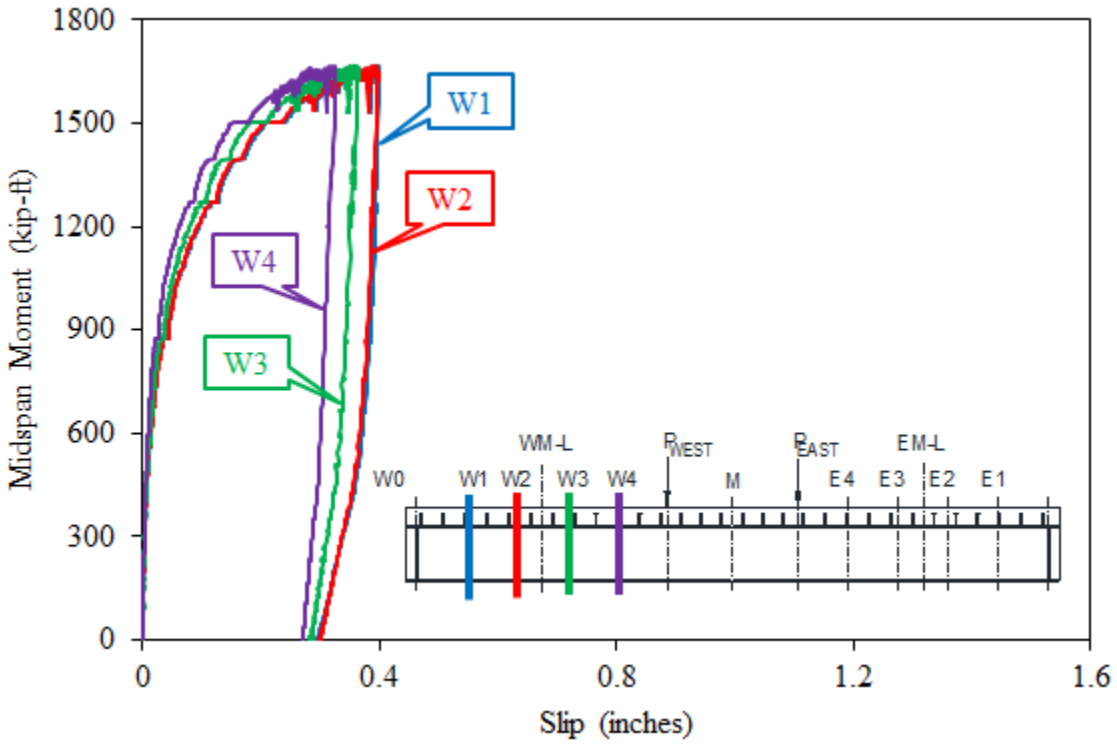

Source: FHWA.

Figure 69. Graph. LVDT slip data for west shear span of 1S1.

The slip data shown in figure 69 are as expected since the east shear span failed first, so a limited amount of slip was present in the west shear span. The sections closest to the end of the beam experienced slightly more slip than those closer to midspan with sections W1 and W2 having approximately equal slip values.

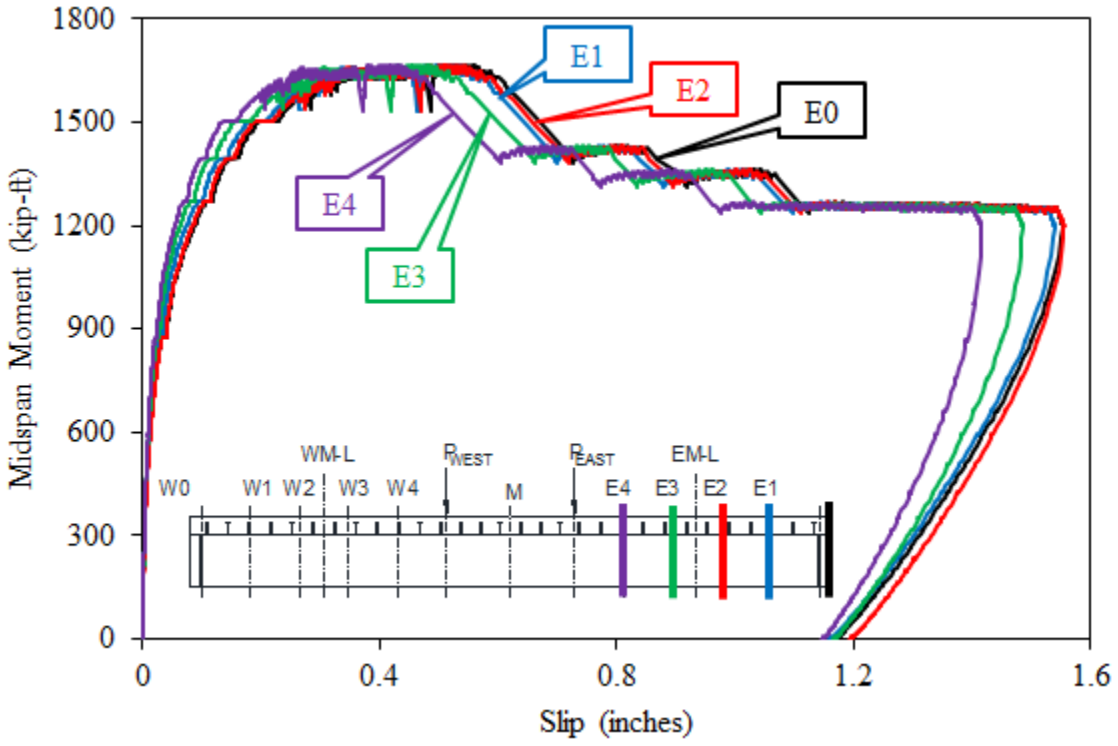

Source: FHWA.

Figure 70. Graph. LVDT slip data for east shear span of 1S1.

As seen in figure 70, the slip damage in the east shear span was much greater than in the west shear span. This beam failed because of a horizontal shear failure at the shear studs. The first shear stud failure occurred at a slip value between 0.5 and 0.6 inch in figure 70. At this point, all of the sections experienced a drop in load and a sudden increase in slip. This occurred again at approximately 0.7–0.8 inch of slip and for a third time at approximately 0.9–1.0 inch of slip. These multiple drops in slip suggest that the studs did not fail in unison but incrementally, although the exact order in which the studs failed cannot be interpreted from the figure. The incremental failure also shows that there was a considerable amount of ductility in the shear connection between the steel beam and concrete deck. As with figure 69, the sections closest to the end of the beam experienced the greatest amount of slip.

Figure 71 shows the uplift at the middle of the east and west shear spans. The uplift appears consistent between the two shear spans until reaching the maximum moment. At that point, the east shear span experienced a sudden increase in uplift. This probably coincided with the first failure of the shear studs in the east shear span.

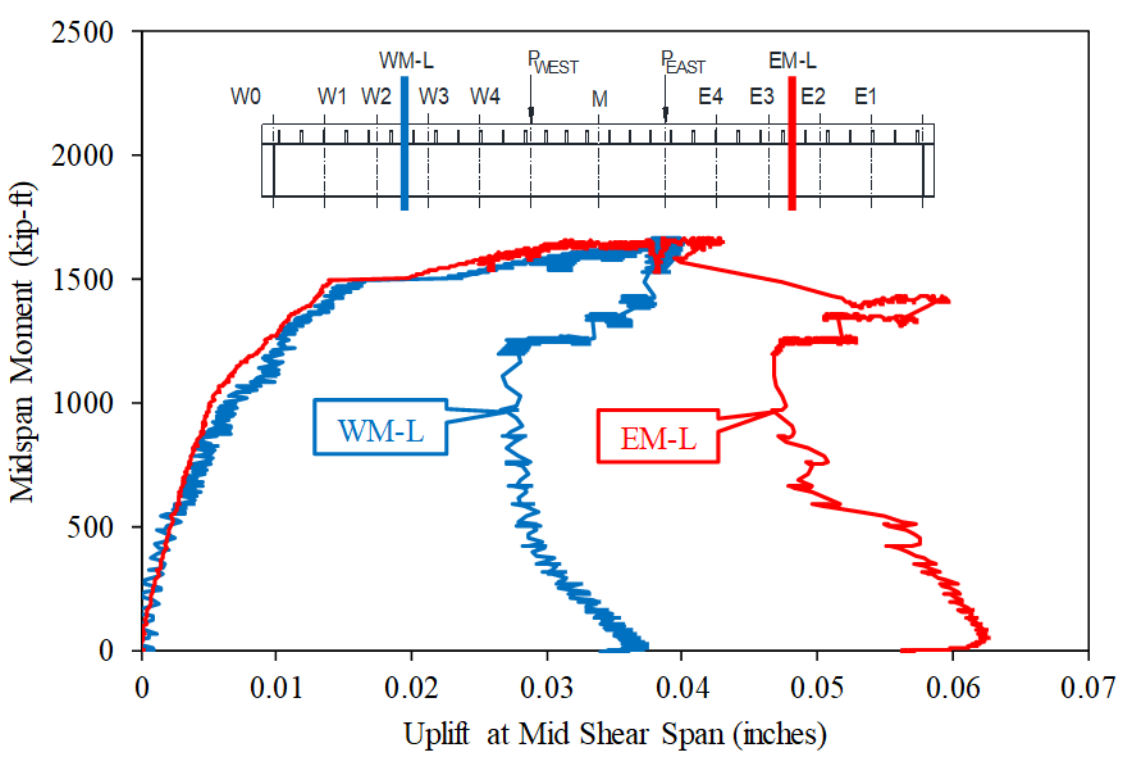

Source: FHWA.

Figure 71. Graph. LVDT results for uplift in both shear spans of beam 1S1.

To provide a comparison between the 12- and 48-inch spacing beams, LVDT data from beam 4S1 are also presented. Figure 72 and figure 73 show the LVDT slip data for beam 4S1 for the west and east shear spans, respectively. As shown in the figures, the west shear span experienced significantly more slip damage than the east shear span. In general, the beam behaved as expected, with the sections near the end of the beam having more slip damage than those near midspan.

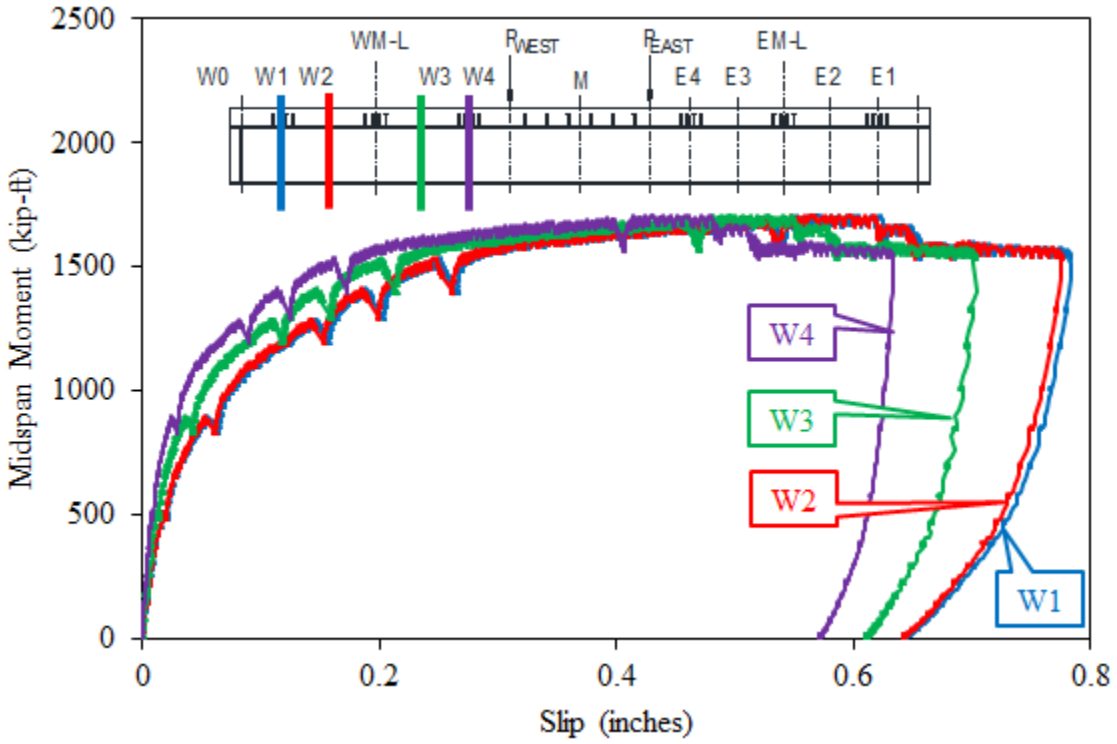

Source: FHWA.

Figure 72. Graph. LVDT results for slip in west shear span of beam 4S1.

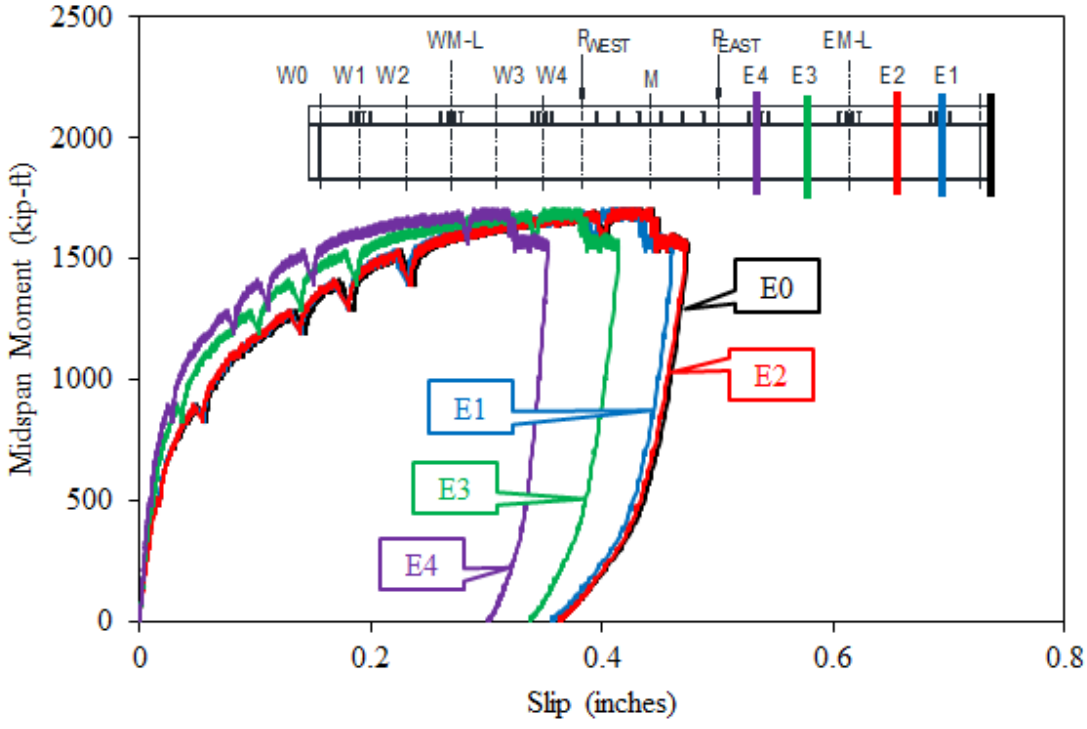

Source: FHWA.

Figure 73. Graph. LVDT results for slip in east shear span of beam 4S1.

When comparing the plots of the moment–LVDT data from the failing shear spans of each beam (i.e., figure 70 for beam 1S1 and figure 72 for beam 4S1), it is important to keep in mind the failure mode for each beam. Initially it may appear that beam 1S1, with a 12-inch shear stud spacing, had much greater ductility than beam 4S1, with a 48-inch spacing, since the maximum recorded slip on beam 1S1 was nearly 1.6 inches compared to nearly 0.8 inch for beam 4S1. However, beam 1S1 failed because of a horizontal shear failure at the studs, whereas beam 4S1 failed because of grout crushing at the midspan prior to any shear stud failures. Therefore, one would expect significantly more horizontal slip in beam 1S1 than in beam 4S1 because of these different failure modes. Because of this difference in failure modes, it was difficult to draw any conclusions based on the LVDT data on the difference in ductility because of the shear stud spacing. Regardless, there were no apparent negative slip characteristics between beams 1S1 and 4S1, which suggests that increasing the spacing from 12 to 48 inches should not negatively influence the overall behavior of the beams.

Figure 74 shows the uplift behavior at the middle of the shear span of beam 4S1. Throughout the test, the east shear span experienced greater uplift than the west shear span. This was surprising since the west shear span accumulated more slip damage than the east did. However, the relative difference between the two was quite small.

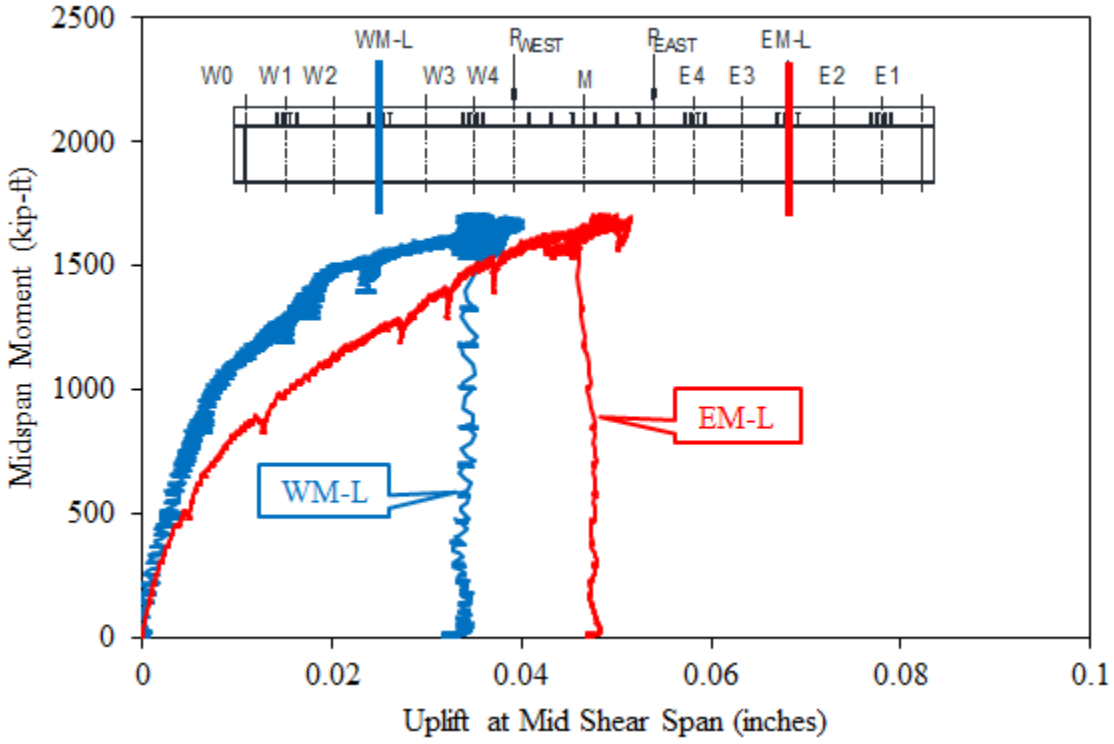

Source: FHWA.

Figure 74. Graph. LVDT results for uplift in both shear spans of beam 4S1.

The uplift was similar in behavior and relative magnitude between beams 1S1 and 4S1 (compare figure 71 and figure 74). As expected, the difference in failure mode between the beams affected the slip behavior but not the uplift behavior in the beams. As with the slip behavior, it does not

appear that the 48-inch spacing had any negative impact on the overall performance of the beams. LVDT data for the remaining large-scale static tests are shown in appendix F.

Laser Tracker Slip Results

As during the large-scale fatigue tests, the team took laser tracker measurements throughout the static testing process. Figure 75 through figure 78 show the relative slip measurements for beams 1S1, 2S1, 3S1, and 4S1 taken at applied moments of 460; 860; 1,270; 1,380; and 1,500 kip-ft, which correspond to approximately 25, 50, 75, 80, and 90 percent, respectively, of the maximum applied moment. Comparing these figures shows how beams with different shear stud–cluster spacings performed throughout loading. Unfortunately, many of the aluminum spacers fell off during testing of beam 1S2, so data could not be collected and are therefore not presented. Researchers also took laser tracker measurements after the beams failed; these data are included in the figures. The general format of these figures is the same as those for laser tracker slip data for the large-scale fatigue tests. The main difference is that each line represents data taken at a different load level rather than a cycle count. Note that in some cases, such as the failure data for beam 3S1, data points are missing on the figures. These are locations in which the aluminum spacers fell off during testing; therefore, data could not be collected. Figure 77 shows this for beam 3S1 between approximately 80 and 100 inches from the east end of the beam.

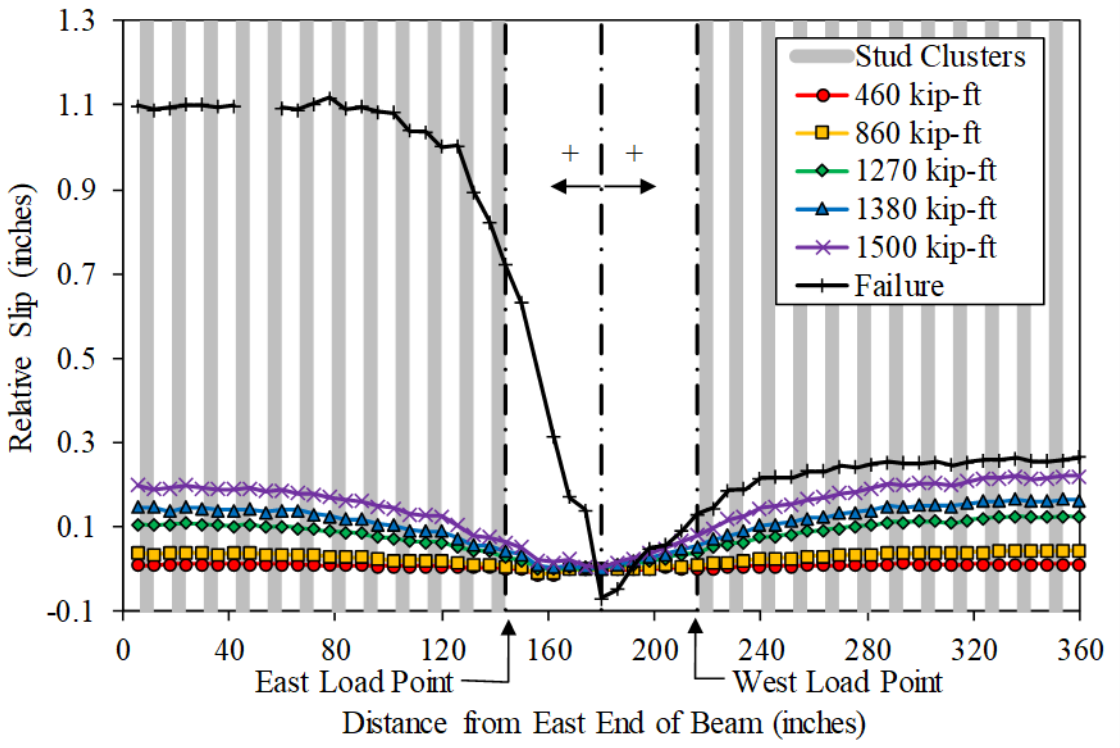

Source: FHWA.

Figure 75. Graph. Laser tracker slip results for 1S1 at various applied moments.

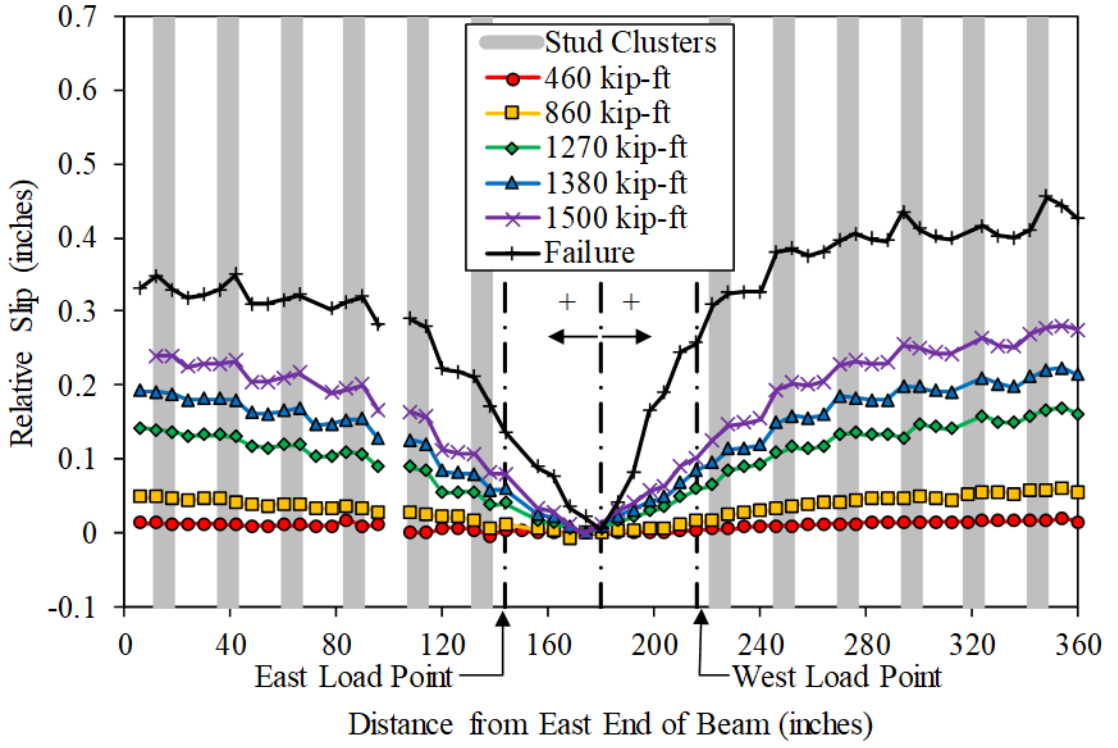

Source: FHWA.

Figure 76. Graph. Laser tracker slip results for 2S1 at various applied moments.

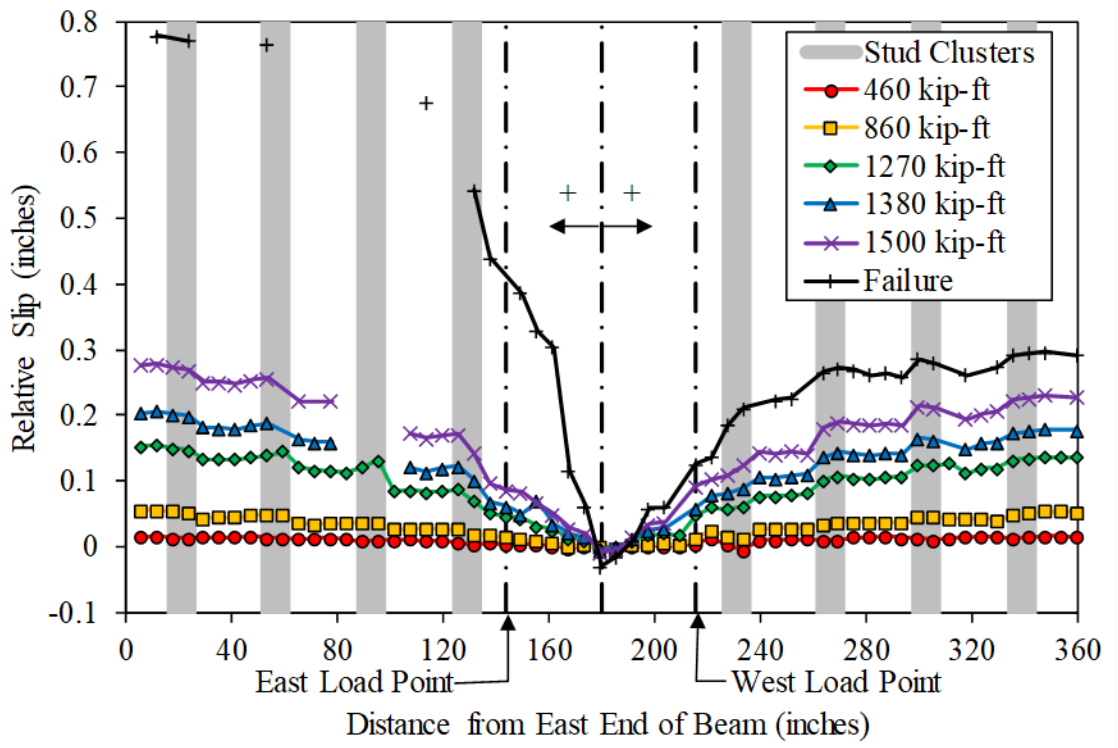

Source: FHWA.

Figure 77. Graph. Laser tracker slip results for 3S1 at various applied moments.

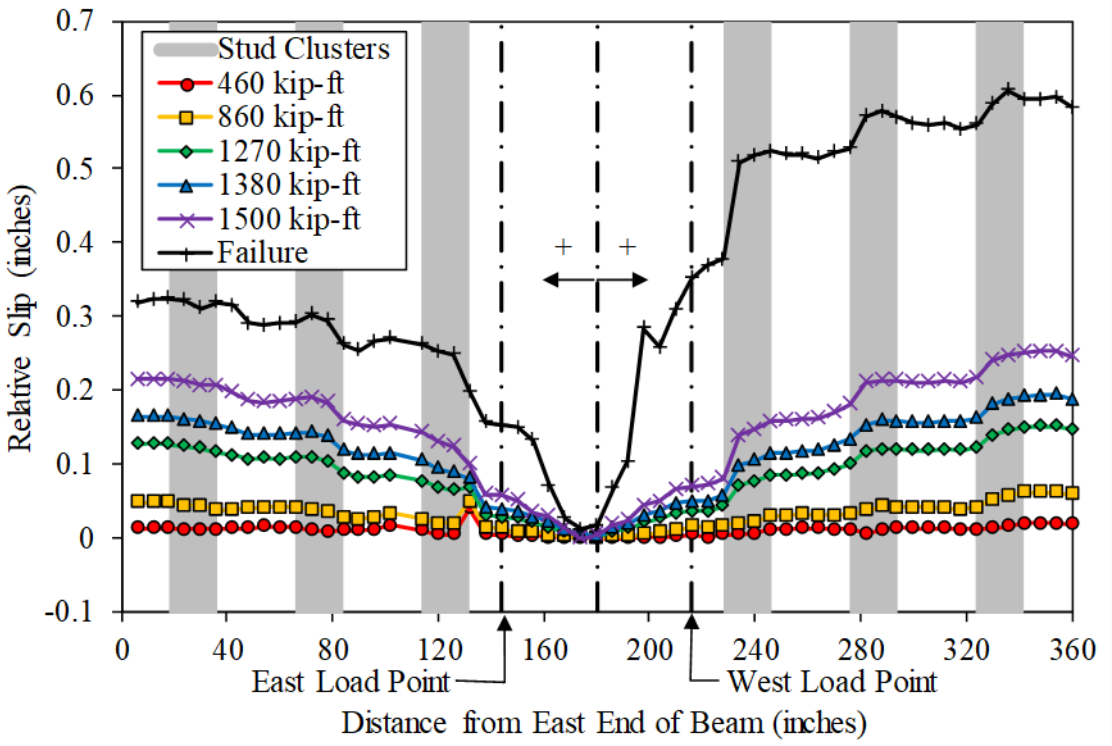

Source: FHWA.

Figure 78. Graph. Laser tracker slip results for 4S1 at various applied moments.

Overall, the slip behavior for the four beams was as expected. Slip was approximately 0 near the midspan and gradually increased until reaching a maximum value at each end of the beam. This was true for all load levels during testing. For the beams with extended shear stud spacing (2S1, 3S1, and 4S1), the slip appears stairlike in the graph, similar to that seen in the large-scale fatigue data. The local increases in slip for the steps correspond to the midspan side of the shear stud clusters. Damage was concentrated here likely because of shear lag. Between the shear stud clusters, the slip remained fairly constant. Despite the stairlike slip behavior, the magnitude of the maximum slip was similar for all four beams at 90 percent of the ultimate load, ranging from approximately 0.2 to 0.3 inch. It does not appear that the extended shear stud–cluster spacing had a negative effect on the relative slip behavior.

As mentioned previously, the difference in failure modes made a ductility comparison between the beams based on the LVDT data impossible. The laser tracker measurements taken at 90 percent of the maximum applied moment can be used, however, since these measurements were taken prior to failure. Using these data, the team calculated a cumulative slip across both shear spans of each large-scale static test beam. In locations where the aluminum spacers had fallen off during testing, researchers used linear interpolation to calculate individual slip values between the intact spacers. Table 12 shows these cumulative slip values for the shear span that accumulated the most slip, which was deemed the failing shear span. In general, the cumulative slip was relatively similar between both shear spans in a particular beam.

Table 12. Cumulative slip of failing shear span in large-scale static tests at 90 percent applied moment.

Specimen	Failing Shear Span	Cumulative Slip (Inches)
1S1	West	4.29
2S1	West	5.23
3S1	East	5.05
4S1	West	4.44

Overall, the cumulative slip values for each of the four beams are relatively similar, ranging from 4.29 to 5.23 inches. Since there are not any significant differences in these values at 90 percent of the maximum applied moments, there should not be any concerns about slip ductility when increasing the shear stud spacing from 24 to 48 inches.

Laser Tracker Uplift Results

In addition to the relative slip, the team used laser tracker measurements to determine the relative uplift between the steel girder and haunch during the static tests. Figure 79 through figure 82 show the relative uplift results at applied moments of approximately 25, 50, 75, 80, and 90 percent of the maximum applied moment.

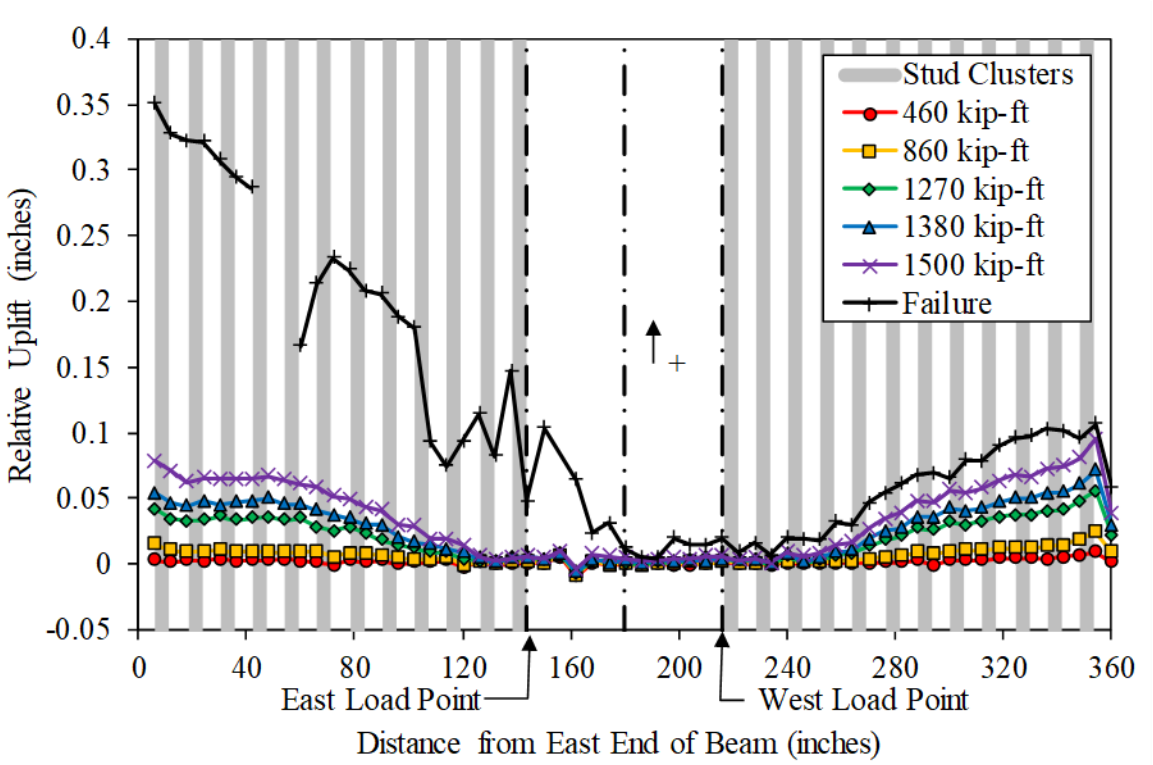

Source: FHWA.

Figure 79. Graph. Laser tracker uplift results for 1S1 at incremental applied moments.

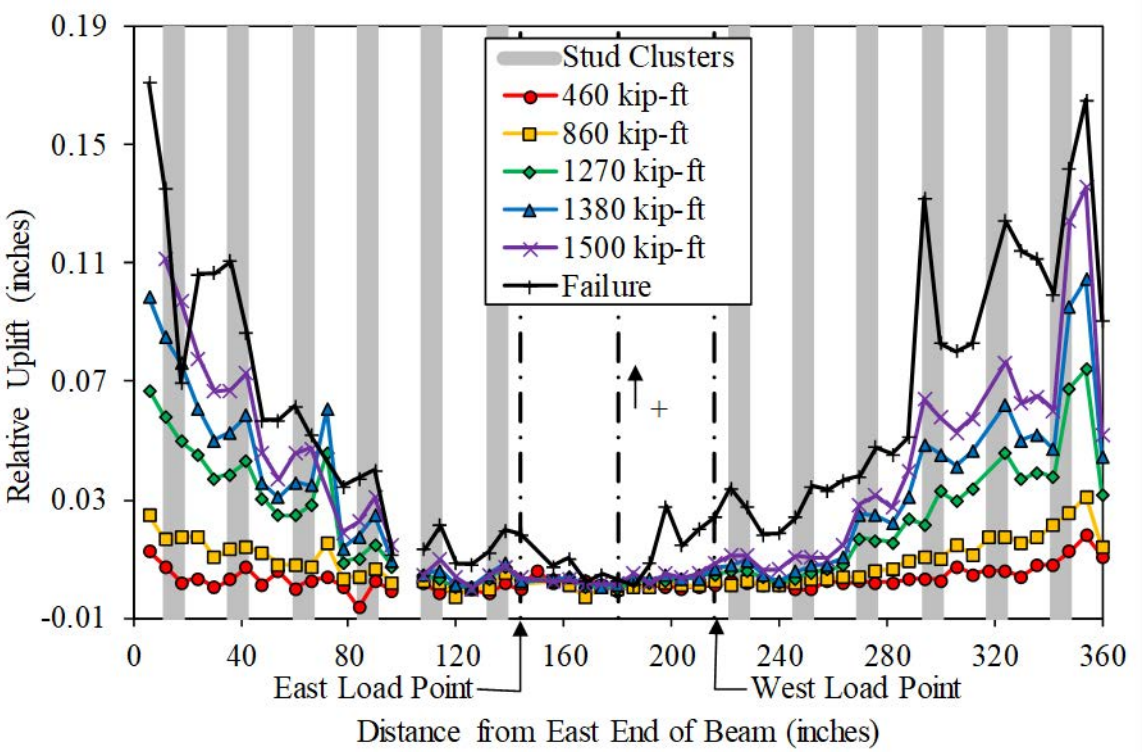

Source: FHWA.

Figure 80. Graph. Laser tracker uplift results for 2S1 at incremental applied moments.

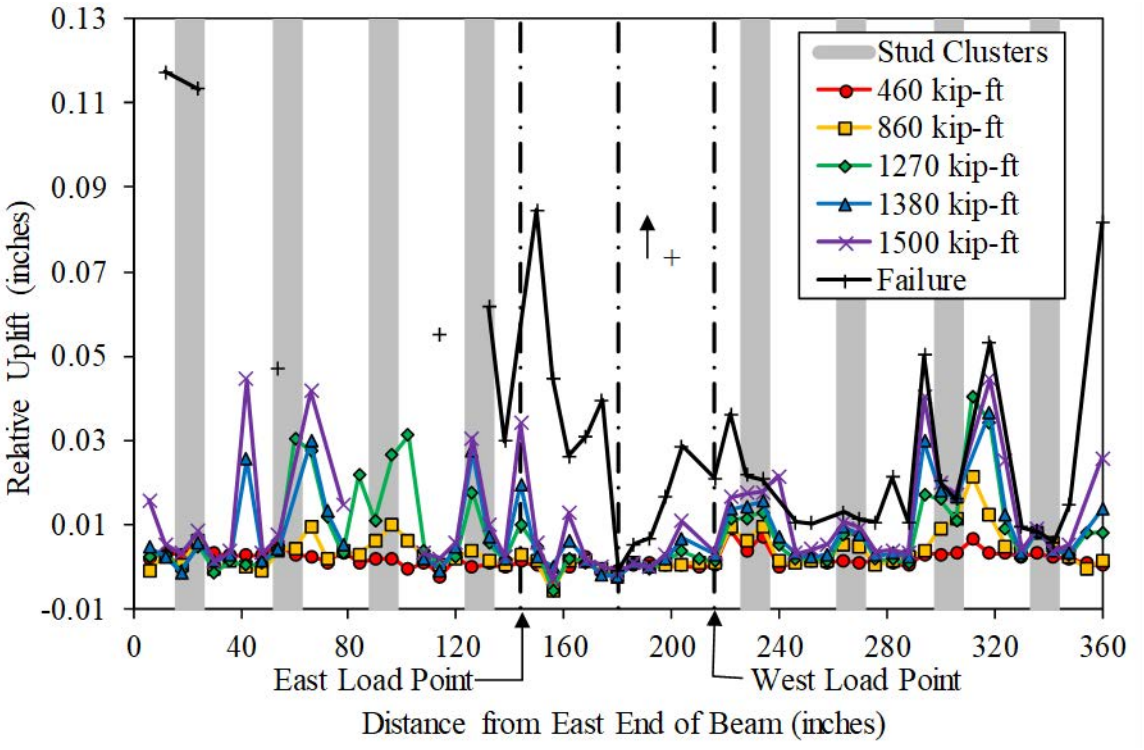

Source: FHWA.

Figure 81. Graph. Laser tracker uplift results for 3S1 at incremental applied moments.

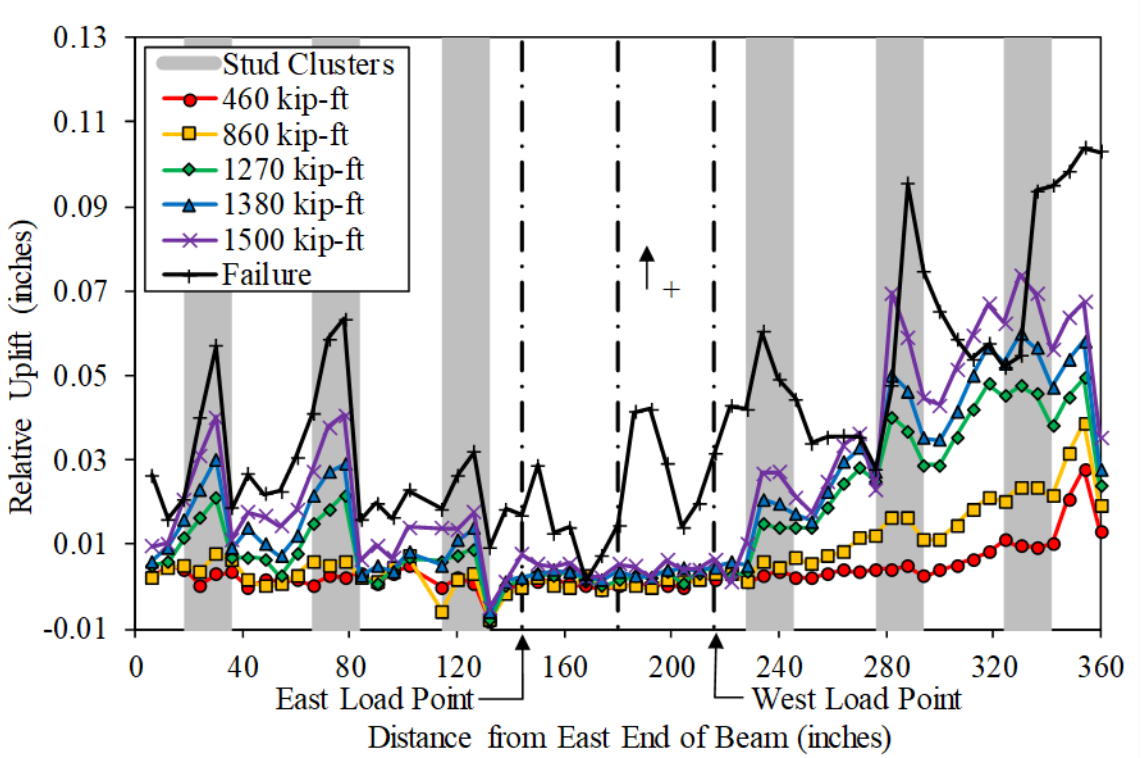

Source: FHWA.

Figure 82. Graph. Laser tracker uplift results for 4S1 at incremental applied moments.

The uplift behavior for each of the four beams was generally as expected. The uplift remained approximately 0 at the constant-moment region and then gradually increased toward each end of the beam for each different load level. This behavior was most apparent in beams 1S1, 2S1, and 4S1. For the beams with extended shear stud spacing, there were local peaks in uplift at the shear stud clusters. This was most apparent in beams 2S1 and 4S1. Damage occurred at these locations such that the shear studs could not maintain vertical compatibility between the concrete deck and steel beam. The uplift behavior was similar for all four beams, though this similarity was not as definitive as for the slip behavior. At approximately 90 percent of the ultimate load, the maximum uplift in each of the beams ranged from 0.05 to 0.13 inch. The extended shear stud–cluster spacing did not appear to have any negative effect on the relative uplift behavior.

As with the slip measurements, researchers calculated the cumulative uplift for the failing shear span of each large-scale static test beam. These results are shown in table 13.

Table 13. Cumulative uplift of failing shear span in large-scale static tests at 90 percent applied moment.

Specimen	Failing Shear Span	Cumulative Uplift (Inches)
1S1	East	1.04
2S1	West	1.04
3S1	West	0.34
4S1	West	1.02

In table 13, three of the four beams have nearly identical cumulative uplift values; beam 3S1 is the anomaly. It is unclear why the cumulative uplift results for beam 3S1 are so disparate, other than that most of the damage occurred after the 90 percent moment mark unlike the other three specimens. However, this is not a concern; there is similitude in the cumulative uplift between the 12-, 24- and 48-inch spacings and, overall, there does not appear to be any significant difference in the uplift ductility between 12- and 48-inch shear stud spacings.

Summary of Large-Scale Static Tests

A total of five large-scale static tests were conducted, which included shear stud–cluster spacings of 12, 24, 36, and 48 inches. The first beam tested had a 12-inch shear stud spacing and two shear studs placed transversely across the flange in each shear stud location. When this beam failed because of grout crushing at the midspan rather than a horizontal shear failure of the studs, the team decided to reduce the number of shear studs in each of the remaining beams. Therefore, each of the other four beams had a single shear stud placed transversely across the flange at each shear stud location.

Of the remaining four beams tested, the 12-inch spacing beam failed because of a horizontal shear failure at the studs. The shear factor—a reduction value applied to a shear stud's strength to match the applied moment to the beam's M_n—for the four beams ranged from 0.71 to 0.78. Since one shear stud failure occurred initially (in beam 1S1) and another occurred closely after grout crushing (beam 3S1), these shear factors probably represent the resistance of a shear stud under statically loaded conditions. These values are similar to the Australian shear stud–strength design provisions, which include a shear factor of 0.80.[9] The authors recommend the AASHTO shear stud–strength design provisions be amended to use a shear factor of 0.70.

The LVDT and laser tracker test data indicated that, as expected, a greater amount of slip occurred in the sections closer to the ends of the beams than at the midspan. Cumulative slip and uplift values across the failing shear span of each beam did not indicate any differences in the slip and uplift ductility of the extended spacing beams. Overall, there were no negative differences observed in the slip and uplift behavior between the beams with shear stud–cluster spacings from 12 to 48 inches.

SMALL-SCALE FATIGUE TEST RESULTS

The following subsections detail the results of the small-scale fatigue tests. Only data that resulted in meaningful findings are presented. As with the large-scale fatigue tests, the strain gauges installed on the shear studs did not provide any meaningful results and, therefore, are not discussed in this report.

Visual Observations

After the fatigue tests concluded, researchers examined the studs. They first removed the concrete decks using a similar process as after the large-scale tests. They removed grout with a jackhammer so that the decks were no longer connected to the steel beams. In some cases, the researchers also removed cores of the grout surrounding the shear studs for examination. Overall, visual observations from the small- and large-scale fatigue tests were nearly identical; thus, no photos of failed specimens are presented in this subsection. Fatigue cracks on the shear studs initiated either at the toe or the top of the weld flash and propagated into the steel beam flange. Shear failures in the grout were also visible on both the top and bottom of the shear stud in the direction of loading.

S-N Data

Unlike the large-scale tests, a fatigue failure was much easier to define in the small-scale tests. For these tests, a fatigue failure is defined as the point at which one or both of the two concrete slabs completely separated from the steel beam. In most cases, one slab separated first, but there were cases in which the two slabs separated at approximately the same cycle count. Note that four tests (PO-F1, PO-F6, PO-11, and PO-F12) were stopped at 50 million cycles. These tests were considered runouts since none of the four tests experienced a fatigue failure; testing was terminated in the interest of time. Cross-sectional pictures of studs from these four runout specimens can be found in appendix E. It is unclear how these studs could continue to transmit shear forces with these cracks in place. Table 14 shows a table of the S-N data from the small-scale tests, and figure 83 shows a plot of the same data.

Table 14. S-N results for small-scale fatigue tests.

Specimen	Actuator Minimum Load (kips)	Actuator Maximum Load (kips)	Stress Range (ksi)[a]	Cycles to Failure
PO-F1	6.0	22.8	14.0	50,000,000[b]
PO-F2	6.0	30.1	20.0	148,935
PO-F3	6.0	27.7	18.0	817,519
PO-F4	6.0	25.3	16.0	7,472,601
PO-F5	6.0	24.0	15.0	1,792,647
PO-F6	6.0	21.7	13.0	50,000,000[b]
PO-F7	6.0	24.0	15.0	712,456
PO-F8	6.0	24.0	15.0	12,884,837
PO-F9	6.0	24.0	15.0	2,846,232
PO-F10	6.0	24.0	15.0	3,425,611
PO-F11	6.0	24.0	15.0	50,000,000[b]
PO-F12	6.0	25.3	16.0	50,000,000[b]
PO-F13	6.0	26.5	17.0	25,383,641
PO-F14	6.0	26.5	17.0	6,765,002

[a]Calculated as the actuator load range divided by the cross-sectional area of all the studs.
[b]Specimen never failed; declared a runout.

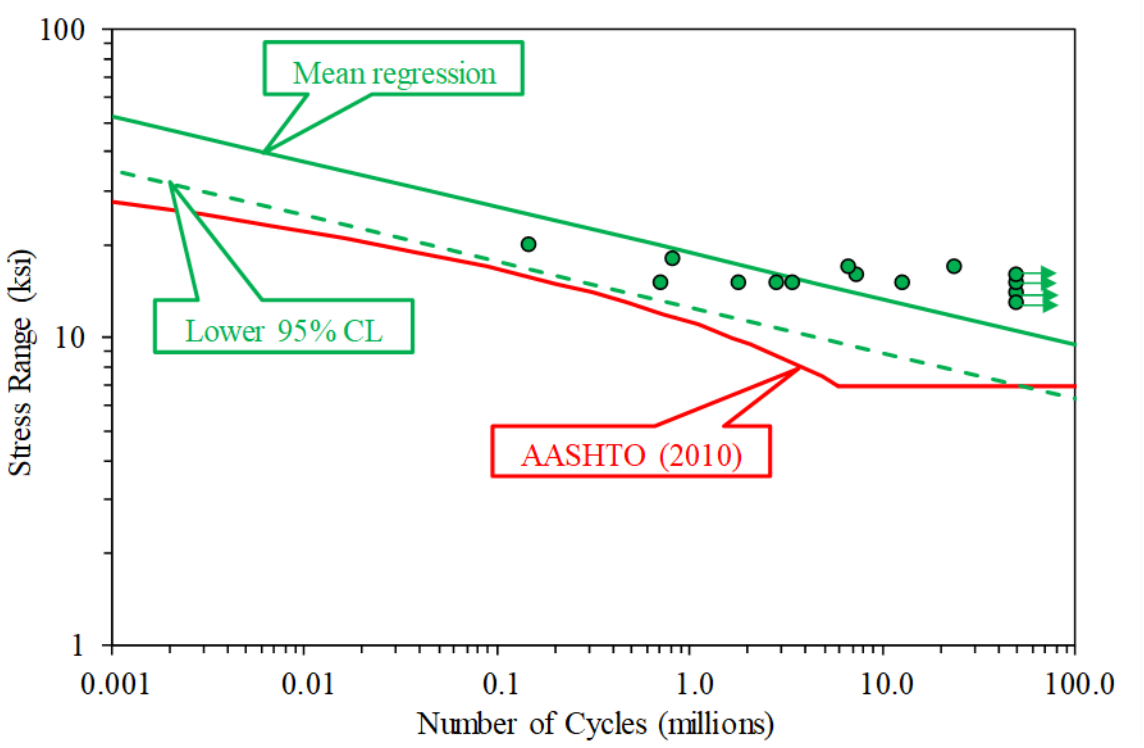

Source: FHWA.

Figure 83. Graph. S-N data for small-scale fatigue tests.

Figure 83 also includes the AASHTO LRFD BDS shear stud–fatigue design curve.[(1)] As with the large-scale fatigue tests, the small-scale tests fall well above the fatigue design curve, especially at larger cycle counts, such as the four tests that were declared runouts at 50 million cycles. Lines for mean regression and lower 95 percent CL are also included in the plot. The line for the lower 95 percent CL is represented by the equation in figure 84.

$$S_{r,\,SS,\,95} = \left(\frac{276{,}200 \times 10^{8}}{N}\right)^{\frac{1}{6.8}}$$

Figure 84. Equation. Equation of lower 95 percent CL through small-scale fatigue test data.

Where $S_{r,SS,95}$ is the shear stress range acting on studs for small-scale tests using a lower 95 percent CL (ksi).

Similar to the large-scale fatigue data, this line is a log-log plot to match the typical AASHTO fatigue details. The slope of the lower 95 percent CL is −6.8, whereas the typical details follow a slope of −3. Again, the difference in slope is because of the difference in loading: the typical details are loaded in pure tension, while shear studs are loaded in a combination of shear and tension. The AASHTO shear stud–fatigue design curve and the 95 percent CL line are very similar from approximately 10,000 to 1 million cycles but become quite different past 1 million cycles because of the semi-log nature of the fatigue design curve.

LVDT Data

During the fatigue testing, LVDT measurements were recorded intermittently throughout the loading process. As described previously, one LVDT was used on each side of a specimen to measure the relative slip between the concrete deck and steel beam. The slip range at particular cycle counts was then determined for the fatigue life of the specimen.

Figure 85 shows a plot of the relative range for each side of specimen PO-F3 over the life of the fatigue test. From the figure, it is clear that side 1 of the specimen failed first. Fatigue damage seemed to accumulate evenly on both sides for approximately the first 300,000 cycles. At that point, the relative slip in side 1 began to increase at a slightly faster rate than side 2. At approximately 700,000 cycles, the slip range on side 1 began to increase at a significantly faster rate before eventually failing at 817,519 cycles. Remaining test data from the small-scale fatigue tests are shown in appendix G.

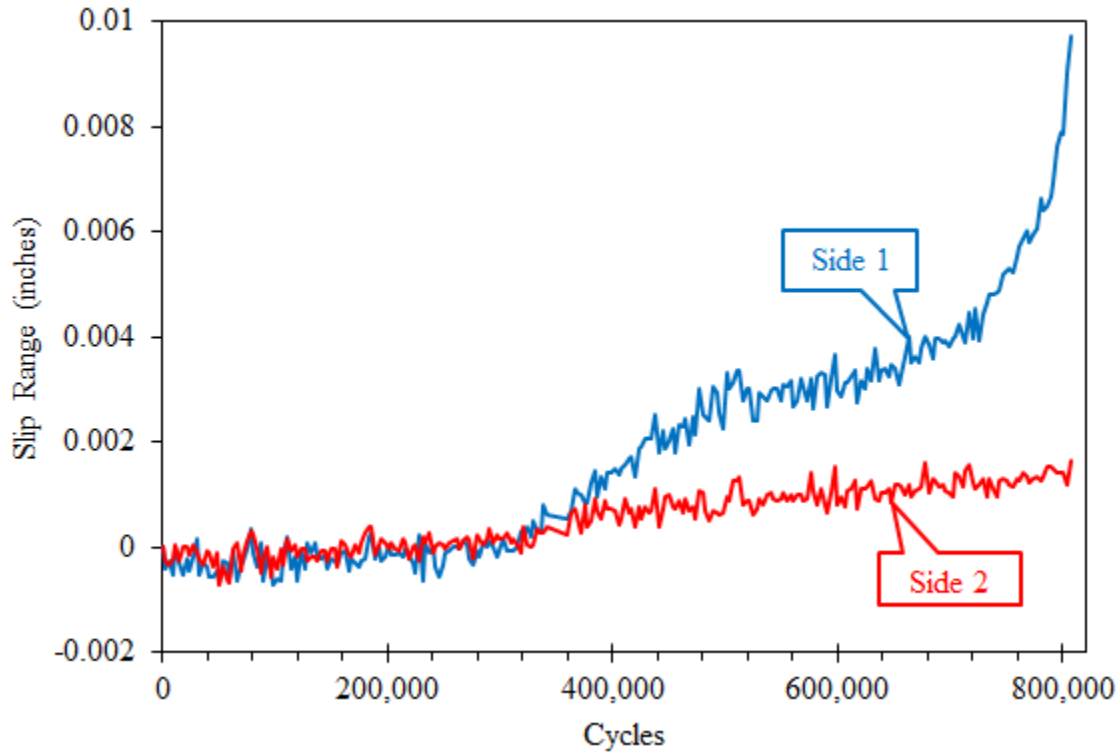

Source: FHWA.

Figure 85. Graph. Relative slip range on both sides of PO-F3.

Summary of Small-Scale Fatigue Tests

A total of 14 small-scale fatigue tests were conducted at various stress ranges. The failure criterion used to define a fatigue failure was the cycle count at which one or both of the two concrete slabs became completely separated from the steel beam. This failure definition was used to construct an S-N plot of the fatigue data. A regression analysis of the S-N data revealed that a log-log line with a slope of −6.8 represented the test data. A lower 95 percent CL of the regression line closely mimics the AASHTO shear stud–fatigue design curve from

approximately 10,000 to 1 million cycles. After this cycle count, the AASHTO curve appears extremely conservative compared to the test data. The LVDT data did provide indications about the behavior of the shear studs during testing and confirmed the failure criterion.

SMALL-SCALE STATIC TEST RESULTS

The following subsections describe the results of the small-scale static tests. Only data that resulted in relevant and meaningful findings are presented.

Visual Observations

After each small-scale static test was complete, the specimen was examined to observe how the shear studs and surrounding concrete behaved. The research team examined both the steel beam and two concrete decks on each specimen. Overall, the shear studs completely sheared off the steel beam in every one of the tests. Further examination determined whether the concrete had locally failed around the shear studs; this was most visible on the side of the concrete decks facing the steel beam. If failure was present, the specimen was considered to have failed because of concrete crushing rather than shear stud shearing.

The longitudinally spaced CIP specimens were examined first. The specimens with a shear stud spacing of 3*d* appeared to have concrete crushing locally around the shear studs, as shown in figure 86. This photo was taken of a concrete deck on specimen PO-S2-L3D-CIP after testing.

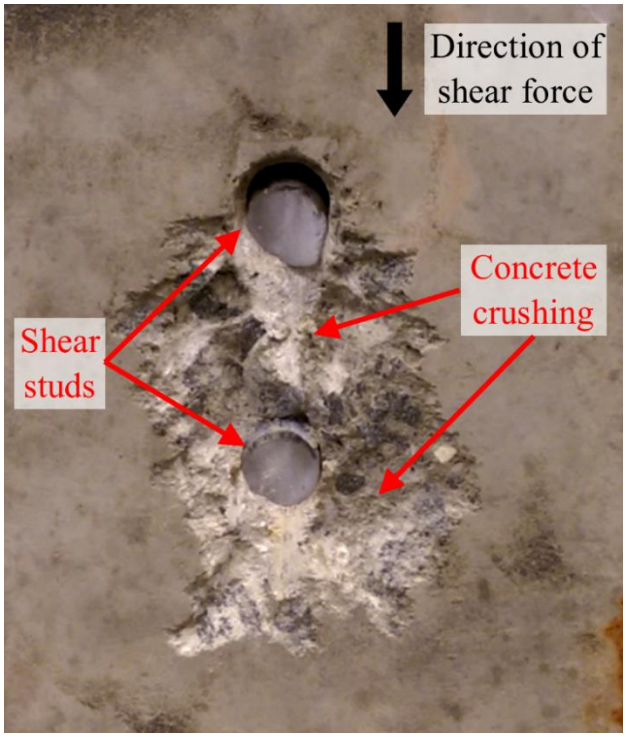

Source: FHWA.

Figure 86. Photo. Concrete crushing failure on PO-S2-L3D-CIP.

The team compared this photo to specimens from Slutter and Fisher, whose work was used to define shear stud capacity based on concrete strength (figure 6).[4] Slutter and Fisher's failure specimens never resulted in shear stud shearing and had extensive diagonal cracking of the concrete.[4] Based on this comparison, the photo in figure 86 shows minor concrete spalling, and this is still a stud shear failure. Figure 87 shows how the remaining CIP specimens with longitudinally spaced shear studs failed with an obvious shearing of the studs with no effect on the concrete.

Source: FHWA.

Figure 87. Photo. Shear stud shearing failure on PO-S1-L4D-CIP.

After examining the concrete decks, researchers observed the shear stud fracture surfaces on the steel beams. A typical fracture surface is shown in figure 88. This photo shows specimen PO-S1-L6D-CIP but is representative of all of the shear stud fracture surfaces on the steel beams. The shear studs typically sheared at the interface between steel beam and concrete deck interface, as shown in the figure.

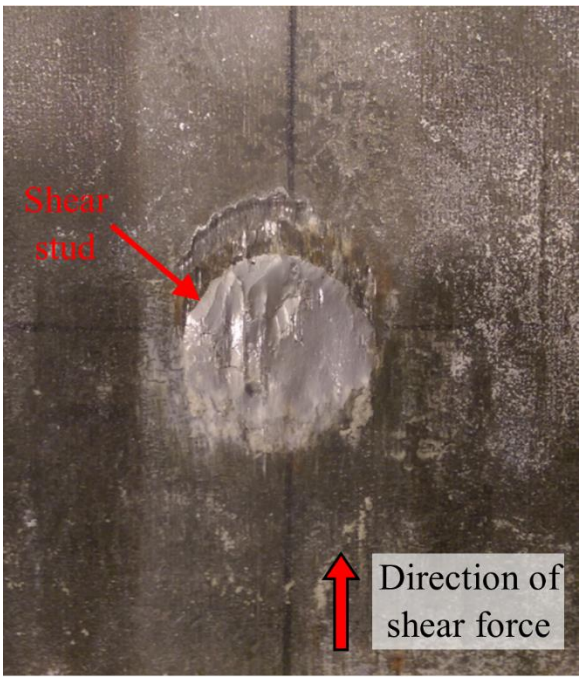

Source: FHWA.

Figure 88. Photo. Typical shear stud fracture on steel beam in small-scale static tests.

Next, the team studied the specimens with longitudinally spaced shear studs and PC decks. All of these specimens appeared to have failed because of shear stud shearing. This was evident by a lack of concrete damage around the shear studs regardless of shear stud spacing. Figure 89 shows an example from specimen PO-S2-L3D-PC; it is representative of all of the specimens with longitudinally spaced shear studs and PC decks. The specimen in this photo represents a worst-case scenario for these specimens since the longitudinal shear stud spacing was at a minimum of 3*d*, but the mode of failure remained in the shear studs.

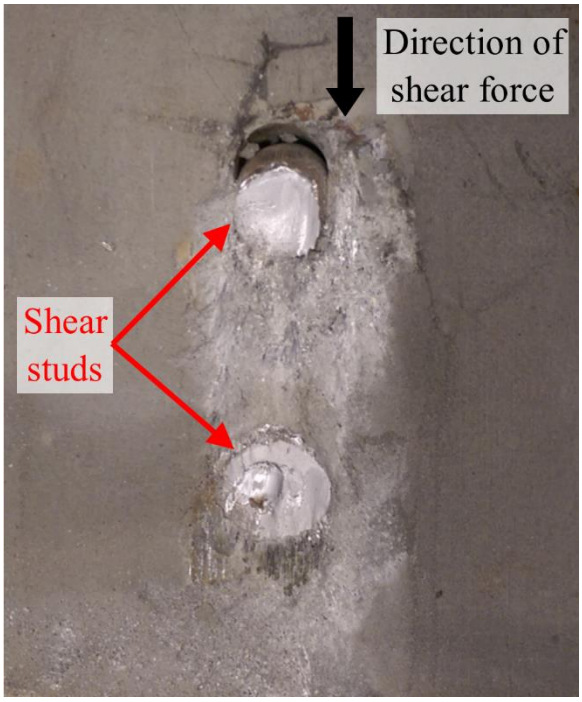

Source: FHWA.

Figure 89. Photo. Typical shear stud failures on specimens with longitudinally spaced shear studs and PC decks.

All of the specimens with transversely spaced shear studs failed because of shear stud shearing. This was the case for both the CIP and PC deck specimens. This behavior was expected since the shear stud spacing was decreased transversely and not in the direction of loading. Figure 90 shows a typical photo of the CIP concrete slab surface with the fractured shear studs still embedded. This photo of specimen PO-S1-T3D-CIP shows minimal damage to the concrete surrounding the shear studs, indicating that the specimen failed because of shear stud shearing.

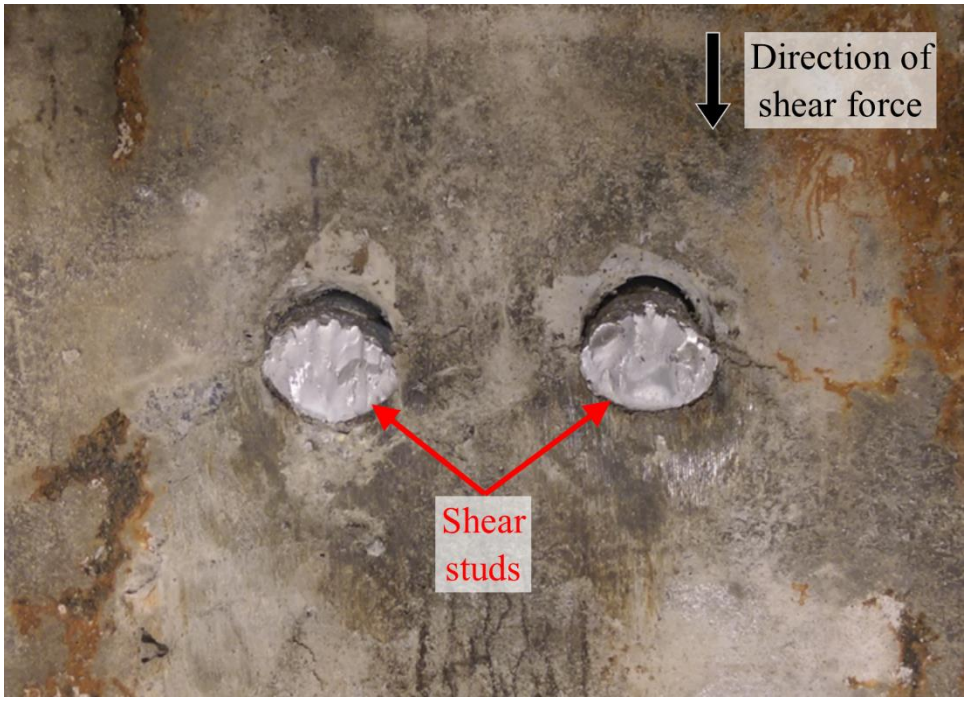

Source: FHWA.

Figure 90. Photo. Typical shear stud failures on specimens with transversely spaced shear studs and CIP decks.

Figure 91 shows the PC concrete slab surface from specimen PO-S1-T3D-PC, a typical example of the specimens with transversely spaced studs and PC decks. Again, it is clear that the shear studs were the dominant failure mode.

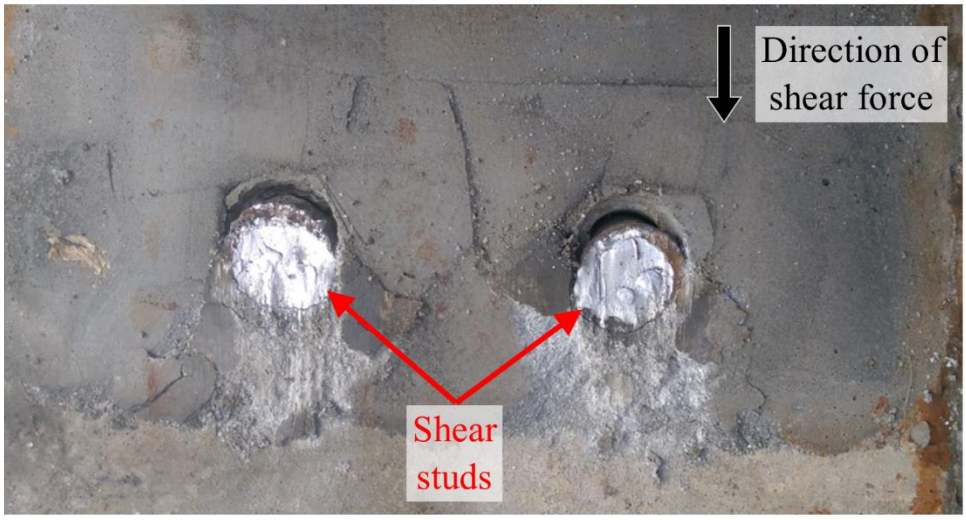

Source: FHWA.

Figure 91. Photo. Typical shear stud failures on specimens with transversely spaced shear studs and PC decks.

Video Extensometer Data

A video extensometer was used in the small-scale static tests; it provided a better spatial resolution of data than the LVDTs, so only video extensometer data are discussed in this report. Using the video extensometer data, researchers developed load–slip data for each test. They recorded slip data between the steel beam and both concrete slabs, which were located on the east and west sides of the specimens during testing.

Figure 92 shows the load–slip data for the eight CIP static tests in which the shear studs were oriented longitudinally (in the direction of loading). Plots for each test are labeled, with the last two digits indicating spacings of 3*d*, 4*d*, 5*d*, and 6*d*. Note the initial two letters of each specimen name (PO) were not included in the labels for brevity. The AASHTO shear stud–strength portions, as calculated using the equation in figure 6, are also included in the figure as dashed lines. The concrete and stud portions were calculated to be 280 and 177 kips, respectively, using the material test results.[1] Since the shear stud–strength value was less than the concrete strength, it would govern the design strength of the connection.

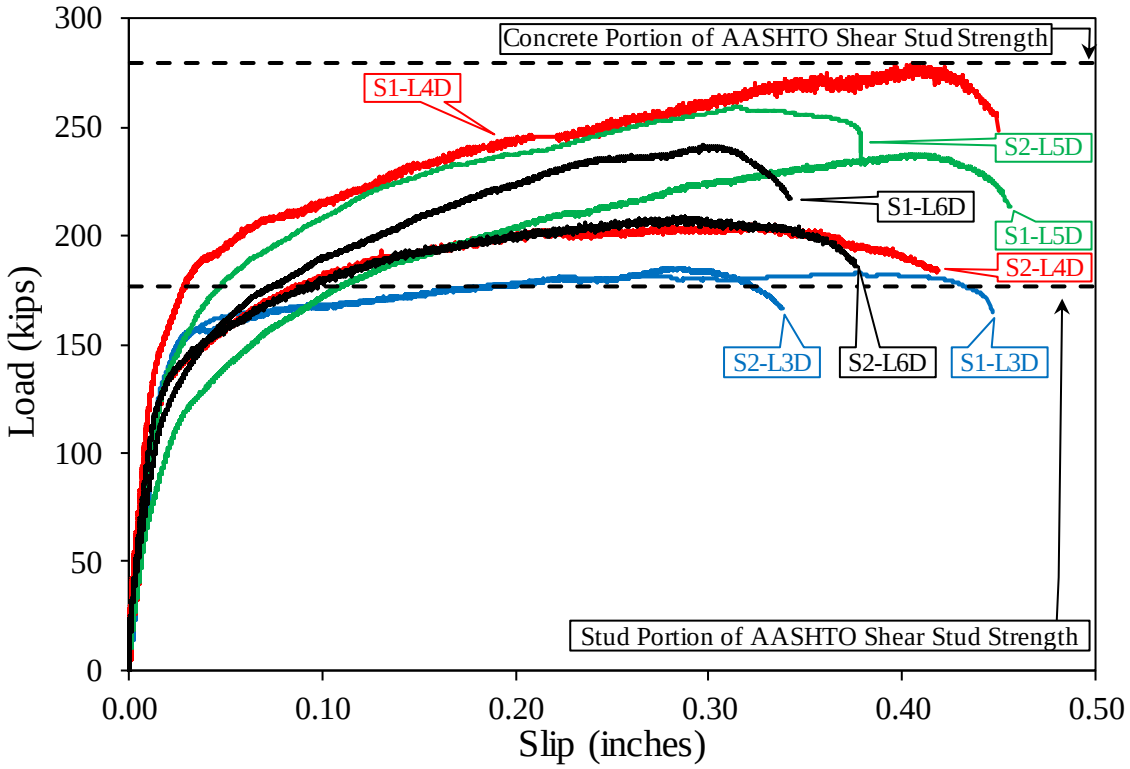

Source: FHWA.

Figure 92. Graph. Load–slip data for small-scale static tests with longitudinally spaced shear studs and CIP decks.

[1]The concrete portion of 280 kips was calculated using a modulus of elasticity of concrete (E_c) of 5,700 ksi, which came from AASHTO empirical equations relating concrete compressive strength to concrete modulus.[(1)]

As seen in the figure, there is a good deal of variability in the test results. The results for the studs oriented longitudinally at a spacing of 3*d* show a consistent lower strength then the other test results, but there does not seem to be any strong correlation between the maximum load and longitudinal shear stud spacing when studs are spaced at a distance greater than 3*d*. That is, the specimens with spacings of 4*d*, 5*d*, and 6*d* all appear somewhat variable.

Table 15 shows the maximum loads for each specimen tested with longitudinally oriented studs and CIP concrete decks. The table also includes the dominant mode of failure for each specimen, which was determined through visual observations of the specimens after testing was complete. The last column of the table lists the performance ratio for each specimen, which is the maximum load recorded during testing divided by the calculated shear stud–strength limit from figure 6. However, because all specimens failed via shear stud shearing, these performance ratios are the maximum load divided by the capacity of four individual studs (177 kips). The performance ratio fulfills the same function as the shear factor used for the large-scale tests, but the shear factor could be applied only to the shear stud portion of the equation in figure 6 to make the applied loading match the predicted capacity. The performance ratio, on the other hand, can be used as a measure of conservatism of the shear stud portion of the equation in figure 6. Performance ratios less than 1.00 indicate unconservative predictions of shear stud capacity.

Table 15. Small-scale static test results with longitudinally spaced studs and CIP decks.

Specimen	Longitudinal Shear Stud Spacing	Maximum Load (kips)	Slip at Maximum Load (Inches)	Failure Mode	Performance Ratio to AASHTO Stud Limits
PO-S1-L3D-CIP	3*d*	183.1	0.38	Stud shear	1.03[a]
PO-S2-L3D-CIP	3*d*	185.4	0.28	Stud shear	1.05[a]
PO-S1-L4D-CIP	4*d*	279.5	0.41	Stud shear	1.58[a]
PO-S2-L4D-CIP	4*d*	205.5	0.32	Stud shear	1.16[a]
PO-S1-L5D-CIP	5*d*	237.6	0.41	Stud shear	1.34[a]
PO-S2-L5D-CIP	5*d*	259.2	0.31	Stud shear	1.47[a]
PO-S1-L6D-CIP	6*d*	241.7	0.30	Stud shear	1.37[a]
PO-S2-L6D-CIP	6*d*	208.7	0.29	Stud shear	1.18[a]

[a]Calculated by dividing maximum load for the specimen by 177 kips since specimen failed via stud shearing.

Although the specimens with a longitudinal spacing of 3*d* (PO-S1-L3D-CIP and PO-S2-L3D-CIP) appeared to meet the AASHTO strength predictions, their ratios are close to 1.00. The other three shear stud–spacing ratios range from 1.18 to 1.58. While it would be technically acceptable to use shear stud spacings as low as 3*d*, because performance ratios are close to a perfect prediction, it would be safer to not allow longitudinal shear stud spacings less than 4*d*.

Figure 93 is similar to figure 92 but shows the eight test results for the PC static tests with longitudinally spaced studs. Since these tests were constructed using PC decks, grout surrounded the shear studs rather than concrete. Therefore, the grout material properties were used in the left

side of the equation in figure 6. The grout and shear stud portions of the shear stud strength were calculated to be 161 and 177 kips, respectively.[2]

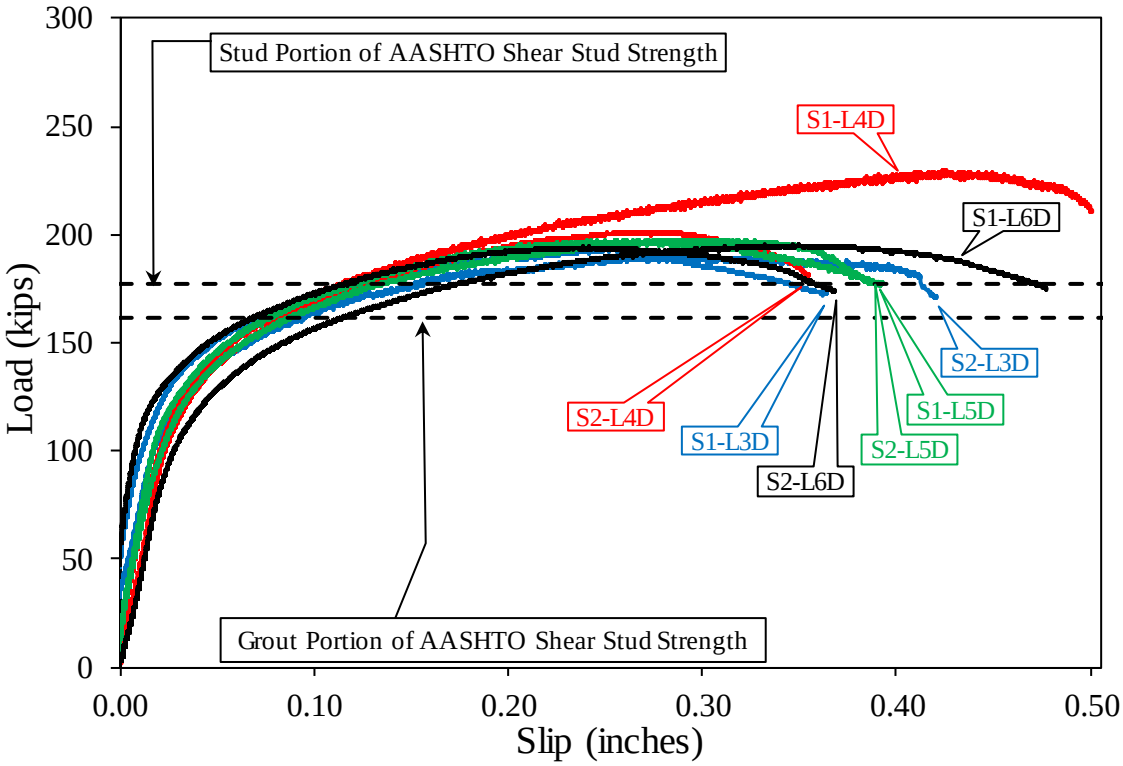

Source: FHWA.

Figure 93. Graph. Load–slip data for small-scale static tests with longitudinally spaced shear studs and PC decks.

When compared to the CIP data, the PC data shown in figure 93 are much more consistent. All but one of the tests (PO-S1-L4D-PC) behaved in a similar manner and had consistent maximum loads. Specimen PO-S1-L4D-PC had a much greater maximum load; the reason for this is unknown. PC tests were probably more consistent because there was grout around the shear studs rather than concrete. Grout is a much more consistent material, especially regarding local crushing around something small, such as a shear stud. It is likely that the CIP specimens produced more variability because of the distribution of coarse aggregates. All of the PC tests had maximum loads greater than the strength predicted by figure 6, which was governed by the grout. Table 16 shows the maximum loads for each PC specimen with longitudinally spaced shear studs.

[2]The modulus of grout is much different than concrete because it does not contain aggregate, therefore the AASHTO empirical equations relating compressive strength to modulus are not valid. The strength of a shear stud in grout of 161 kips was calculated using E_c = 2,300 ksi. This value was calculated in prior FHWA research that used the same grout product as in this study.(34)

Table 16. Small-scale static test results with longitudinally spaced studs and PC decks.

Specimen	Longitudinal Shear Stud Spacing	Maximum Load (kips)	Slip at Maximum Load (Inches)	Failure Mode	Performance Ratio to AASHTO Stud Limits
PO-S1-L3D-PC	3*d*	193.3	0.25	Stud shear	1.20[a]
PO-S2-L3D-PC	3*d*	191.0	0.28	Stud shear	1.19[a]
PO-S1-L4D-PC	4*d*	229.7	0.43	Stud shear	1.43[a]
PO-S2-L4D-PC	4*d*	201.5	0.28	Stud shear	1.25[a]
PO-S1-L5D-PC	5*d*	197.9	0.30	Stud shear	1.23[a]
PO-S2-L5D-PC	5*d*	197.7	0.26	Stud shear	1.23[a]
PO-S1-L6D-PC	6*d*	195.5	0.35	Stud shear	1.21[a]
PO-S2-L6D-PC	6*d*	194.4	0.24	Stud shear	1.21[a]

[a]Calculated by dividing maximum load for the specimen by 177 kips since specimen failed via stud shearing.

Visual inspection after testing showed that all the specimens in table 16 failed because of shear stud shearing; therefore, the performance ratios in the table measure the conservativism of the shear stud connection design equation in figure 6. The performance ratios are well above 1.00 for all spacings, which indicates that the AASHTO shear stud connection strength design equation is appropriate at a minimum spacing of 3*d* when using grout to connect shear studs to a PC concrete deck panel. These results differ from those seen with CIP concrete, which were not able to achieve strength requirements at a longitudinal shear stud spacing of 3*d*. The grouted connection probably produced greater strengths at the smaller spacing because the lack of large aggregates makes grout a more consistent material in small spaces.

Figure 94 shows load–slip results for the four small-scale static test specimens with transversely spaced shear studs and CIP decks. As in the previous figures, the individual strength portions of figure 6 are included on the figure as dashed lines. Since these tests contain CIP decks, concrete material properties were used in calculating the left side of the AASHTO equation in figure 6. The concrete and stud portions were determined to be 280 and 177 kips, respectively.[3] The shear studs governed the design strength.

[3]The value of 280 kips is based on an average measured elastic modulus of the CIP of 5,700 ksi.

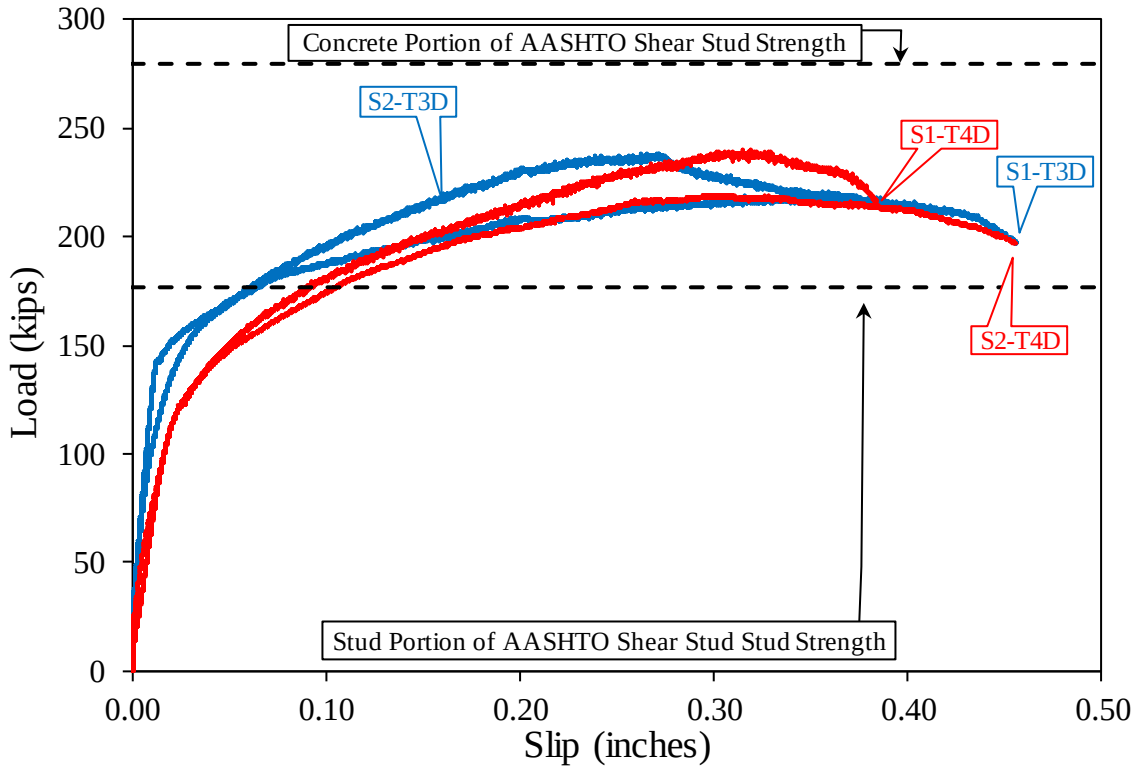

Source: FHWA.

Figure 94. Graph. Load–slip data for small-scale static tests with transversely spaced shear studs and CIP decks.

In terms of maximum load, the test data shown in figure 94 are relatively consistent. Unlike the longitudinal spacing tests, these studs were transversely spaced and only varied from 3*d* to 4*d* rather than from 3*d* to 6*d*. These test data were also probably more consistent because there was a greater amount of concrete in front of the shear studs, so the distribution of coarse aggregates in the concrete was not as critical. All four of the test results had maximum loads greater than the calculated strength from figure 6. Table 17 shows the maximum loads for the test results.

Table 17. Small-scale static test results with transversely spaced studs and CIP decks.

Specimen	Transverse Shear Stud Spacing	Maximum Load (kips)	Slip at Maximum Load (Inches)	Failure Mode	Performance Ratio to AASHTO Stud Limits
PO-S1-T3D-CIP	3*d*	219.6	0.35	Stud shear	1.24[a]
PO-S2-T3D-CIP	3*d*	238.2	0.27	Stud shear	1.35[a]
PO-S1-T4D-CIP	4*d*	240.0	0.32	Stud shear	1.36[a]
PO-S2-T4D-CIP	4*d*	219.2	0.31	Stud shear	1.24[a]

[a]Calculated by dividing maximum load for the specimen by 177 kips since specimen failed via stud shearing.

Since visual inspection showed that all of the specimens failed because of shear stud shearing, the performance ratios shown in table 17 all compare the maximum load to the shear stud limit portion of figure 6. All of performance ratios are greater than 1.00, which indicate figure 6 can be used to predict a shear stud's strength when the transverse spacing of shear studs is reduced to 3*d* and the studs are encased in concrete.

Figure 95 shows the load–slip results for the four small-scale static tests with PC decks and transversely spaced shear studs. The grout and shear stud portions of figure 6 are also indicated in the figure as dashed lines at 161 and 177 kips, respectively.[4]

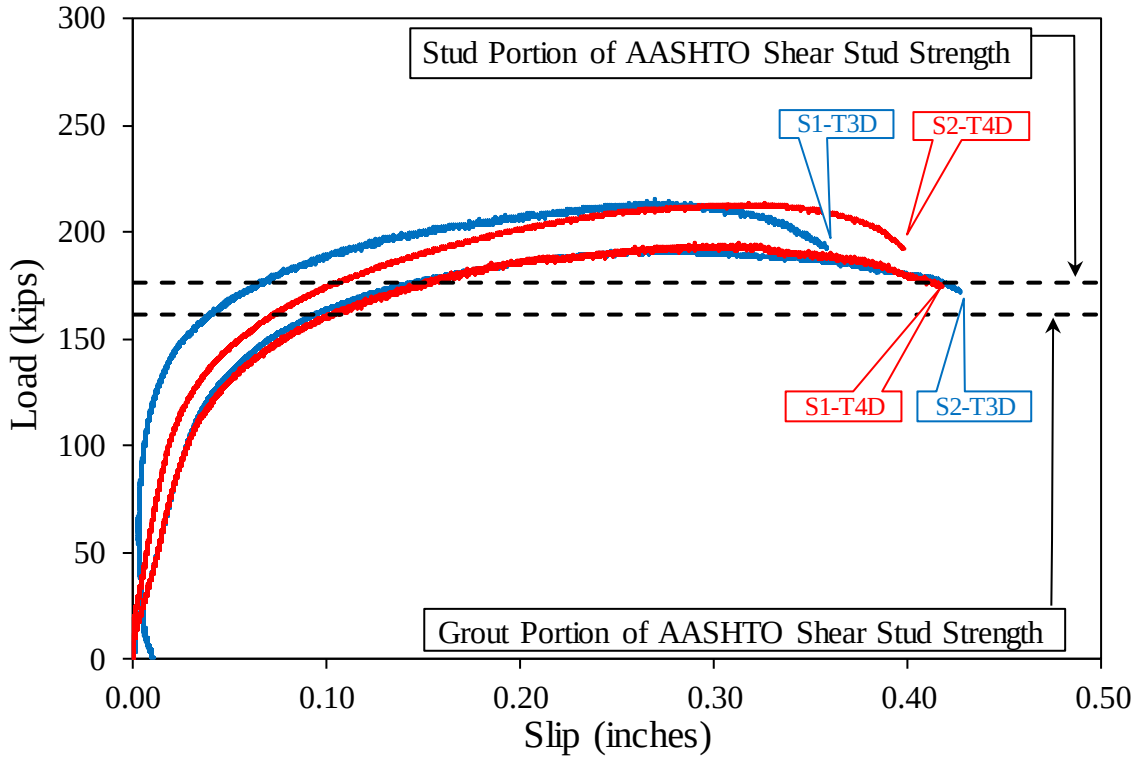

Source: FHWA.

Figure 95. Graph. Load–slip data for small-scale static tests with transversely spaced shear studs and PC decks.

Similar to the CIP decks, the PC static tests with transversely spaced studs were also relatively consistent and behaved as expected. As the figure shows, all of the specimens had maximum loads greater than those predicted by figure 6. Table 18 shows the maximum loads reached by the four PC specimens as well as the failure modes and performance ratios.

[4]The value of 161 kips is based on an elastic modulus of 2,300 ksi for the grout. This value was calculated in prior FHWA research that used same grout product as in this study.(34)

Table 18. Small-scale static test results with transversely spaced studs and PC decks.

Specimen	Transverse Shear Stud Spacing	Maximum Load (kips)	Slip at Maximum Load (Inches)	Failure Mode	Performance Ratio to AASHTO Stud Limits
PO-S1-T3D-PC	3*d*	215.4	0.27	Stud shear	1.34[a]
PO-S2-T3D-PC	3*d*	191.3	0.28	Stud shear	1.19[a]
PO-S1-T4D-PC	4*d*	194.9	0.31	Stud shear	1.21[a]
PO-S2-T4D-PC	4*d*	213.6	0.33	Stud shear	1.33[a]

[a]Calculated by dividing maximum load for the specimen by 177 kips since specimen failed via shear stud shearing.

Visual inspection after testing revealed that all four of these specimens failed because of shear stud shearing, so the performance ratios were calculated by comparing the maximum load to the predicted strength from the shear stud portion of figure 6. All of the performance ratios are greater than 1.00, which shows that figure 6 can be used to predict a shear stud's strength when the transverse spacing of shear studs is reduced to 3*d* and the studs are surrounded by grout.

Summary of Small-Scale Static Tests

The team conducted a total of 24 small-scale static tests with shear studs spaced longitudinally and transversely. Longitudinal spacings of 3*d*, 4*d*, 5*d*, and 6*d* were tested, while only transverse spacings of 3*d* and 4*d* were tested. Tests were conducted for both CIP concrete decks and PC decks grouted into place. The intent of the testing was to determine if current AASHTO longitudinal and transverse spacing limitations could be relaxed.

Technically, for the longitudinal spacings investigated, a 3*d* spacing could be tolerated based on the test results. However, because the actual capacity of the CIP deck specimens at this spacing was so close to the calculated capacity, the team recommends that minimum longitudinal spacing only be reduced to 4*d*. This recommendation would apply to both CIP and PC decks. All of the transversely spaced specimens produced acceptable performance ratios at both of the tested spacings and for both deck types. The team recommends that minimum transverse shear stud spacing be reduced to 3*d*.

ANALYSIS

SUMMARY OF FATIGUE TEST RESULTS AND COMPARISON TO HISTORICAL DATA

This section presents a summary of all the fatigue tests conducted in this research project and a comparison with existing historical data. All of the fatigue tests, both large- and small-scale, were conducted to evaluate whether the current AASHTO shear stud–fatigue design provisions were too conservative and, if so, to develop a proposed alternative fatigue design curve.[(1)] The independent analysis results from both the large- and small-scale tests showed that the AASHTO shear stud–fatigue design provisions appears conservative, especially at higher cycle counts.[(1)] Figure 96 shows an S-N plot of the regression lines for the large- and small-scale test results as well as the shear stud–fatigue design provisions for the AASHTO LRFD BDS and Eurocode.[(1,8)]

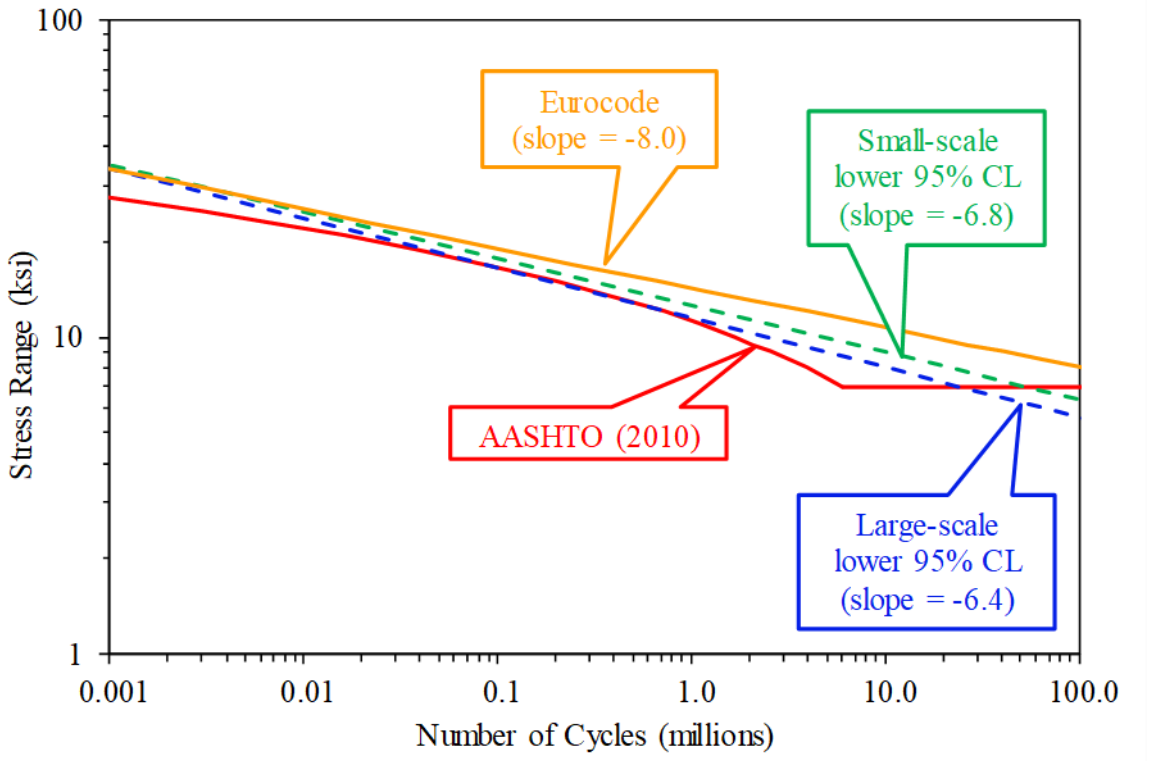

Source: FHWA.

Figure 96. Graph. Comparison of S-N data between current test data and specifications.

When comparing the large- and small-scale test results in the figure, it is clear that the slopes of the regression lines of the two data sets are similar at −6.4 and −6.8, respectively. This is interesting because the two tests were thought to have different loading mechanisms; previous assumptions considered shear studs in the large-scale tests loaded in a combination of shear and bending, while studs in the small-scale tests were thought to be loaded in pure shear. The similar slopes suggest that the loading between the two types of tests may be similar and that the fatigue cracking of the shear studs in both instances may be driven predominantly by shear stresses. The researchers also noted that the small-scale regression lines fell above the large-scale regression

lines, meaning the small-scale tests produced longer fatigue lives. This is as expected because of the size effect when conducting fatigue tests.

In addition to comparing the large- and small-scale fatigue tests in the current study, the team compared this study's results with known historical fatigue tests conducted on shear studs. To be included for comparison to the large-scale tests, historical tests must have been conducted on a large-scale steel girder with a composite concrete deck and shear studs of a similar diameter that provided composite action. This requirement excluded any beams constructed using any other means of composite action, such as channels, hooked studs, bent studs, reinforcing bars, and threaded rods, that were either welded or mechanically fastened to the steel beam. While these other means of composite action may have merit, the current study focused on the use of traditional shear studs. The test beams also must not have been constructed with a ribbed steel deck pan since the researchers expected the ribs to alter the behavior and horizontal shear stress distribution of shear studs, thereby affecting the fatigue performance of the shear studs. This consideration was also justified since ribbed steel deck pans are typically not continuous over the flange for steel bridge construction. The last primary consideration was that the large-scale beams tested must have produced a fatigue failure in the shear studs. Many research projects have been conducted in which beams with shear studs were cycled for a predetermined cycle count, such as 2 million cycles, and then were statically tested to failure. Tests such as these were not included in the comparison because they did not produce a data point on an S-N plot and, thus, could not be included in a fatigue linear regression analysis.[18,35]

There were only two known prior studies on large-scale tests that met the stated criteria. One study was done by Toprac in 1965 on seven 36-foot-long composite beams with ¾-inch-diameter shear studs.[6] Toprac gave cycle counts for multiple failure definitions, including when the first shear stud failed, when the first pair of studs failed (studs were placed in pairs across the flange), and when the beam experienced a complete loss of composite action. The last measurement was used as a means of comparison to the current study because it was most similar to this study's failure definition. Of the seven beams tested in Toprac's study, four had good welds on the studs, while the other three had poor quality welds. However, when all seven data points were plotted on an S-N plot, there did not appear to be any difference in the fatigue behavior between any of the seven beams other than typical fatigue scatter; therefore, all seven data points were included in the comparison.

The other known study that fit the criteria was done by King et al. in 1965 on eight 15-foot-long composite beams with ½-inch-diameter shear studs.[5] Similar to Toprac, King et al. provided multiple fatigue failure definitions. In this case, there were two: the beam was considered failed when the first pair of studs failed or when there was a complete loss of composite action. The latter definition was used in the comparison to this study. However, once King et al.'s data were plotted on an S-N curve with the data from the current study and Toprac, it was clear that there was a size effect; the data from King et al. plotted higher than the other data sets. Because the King et al. studs were much smaller in diameter, they probably had less residual stress, and scaling effects led to longer fatigue lives. For this reason, the data from King et al. were discarded from the comparison.

The data from the current study and Toprac were combined on an S-N plot shown in figure 97. A regression analysis was also conducted on the combined test results. The line for the lower 95 percent CL is shown in the equation in figure 98. Toprac's S-N data are shown in tabular form in appendix H.

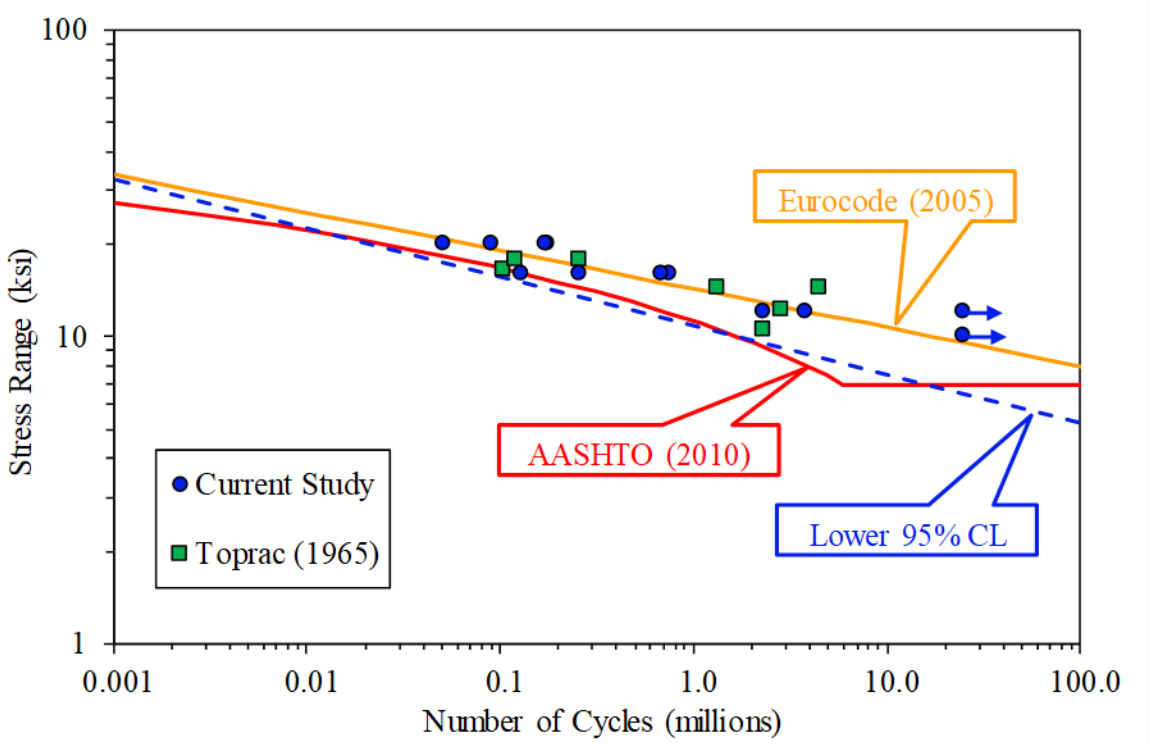

Source: FHWA.

Figure 97. Graph. Comparison of large-scale shear stud S-N results between current and historical test data.

$$S_{r,HLS,95} = \left(\frac{32{,}600 \times 10^8}{N}\right)^{\frac{1}{6.3}}$$

Figure 98. Equation. Equation of lower 95 percent CL using large-scale fatigue test results from current study and historical data.

Where $S_{r,HLS,95}$ is the shear stress range acting on studs using a lower 95 percent CL for the historical large-scale fatigue tests (ksi).

Based on figure 97, the two data sets appear quite similar, thus lending validity to completing a regression analysis on the combined data set. Using the combined data set allows for a greater number of data points to be included in the analysis, which should make it more accurate. The slope of the lower 95 percent CL regression line is −6.3, which is similar to the slope of −6.4 of the regression line for the large-scale test results from this study. The regression line of the combined data set is shifted down slightly from the regression line for the large-scale tests from this study only. This is noted by the difference in the fatigue constants of the two equations; 57,700 in figure 61 and 32,600 in figure 98.

The current AASHTO LRFD BDS shear stud–fatigue design provisions were shown to be conservative at higher cycle counts.[1] Therefore, the team recommends the lower 95 percent CL regression line for this combined data set as a proposed alternative fatigue design curve. This curve provides more realistic expected fatigue lives than the current AASHTO fatigue design curve, especially at longer fatigue lives. This proposed fatigue design curve still falls below the Eurocode design provisions, so it is still expected to be reasonably conservative while allowing slightly relaxed fatigue limit state provisions.[8]

The team recommends that the current AASHTO shear stud–fatigue CAFT of 7.0 ksi remain as is. As mentioned in the Introduction of this report, analysis of recent push-out fatigue tests has confirmed this value.[12] The cycle count at which the CAFT would govern the fatigue design, however, would change with the recommended fatigue design curve. According to the current AASHTO LRFD BDS, finite life design is applicable until 5,973,350 cycles. At this point, infinite life design governs, and the CAFT of 7.0 ksi would be used for fatigue design of the shear studs. Using the proposed fatigue design curve in figure 98 instead, the cycle count at which the design would change from finite to infinite would be 15,456,093 cycles. As shown in figure 96, this is the point at which the proposed fatigue design curve and the CAFT of 7.0 ksi intersect.

Similar to the large-scale fatigue test results, the small-scale data were also compared to historical data. Researchers developed a set of criteria for historical data as with the large-scale tests. The historical small-scale tests must have been conducted on steel beams with composite concrete decks with shear studs of a similar diameter. Again, this requirement excluded other means of composite action, such as channels and threaded rods. The specimens also must not have been constructed with a ribbed steel deck pan and must have produced a fatigue failure. One new requirement specific to small-scale tests was that they must have been conducted on two-sided push-out specimens. As noted previously, an analytical study showed that one-sided push-out tests can induce up to 20 percent more tensile forces in the shear studs, which causes a reduction in the fatigue life.[31] Because of this requirement, the team excluded the data used to develop the current AASHTO shear stud–fatigue design provisions, as well as other push-out tests constructed with PC concrete deck panels.[4,18]

With these criteria in place, the team identified 12 other studies with a total of 116 push-out tests. Overall, these included tests using shear studs with a diameter from 0.39 to 1.25 inches; those constructed with lightweight concrete; and those with one, two, or four shear studs per specimen side. Individual test data from each of these studies are shown in appendix H. One study that appeared to meet the criteria but was not included in the comparison was done by Mainstone and Menzies.[36] When the test results from this study were plotted on a common S-N plot, it was clear that study produced failures with significantly shorter fatigue lives than any of the other data. The authors of this report are unsure of the cause of this discrepancy, but nonetheless the Mainstone and Menzies data were characterized as outliers and were removed from the data set.

The data from the current study and the historical push-out fatigue data were combined on an S-N plot shown in figure 99. A regression analysis was also conducted on the combined test results. The equation for the line for the lower 95 percent CL is shown in figure 100.

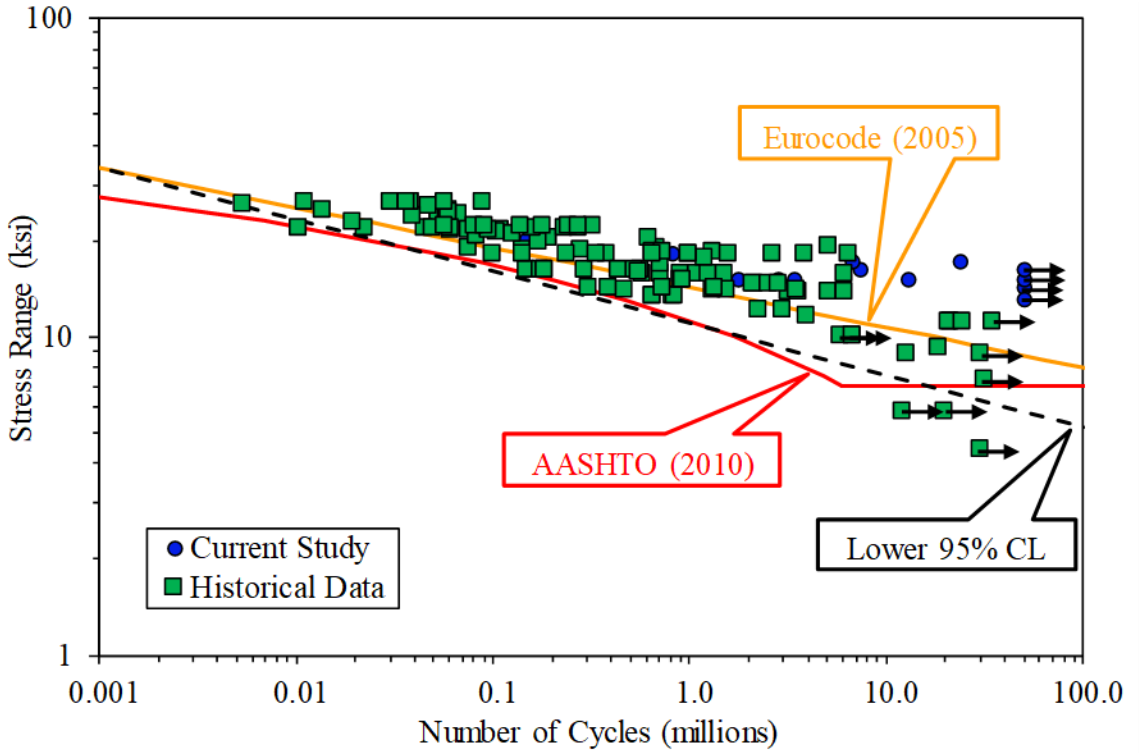

Source: FHWA.

Figure 99. Graph. Comparison of small-scale shear stud S-N results between current and historical test data.

$$S_{r,HSS,95} = \left(\frac{24{,}500 \times 10^8}{N}\right)^{\frac{1}{6.1}}$$

Figure 100. Equation. Equation of lower 95 percent CL through small-scale fatigue test results from current study and historical data.

Where $S_{r,HSS,95}$ is the shear stress range acting on studs for small-scale tests based on a lower 95 percent CL using the historical small-scale fatigue tests (ksi).

In figure 99, the S-N results from the current study and the historical data appear similar, as expected, when compared to the equation in figure 84 that was based only on the current study data. The slope of the entire data set was found to be −6.1, compared to the slope of −6.8 for the results of the current study only. However, the line intercepts are different, with the current study data producing a constant of 276,200, and the entire data set producing a constant of 24,500.

To contrast any differences between large- and small-scale testing effects, figure 101 shows a comparison between the lower 95 percent CL regression lines of the combined data sets for both large- and small-scale shear stud–fatigue data (equations shown in figures 98 and 100).

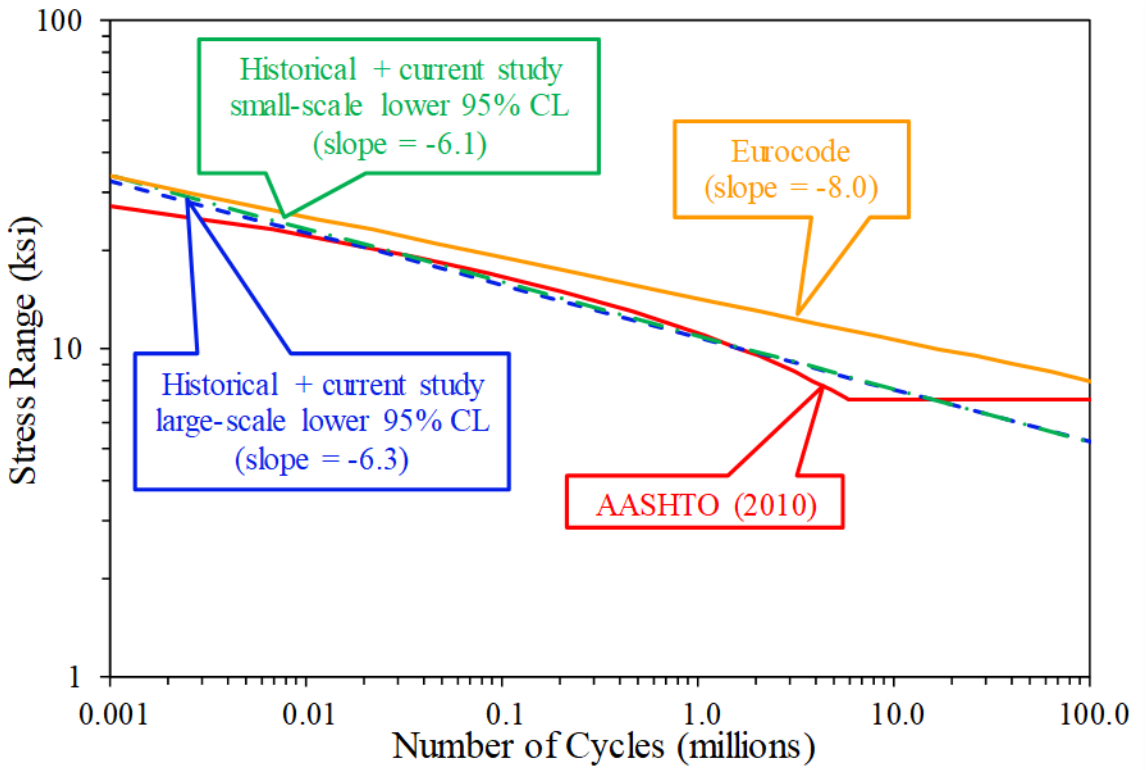

Source: FHWA.

Figure 101. Graph. Comparison of lower 95 percent CL regression lines between historical large- and small-scale shear stud–fatigue data.

When comparing the large- and small-scale data sets, the lower 95 percent CL regression lines are nearly identical. The slopes of the lines between the large-scale (−6.3) and small-scale (−6.1) data are even more similar in the combined data set than when only using data from the current study. The close similarity of the regression lines suggests that two-sided push-out tests can be used to accurately simulate large-scale testing of shear stud–fatigue behavior. This also reinforces the notion that fatigue cracking of shear studs in large-scale beams is driven by shear stresses.

In terms of shear stud–cluster spacing, the large-scale fatigue test specimens were constructed with spacings of 12, 24, 36, and 48 inches. In examining the totality of the test data, the shear stud–cluster spacing did not appear to have any negative impact on the fatigue performance of the beams. There were slight differences in the slip and uplift behavior of the 36- and 48-inch spacing test beams, but this difference in behavior did not affect the fatigue performance of the beams. Using PC concrete deck panels connected to steel girders via grouted pockets for both the large- and small-scale fatigue tests also did not cause any undesired fatigue behavior. Because of the successful fatigue performance of the extended shear stud–cluster spacings and PC deck construction of the test specimens, the current and proposed AASHTO fatigue design provisions for shear studs can be applied to PC concrete deck systems used for ABC.

SUMMARY OF STATIC TEST RESULTS AND COMPARISON TO HISTORICAL DATA

This section presents a summary of all the static tests conducted in this research project and a comparison to existing historical data. The large- and small-scale static tests were conducted to evaluate whether the current AASHTO shear stud–strength design provisions were unconservative and, if so, develop recommendations for proposed design provisions.

The five large-scale static test specimens were designed to induce a horizontal shear failure along the welded interface between the shear studs and the top flange of the steel beam. Of these five tests, only one (beam 1S1) failed initially because of horizontal shear; the remaining tests failed because of concrete crushing at the midspan, although the shear studs in another beam (3S1) did fail soon after an initial grout crushing failure. Of the five beams tested, none exceeded their M_n. The shear factors—defined as the factor applied to a shear stud's resistance to match the applied moment to the calculated moment capacity of the beam—in the five beams ranged from 0.71 to 0.86. Note that beam 1S1 did produce a horizontal shear stud failure, so its shear factor of 0.71 is directly applicable. The other beams initially failed because of concrete crushing, so their shear factors are minimum values.

As with the fatigue tests, the team defined criteria to select historical data for comparison to the large-scale static test results from this study. The historical static testing must have been conducted on a large-scale steel girder with a composite concrete deck with round, unbent shear studs and completed in positive flexural bending with simple support conditions. The beams must not have been constructed with a ribbed steel deck pan since this is known to affect the strength of shear stud connections. Since the beams in this study were constructed without any PT on the concrete deck and PT would probably alter the static behavior during testing, beams utilizing PT were not considered. This precluded one study on the composite behavior of shear studs that were used as a means of providing composite action to PC concrete decks.[35] Another requirement was that the static tests must have been conducted on beams that had not been subject to damage from previous loading. This requirement excluded two other studies in which either static or fatigue tests had been conducted on the beams prior to the static loading to failure.[18] The last consideration was that the composite beams must have been designed such that the strength of the steel shear studs controlled the moment capacity of the beams; this is important for calculation of shear factors. This requirement implies that the beam(s) tested must be partially composite since this is the only way that the shear studs can govern the moment capacity of a composite beam.

One study that fit the criteria was completed in 2013 at the University of Auburn.[37] In this study, four 34-foot-long composite beams were statically tested to failure. Two of the beams used traditional ⅞-inch-diameter shear studs, while the other two used 1¼-inch-diameter studs. One beam for each shear stud diameter size had a shear stud spacing of 2 ft, while the other two beams had shear stud spacings of 4 ft. The beams were designed for approximately 84–92 percent composite action. During the static testing, all four beams failed owing to concrete crushing at the midspan and did not experience any shear stud failures. Two of these beams exceeded their calculated moment capacities by approximately 1–2 percent. The other two beams (specimens 3 and 4) experienced maximum moments of approximately 2–3 percent less than their calculated moment capacities. Shear factors were calculated to be approximately 0.70 and

0.76 for specimens 3 and 4, respectively. It is important to note that these are minimum values, however, since the beams failed because of concrete crushing and not because of a shear stud failure.

Based on the large-scale static tests conducted in this study and results found in the literature, the team recommends a factor of 0.70 be applied to the strength design equation of a shear stud within the AASHTO provisions. This value conservatively takes the lower bound of the test data. It also signifies that shear studs are loaded in a combination of bending and shear rather than pure tension as the current AASHTO shear stud–strength design provisions imply. Some international shear stud–strength design provisions include a factor of 0.80, similar to the value of 0.70 recommended here.

The large-scale tests were conducted with shear stud–cluster spacings of 12, 24, 36, and 48 inches. The static test results showed no negative impact on the strength behavior of the beams with the extended cluster spacings. There were no noticeable differences in the slip and uplift behavior between any of the cluster spacings in the large-scale static tests.

The small-scale static tests were conducted to evaluate the minimum longitudinal and transverse spacing limits in the AASHTO shear stud provisions. Both CIP and PC specimens were tested to evaluate these spacing limits from a strength perspective. Static tests with longitudinally spaced shear studs showed that the minimum longitudinal spacing can be reduced from 6*d* to 4*d*. When the longitudinal spacing was reduced to 3*d*, the shear stud strength was nearly identical to its calculated resistance for CIP decks, hence the recommendation of 4*d*. The specimens with transversely spaced shear studs showed that the minimum transverse spacing can be reduced from 4*d* to 3*d* and still meet the assumed strength requirements of a shear stud connection.

The team compared the small-scale static tests to previous projects that investigated variable shear stud spacing. Again, the team defined criteria to select historical data for comparisons. The push-out tests must have been constructed with a steel beam, two concrete decks (two-sided), and no ribbed deck. Shear studs must have been used to provide composite action between the steel beam and concrete decks. Using these criteria, three studies that investigated longitudinal shear stud spacing were compared to the results in this study.

One was conducted in Japan and included 12 push-out tests constructed with CIP concrete decks.[25] The specimens had longitudinal shear stud spacings of 16*d*, 11.4*d*, and 5*d*. The static test results revealed that the 5*d* spacing specimens had a strength of approximately 5 percent lower than the 16*d* specimens. Analytical analyses were also conducted using finite element modeling. The analytical models consisted of specimens with longitudinal shear stud spacings of 13*d*, 11*d*, 9*d*, 7*d*, 5*d*, 4*d*, and 3*d*. The analytical results were compared using the 13*d* spacing as the baseline and are thus expressed in percentages of the 13*d* specimen strength. The results showed that the 9*d* specimens reached loads of approximately 90–95 percent, the 5*d* specimens reached loads of approximately 82–91 percent, the 4*d* specimens reached loads of approximately 79–89 percent, and the 3*d* specimens reached loads of approximately 77–87 percent of the 13*d* specimens. The variation of the test results at a particular shear stud spacing were caused by a difference in concrete strength. Clearly the 3*d*, 4*d*, and 5*d* specimens produced lower loads than the specimens with greater spacings; when compared to each other, the 3*d* specimens produced approximately 10–20 percent lower loads compared to the 5*d* specimens.

Another study was conducted at Chung-Ang University in South Korea.[26] This test program was conducted on push-out specimens constructed with PC concrete slabs. The PC slabs were then grouted in place and connected to the steel beam via a shear stud. The specimens had longitudinal shear stud spacings of 3*d*, 4*d*, and 5*d*. The results of the static tests showed that the specimens with spacings of 4*d* had approximately 75 percent of the strength of the 5*d* specimens, while the 3*d* spacing specimens had a strength of approximately 70 percent of the 5*d* specimens. Unfortunately, no experimental test loads were provided in the study so the strength resistance of the specimens could not be compared using the AASHTO shear stud–strength design provisions. The study did provide an equation for a strength reduction factor to apply to the connection where the longitudinal shear stud spacing was less than 5*d*.

Push-out tests were also conducted at Ryerson University as a means of connecting PC concrete bridge decks to steel girders.[38] The push-out tests included specimens with PC decks, CIP decks, and those with regularly spaced shear studs and clustered shear studs. The regularly spaced studs were placed at a longitudinal spacing of 16.7*d* while the studs within clusters were placed at spacings of 4.2*d*. Instead of using grout, normal concrete was used to fill the shear pockets as a means of connection to the shear studs. The PC specimens with the shear stud clusters sustained nearly the same load as specimens with CIP decks and regularly spaced studs. This showed that the difference between 16.7*d* and 4.2*d* longitudinal spacing of the shear studs had a negligible effect on the strength of the connection.

Based on these three referenced studies, when reducing the longitudinal shear stud spacing from a greater distance (e.g., 16*d*) to a shorter distance (e.g., 4*d*), a small reduction in strength could occur, but not in all cases. However, there was sufficient evidence to determine that when reducing the longitudinal spacing from 5*d* to 3*d*, a strength reduction of 10–30 percent was likely. This matched test results in the current study. Although the referenced studies did not speculate why this occurred, it is likely because the concrete between the closely spaced studs did not develop its full strength. Based on the results of this study and those found in the literature, the team recommends that the minimum longitudinal shear stud spacing be reduced to 4*d* and the minimum transverse shear stud–spacing limit be reduced to 3*d*.

Based on the static tests, all of the current and proposed shear stud–strength provisions in AASHTO appear to be well suited when using PC concrete decks for ABC.[1] The research team proposes increasing the AASHTO maximum longitudinal shear stud–spacing of 48 inches, along with the new proposed minimum longitudinal spacing of 4*d* and minimum transverse spacing limit of 3*d* allowing for PC concrete decks to be designed, detailed, and erected more efficiently.

CONCLUSIONS

The large- and small-scale fatigue and static tests and resulting analyses led to the following conclusions:

- A comparison of historical and current fatigue data on shear studs revealed that the slopes of the linear regression lines were similar between the large-scale (−6.3) and small-scale (−6.1) data sets. The lines were also nearly identical on a typical S-N plot. This signifies that the shear stud–fatigue performance is extremely similar between large-scale composite beams and two-sided push-out tests. Since the small-scale tests are loaded in pure shear, this similarity suggests that fatigue cracking in shear studs on large-scale tests is dominated by shear stresses as well.

- The linear regression analysis and results shown in figure 97 demonstrate that a log-log fatigue design curve with a slope of −6.3 would be appropriate for shear studs. The existing CAFT of 7.0 ksi for shear studs appears reasonable. Given the current AASHTO shear stud design equation is in semi-log format, it yields overly conservative design strengths between 1.7 and 16 million design cycles.

- The AASHTO shear stud–strength design provisions appear to overestimate the capacity of a shear stud, making the provisions unconservative. The large-scale static test results showed that placing a factor of 0.70 in front of a shear stud's strength calculation in the strength limit state would make this provision conservative and more representative of actual behavior seen during testing. Using a factor of 0.70 in the equation implies that shear studs are loaded in a combination of bending and shear rather than in pure tension as the current provision suggests.

- Increasing the maximum longitudinal spacing between shear stud clusters up to 48 inches did not have a negative impact on the fatigue or strength performance of the shear studs. There were differences noted in the slip and uplift behavior in beams with 36- and 48-inch spacings, but these differences were not detrimental to the fatigue or strength performance of the beams.

- The minimum longitudinal shear stud–spacing limit in AASHTO can be safely reduced from 6*d* to 4*d*.[1] The CIP static tests showed that studs can be placed at a spacing of 4*d*, while the PC small-scale static tests showed that shear studs can be placed at a longitudinal spacing of 3*d* and still meet the AASHTO shear stud–strength design requirements. For simplicity's sake, the greater of the two spacings was chosen as the recommended minimum value. There was no strong correlation between failure load and longitudinal shear stud spacings greater than 3*d*.

- The minimum transverse shear stud spacing in AASHTO can be safely reduced from 4*d* to 3*d*. The CIP and PC small-scale static tests showed that shear studs placed at a transverse spacing of 3*d* can meet the AASHTO shear stud–strength provisions. There was no strong correlation between the failure load and either a 3*d* or 4*d* transverse shear stud spacing.

- The large-scale tests of composite beams with PC deck panels and shear pockets showed similar fatigue and strength performance as expected of beams with CIP concrete decks.

RECOMMENDATIONS

The following recommendations were presented to the AASHTO Committee of Bridges and Structures, T-14 Structural Steel Design subcommittee, for potential incorporation into the AASHTO LRFD BDS. Recommendations are in the same order that they would appear in the specification:

1. Consider increasing the maximum center-to-center pitch of shear connectors to 48 inches in AASHTO LRFD BDS section 6.10.10.1.2.[5]

2. Consider decreasing the minimum center-to-center pitch of shear connectors to four shear stud diameters in AASHTO LRFD BDS section 6.10.10.1.2.

3. Consider decreasing the minimum center-to-center transverse spacing of shear connectors to three shear stud diameters in AASHTO LRFD BDS section 6.10.10.1.3.

4. Consider revising the fatigue resistance provisions of shear studs to be written in terms of a horizontal shear stress range rather than a horizontal shear force range, in AASHTO LRFD BDS sections 6.10.10.2 and 6.10.10.3. This revision would make this section similar to the fatigue provisions for typical bridge details other than shear studs, which would make the specifications more consistent throughout.

5. Consider revising the shear stud–fatigue resistance equations in AASHTO LRFD BDS section 6.10.10.2 to follow a similar form to the general fatigue design provisions in AASHTO LRFD BDS section 6.6.1.2.5; this will provide more consistency throughout the specifications. This includes the following considerations:

    a. For infinite life design, use a CAFT as the nominal fatigue resistance, similar to AASHTO LRFD BDS equation 6.6.1.2.5-1. A CAFT of 7.0 ksi is recommended for shear studs.

    b. For finite life design, use an equation similar to AASHTO LRFD BDS equation 6.6.1.2.5-2 to specify the nominal fatigue resistance and the slope of the shear stud–fatigue design curve on an S-N plot. The following equation is recommended:

$$(\Delta F)_n = \left(\frac{A}{N}\right)^{\frac{1}{6.3}}$$

Figure 102. Equation. Recommended shear stud–fatigue design equation.

[5]This report considers the AASHTO LRFD BDS seventh edition as the current edition.(1) By the time of this report's publication, this recommendation was already adopted by AASHTO and implemented in the eighth edition in part because of preliminary test results from this study.(3)

Where:
$(\Delta F)_n$ = nominal fatigue resistance (ksi).
A = fatigue detail constant for shear studs, equal to $32{,}600 \times 10^8$ (ksi^3).
N = number of cycles, determined from AASHTO LRFD BDS Equation 6.6.1.2.5-3.

6. Consider including a factor of 0.70 on the right side of the equals sign in AASHTO LRFD BDS Equation 6.10.10.4.3-1. This side of the equation represents the capacity of the shear stud as part of the nominal shear resistance of the shear stud embedded in concrete (or grout). The following equation is recommended:

$$Q_n = 0.5\, A_{SC} \sqrt{f'_c E_c} \leq 0.7\, A_{SC} F_u$$

Figure 103. Equation. Recommended shear stud capacity equation.

Where:
A_{sc} = cross sectional area of a shear stud (inch^2).
f'_c = concrete design compressive strength (ksi).
E_c = modulus of elasticity of concrete (ksi).
F_u = ultimate strength of shear stud (ksi).

7. Because shear studs may be grouted rather than cast in concrete, guidance must be provided to engineers on whether the E_c term in figure 103 is for concrete or grout. Additionally, and more importantly, the modulus of elasticity is different between normal concrete and grout because of the grout does not contain aggregates. Therefore, the predictive equations for E_c elsewhere in the AASHTO LRFD BDS are not applicable when calculating the modulus of grout. Doing so results in unconservative shear stud capacity using the recommended equation in figure 103.

8. Consider adding commentary resulting from the above changes to aid engineers in understanding the development of the AASHTO LRFD BDS shear stud design provisions.

APPENDIX A. DECK PANEL DRAWINGS FOR LARGE-SCALE TESTS

This appendix contains drawings of the PC concrete deck panels used for the large-scale fatigue and static tests.

GENERAL NOTES:

1. POSITION OF REINFORCEMENT TO BE MAINTAINED WITH THERMOPLASTIC CHAIRS OR PLASTIC TIPPED SLAB BOLSTERS.
2. AIR CONTENT SHALL BE 5.0 – 9.0%.
3. CURING WITH MEMBRANE CURING COMPOUND SHALL CONFORM TO NYSDOT STANDARD SPECIFICATION 711–05/704–03.
4. FORMICA COATED WOOD FORM SHALL BE USED TO FORM BOTTOM AND SIDES OF PANELS.
5. REINFORCEMENT SHALL CONFORM TO ASTM A615 GR. 60 (BLACK), AND MUST COME FROM THE SAME HEAT.
6. (4) ADDITIONAL #8 x 1'–7" REBAR LENGTHS SHALL BE CUT PER EACH 4'–0"x8'–0" PANEL (DESIGN #1 & #2), PER DAY, BUNDLED IN (4) TO A BUNDLE.

DESIGN NOTES:

1. CONCRETE STRENGTH TO BE 6,000 PSI AT 28 DAYS
2. STRIPPING STRENGTH = 3,500 PSI

DIMENSIONAL TOLERANCES:

1. SLAB WIDTH, LENGTH, AND THICKNESS = $\pm \frac{1}{8}$"
2. SPECIAL REINFORCEMENT POSITION: COVER $\pm\frac{1}{8}$" FOR DESIGN #1 & #2 PANELS, & $\pm\frac{1}{4}$" FOR ALL OTHER PANELS. SPACING: SEE SLAB LAYOUTS
3. LOCATION OF INSERTS WITHIN UNITS: $\pm\frac{1}{8}$"
4. LOCATION OF LIFTING DEVICES: ±1"

TABLE OF CONTENTS

SHEET No.	DRAWING No.	TITLE	REVISION No.
1	D1	PRODUCTION NOTE SHEET	0
3	D3		
4	D4	DECK PANEL TYPE #1 DETAILS	0
5	D5	DECK PANEL TYPE #2 DETAILS	0
6	D6	DECK PANEL TYPE #3 DETAILS	0
7	D7	DECK PANEL TYPE #4 DETAILS	0
8	D8	TYPICAL DETAILS	0

TESTING/INSPECTION

DELIVERY SCHEDULE:

1. ALL SLABS SHALL BE DELIVERED TO THE TURNER FAIRBANK HIGHWAY RESEARCH CENTER IN McLEAN, VIRGINIA ON SEPT. 28, 2012.

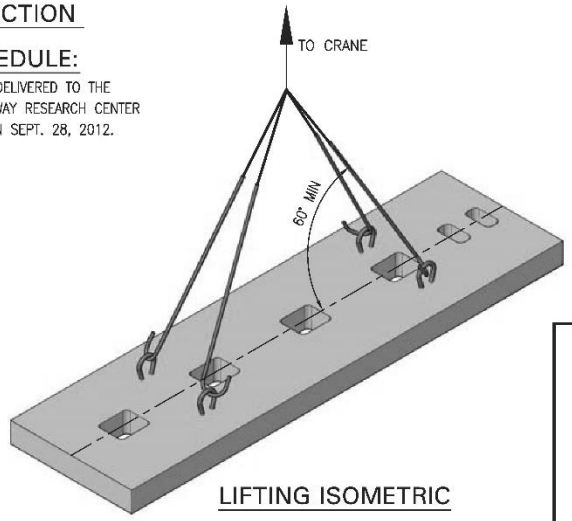

LIFTING ISOMETRIC

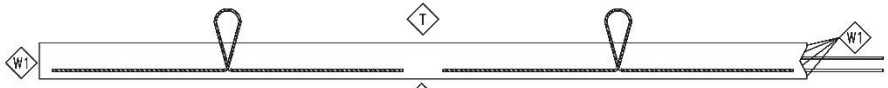

FINISHING SCHEDULE

W1 – FORMICA COATED WOOD FORM

T – (1) PASS HARD STEEL TROWEL

NO.	DATE	BY	DESCRIPTION
1	8/3/12	PJR	PER CONTRACTOR COMMENTS

REVISIONS

FHWA TURNER FAIRBANK
HIGH WAY RESEARCH CENTER
McLEAN, VIRGINIA
PRODUCTION NOTE SHEET

ENGINEER:
FEDERAL HIGHWAY ADMINISTRATION

DRAWN	DATE	CHK'D	SHEET	SCALE	DWG.
PJR	8/2/12	JRO	1	NONE	D1

Source: FHWA.

Figure 104. Schematic. Overview drawing of PC concrete deck panels used for large-scale tests.

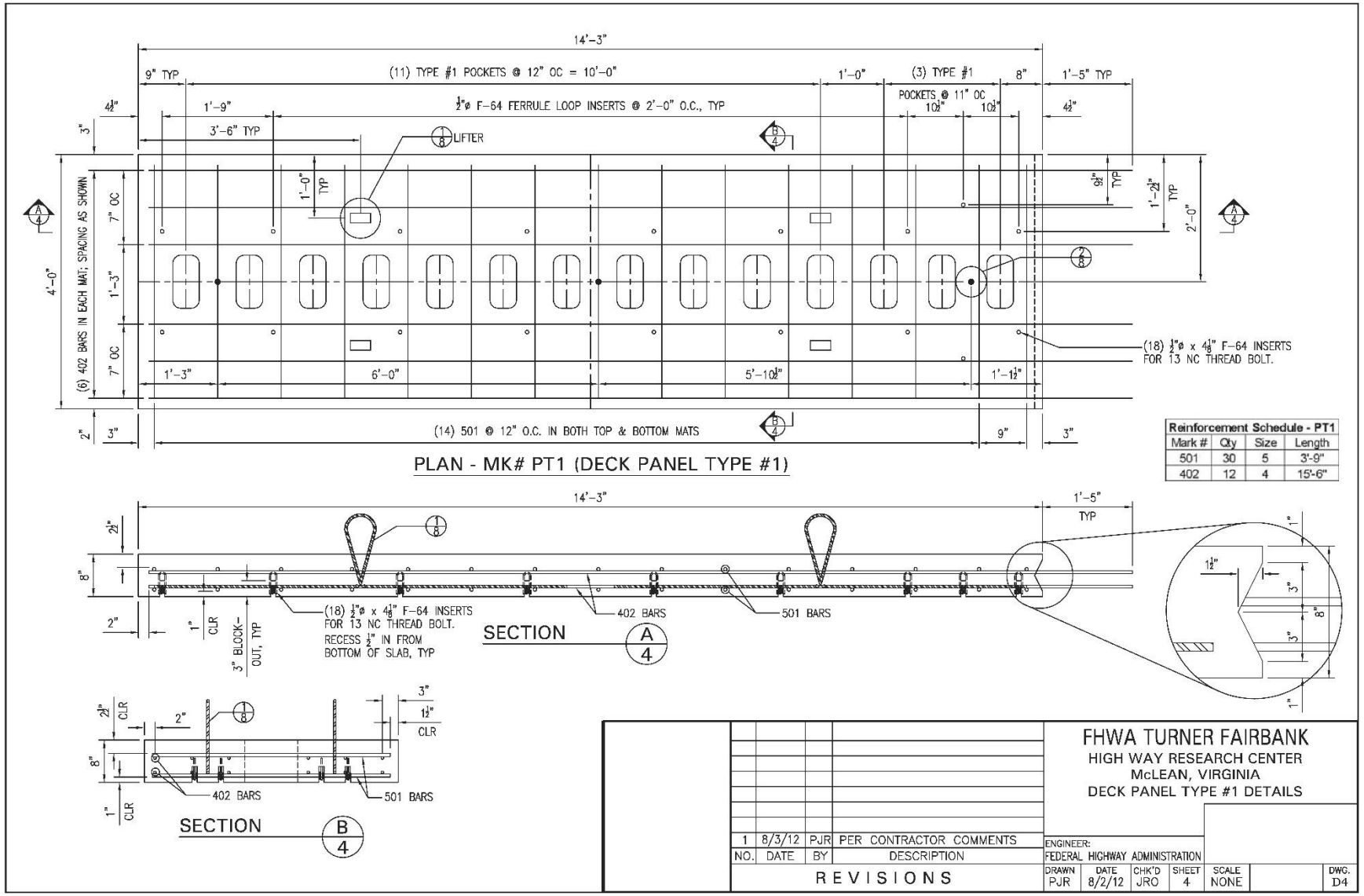

Source: FHWA.

Figure 105. Schematic. Drawing of PC concrete deck panel with 12-inch shear stud spacing.

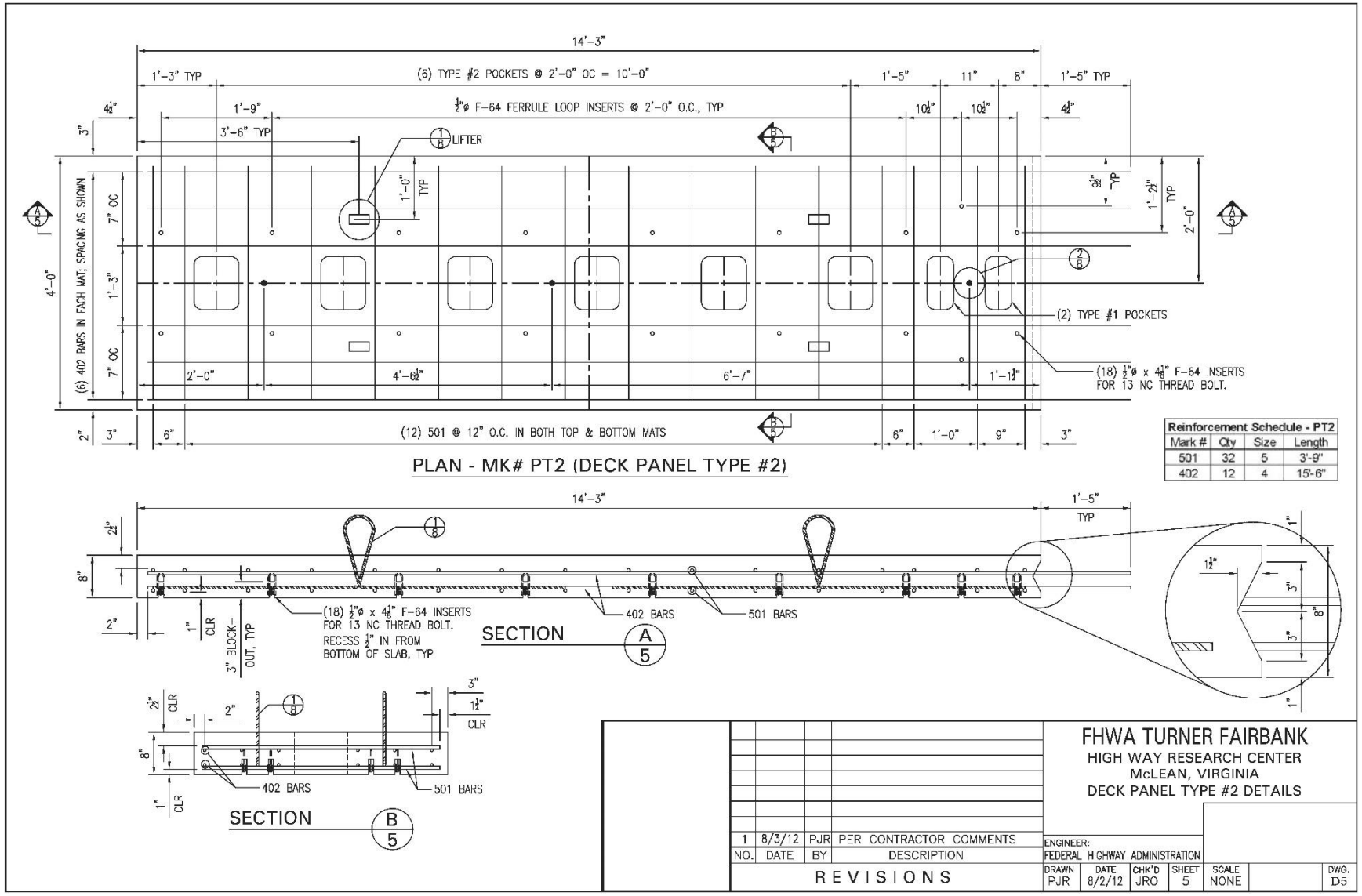

Source: FHWA.

Figure 106. Schematic. Drawing of PC concrete deck panel with 24-inch shear stud spacing.

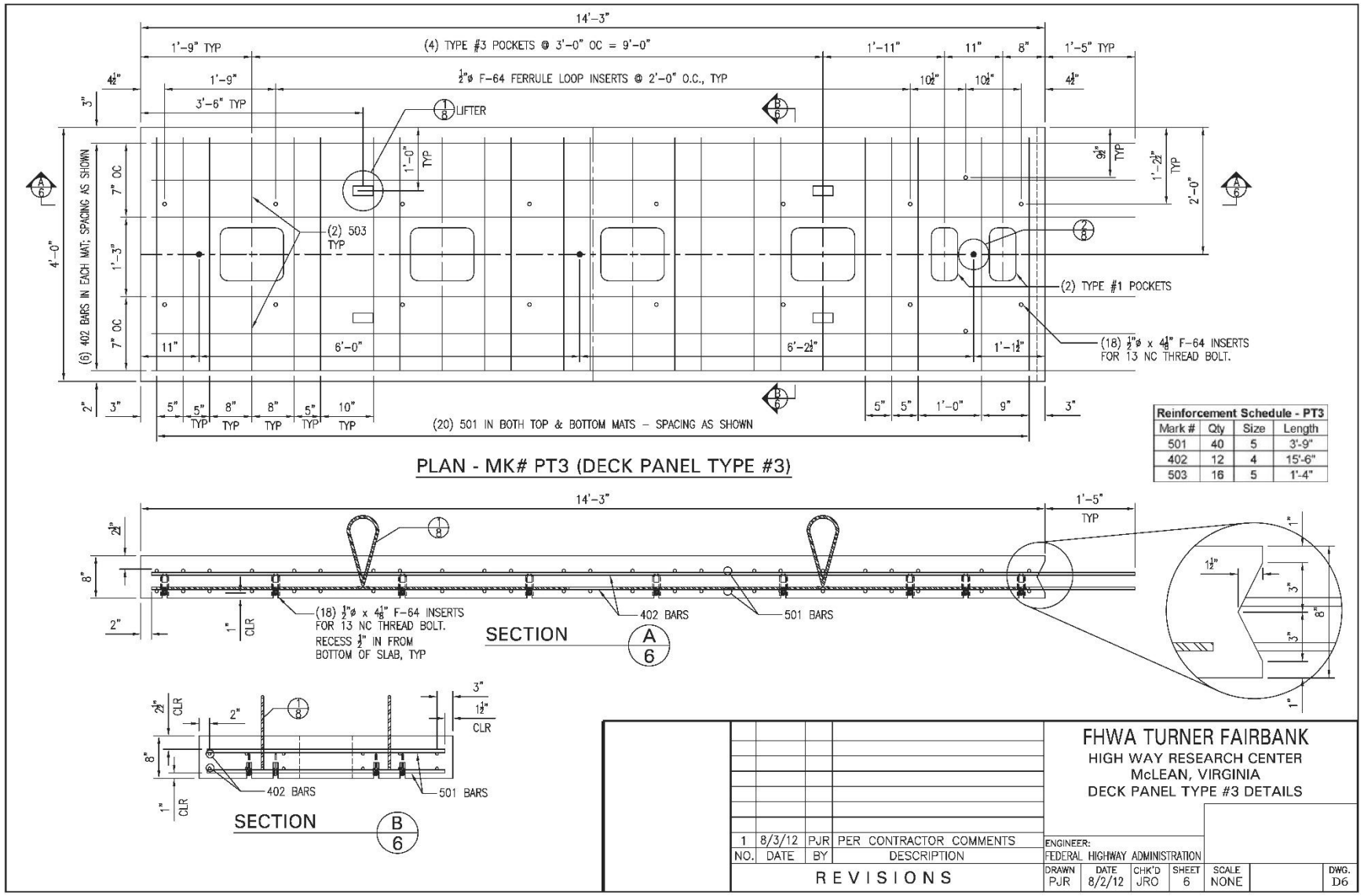

Source: FHWA.

Figure 107. Schematic. Drawing of PC concrete deck panel with 36-inch shear stud spacing.

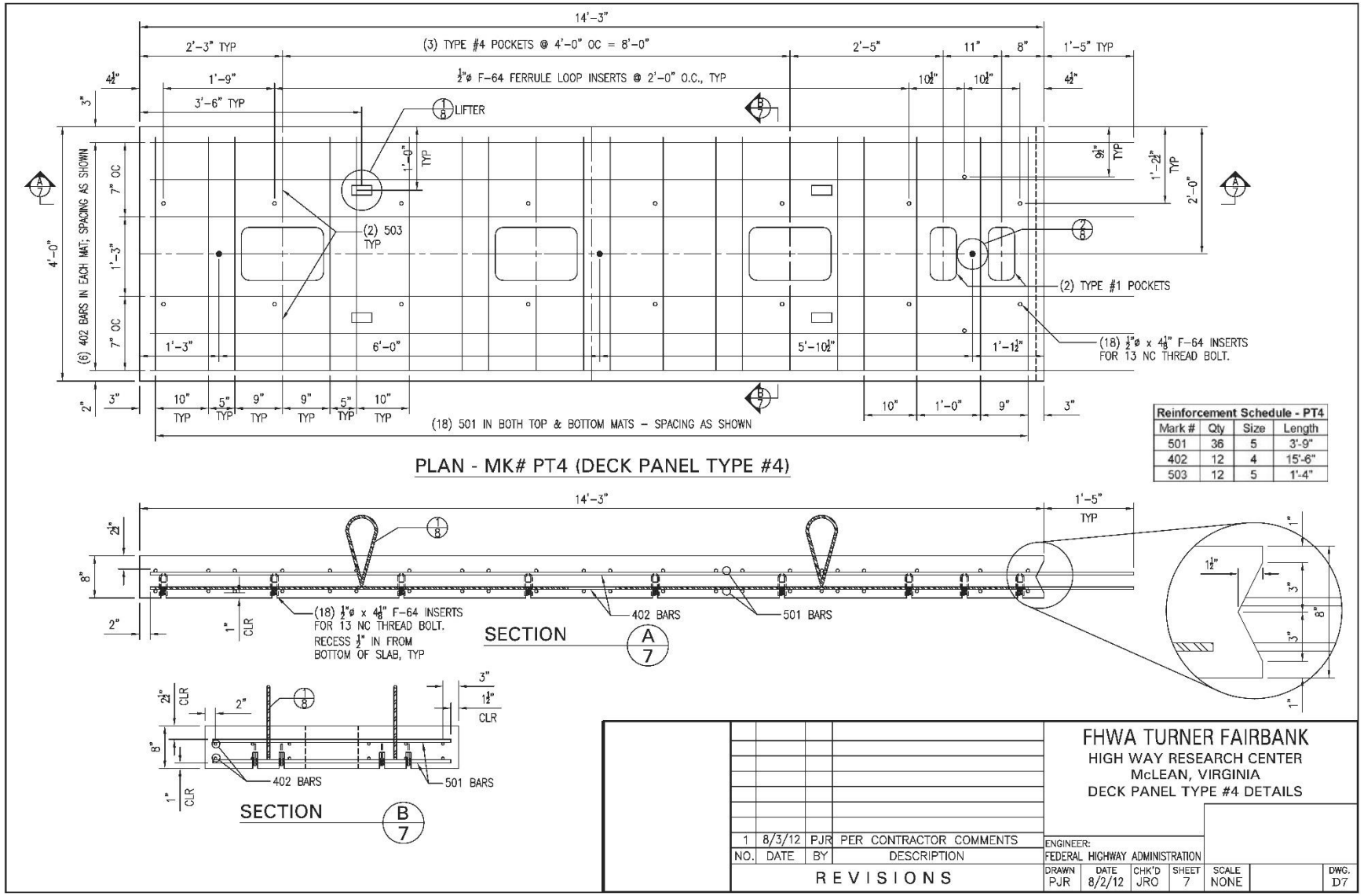

Source: FHWA.

Figure 108. Schematic. Drawing of PC concrete deck panel with 48-inch shear stud spacing.

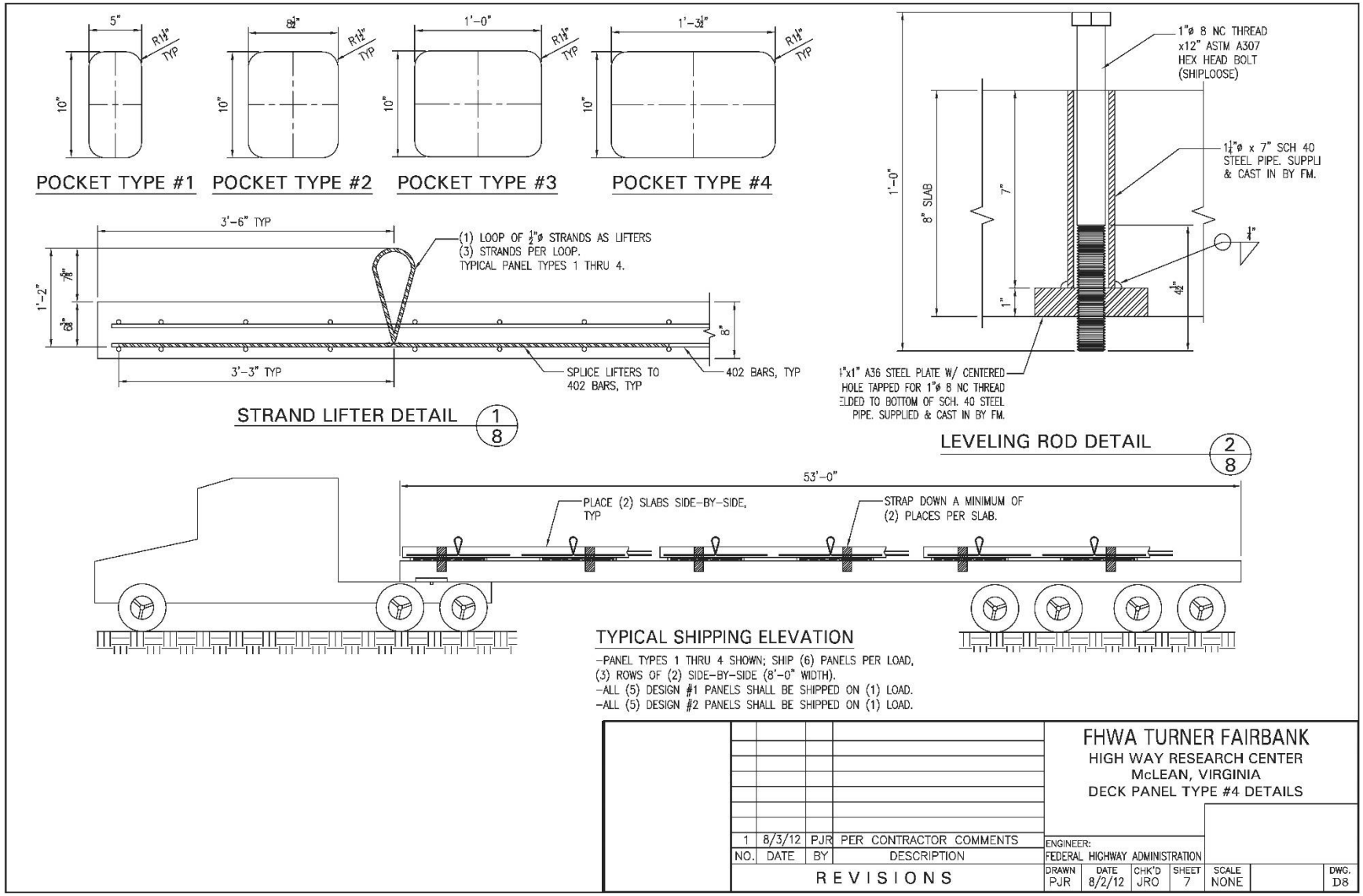

Source: FHWA.

Figure 109. Schematic. Drawing details for PC concrete deck panels.

APPENDIX B. MATERIAL TEST RESULTS

This appendix contains the individual results of steel and cemetious material tests performed in support of this study.

STEEL MATERIAL TESTS

Tensile testing of all steel materials was conducted according to the ASTM A370 specification.[39] Testing was conducted in a servo-hydraulic controlled frame with hydraulic wedge grips using loading rates as prescribed by the ASTM A370 specification.[39] The only deviation from ASTM A370 was a TFHRC preference to also assess static yield related to a Structural Stability Research Council (SSRC) recommendation in the *Guide to Stability Design Criteria for Metal Structures*.[40] SSRC recommends three pauses in loading after yielding to observe the load drop as the material relaxes under 0 strain rate (i.e., static conditions). Holds were maintained for 90 s each. The static yield is included in this appendix for information purposes only; it was defined as the point where the best-fit line through the three static holds intersected the 0.02-percent offset line.

W27x84 Beam Sections

All of the large-scale steel beams were produced from the same heat number, and material properties were assessed from an extra 3-foot-long portion of W27x84 purchased with the beams. Standard ASTM A370, plate-type specimens with an 8-inch gauge length were machined from the flange and web as shown in figure 110.[39] Because the section was deep enough, transversely oriented specimens were made from the web along with the longitudinally oriented specimens in the web and flange. Strain was measured over the 8-inch gauge length using a laser extensometer.

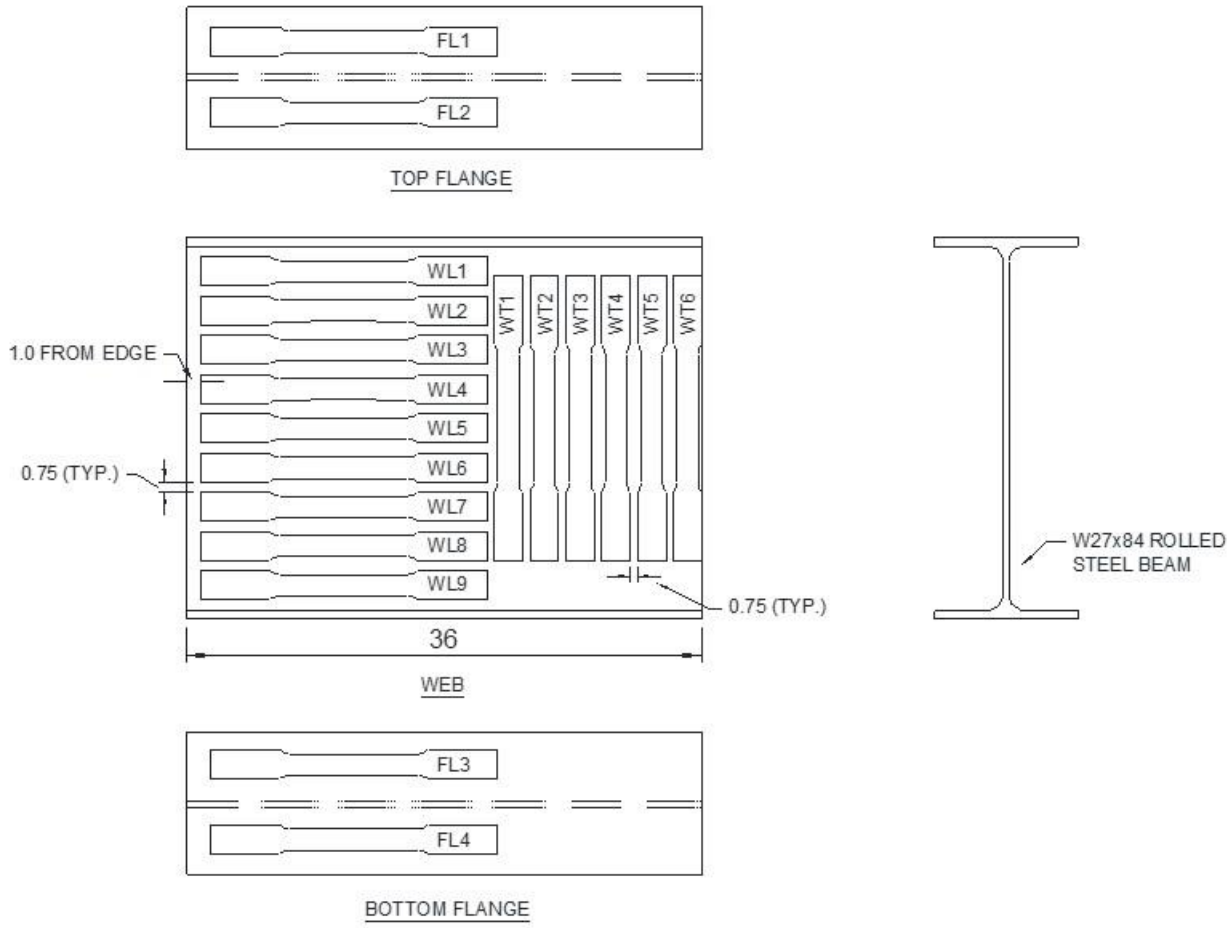

Source: FHWA.
Note: Measurements are in inches.

Figure 110. Schematic. Location of W27x84 tensile test specimens.

The stress–strain curves for the flange specimens are shown in figure 111, longitudinal web specimens in figure 112, and transverse web specimens in figure 113. Most of the stress–strain curves taken from the same sampling location are identical, with the exception of the WL3 and WL9, which were longitudinally oriented specimens from the web. For reasons unknown, both these specimens demonstrated noticeably different yield and tensile strengths from the rest of the population. However, even these two low-strength specimens still met the specification requirements; therefore, this anomaly was not a concern. Table 19 shows a summary of all the tensile test results taken from W27x84.

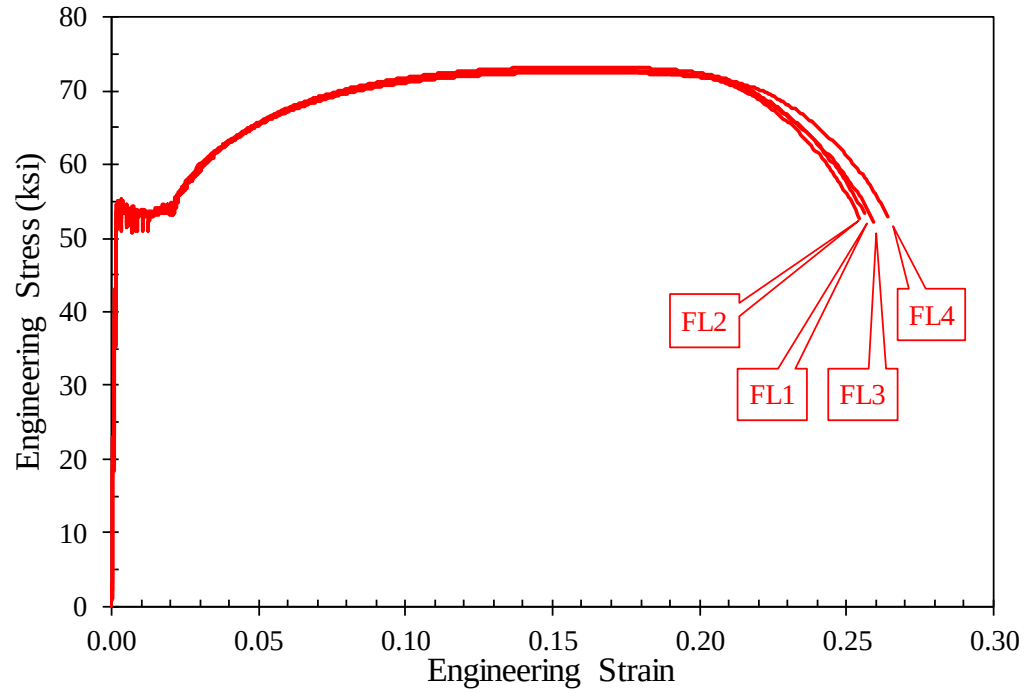

Source: FHWA.

Figure 111. Graph. Stress–strain curves for W27x84 longitudinal flange samples.

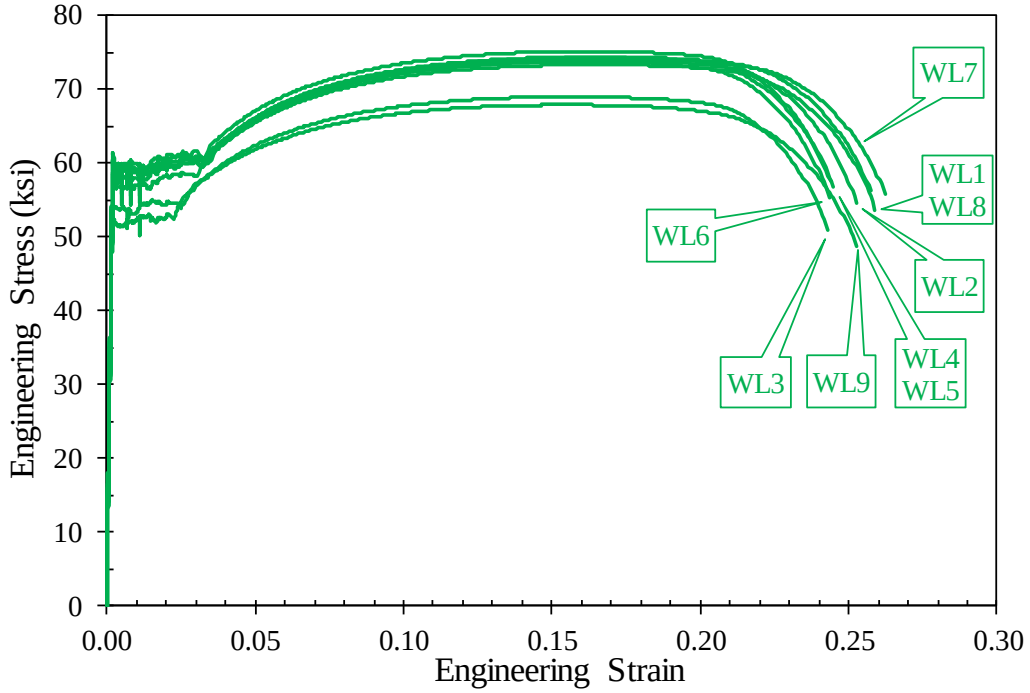

Source: FHWA.

Figure 112. Graph. Stress–strain curves for W27x84 longitudinal web samples.

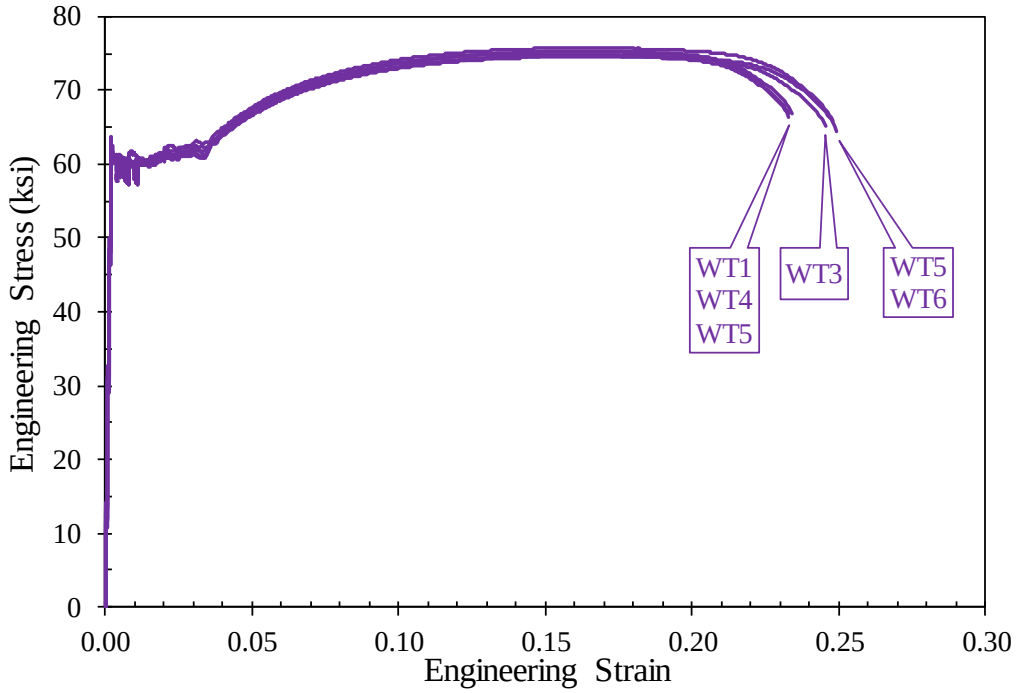

Source: FHWA.

Figure 113. Graph. Stress–strain curves for W27x84 transverse web samples.

Table 19. Summary of W27x84 tensile test results.

Specimen	Static Yield (ksi)	0.2% Offset Yield Stress (ksi)	Tensile Strength (ksi)	Elongation at Fracture (Percent)	Reduction in Area (Percent)
FL1	51.8	54.0	72.9	25	67
FL2	52.5	54.8	73.2	26	65
FL3	51.2	53.6	72.7	26	64
FL4	51.3	53.4	72.5	26	64
FL average	**51.7**	**54.0**	**72.8**	**26**	**65**
WL1	54.4	56.8	73.4	26	75
WL2	55.8	58.1	73.9	25	69
WL3	—	53.8	69.0	24	69
WL4	57.3	59.7	75.2	25	65
WL5	56.7	59.0	74.3	24	66
WL6	56.7	58.9	73.7	24	69
WL7	57.2	59.8	74.1	26	71
WL8	57.4	59.2	74.4	26	69
WL9	—	51.7	67.9	25	72
WL average	**56.5**	**57.4**	**72.9**	**25**	**69**
Overall longitudinal average	**54.8**	**56.4**	**72.9**	**25**	**68**
WT1	58.1	60.2	75.4	23	44
WT2	58.5	61.1	75.2	23	49
WT3	58.2	60.5	74.6	25	51
WT4	57.7	60.0	74.7	23	43
WT5	58.1	60.6	74.8	25	51
WT6	58.2	60.8	75.7	25	47
WT average	**58.2**	**60.5**	**75.1**	**24**	**47**

—Loading program malfunctioned and only performed one static hold, therefore static yield could not be calculated.

W10x60 Beam Sections

All of the small-scale steel beams were produced from the same heat number, and material properties were assessed from an extra 3-foot-long portion of W10x60 purchased with the small-scale beams. Standard ASTM A370, plate-type specimens with an 8-inch gauge length were machined from the flange and web as shown in figure 114. Strain was measured over the 8-inch gauge length using a laser extensometer.

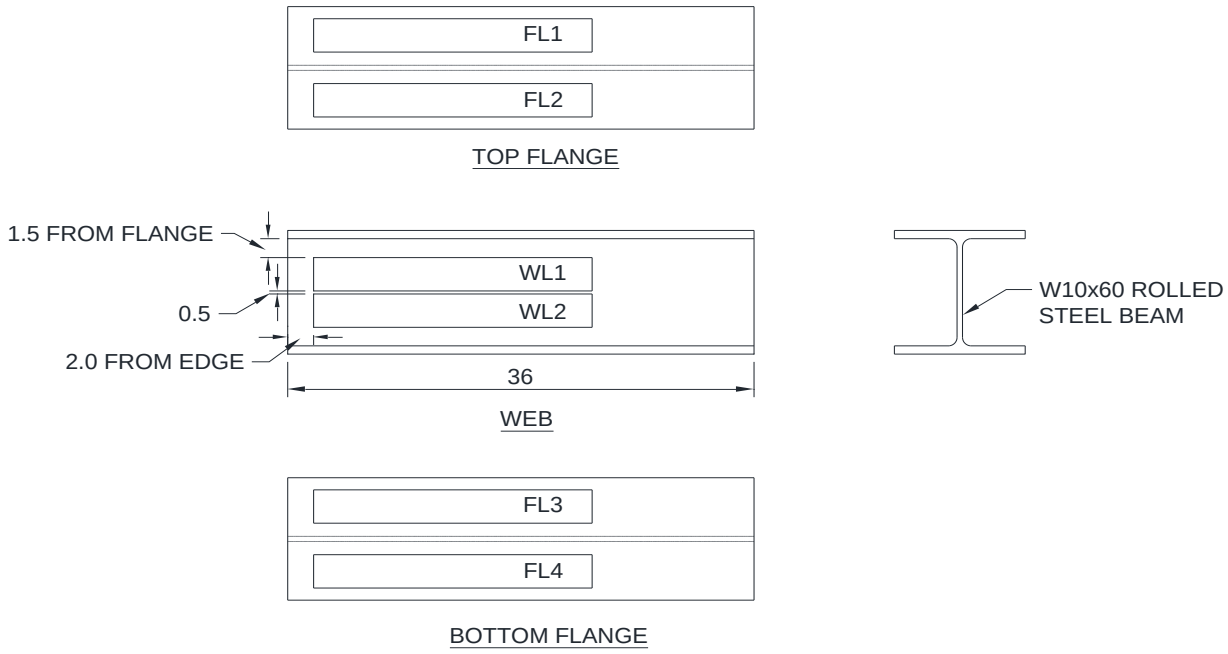

Source: FHWA.
Note: Measurements are in inches.

Figure 114. Schematic. Location of tensile test specimens from small-scale steel beam.

Figure 115 shows the stress–strain results from the longitudinal samples taken from the flange while figure 116 shows the stress–strain curve for the longitudinal samples from the web. There was more variability in the stress–strain results from the small- than from the large-scale beam. For example, in figure 115, all of the specimens produced nearly identical results except for FL1. This specimen showed lower overall stress values than the others and had a yield stress of 49.1 ksi, which is slightly less than the specified value of 50 ksi. Since this value was nearly 50 ksi, and the remaining three tests had yield stresses closer to 55 ksi, this low-stress result was not a particular concern. In figure 116, the test results on the web material were slightly different as well; with only two test results, it is difficult to discern why. Table 20 shows a summary of the tensile test results from the W10x60 small-scale beam properties.

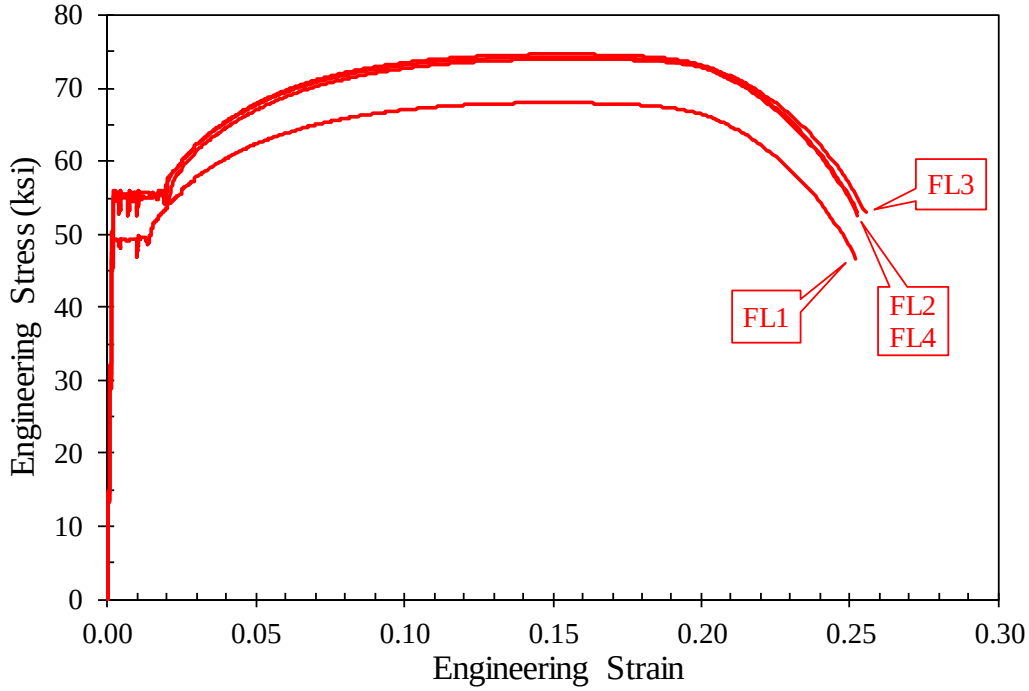

Source: FHWA.

Figure 115. Graph. Stress–strain curves for W10x60 longitudinal flange samples.

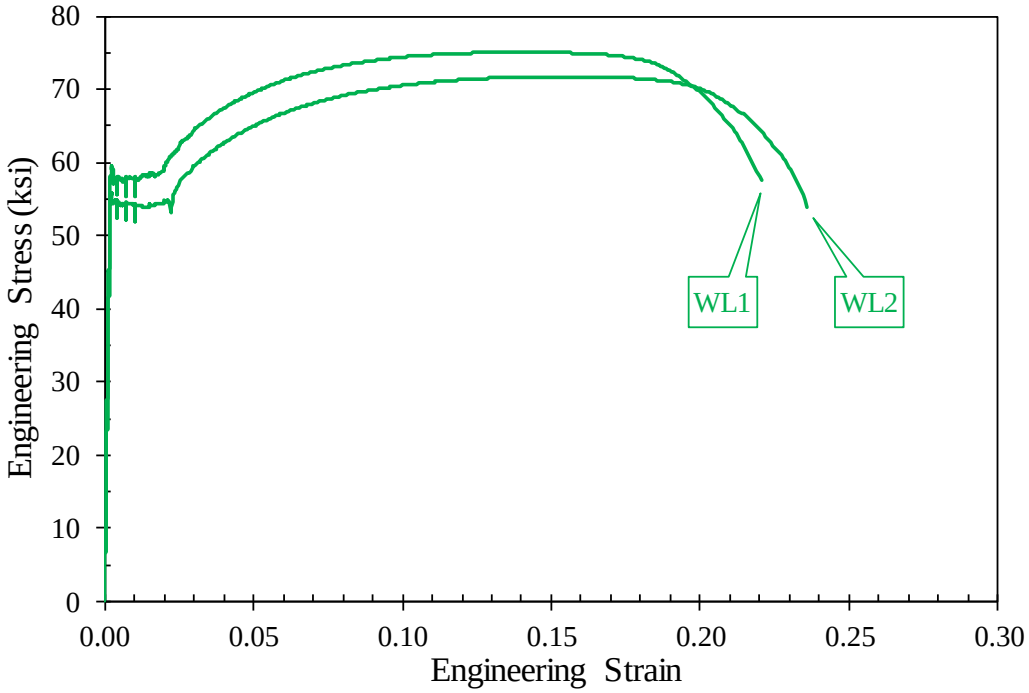

Source: FHWA.

Figure 116. Graph. Stress–strain curves for W10x60 longitudinal web samples.

Table 20. Summary of W10x60 tensile test results.

Specimen	Static Yield (ksi)	0.2% Offset Yield Stress (ksi)	Tensile Strength (ksi)	Elongation at Fracture (Percent)	Reduction in Area (Percent)
FL1	48.3	49.1	68.0	25	64
FL2	52.7	55.0	74.4	25	64
FL3	53.3	55.8	74.0	26	68
FL4	53.3	55.5	74.7	25	68
FL average	**51.9**	**53.9**	**72.8**	**25**	**66**
WL1	55.5	57.8	75.1	22	70
WL2	52.3	54.7	71.7	24	68
WL average	**53.9**	**56.3**	**73.4**	**23**	**69**
Overall average	**52.6**	**54.7**	**73.0**	**24**	**67**

Shear Studs

All of the shear studs used in the research program came from the same heat number, so five studs were randomly selected for tensile testing. The studs were machined into ASTM A370 standard round bar specimens with a 2-inch gauge length. Strain was measured with a 2.000-inch clip-on extensometer. Figure 117 shows the individual stress–strain tensile test results for the five shear studs. The stress–strain results from the shear studs were as expected and provided good agreement with the mill certifications for the shear studs. Table 21 shows the average test results for the static yield, 0.2 percent offset yield, tensile strength, elongation, and reduction in area.

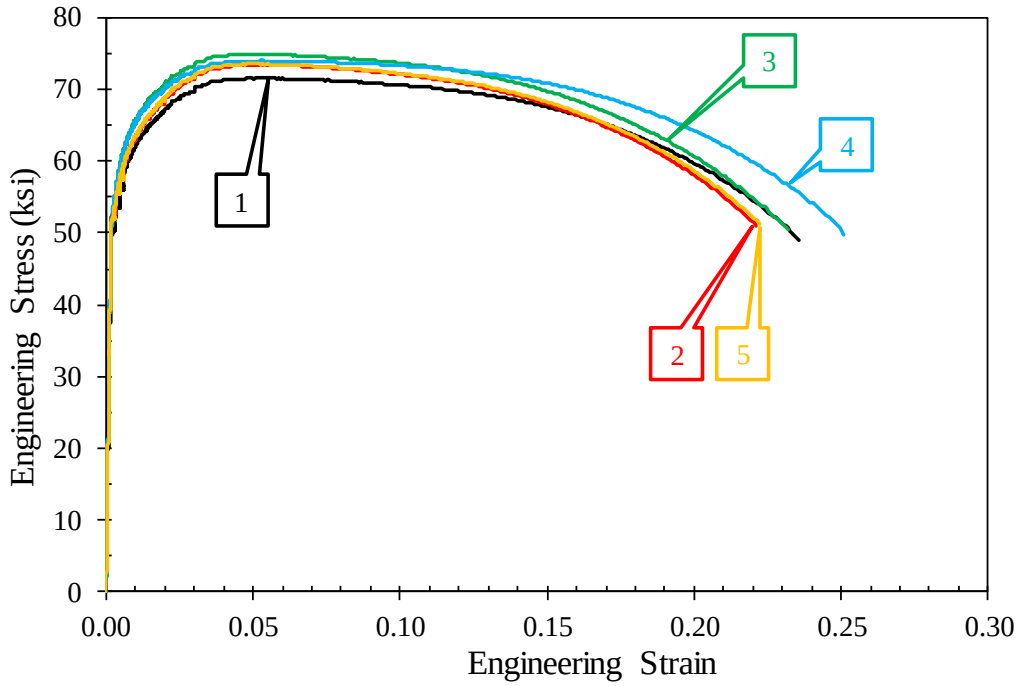

Source: FHWA.

Figure 117. Graph. Stress–strain curves for shear studs.

Table 21. Summary of shear stud tensile test results.

Shear Stud	Static Yield (ksi)	0.2% Offset Yield Stress (ksi)	Tensile Strength (ksi)	Elongation at Fracture (Percent)	Reduction in Area (Percent)
1	52.7	54.9	71.6	24	62
2	53.7	56.0	73.5	23	61
3	55.8	57.6	74.9	24	64
4	55.0	57.4	74.0	25	65
5	54.2	56.0	73.6	23	61
Average	**54.3**	**56.4**	**73.5**	**24**	**63**

CONCRETE AND GROUT

Concrete properties were assessed with 4- by 8-inch cylinders made with the other components described in this section. Concrete cylinders were made and tested according to ASTM C39.[(41)] Grout properties (when applicable) were assessed with 2- by 2-inch grout cubes, made and tested according to ASTM C109.[(42)]

Large-Scale Beams

The concrete deck panels used for the large-scale tests were fabricated at a PC concrete facility. The PC company provided concrete test cylinders that were made using the same concrete

batches used for the deck panels. Each cylinder was labeled with the deck panel it was cast with. At least one but usually two concrete test cylinders were associated with each deck panel. The cylinders for each deck panel were tested 1–2 days after beginning a fatigue or static test with that deck panel. All concrete test cylinders were at least 6 mo old when tested.

When the deck panels were grouted into place on each of the large-scale beams, grout test cubes were also made from the same grout mix. Generally, four separate batches of grout were required to fill the haunch and pockets along a beam. Multiple grout cubes were made from each batch and many were used to assess strength-gain properties to determine if the formwork could be stripped or if the beam specimen test could begin or not. These early-age grout strength results are not presented herein; only the results from the day the testing began are presented. Generally, four to eight grout cubes were tested with the goal of obtaining at least one grout cube result from each batch. However, not all grout cube test results were considered valid according to ASTM C109 criteria and these invalid results were omitted from the data.

Table 22 and table 23 outline the individual concrete cylinder and grout cube results for all the large-scale beam specimens. The tables also report the average results, which were used in any strength calculations of the specimen.

Table 22. Concrete cylinder test results from large-scale composite beams.

Specimen	Cylinder 1 (ksi)	Cylinder 2 (ksi)	Cylinder 3 (ksi)	Cylinder 4 (ksi)	Average (ksi)
1S2	8.0	8.1	—	—	8.0
1S1	8.9	9.2	—	—	9.1
1F1	7.6	7.1	—	—	7.3
1F2	10.0	10.0	10.1	10.3	10.1
1F3	8.8	8.1	—	—	8.4
2S1	10.3	9.6	—	—	10.0
2F1	10.6	11.0	—	—	10.8
2F2	7.0	—	—	—	7.0
2F3	8.6	8.5	—	—	8.5
3S1	10.0	8.4	—	—	9.2
3F1	9.3	9.5	—	—	9.4
3F2	9.5	10.0	—	—	9.7
3F3	10.4	9.3	—	—	9.9
4S1	9.0	8.0	—	—	8.5
4F1	9.0	8.5	—	—	8.8
4F2	10.9	11.0	—	—	11.0
4F3	9.3	11.0	—	—	10.2

—No data.

Table 23. Grout cube test results from large-scale composite beams.

Specimen	Cube 1 (ksi)	Cube 2 (ksi)	Cube 3 (ksi)	Cube 4 (ksi)	Cube 5 (ksi)	Cube 6 (ksi)	Cube 7 (ksi)	Cube 8 (ksi)	Average (ksi)
1S2	7.4	7.7	7.7	—	—	—	—	—	7.6
1S1	6.9	6.8	6.8	7.1	6.9	6.7	6.9	—	6.9
1F1	9.1	10.1	9.9	9.6	9.1	9.7	8.8	8.2	9.4
1F2	5.0	5.8	5.2	6.0	5.0	5.4	5.6	5.1	5.4
1F3	6.0	6.1	5.3	5.6	—	—	—	—	5.7
2S1	6.7	6.7	7.0	7.5	6.7	7.3	7.5	7.0	7.0
2F1	7.9	9.2	7.9	9.4	8.8	9.2	—	—	8.7
2F2	7.6	7.6	7.4	7.4	7.5	7.8	7.2	7.4	7.5
2F3	10.3	9.8	9.5	10.1	10.3	10.6	10.1	10.3	10.1
3S1	6.8	6.2	6.7	7.1	6.9	6.7	6.8	6.8	6.7
3F1	7.5	8.0	8.3	6.9	7.0	8.2	8.0	7.3	7.7
3F2	6.6	7.2	7.1	6.4	6.9	6.7	6.7	—	6.8
3F3	6.5	6.2	7.1	6.6	6.4	6.7	6.3	—	6.6
4S1	7.5	7.6	7.9	7.6	7.5	8.1	7.1	—	7.6
4F1	8.8	8.8	8.7	8.6	8.5	8.7	8.2	8.5	8.6
4F2	7.1	7.2	7.0	6.8	6.5	6.6	7.3	7.4	7.0
4F3	8.2	9.3	9.1	8.7	8.3	8.9	7.9	—	8.6

—No data.

Small-Scale Fatigue Specimens

The concrete PC panels used for the small-scale fatigue tests were cast on September 11, 2012. All 28 of the deck panels as well as the cylinders were cast using concrete from one concrete truck. The deck panels were moist-cured for 7 days using wet burlap. The concrete cylinders from the fatigue deck panel cast were tested on two dates while the small-scale fatigue tests were conducted, which happened to be 3–4.5 yr after casting. Table 24 shows the concrete cylinder strength values and the dates in which the cylinders were tested. Based on the age of the cylinders and the data in table 24, it was clear the cylinders reached a consistent, stable strength. An average concrete strength of 5.3 ksi was assumed for the PC deck panels.

Table 24. Small-scale fatigue PC deck test cylinder results.

Date Tested	Concrete Cylinder Strength (ksi)
June 26, 2015	5.4
June 26, 2015	5.5
June 26, 2015	5.5
June 26, 2015	5.4
June 26, 2015	5.2
December 15, 2016	5.1
December 15, 2016	5.2
December 15, 2016	5.4
December 15, 2016	5.3
December 15, 2016	5.4

In October 2012, the PC decks were grouted into place onto the small-scale fatigue specimens in two stages. First, the steel beam was laid on its side and one PC deck was grouted into place and then, 3 days later, the beam was flipped over and the process was repeated to grout the second deck panel to the opposite flange. Since grout was cast in two stages, test cubes were made for each grout cast. These test cubes were tested over a variety of dates while the small-scale fatigue testing took place. Table 25 shows the results from testing the grout cubes.

Table 25. Individual grout test results for material on small-scale fatigue test specimens.

Date Tested	Mix 1 Grout Strength (ksi)	Mix 2 Grout Strength (ksi)
July 7, 2015	9.9	9.3
July 7, 2015	8.9	8.6
April 19, 2016	10.5	10.4
April 19, 2016	10.6	10.4
April 19, 2016	11.0	10.5
April 19, 2016	11.6	10.1
August 9, 2016	10.8	10.3
August 9, 2016	10.3	10.3
December 15, 2016	10.8	9.4
December 15, 2016	9.8	9.0

In the table, there is no discernable difference between the two grout mixes. Both mixes were tested approximately 3–4 yr after they were cast, so the 3-day difference in casting dates is negligible. Therefore, an average grout strength value of 10.1 ksi can be used for all of the grout in the small-scale fatigue tests.

Small-Scale Static Specimens

The concrete used for the small-scale static tests was cast on two separate occasions; the panels used for the PC static tests were cast on August 8, 2012, and the CIP static test specimens were cast on December 13, 2012. For each concrete cast, a single concrete truck was used to make the panels and the cylinders. Both the PC deck panels and CIP test specimens were moist-cured for 7 days using wet burlap. All of the concrete cylinders were tested in December 2016, near the end of the small-scale static testing. Table 26 shows the concrete cylinder strengths for each test type.

Table 26. Individual concrete test results for concrete deck panels of small-scale fatigue specimens.

Test Type	Concrete Cylinder Strength (ksi)
PC	7.5
PC	7.6
PC	7.8
PC	7.3
PC	7.5
PC	7.4
CIP	10.0
CIP	9.4
CIP	9.7
CIP	9.4
CIP	9.6
CIP	9.8

From looking at the test data in table 26, it is clear that after 4 yr of curing, both concrete mixes reached a consistent, stable strength. Therefore, it is safe to assume that the average concrete strength of the PC deck panels was 7.5 ksi and the average cylinder strength of the CIP test specimens was 9.6 ksi.

The PC decks for the small-scale static test specimens were grouted into place in January 2012. As in the small-scale fatigue tests, the PC panels were grouted in two stages; the first panel was grouted in place and allowed to cure for 3 days, then the specimen was flipped and the second panel was grouted in place. Test cubes were made for each grout cast. The grout cubes were tested in December 2016, near the end of the small-scale static testing. Table 27 shows the results from testing the grout cubes.

Table 27. Individual grout test results for material on small-scale static test specimens.

Mix 1 Grout Strength (ksi)	Mix 2 Grout Strength (ksi)
8.2	8.2
7.5	7.2
7.9	7.6
8.2	7.4
8.6	7.3
8.4	7.4
9.4	6.2
8.3	6.6
6.7	6.0
7.9	6.6
7.9	7.3
8.3	7.5
6.7	7.3
6.9	7.4
9.0	8.8
8.1	8.0
8.5	7.0
8.8	8.1
8.4	8.9
7.9	8.6
7.8	8.6
8.8	9.4

From examining the table, grout mix 1 has an average of 8.1 ksi, with a standard deviation of 0.7 ksi. Grout mix 2 has an average 7.6 ksi, with a standard deviation of 0.9 ksi. These values are similar enough that it seems reasonable to call the two grout mixes equivalent. Therefore, it is safe to assume an average grout strength of 7.8 ksi for all of the grout in the PC small-scale static tests.

APPENDIX C. LARGE-SCALE FATIGUE TEST STRAIN GAUGE AND LVDT TEST RESULTS

This appendix contains the relevant strain gauge and LVDT test results from the large-scale fatigue tests. In general, the data here follow the same order used in the Experimental Results and Discussion section of this report. Data from one beam are presented in the following order: location of the NA in both shear spans, location of the NA in all sections of the shear span that failed first, horizontal slip in both shear spans, horizontal slip in all sections of the shear span that failed first, and vertical uplift in both shear spans. In tests that resulted in runouts, data from both shear spans are presented.

SPECIMEN 1F2

Figure 118 through figure 122 show the strain gauge and LVDT results for specimen 1F2.

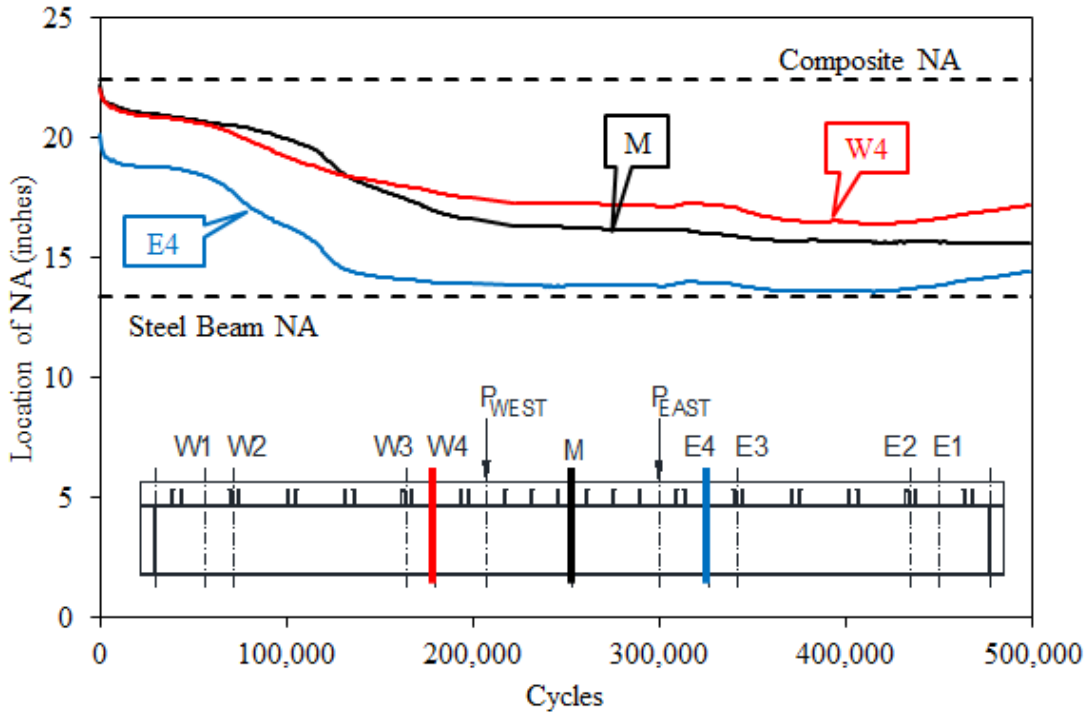

Source: FHWA.

Figure 118. Graph. Location of NA for both shear spans of 1F2.

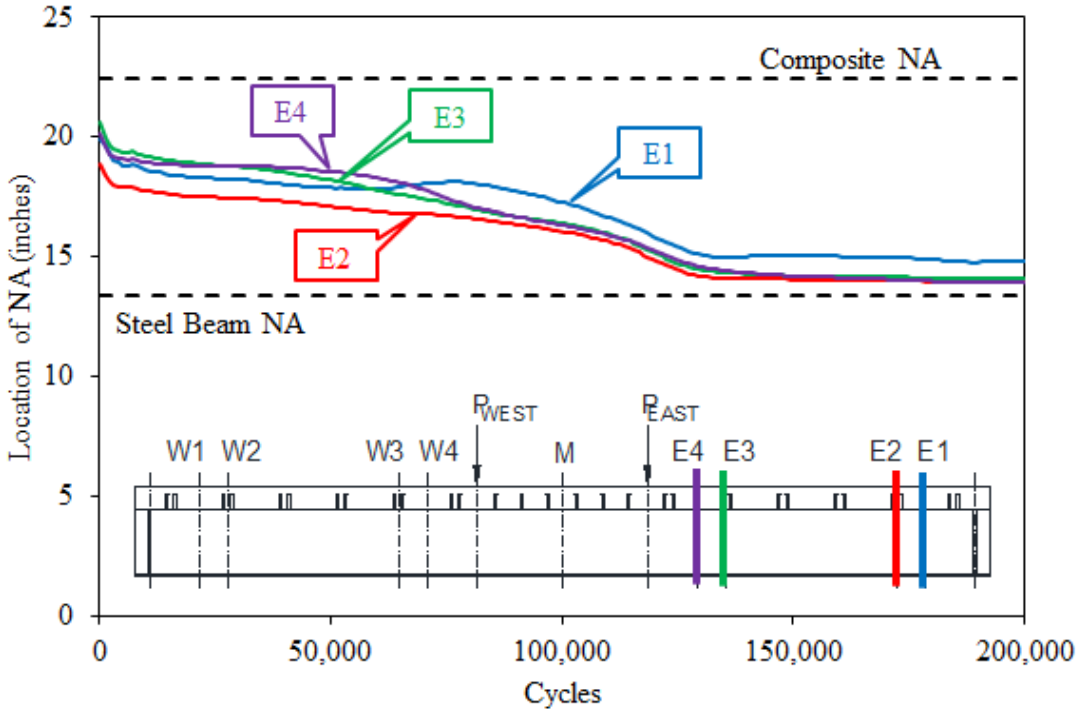

Source: FHWA.

Figure 119. Graph. Location of NA for east shear span of 1F2.

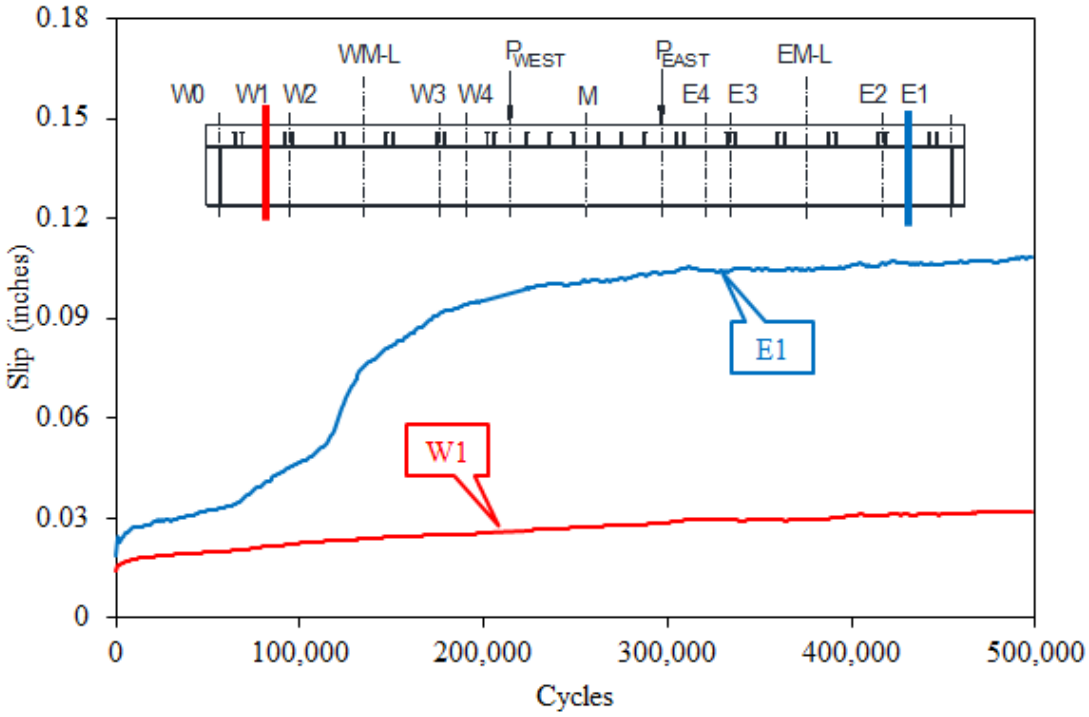

Source: FHWA.

Figure 120. Graph. Horizontal slip in both shear spans of 1F2.

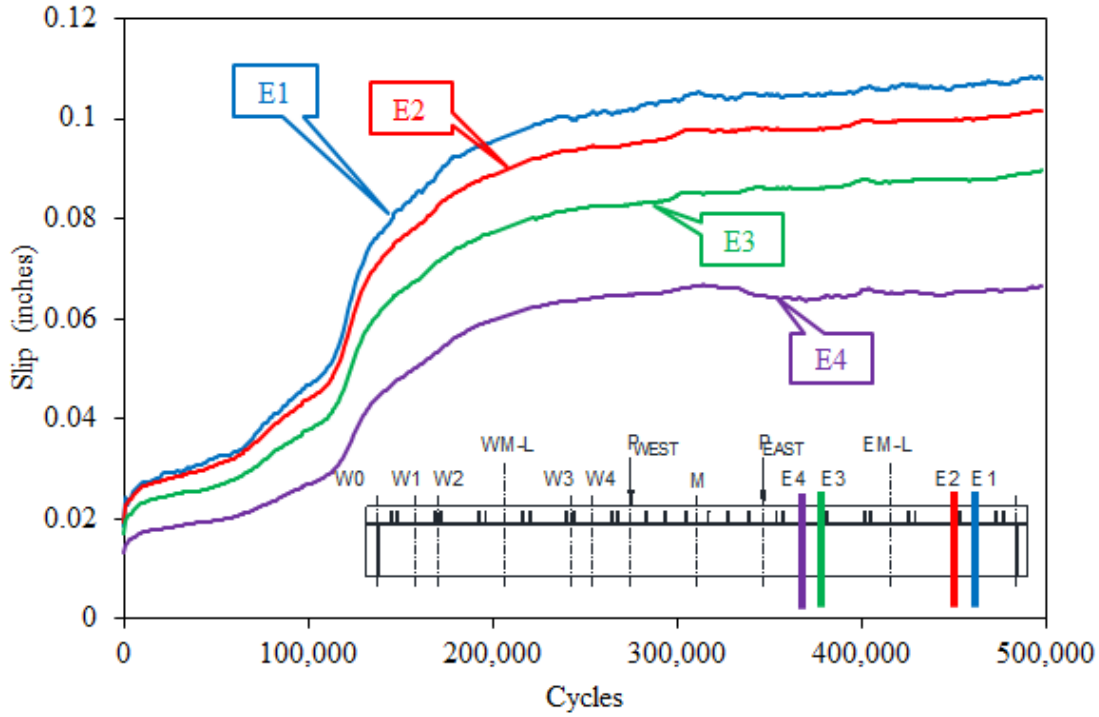

Source: FHWA.

Figure 121. Graph. Horizontal slip in east shear span of 1F2.

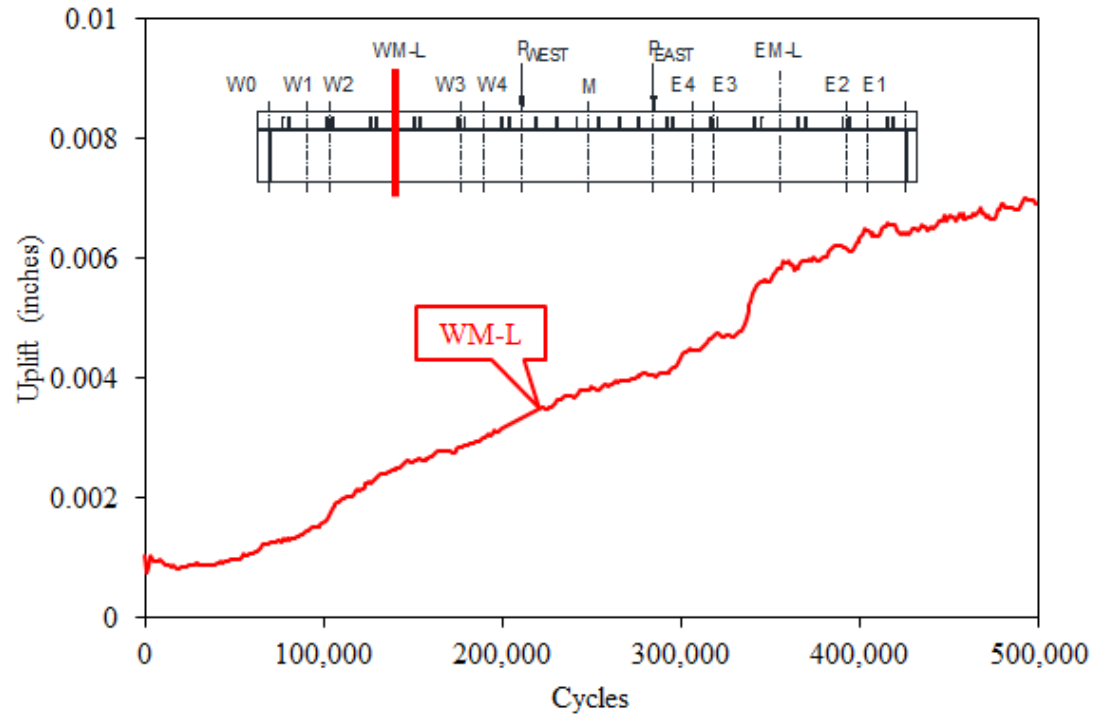

Source: FHWA.

Figure 122. Graph. Vertical uplift in both shear spans of 1F2.

SPECIMEN 1F3

Figure 123 through figure 127 show the strain gauge and LVDT results for specimen 1F3.

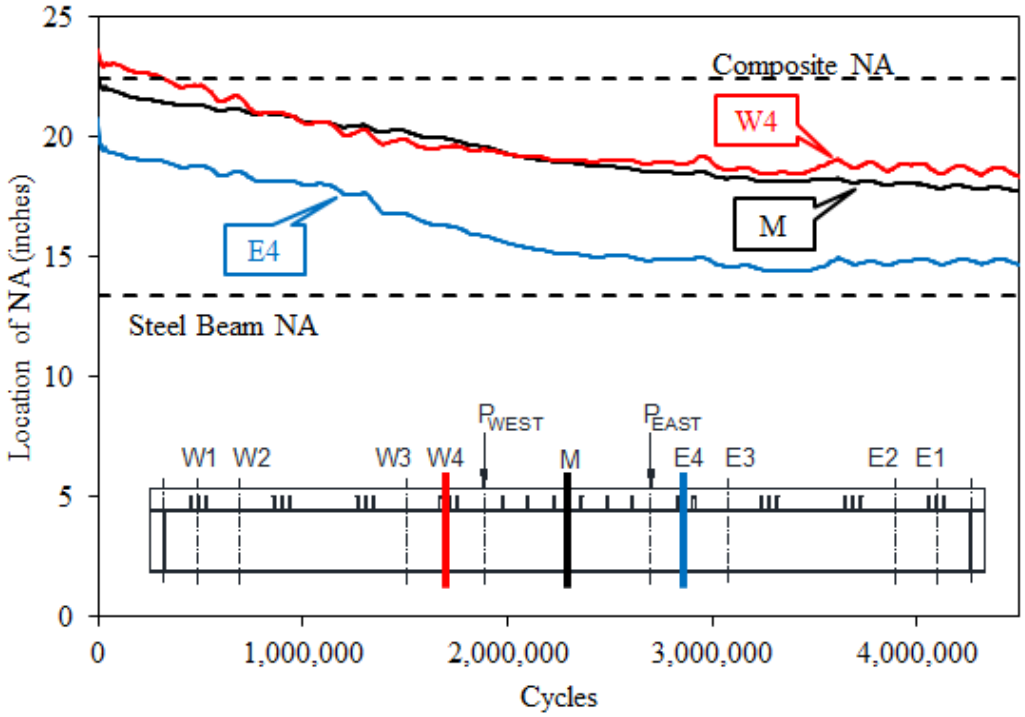

Source: FHWA.

Figure 123. Graph. Location of NA for both shear spans of 1F3.

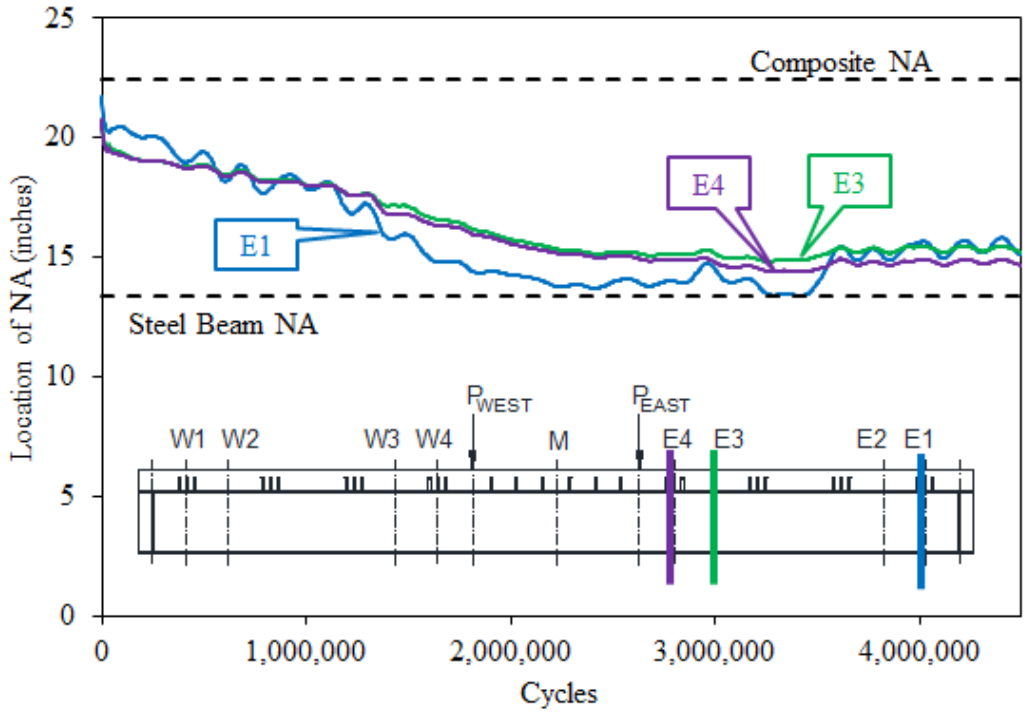

Source: FHWA.

Figure 124. Graph. Location of NA for east shear span of 1F3.

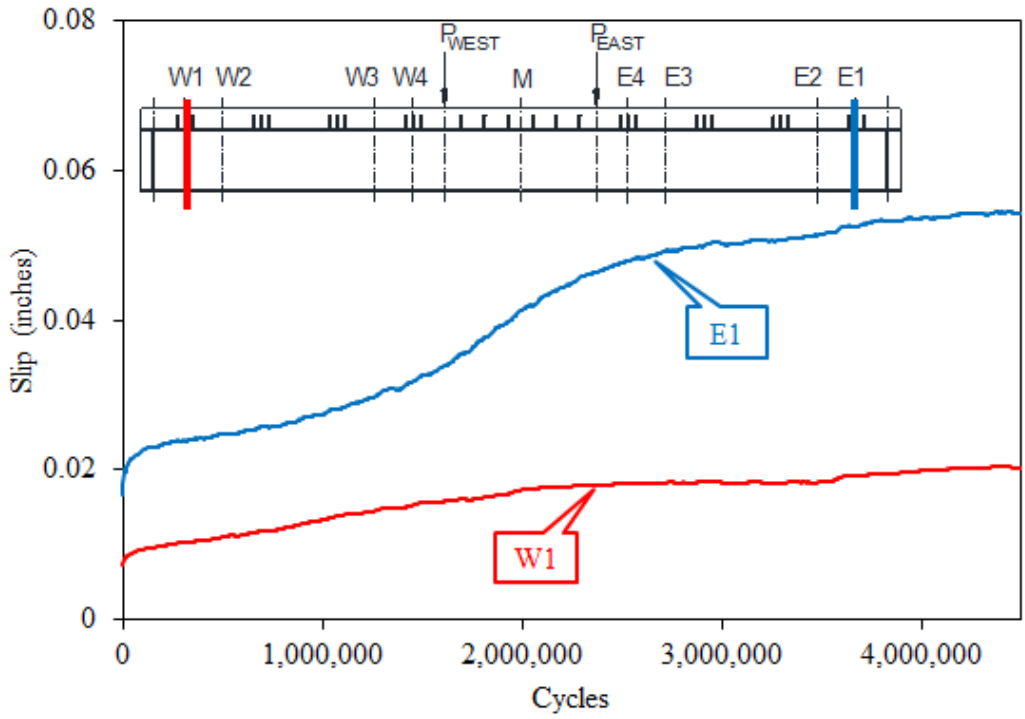

Source: FHWA.

Figure 125. Graph. Horizontal slip in both shear spans of 1F3.

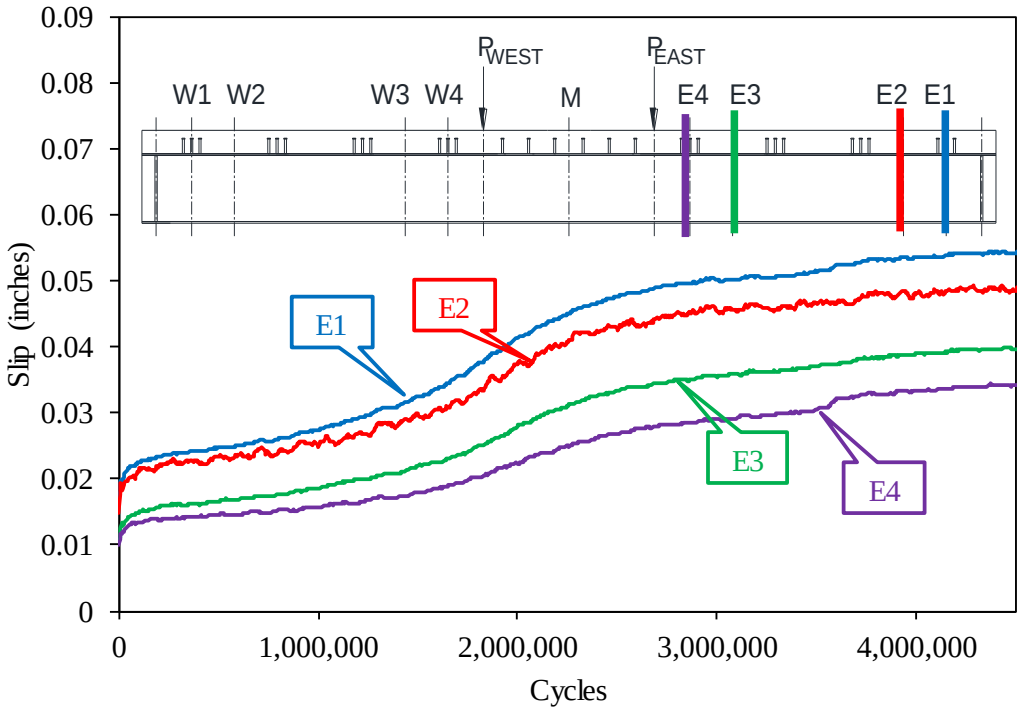

Source: FHWA.

Figure 126. Graph. Horizontal slip in east shear span of 1F3.

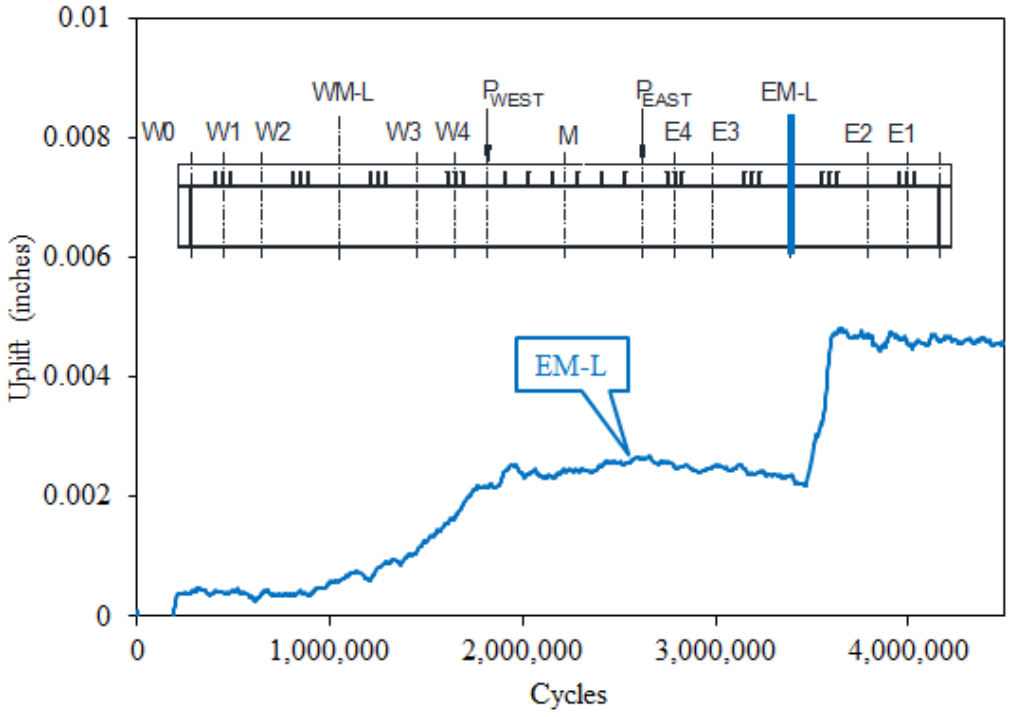

Source: FHWA.

Figure 127. Graph. Vertical uplift in east shear span of 1F3.

SPECIMEN 2F1

Figure 128 through figure 132 show the strain gauge and LVDT results for specimen 2F1.

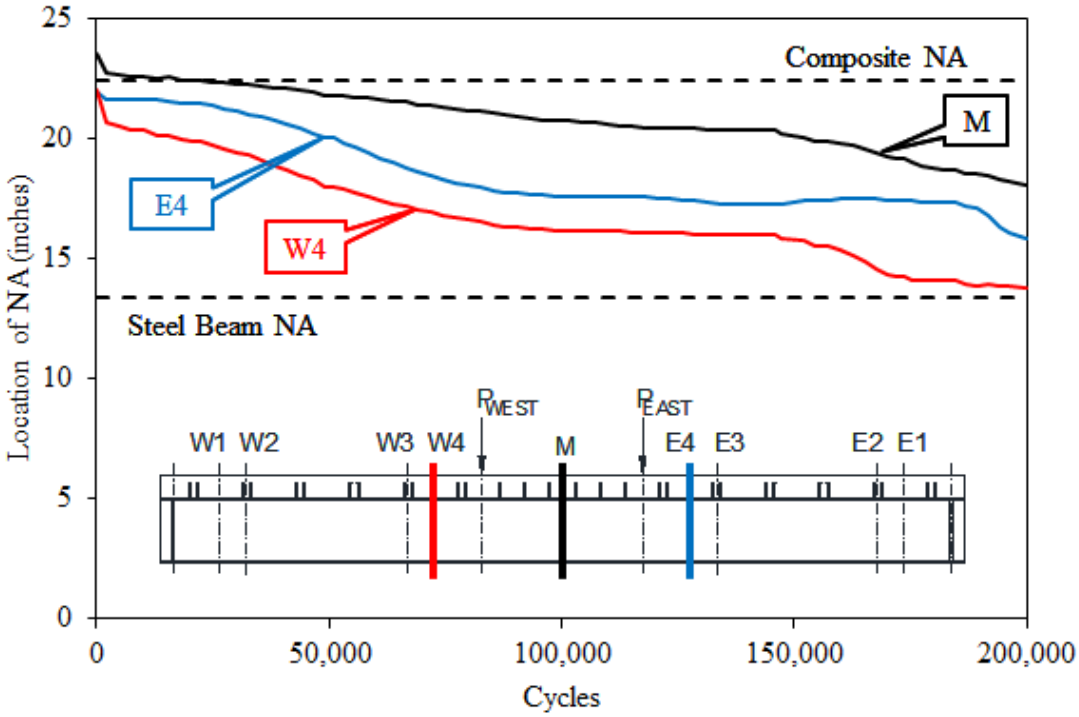

Source: FHWA.

Figure 128. Graph. Location of NA for both shear spans of 2F1.

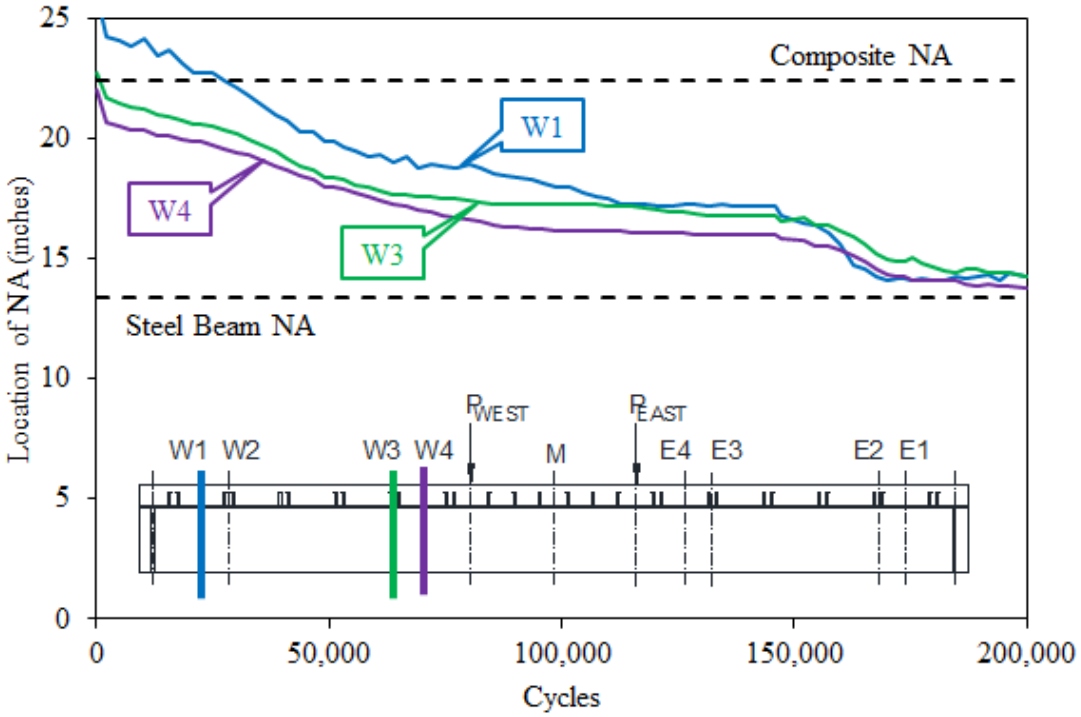

Source: FHWA.

Figure 129. Graph. Location of NA for west shear span of 2F1.

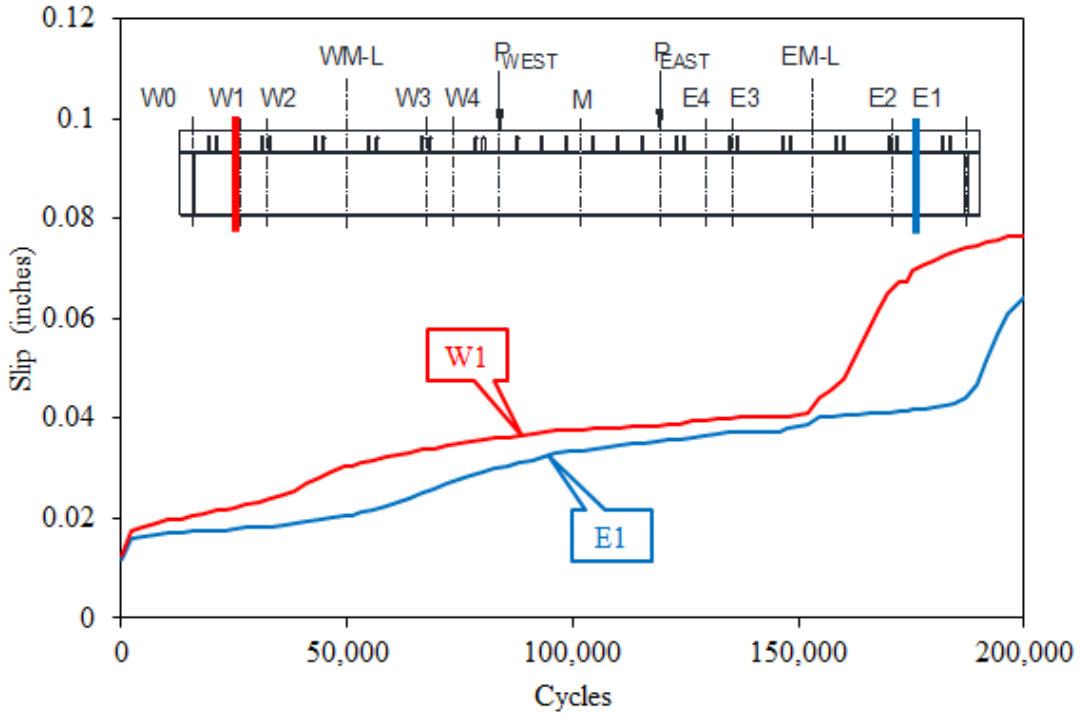

Source: FHWA.

Figure 130. Graph. Horizontal slip in both shear spans of 2F1.

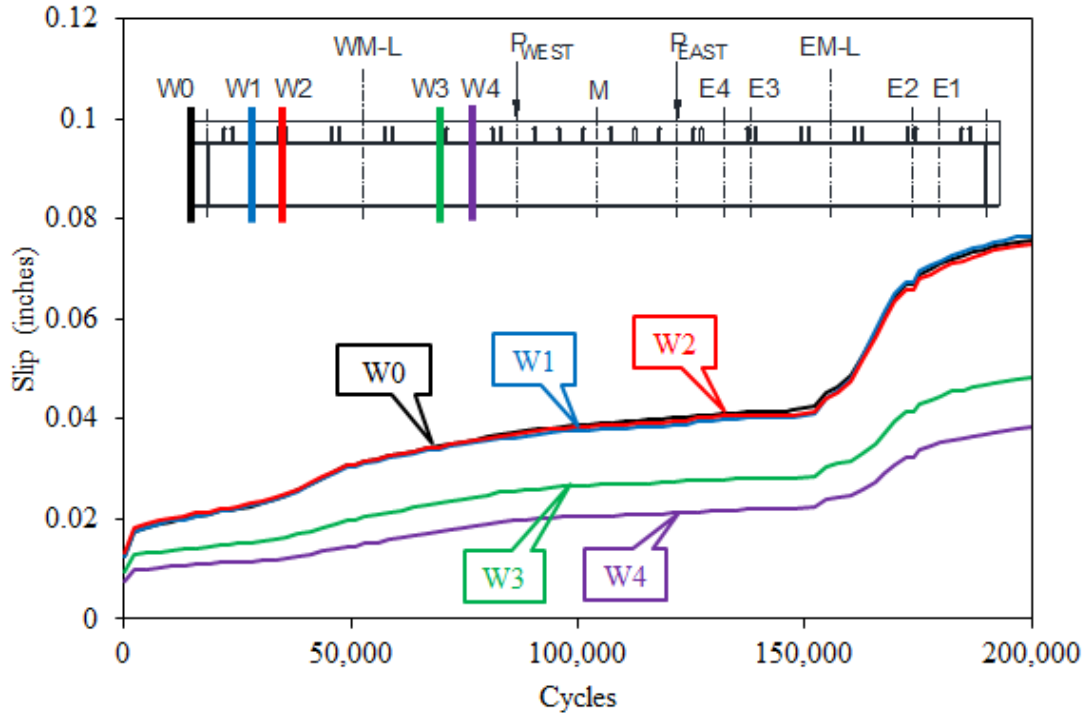

Source: FHWA.

Figure 131. Graph. Horizontal slip in west shear span of 2F1.

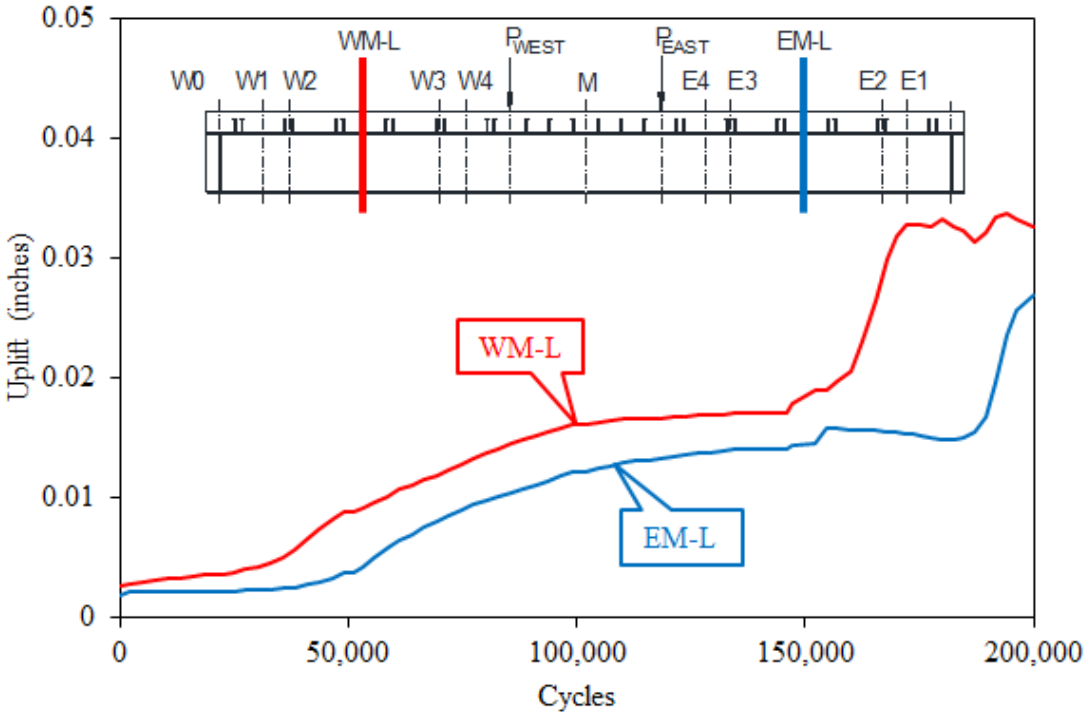

Source: FHWA.

Figure 132. Graph. Vertical uplift in both shear spans of 2F1.

SPECIMEN 2F2

Figure 133 through figure 137 show the strain gauge and LVDT results for specimen 2F2.

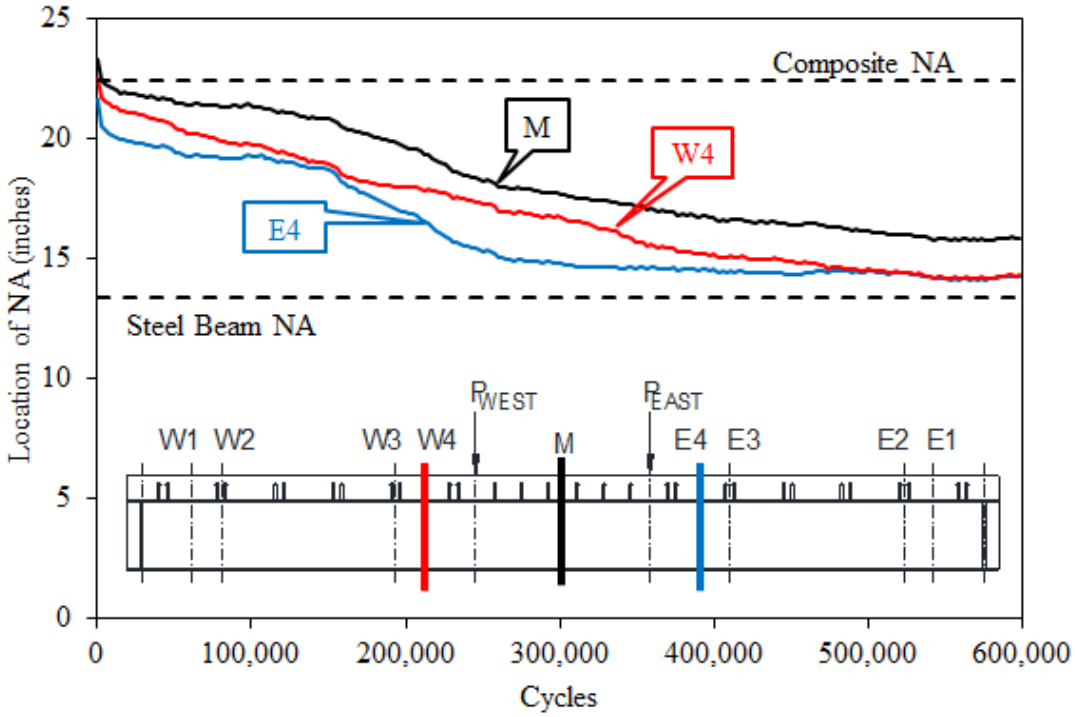

Source: FHWA.

Figure 133. Graph. Location of NA for both shear spans of 2F2.

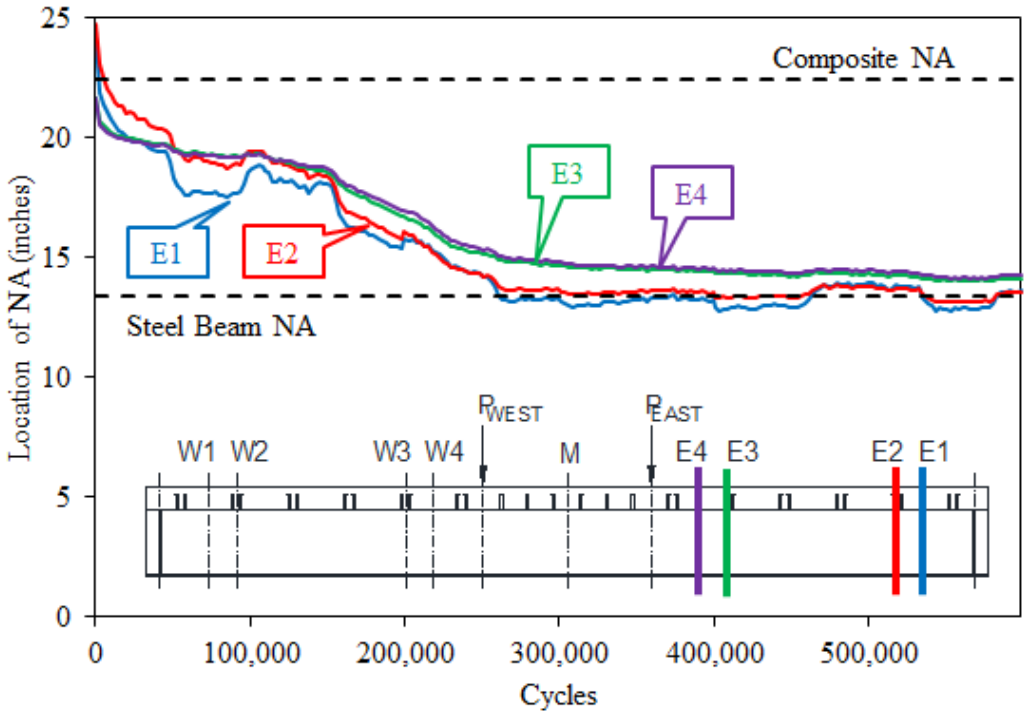

Source: FHWA.

Figure 134. Graph. Location of NA for east shear spans of 2F2.

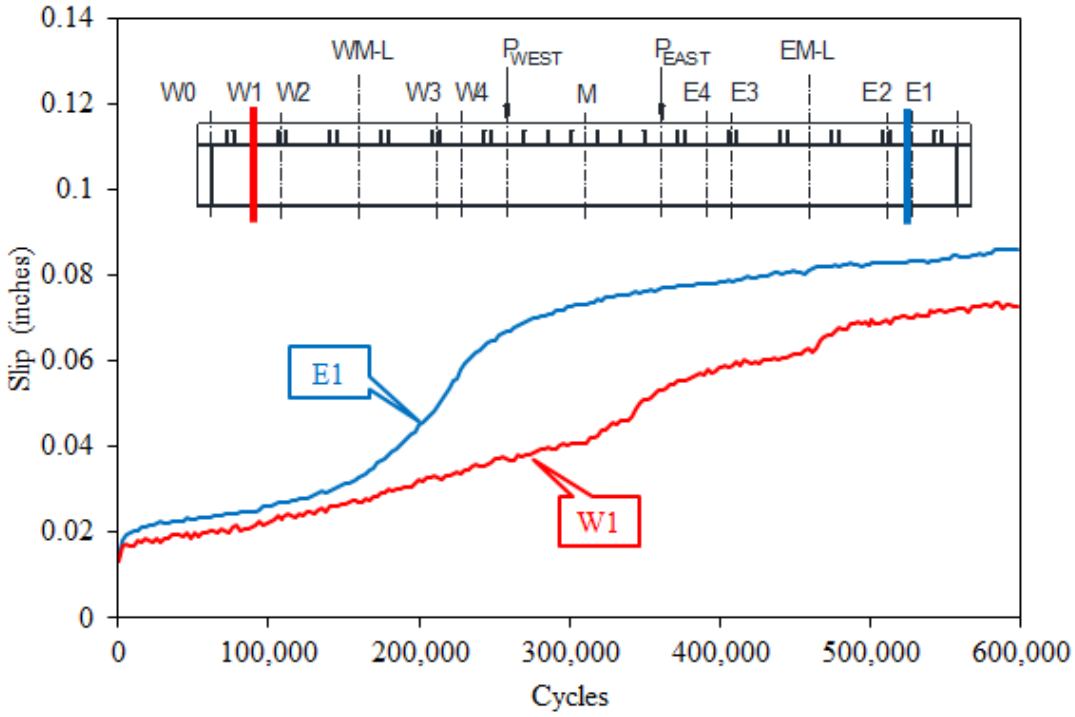

Source: FHWA.

Figure 135. Graph. Horizontal slip in both shear spans of 2F2.

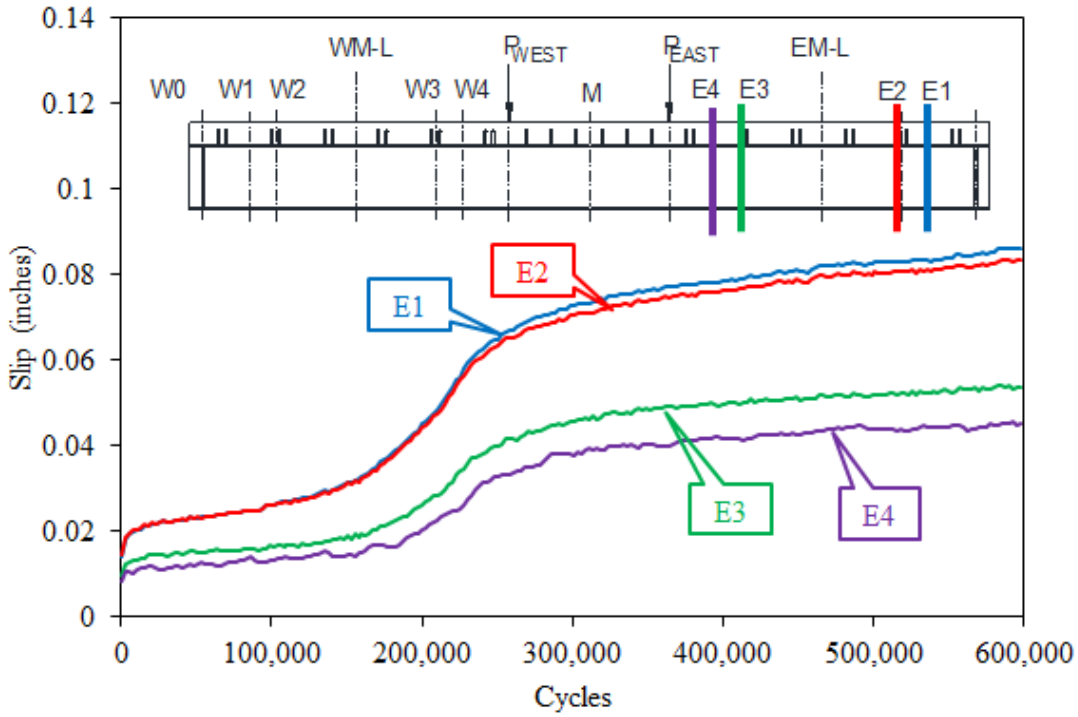

Source: FHWA.

Figure 136. Graph. Horizontal slip in east shear span of 2F2.

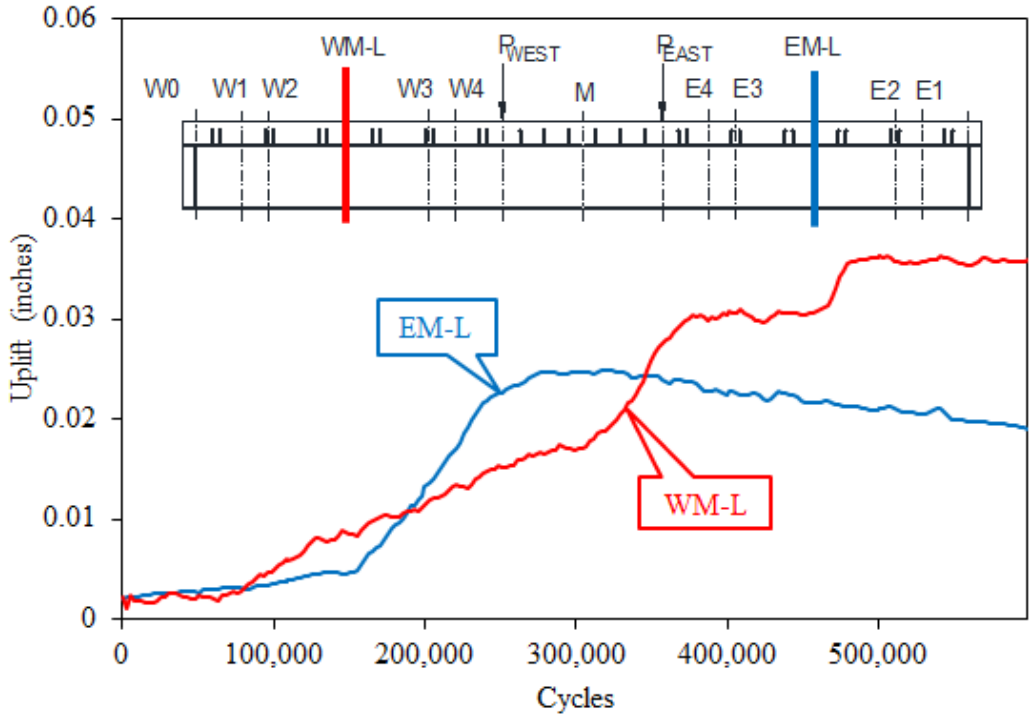

Source: FHWA.

Figure 137. Graph. Vertical uplift in both shear spans of 2F2.

SPECIMEN 2F3

Figure 138 through figure 144 show the strain gauge and LVDT results for specimen 2F3.

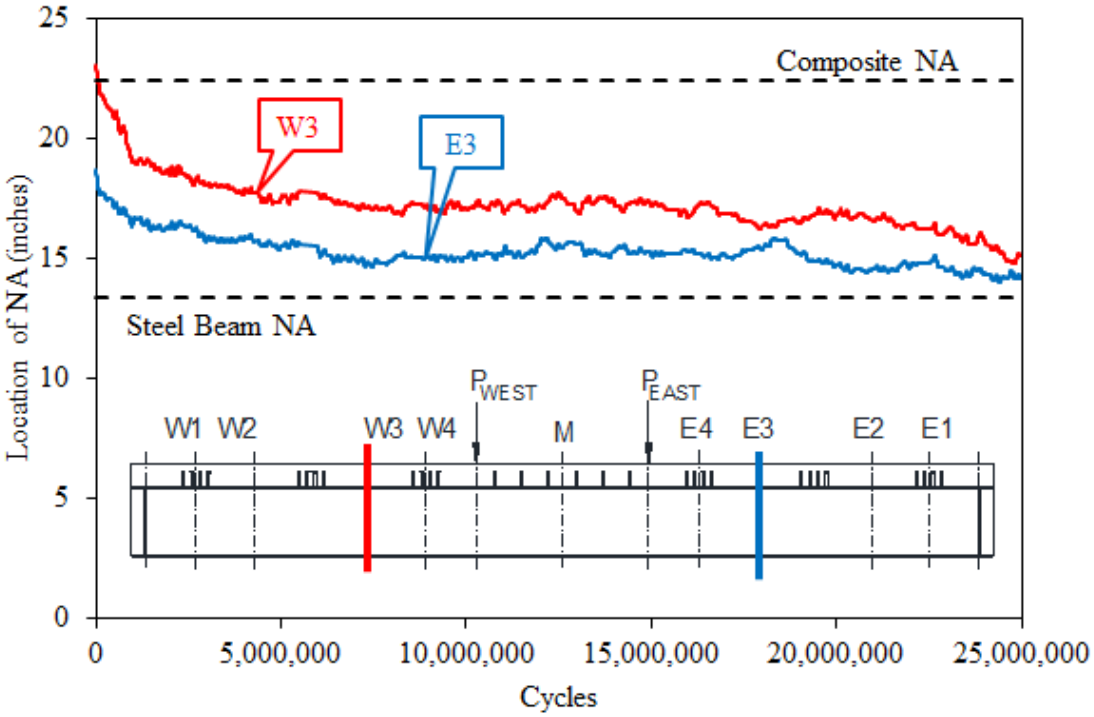

Source: FHWA.

Figure 138. Graph. Location of NA for both shear spans of 2F3.

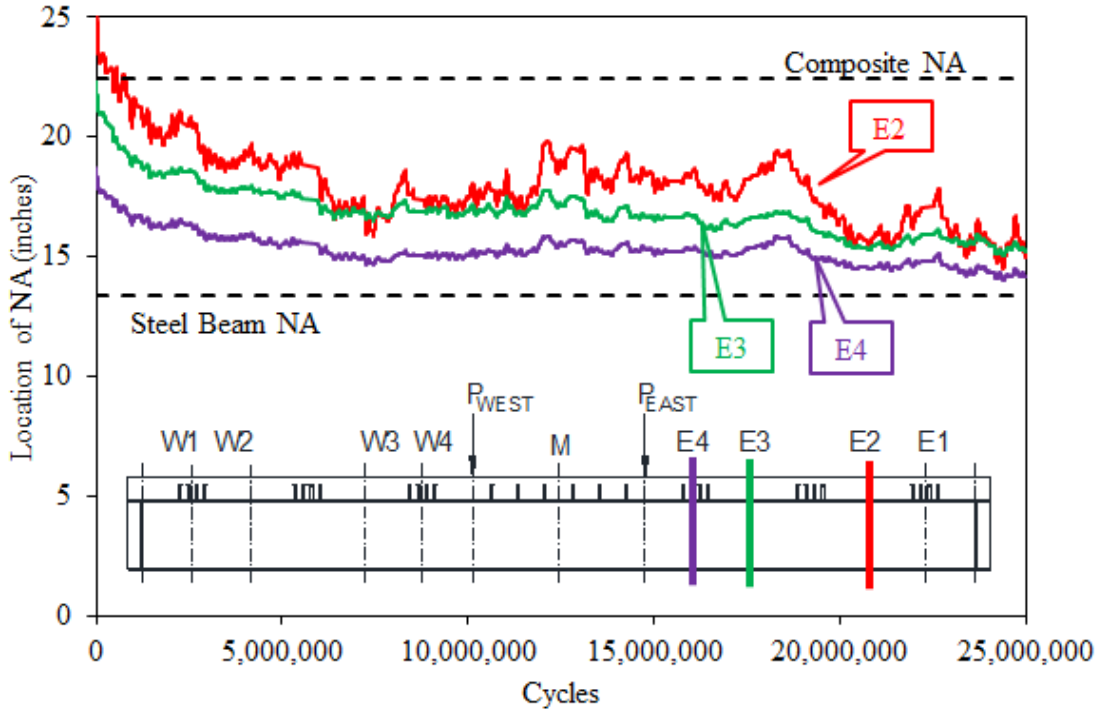

Source: FHWA.

Figure 139. Graph. Location of NA for east shear span of 2F3.

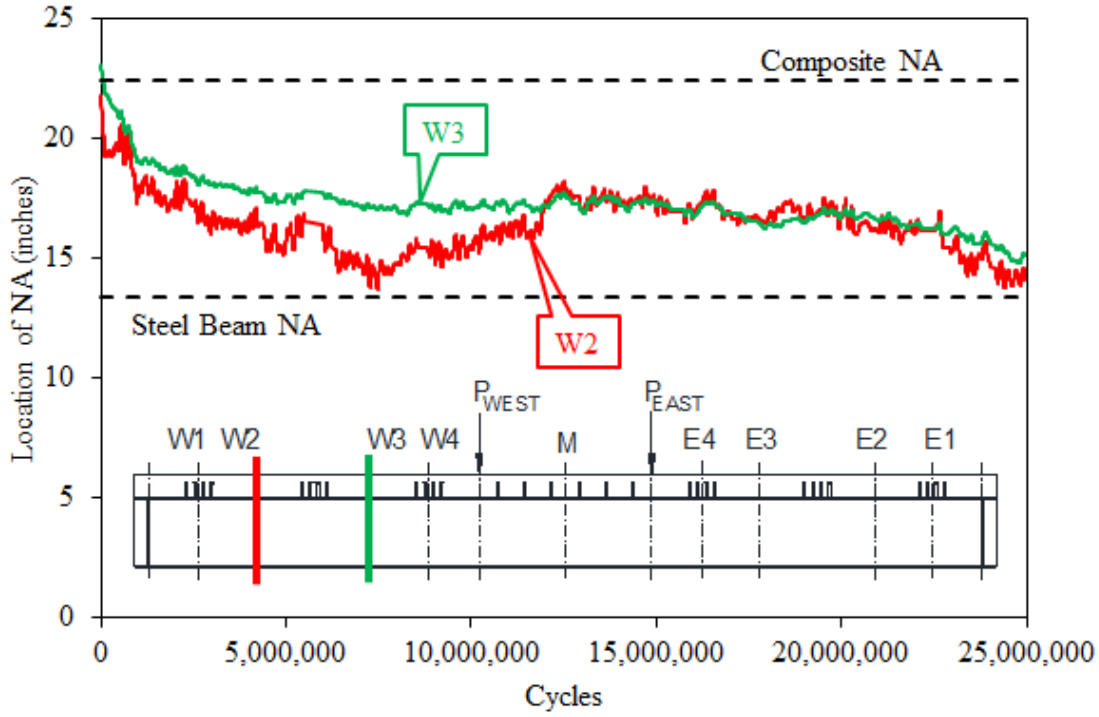

Source: FHWA.

Figure 140. Graph. Location of NA for west shear span of 2F3.

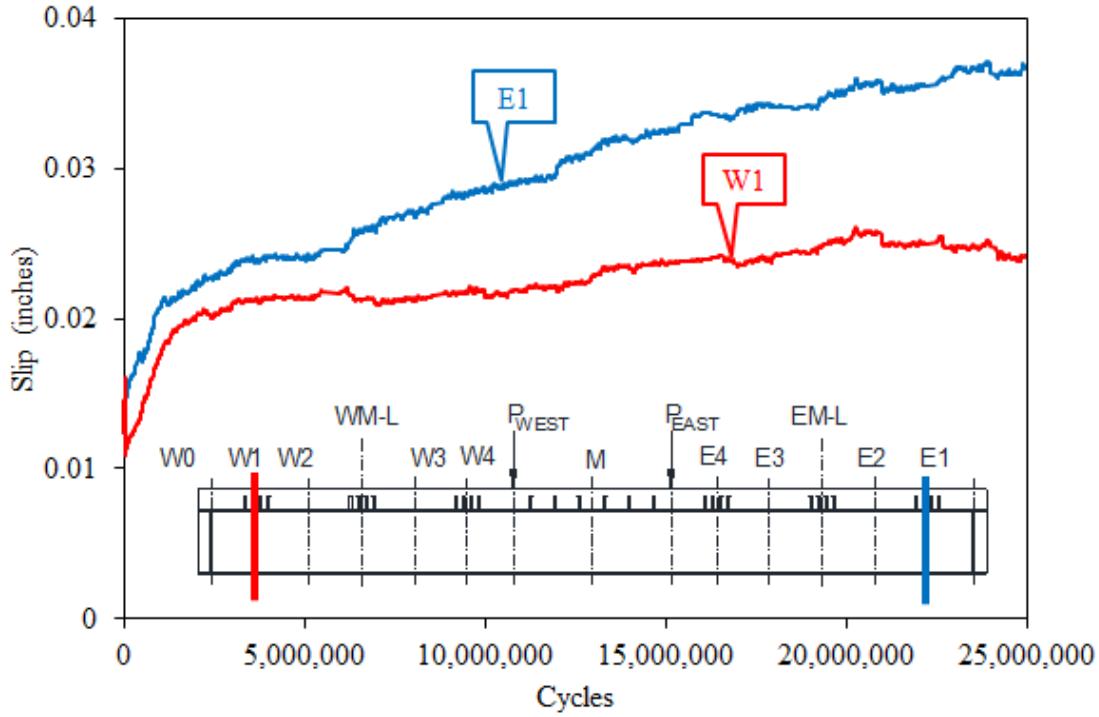

Source: FHWA.

Figure 141. Graph. Horizontal slip in both shear spans of 2F3.

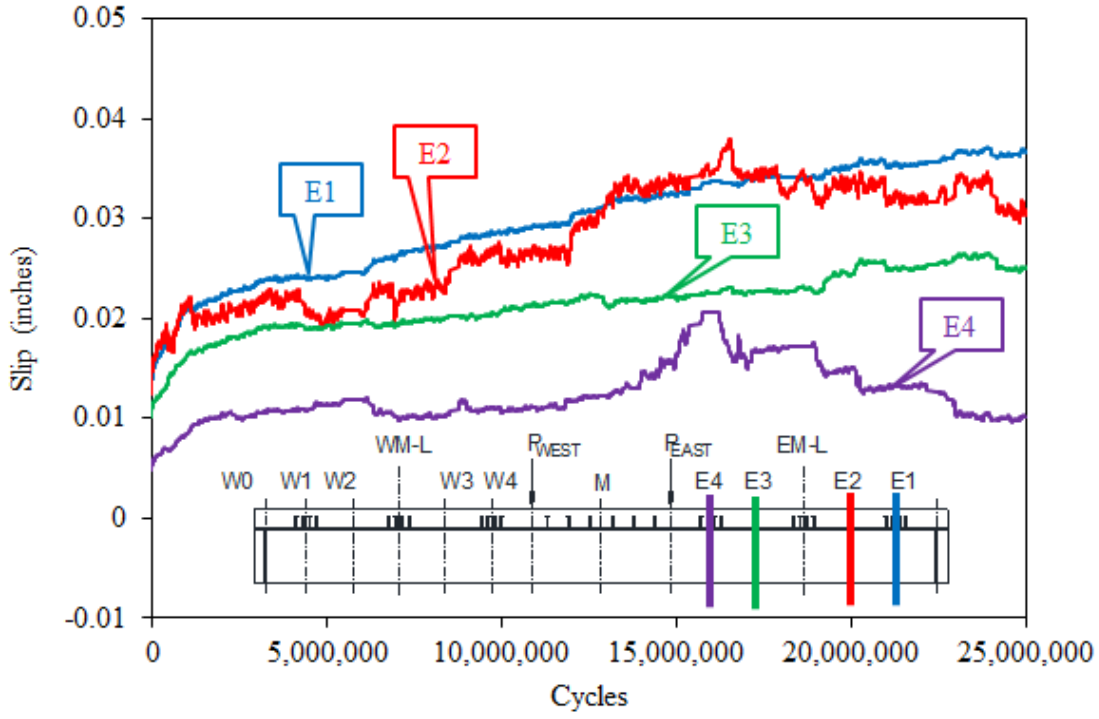

Source: FHWA.

Figure 142. Graph. Horizontal slip in east shear span of 2F3.

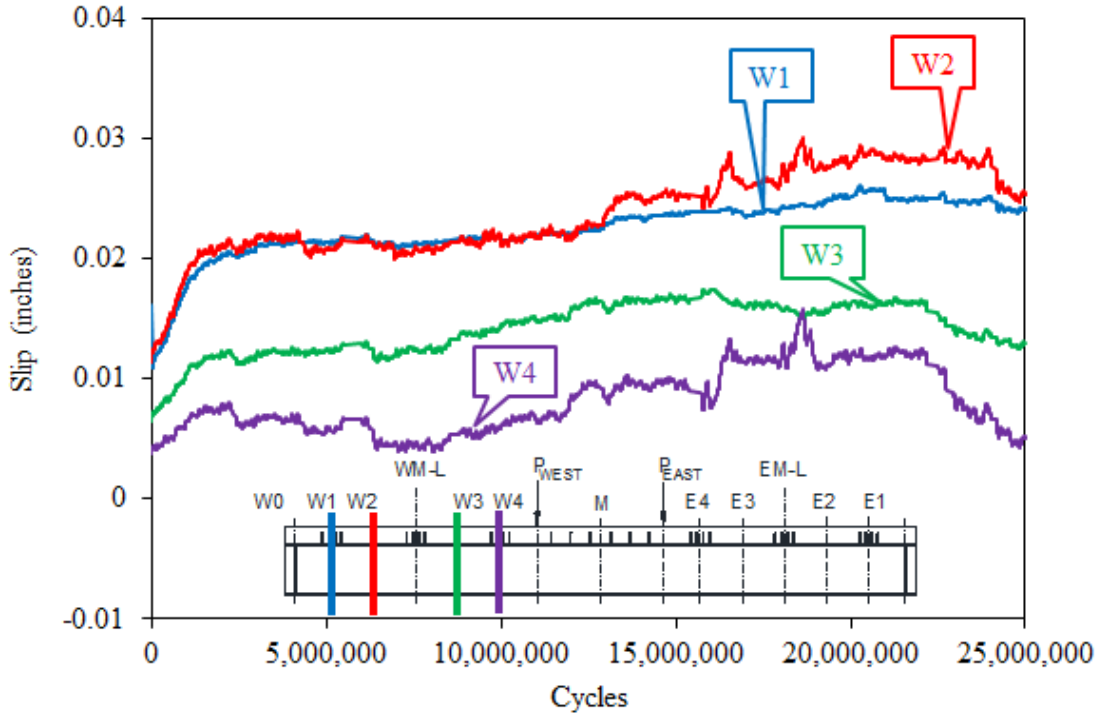

Source: FHWA.

Figure 143. Graph. Horizontal slip in west shear span of 2F3.

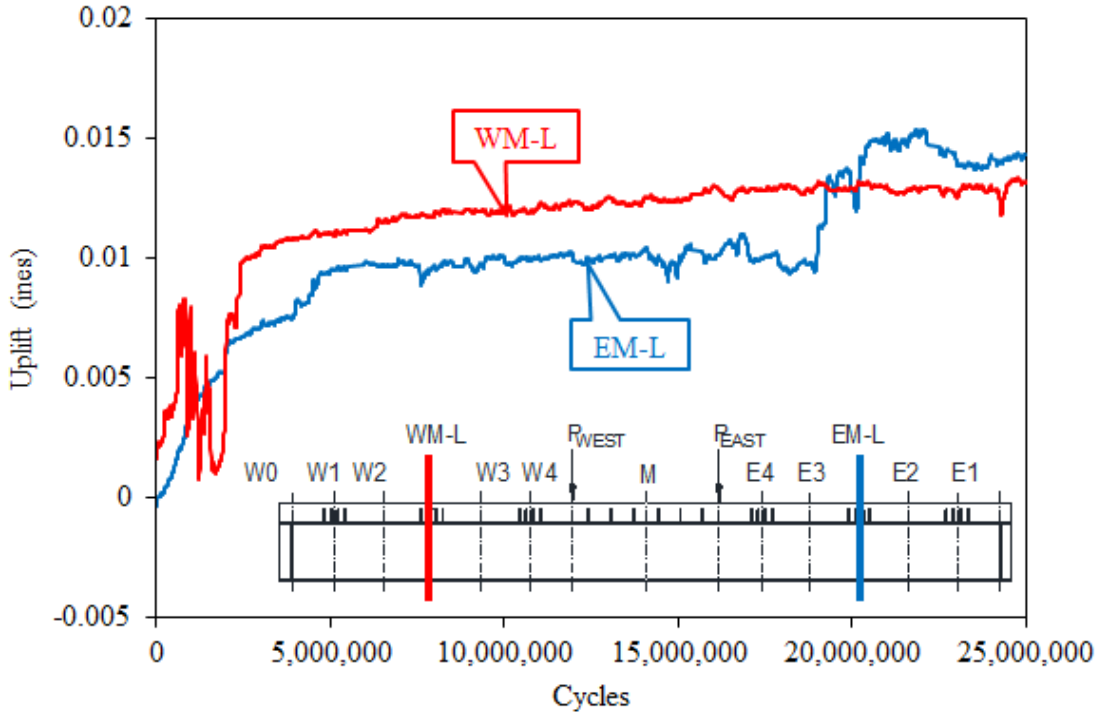

Source: FHWA.

Figure 144. Graph. Vertical uplift in both shear spans of 2F3.

SPECIMEN 3F1

Figure 145 through figure 149 show the strain gauge and LVDT results for specimen 3F1.

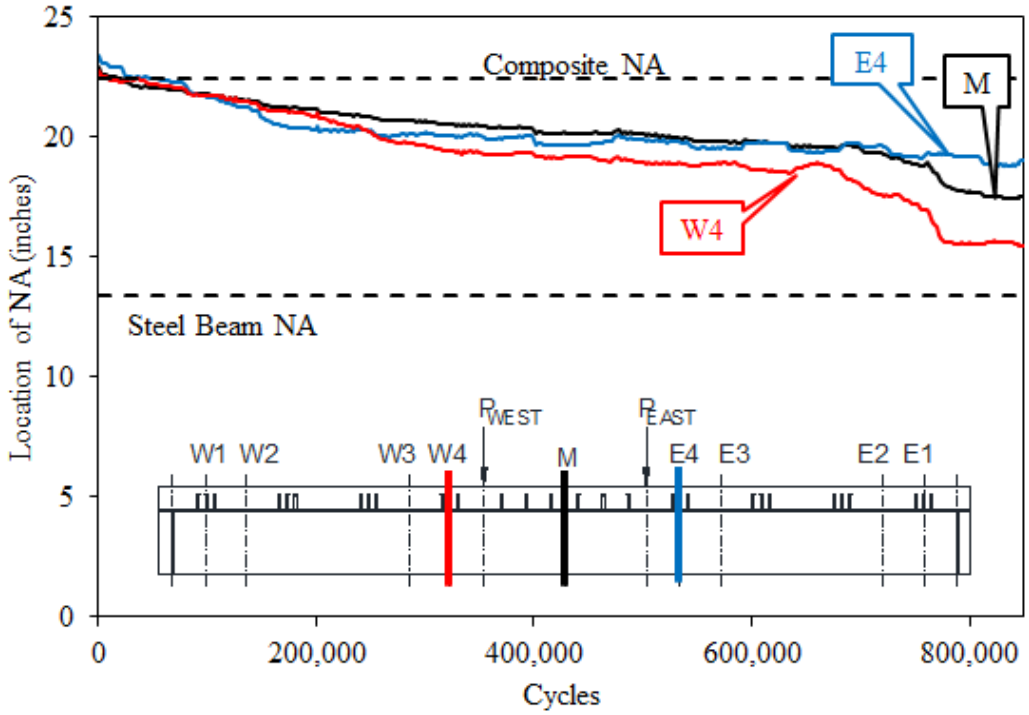

Source: FHWA.

Figure 145. Graph. Location of NA for both shear spans of 3F1.

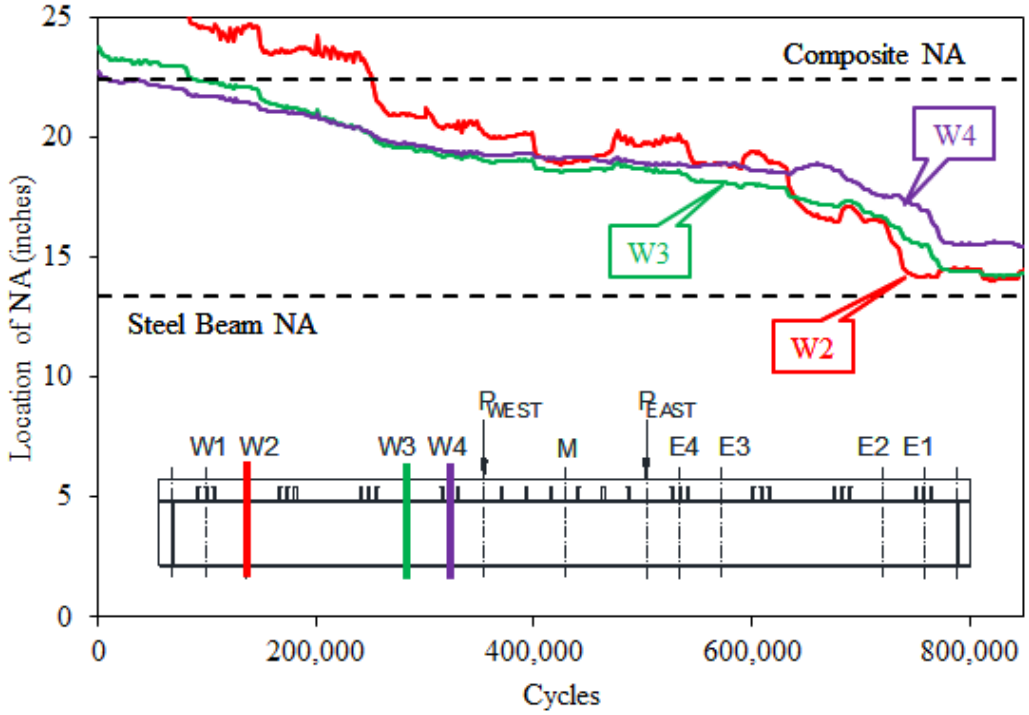

Source: FHWA.

Figure 146. Graph. Location of NA for west shear span of 3F1.

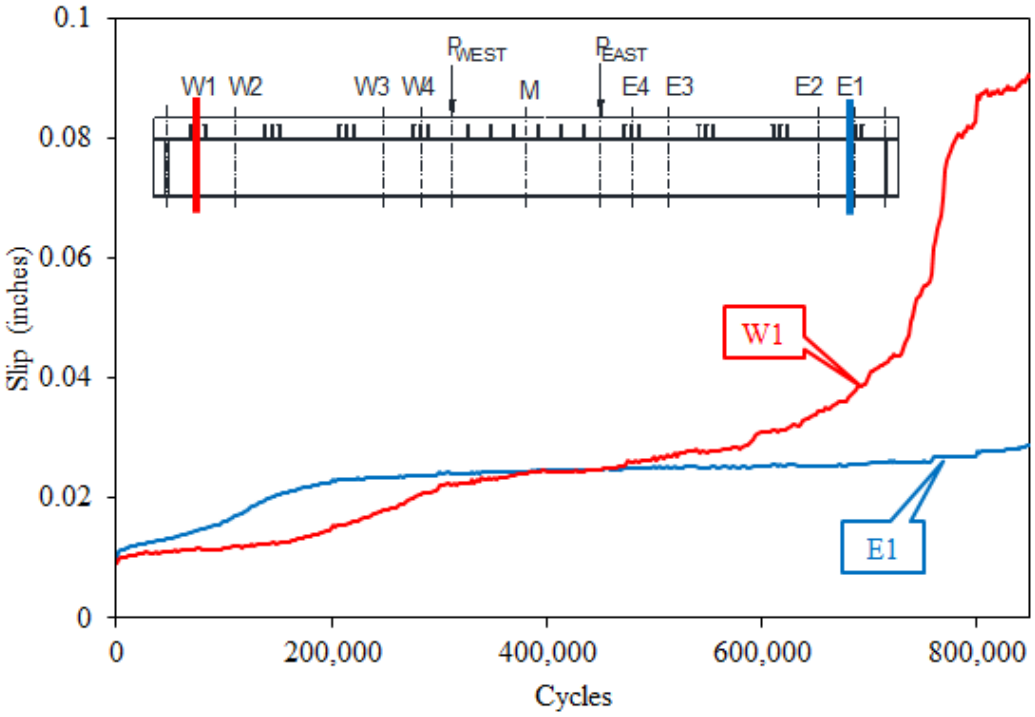

Source: FHWA.

Figure 147. Graph. Horizontal slip in both shear spans of 3F1.

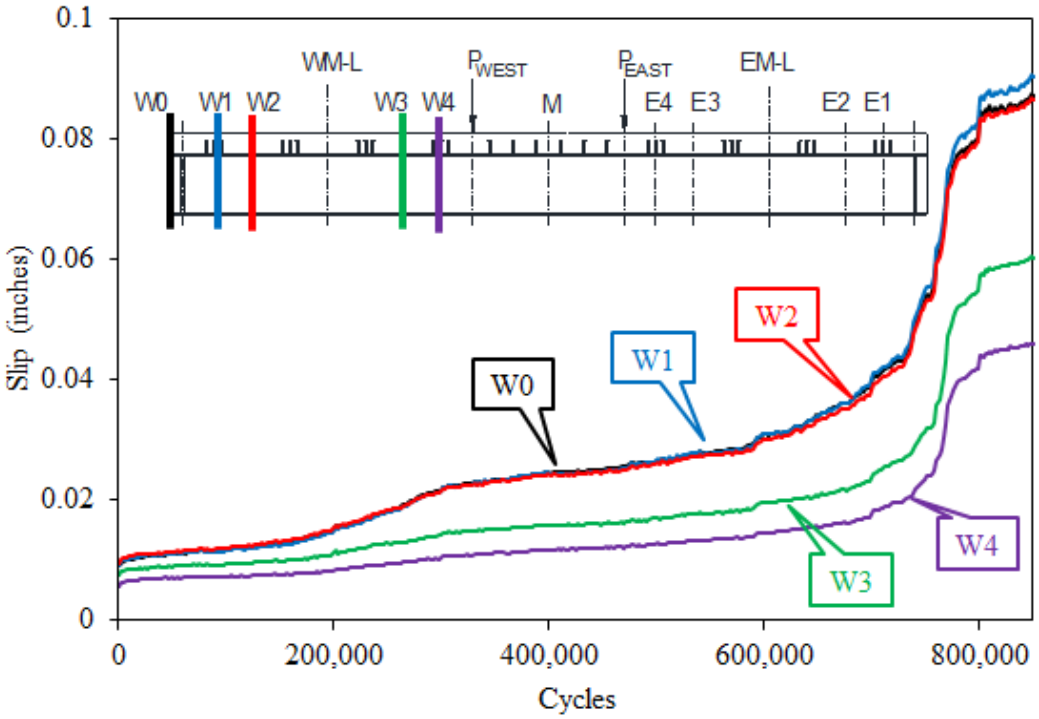

Source: FHWA.

Figure 148. Graph. Horizontal slip in west shear span of 3F1.

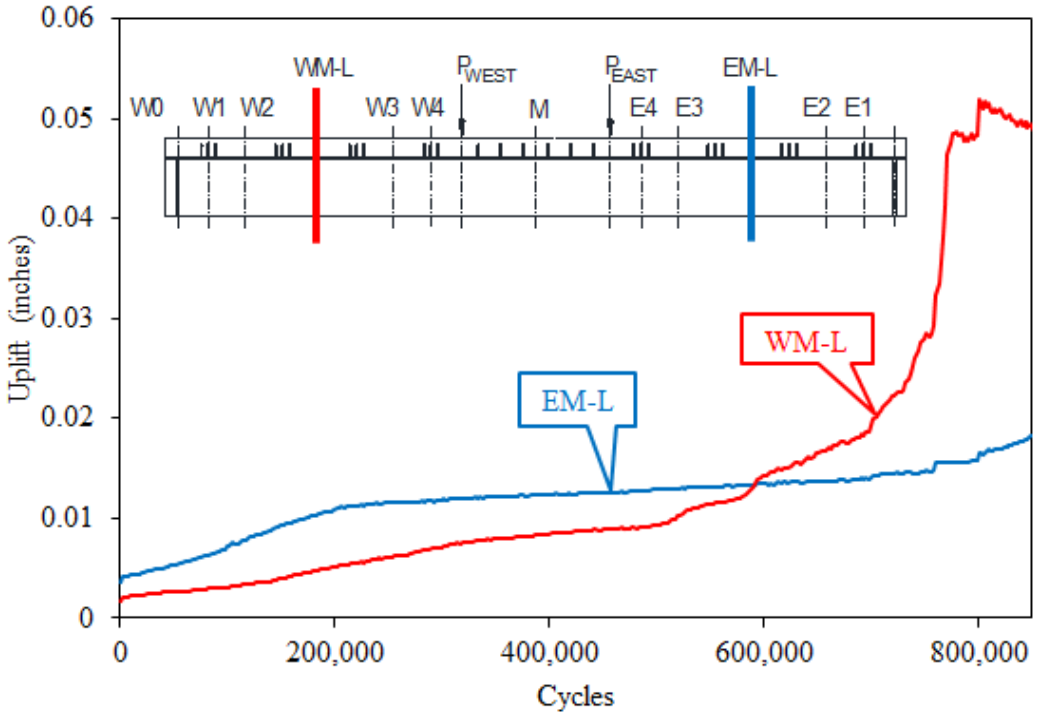

Source: FHWA.

Figure 149. Graph. Vertical uplift in both shear spans of 3F1.

SPECIMEN 3F2

Figure 150 through figure 154 show the strain gauge and LVDT results for specimen 3F2.

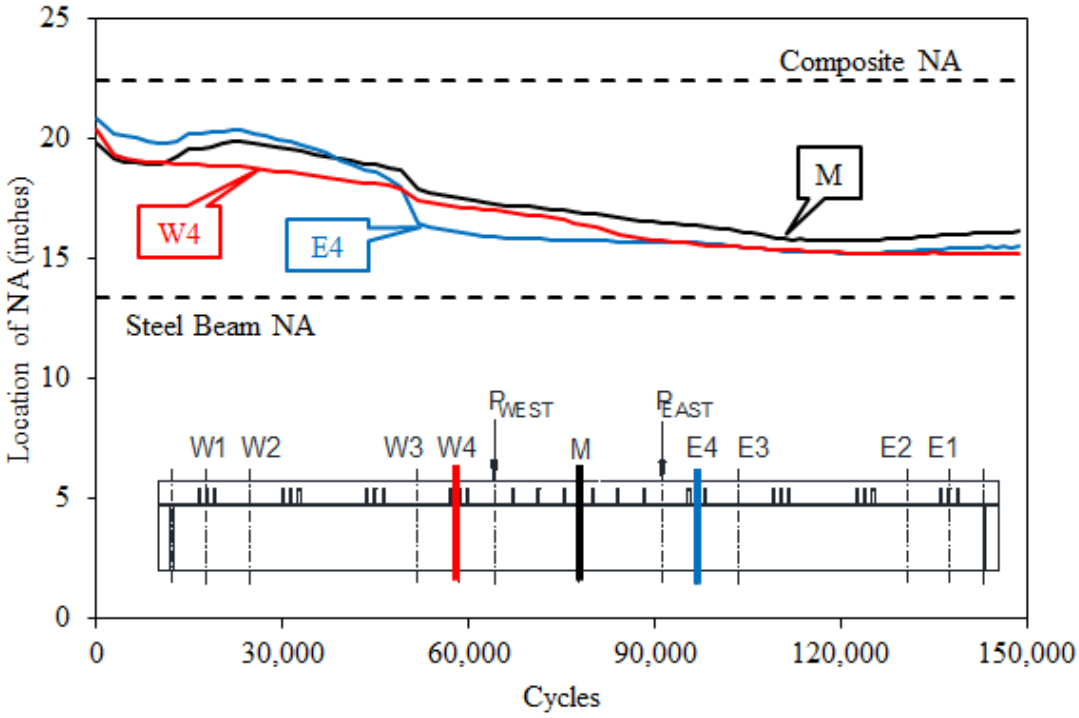

Source: FHWA.

Figure 150. Graph. Location of NA for both shear spans of 3F2.

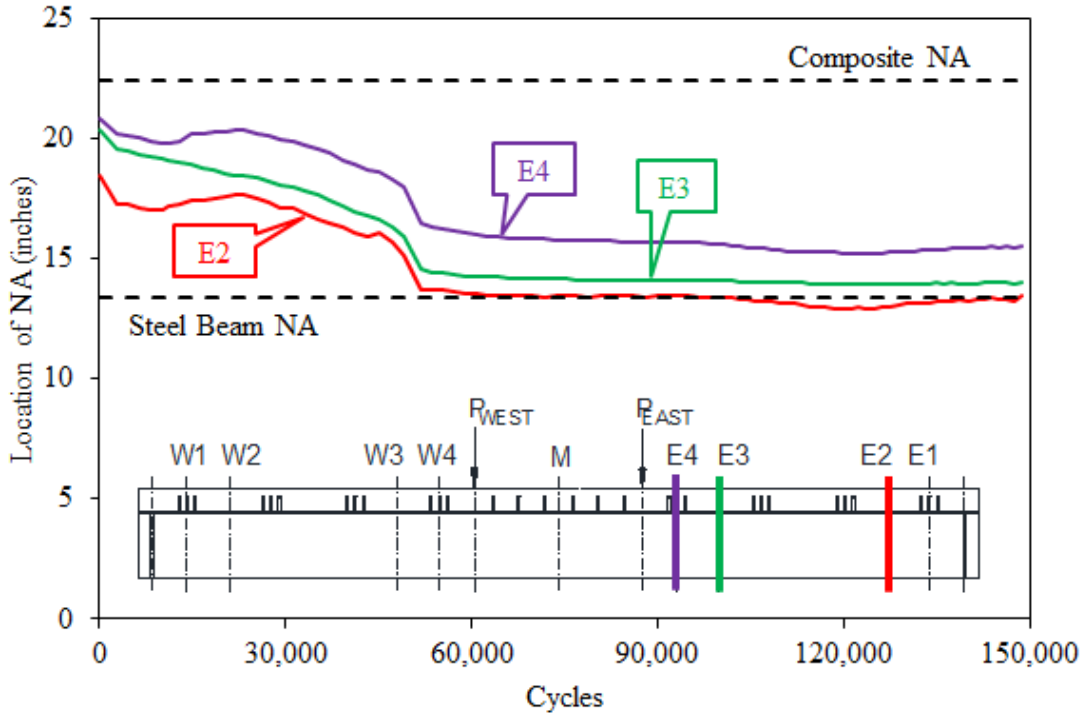

Source: FHWA.

Figure 151. Graph. Location of NA for east shear span of 3F2.

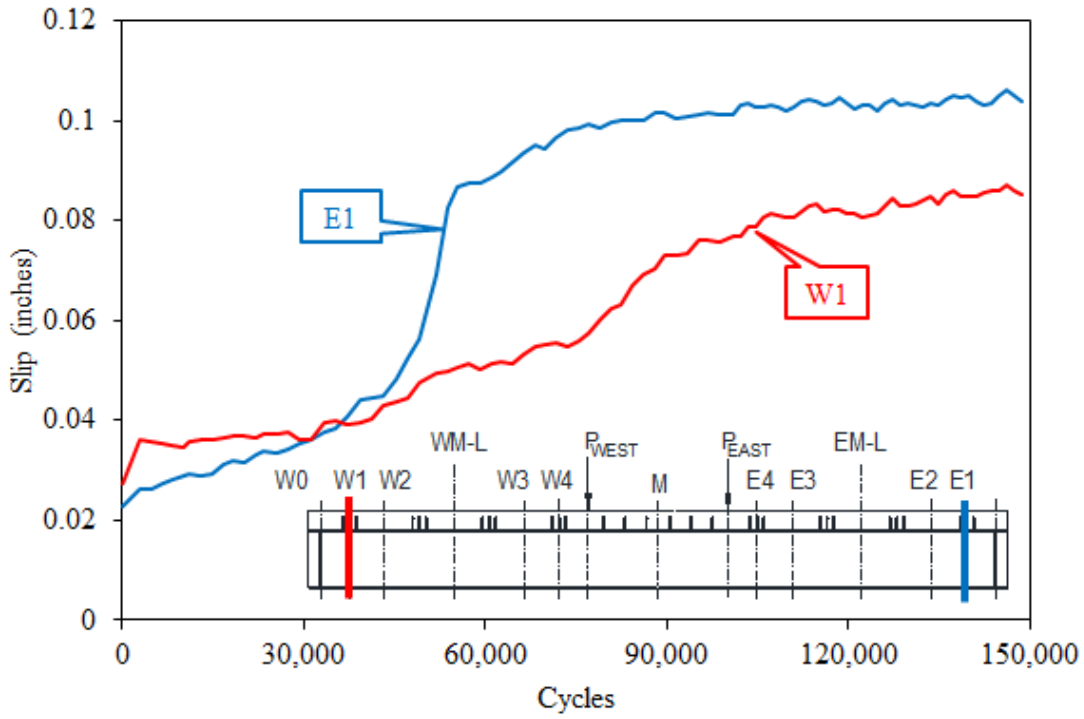

Source: FHWA.

Figure 152. Graph. Horizontal slip in both shear spans of 3F2.

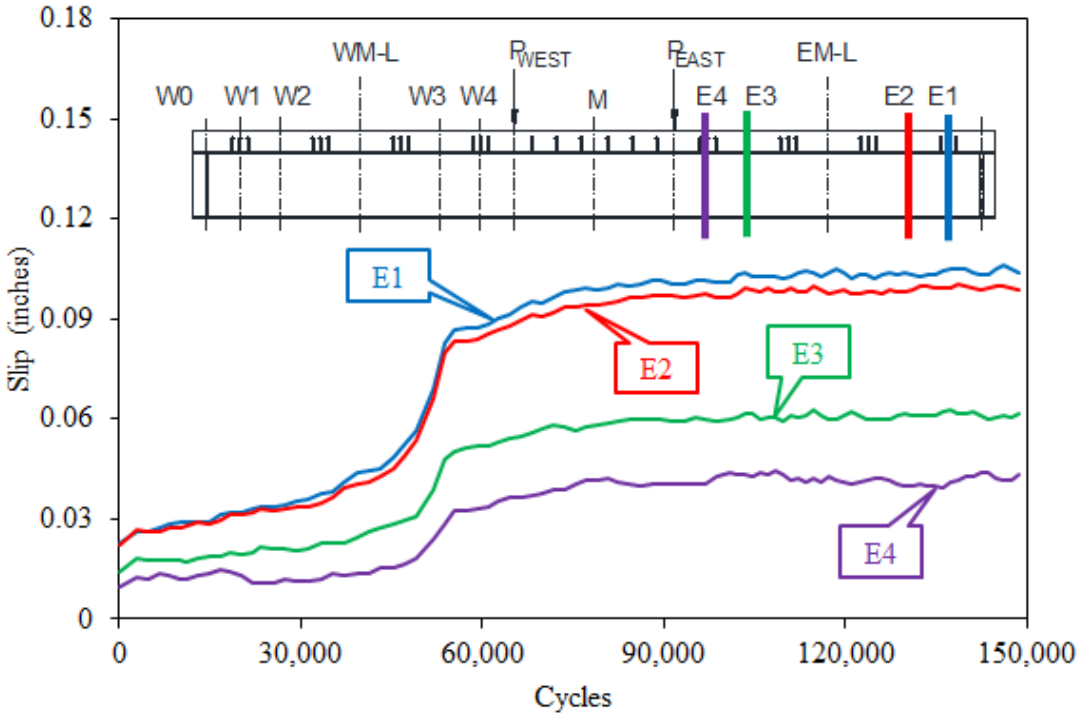

Source: FHWA.

Figure 153. Graph. Horizontal slip in east shear span of 3F2.

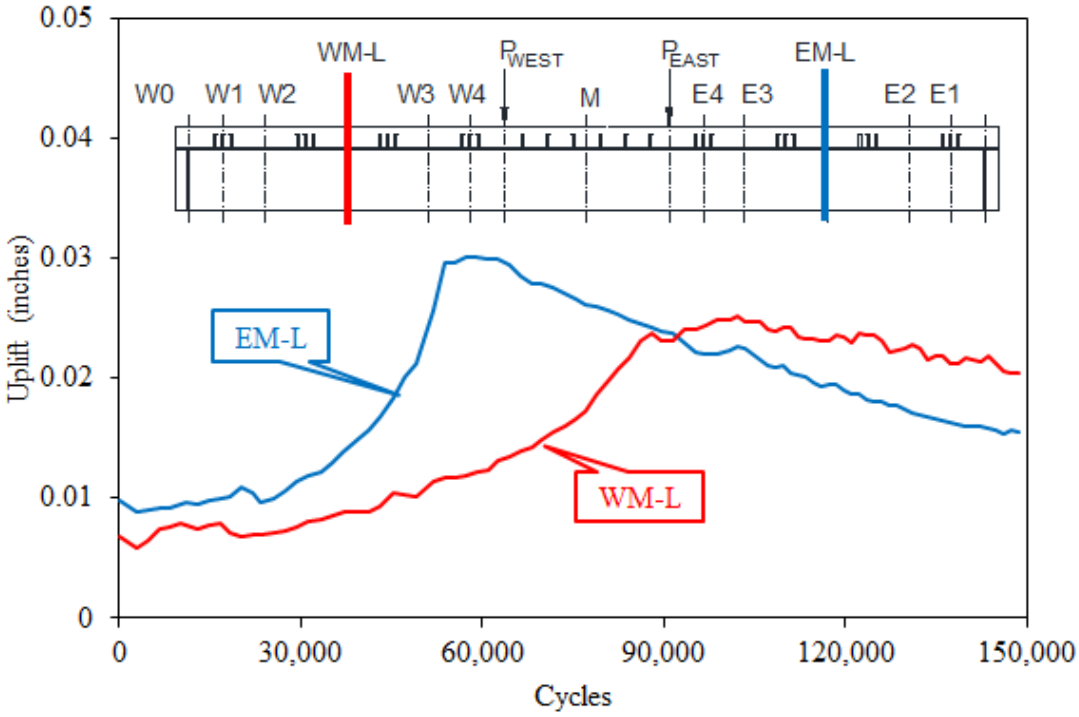

Source: FHWA.

Figure 154. Graph. Vertical uplift in both shear spans of 3F2.

SPECIMEN 3F3

Figure 155 through figure 159 show the strain gauge and LVDT results for specimen 3F3.

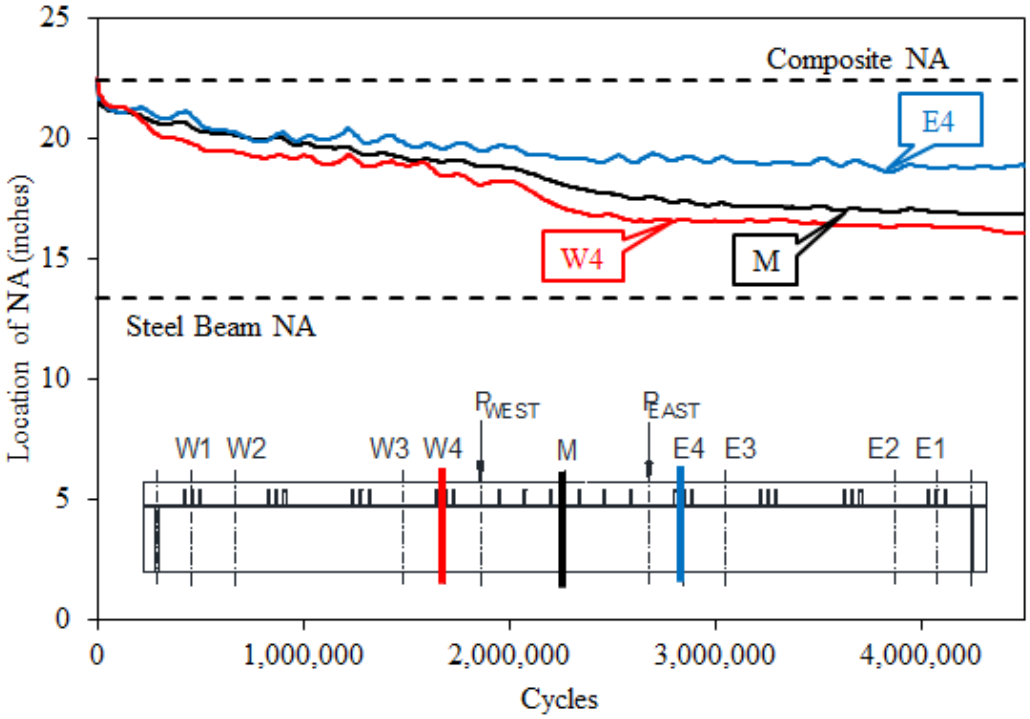

Source: FHWA.

Figure 155. Graph. Location of NA for both shear spans of 3F3.

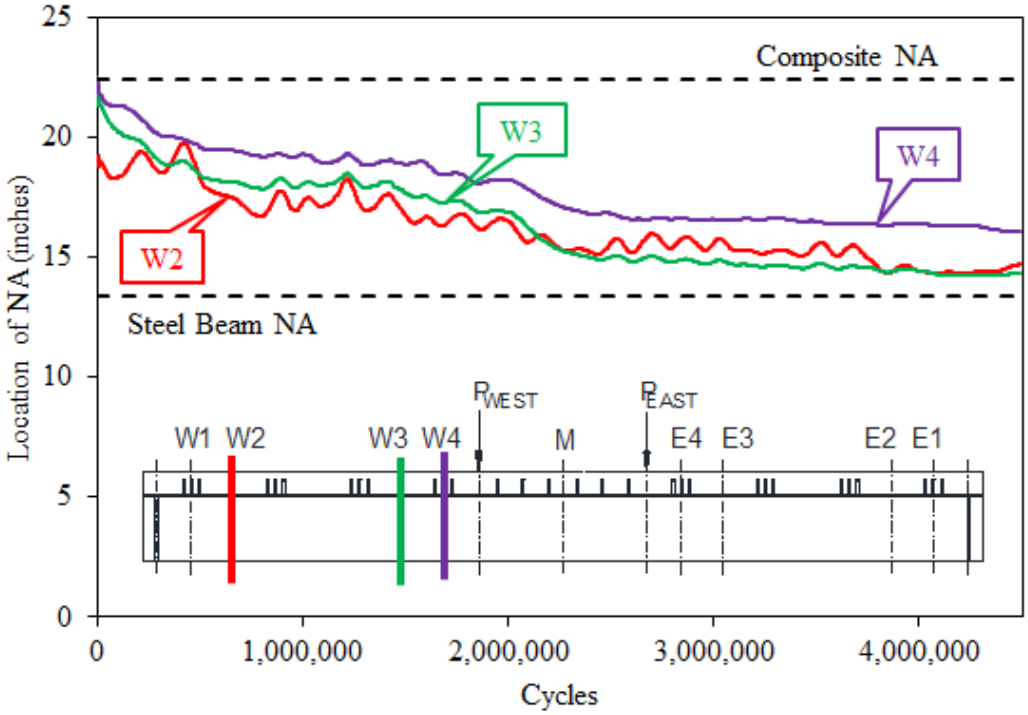

Source: FHWA.

Figure 156. Graph. Location of NA for west shear span of 3F3.

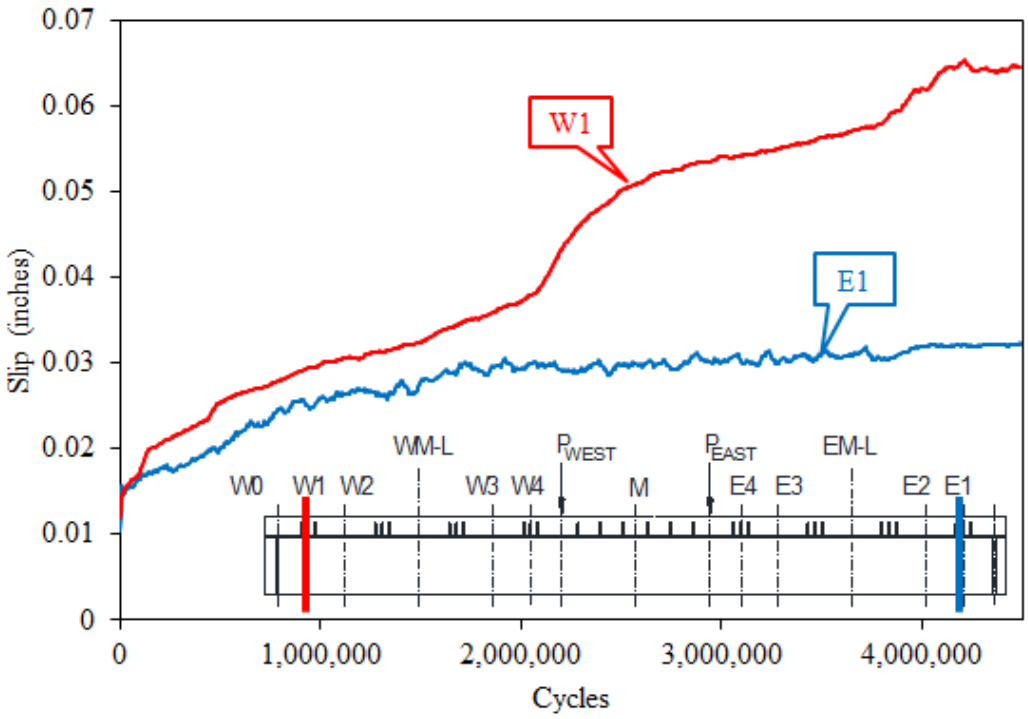

Source: FHWA.

Figure 157. Graph. Horizontal slip in both shear spans of 3F3.

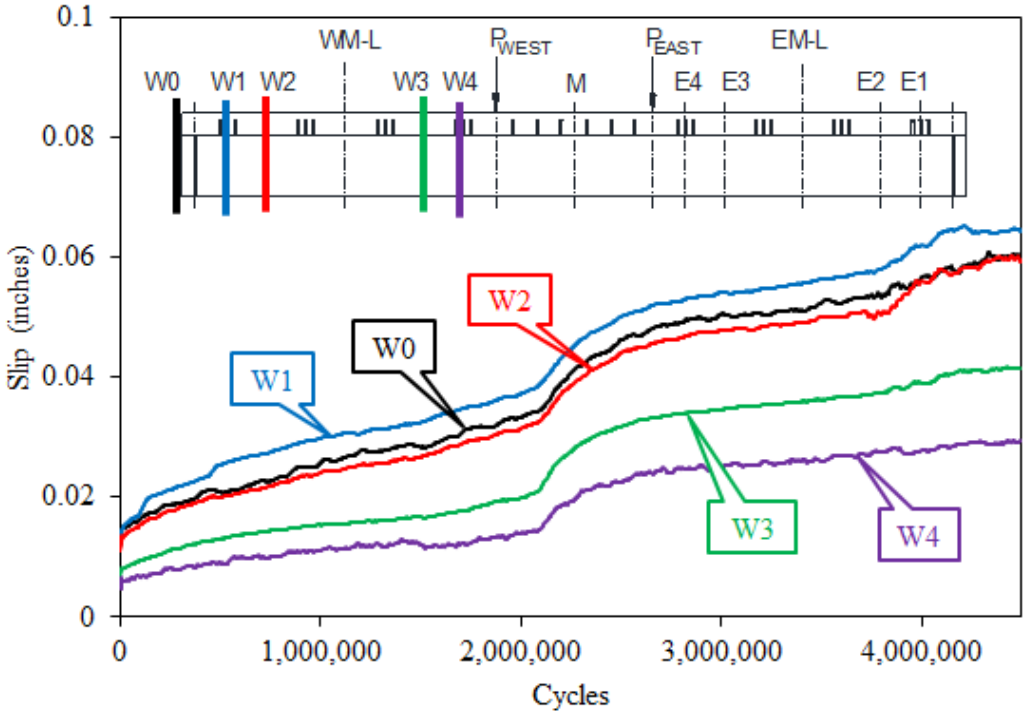

Source: FHWA.

Figure 158. Graph. Horizontal slip in west shear span of 3F3.

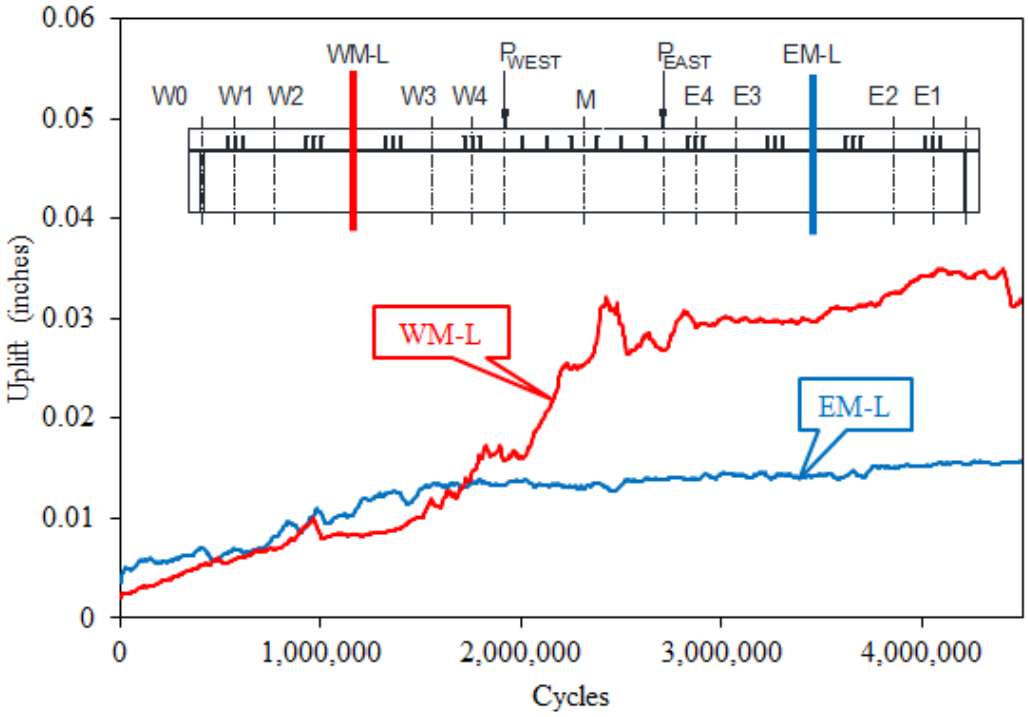

Source: FHWA.

Figure 159. Graph. Vertical uplift in both shear spans of 3F3.

SPECIMEN 4F2

Figure 160 through figure 164 show the strain gauge and LVDT results for specimen 4F2.

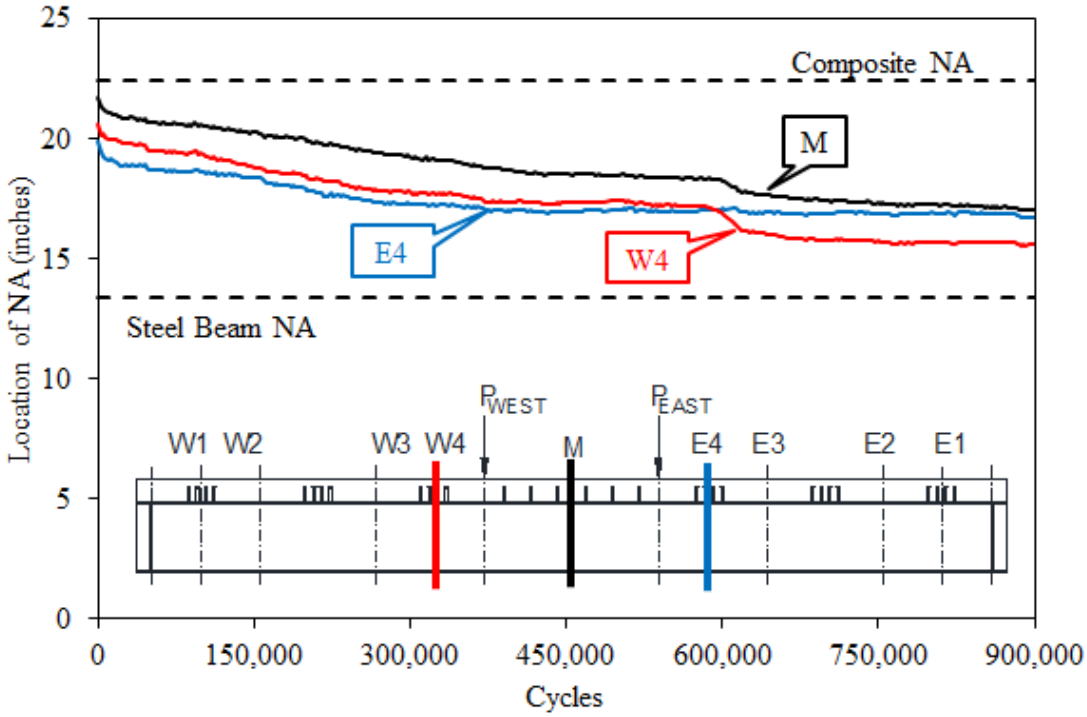

Source: FHWA.

Figure 160. Graph. Location of NA for both shear spans of 4F2.

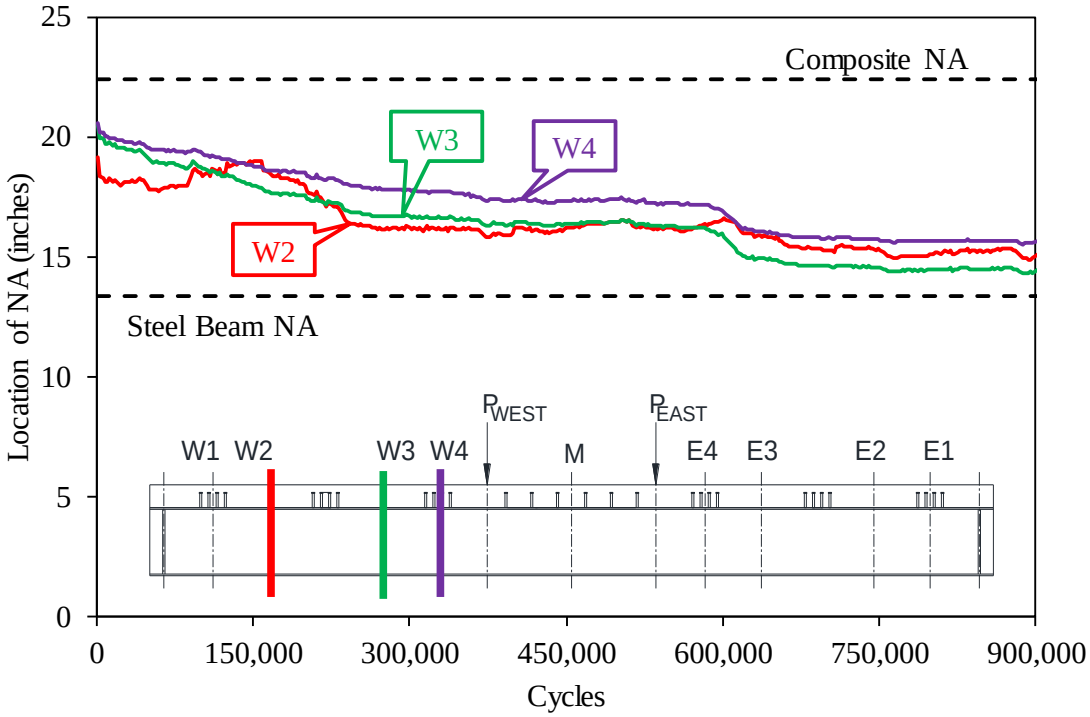

Source: FHWA.

Figure 161. Graph. Location of NA for west shear span of 4F2.

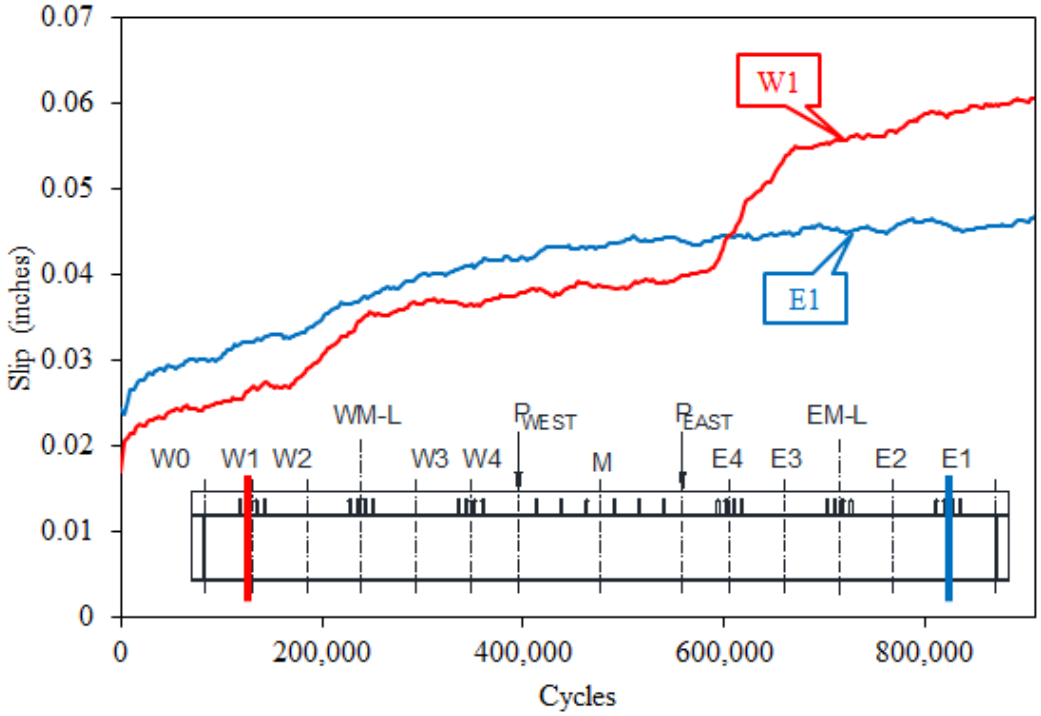

Source: FHWA.

Figure 162. Graph. Horizontal slip in both shear spans of 4F2.

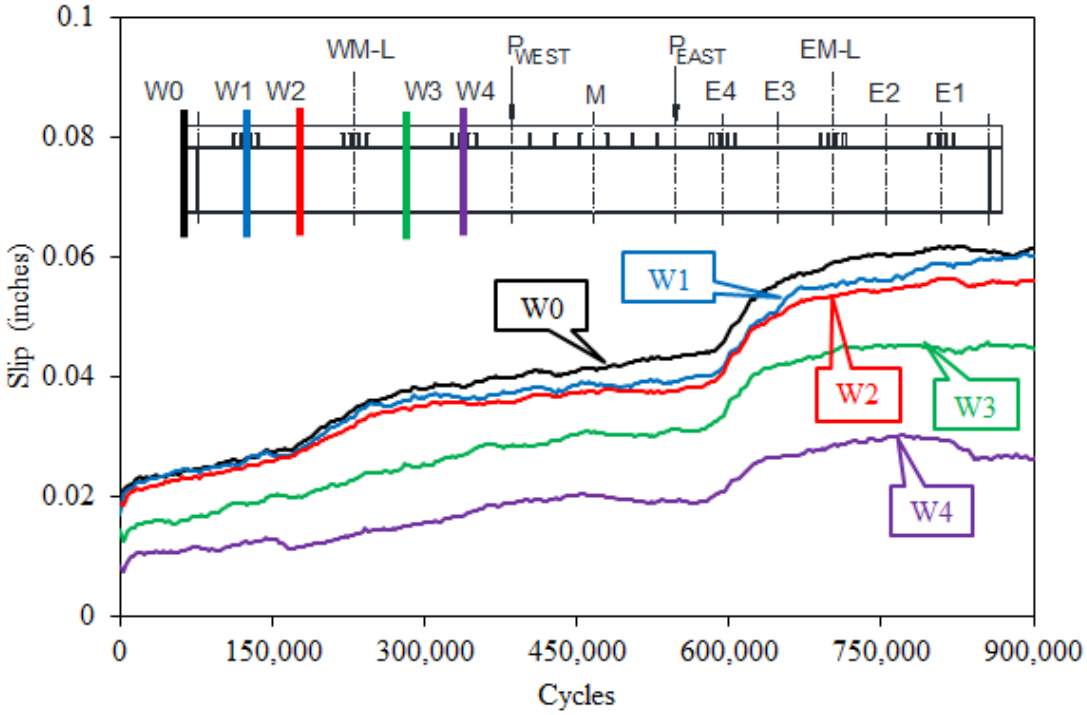

Source: FHWA.

Figure 163. Graph. Horizontal slip in west shear span of 4F2.

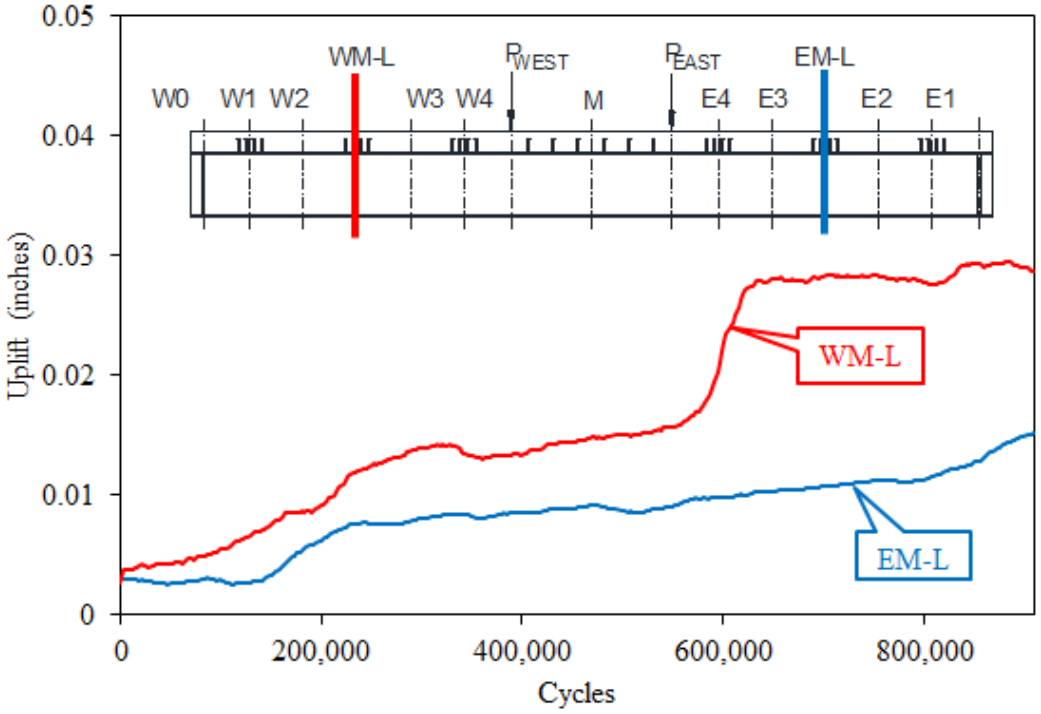

Source: FHWA.

Figure 164. Graph. Vertical uplift in both shear spans of 4F2.

SPECIMEN 4F3

Figure 165 through figure 171 show the strain gauge and LVDT results for specimen 4F3.

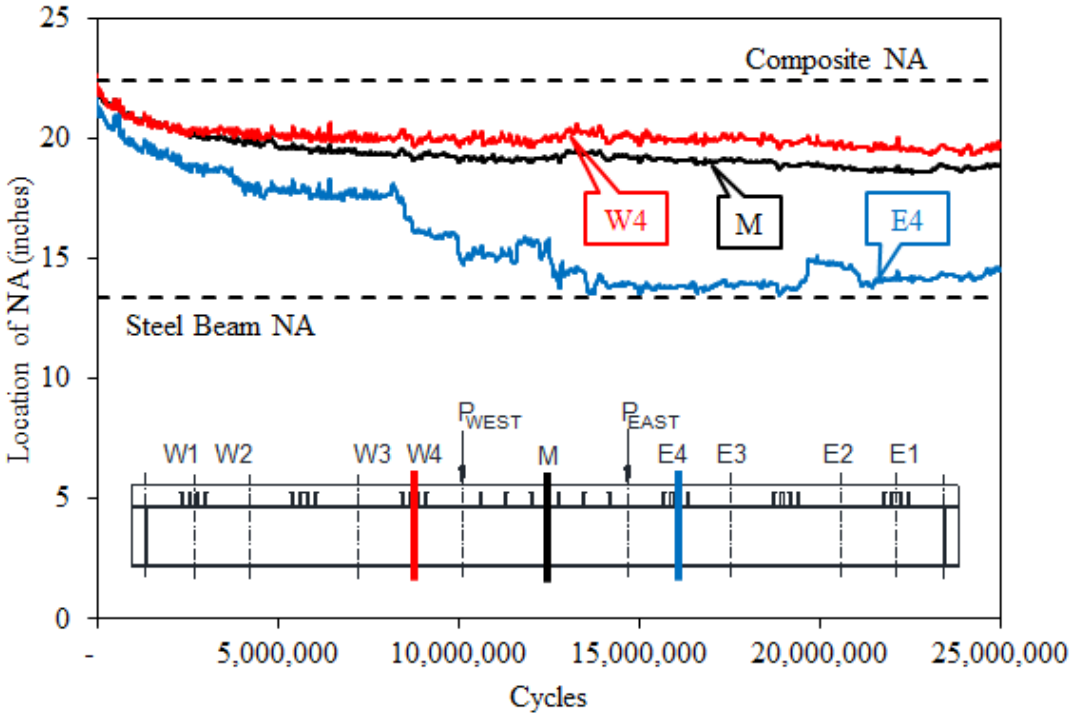

Source: FHWA.

Figure 165. Graph. Location of NA for both shear spans of 4F3.

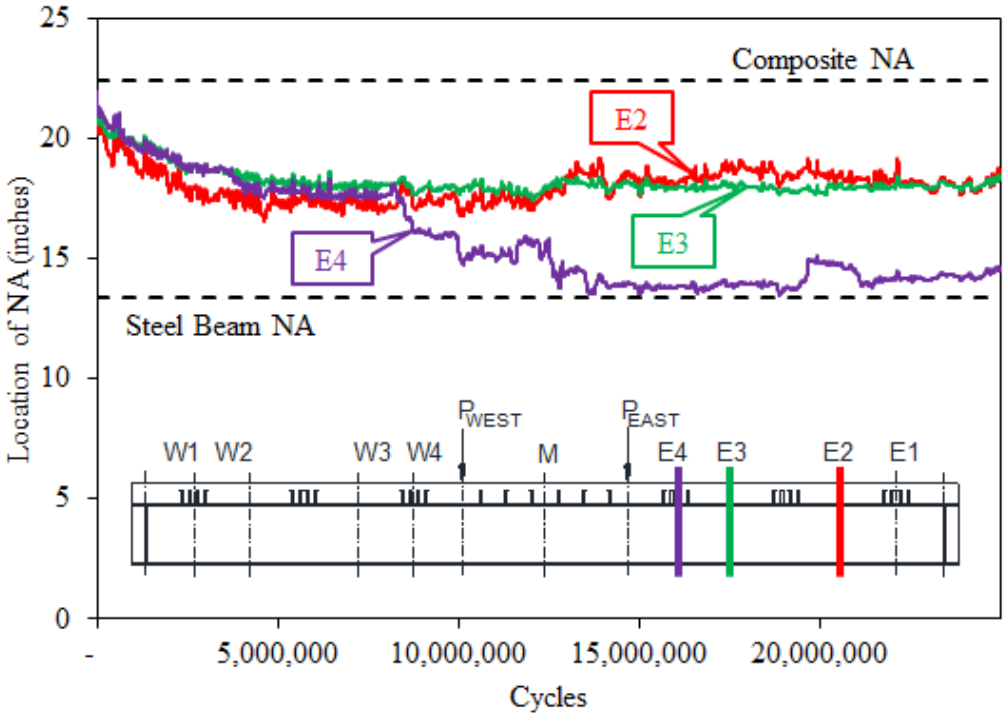

Source: FHWA.

Figure 166. Graph. Location of NA for east shear span of 4F3.

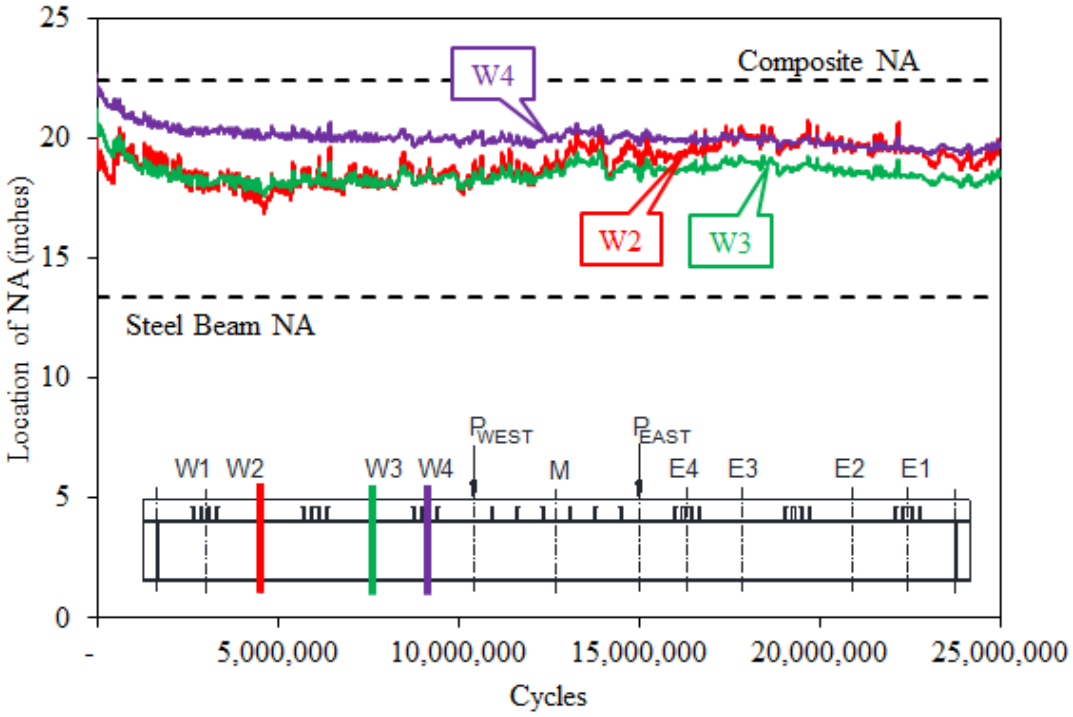

Source: FHWA.

Figure 167. Graph. Location of NA for west shear span of 4F3.

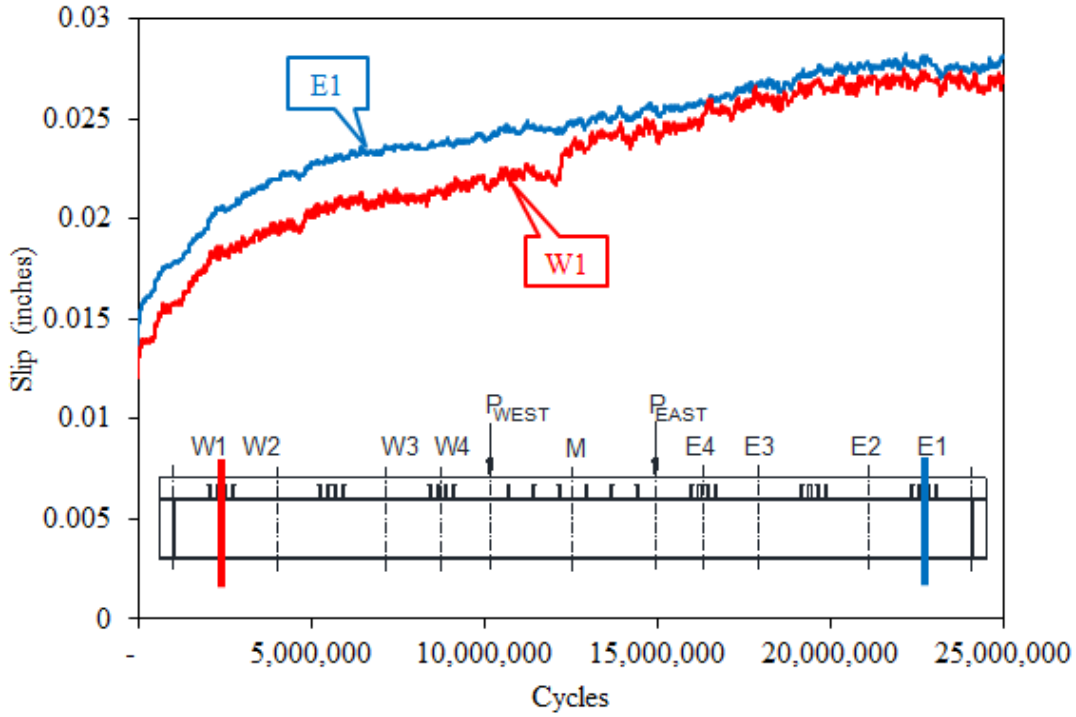

Source: FHWA.

Figure 168. Graph. Horizontal slip in both shear spans of 4F3.

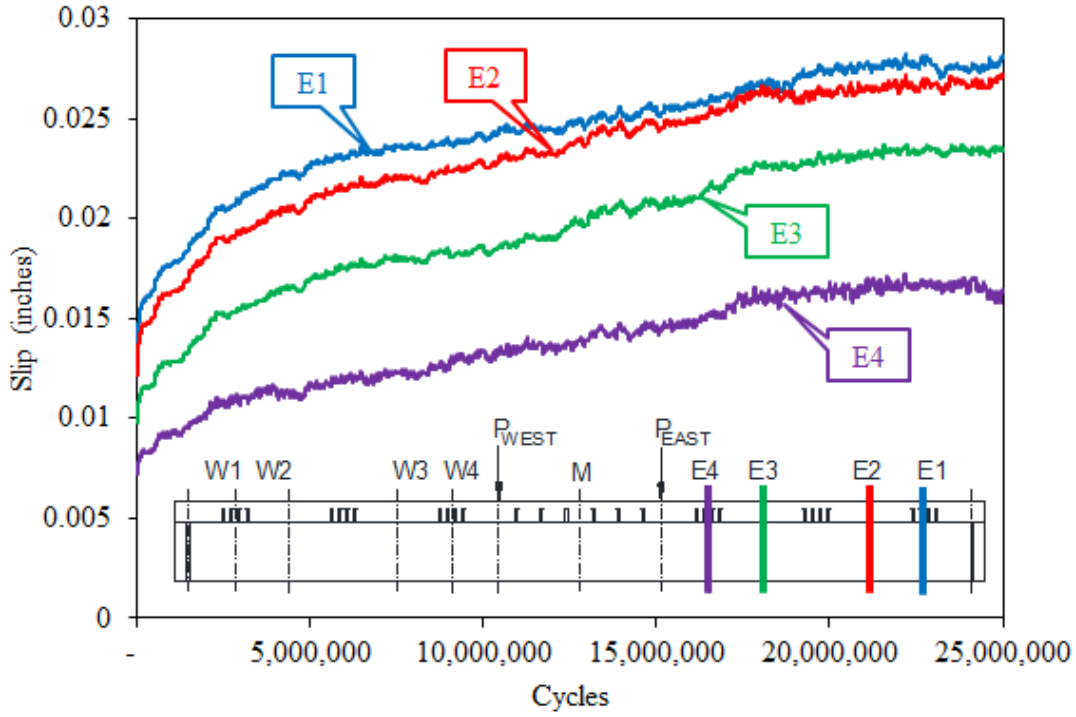

Source: FHWA.

Figure 169. Graph. Horizontal slip in east shear span of 4F3.

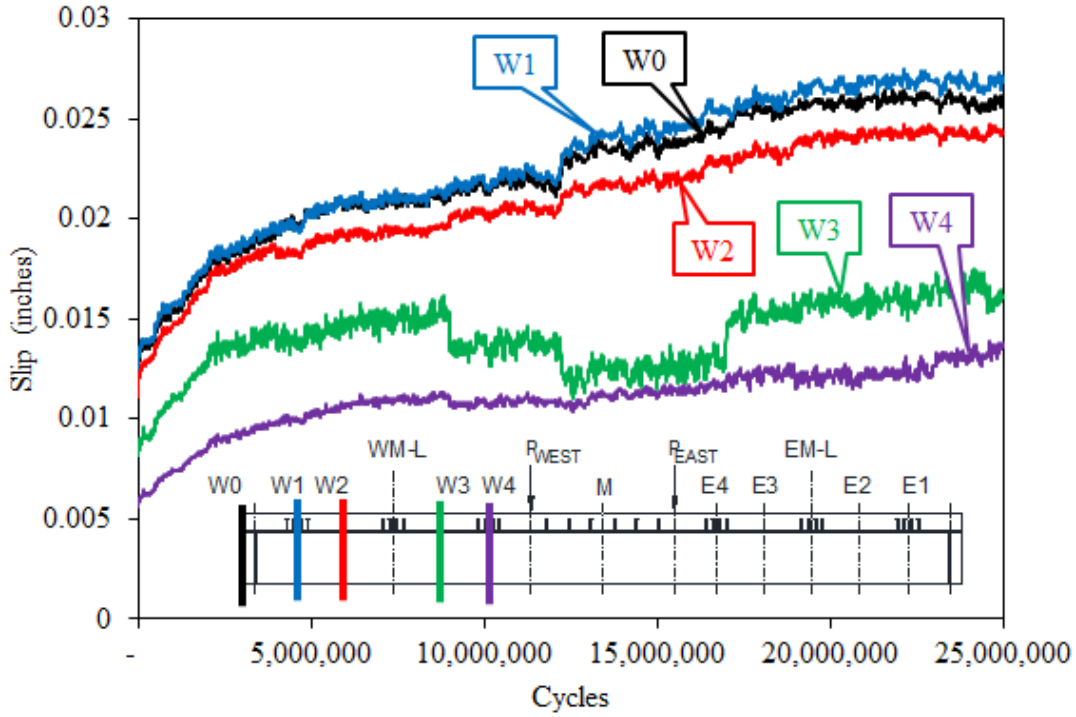

Source: FHWA.

Figure 170. Graph. Horizontal slip in west shear span of 4F3.

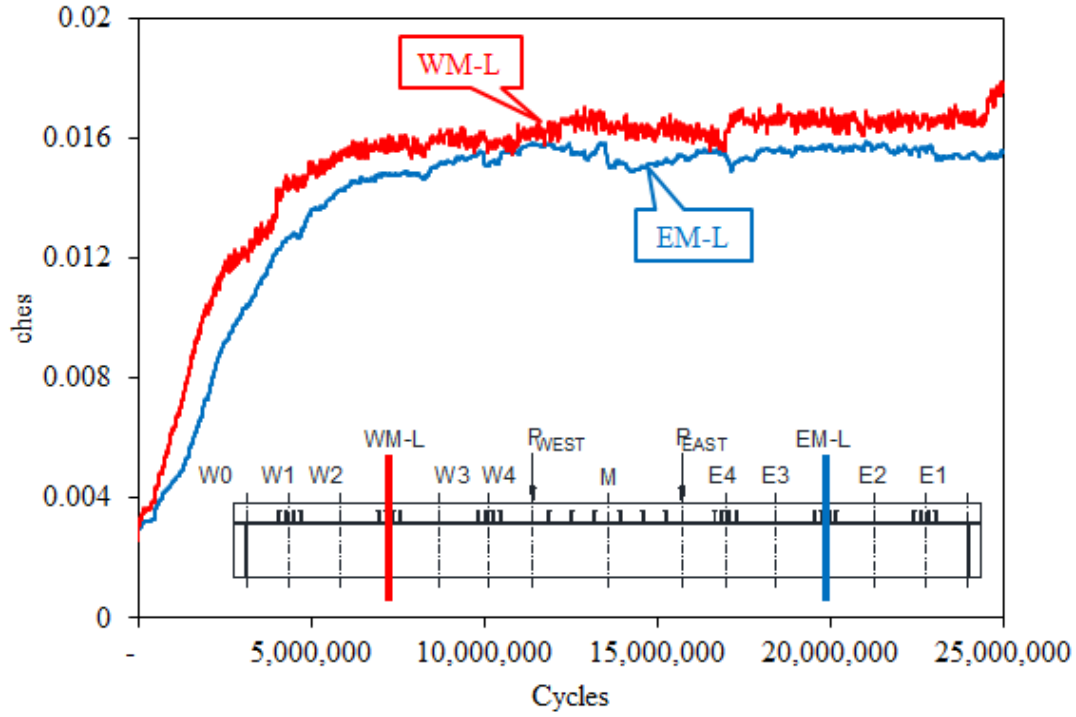

Source: FHWA.

Figure 171. Graph. Vertical uplift in both shear spans of 4F3.

APPENDIX D. LASER TRACKER RESULTS

This appendix contains the laser tracker data collected for all large-scale fatigue specimens. The laser tracker collects three-dimensional coordinate data of measurement points, which can be decoupled into slip and uplift displacements between the concrete deck and beam flange. Figure 172 through figure 180 show graphs of relative slip between the concrete deck and the beam flange collected for each large-scale fatigue specimen. Figure 181 through figure 189 show the relative uplift between the concrete deck and beam flange for each large-scale fatigue specimen.

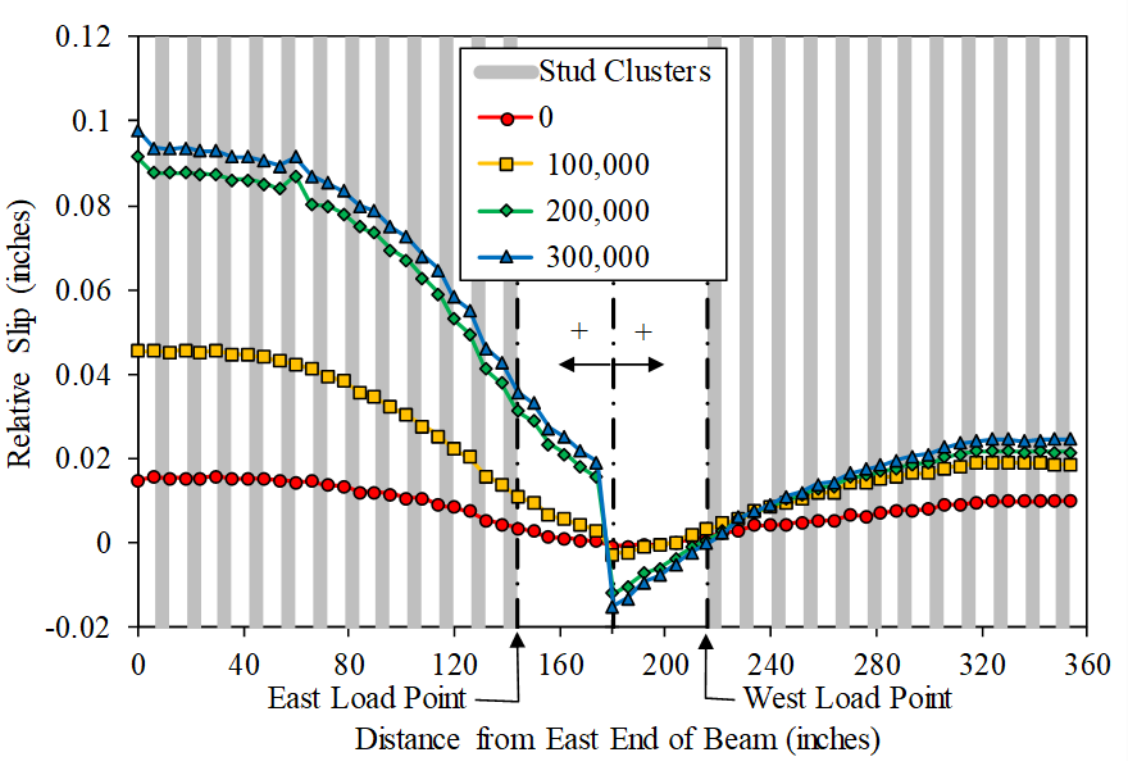

Source: FHWA.

Figure 172. Graph. Laser tracker slip results for beam 1F2.

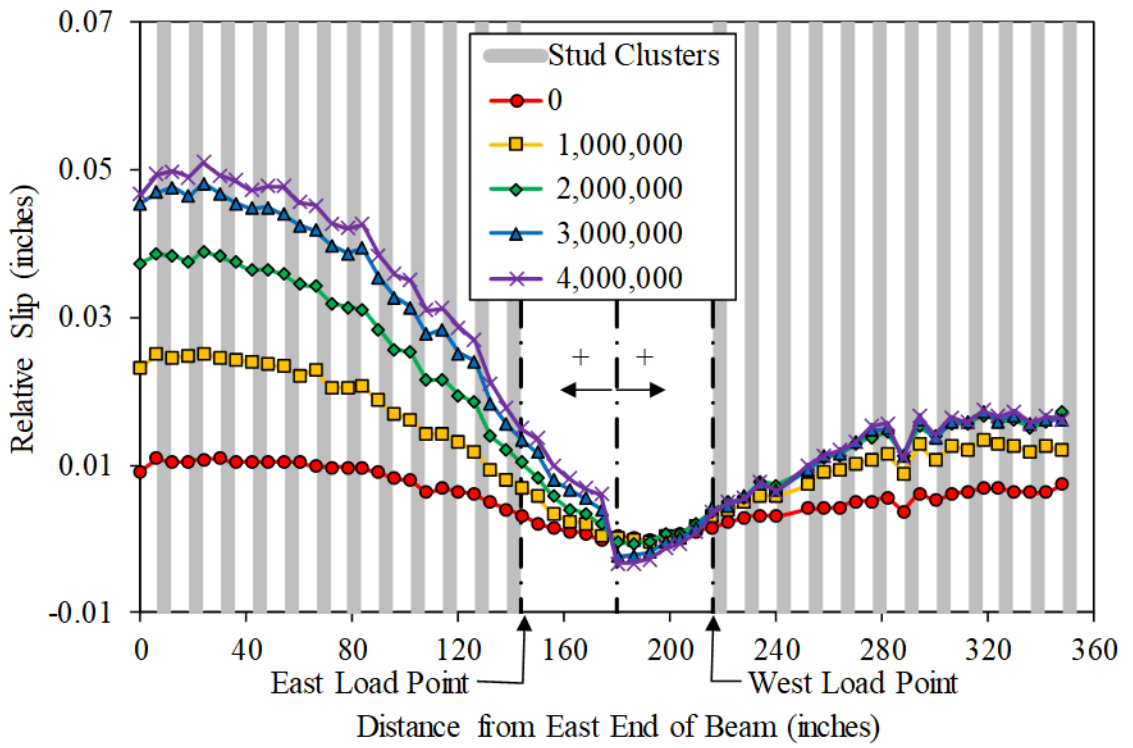

Source: FHWA.

Figure 173. Graph. Laser tracker slip results for beam 1F3.

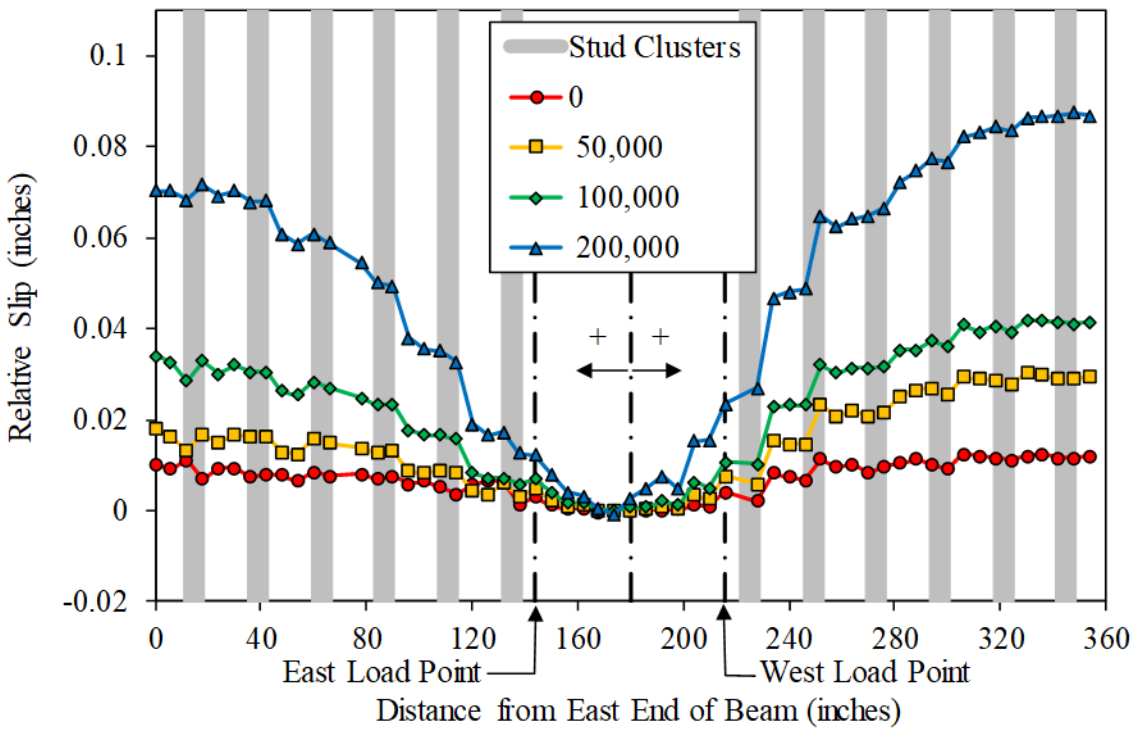

Source: FHWA.

Figure 174. Graph. Laser tracker slip results for beam 2F1.

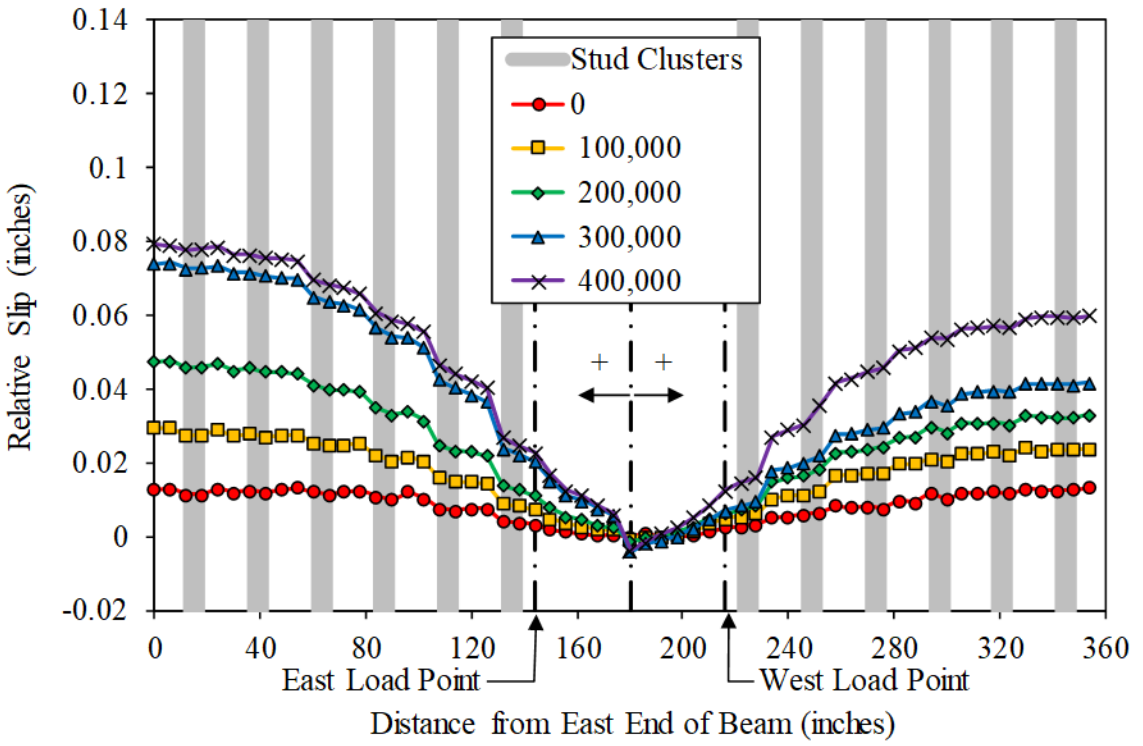

Source: FHWA.

Figure 175. Graph. Laser tracker slip results for beam 2F2.

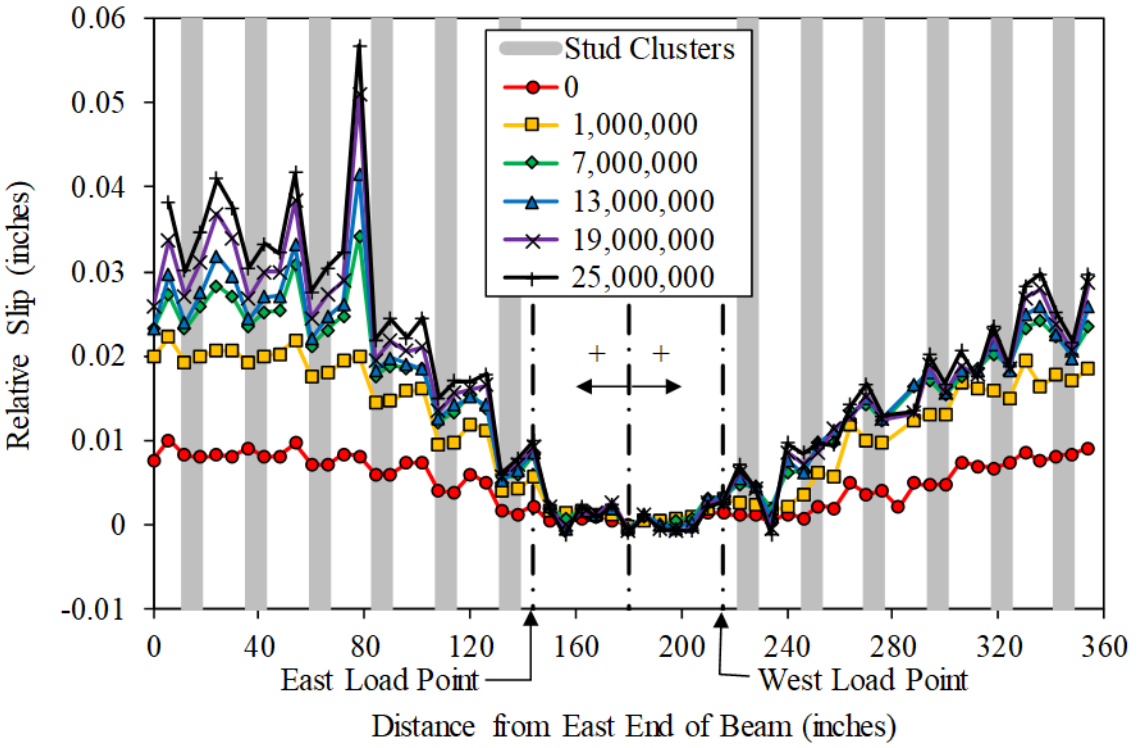

Source: FHWA.

Figure 176. Graph. Laser tracker slip results for beam 2F3.

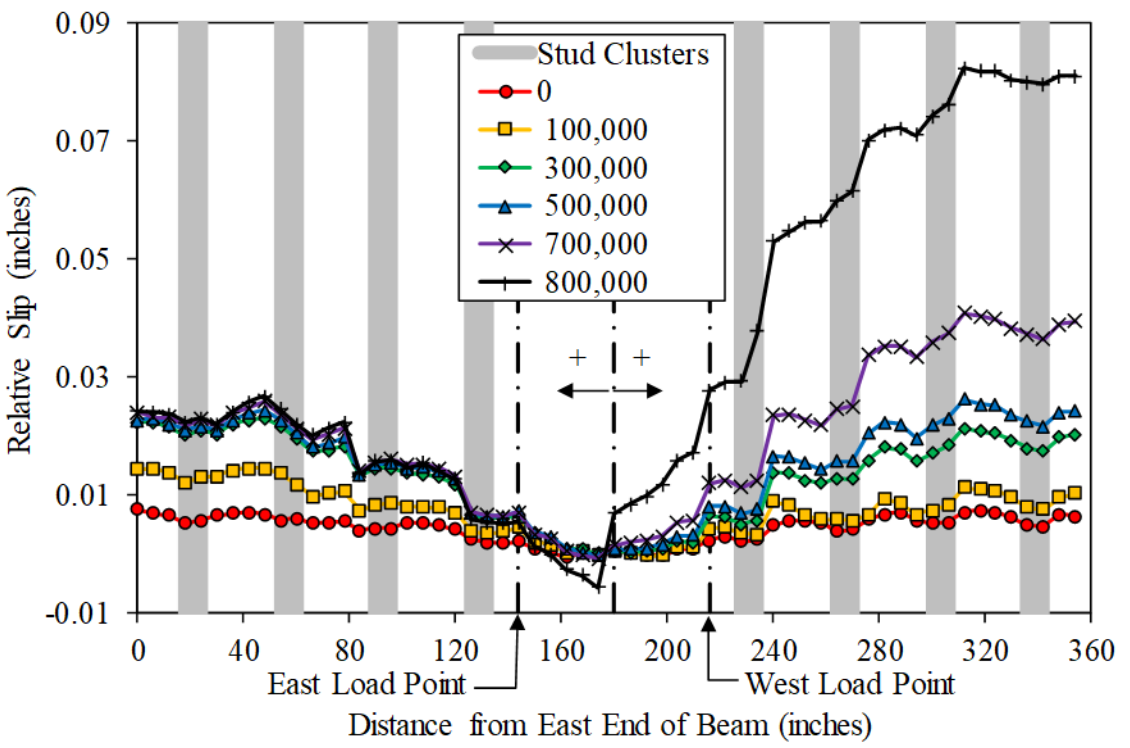

Source: FHWA.

Figure 177. Graph. Laser tracker slip results for beam 3F1.

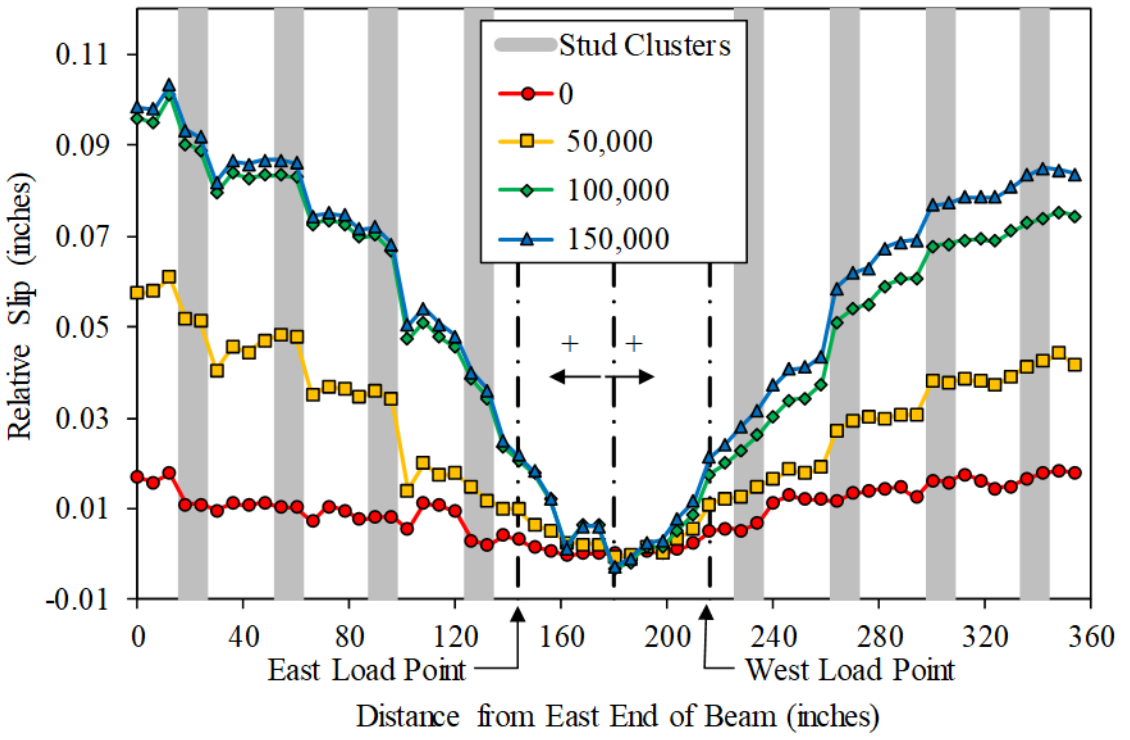

Source: FHWA.

Figure 178. Graph. Laser tracker slip results for beam 3F2.

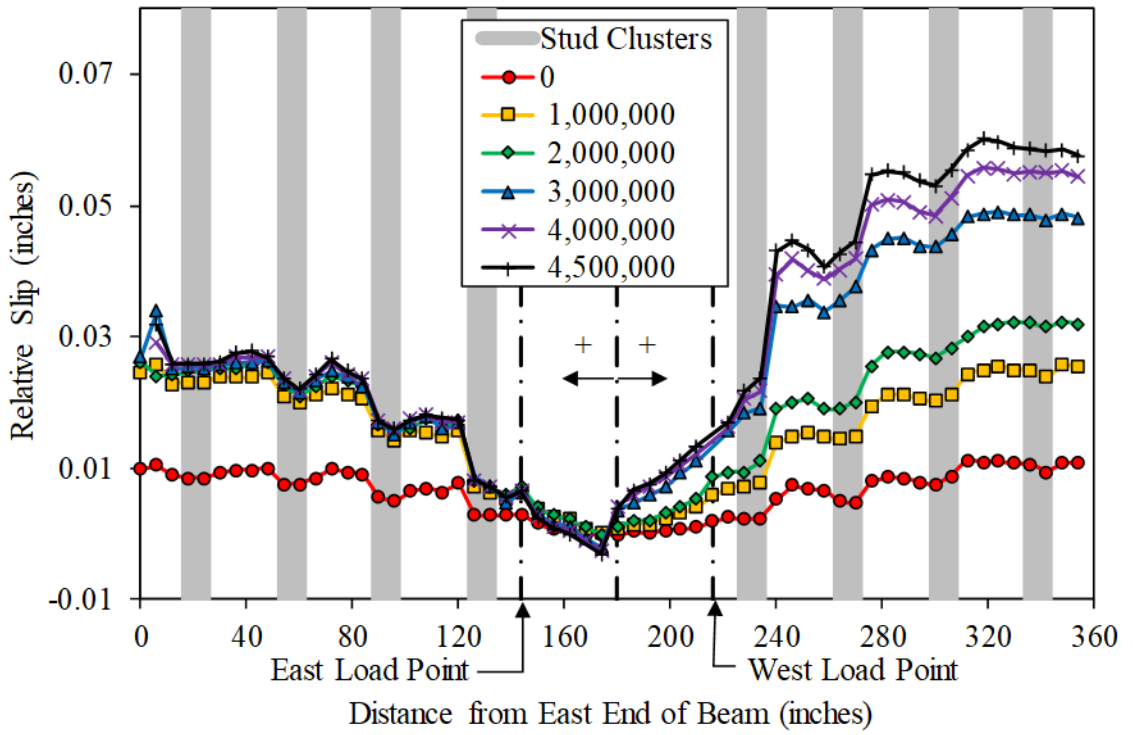

Source: FHWA.

Figure 179. Graph. Laser tracker slip results for beam 3F3.

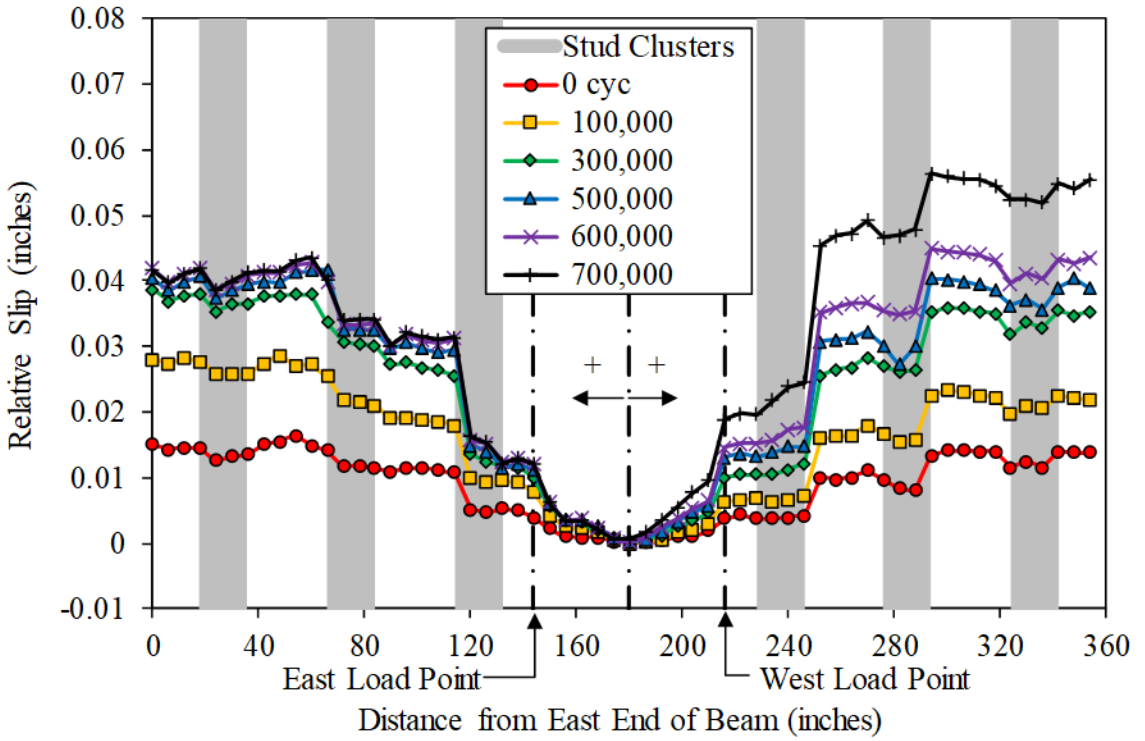

Source: FHWA.

Figure 180. Graph. Laser tracker slip results for beam 4F2.

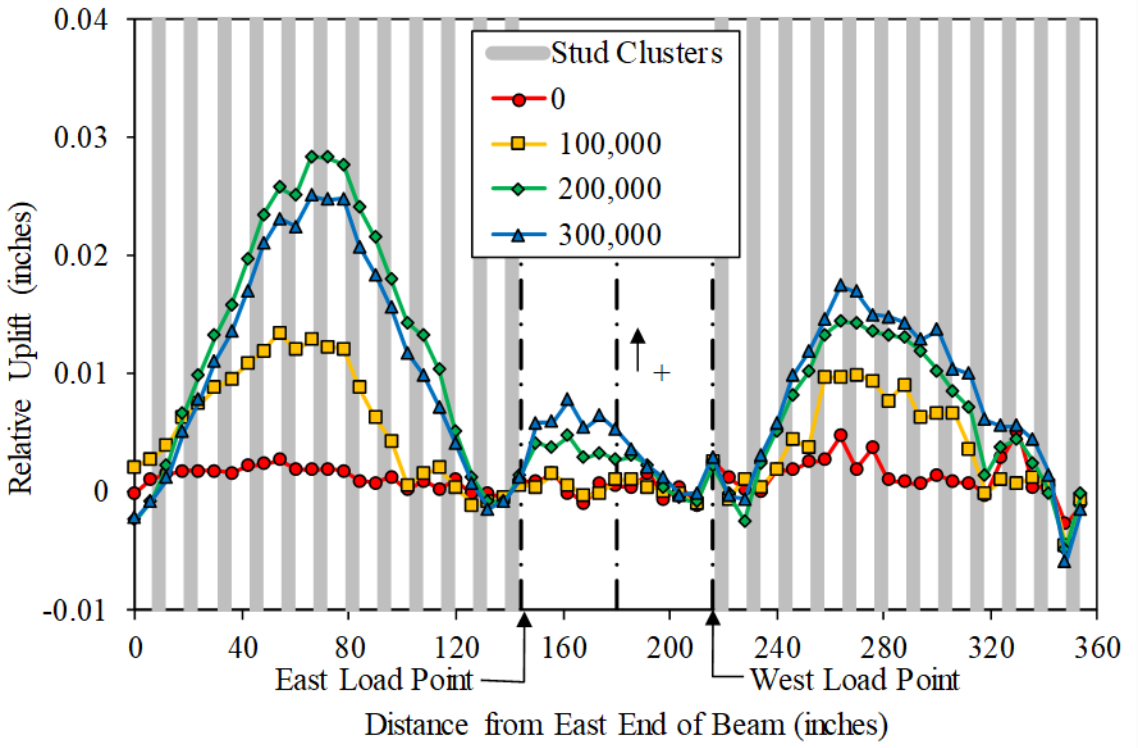

Source: FHWA.

Figure 181. Graph. Laser tracker uplift results for beam 1F2.

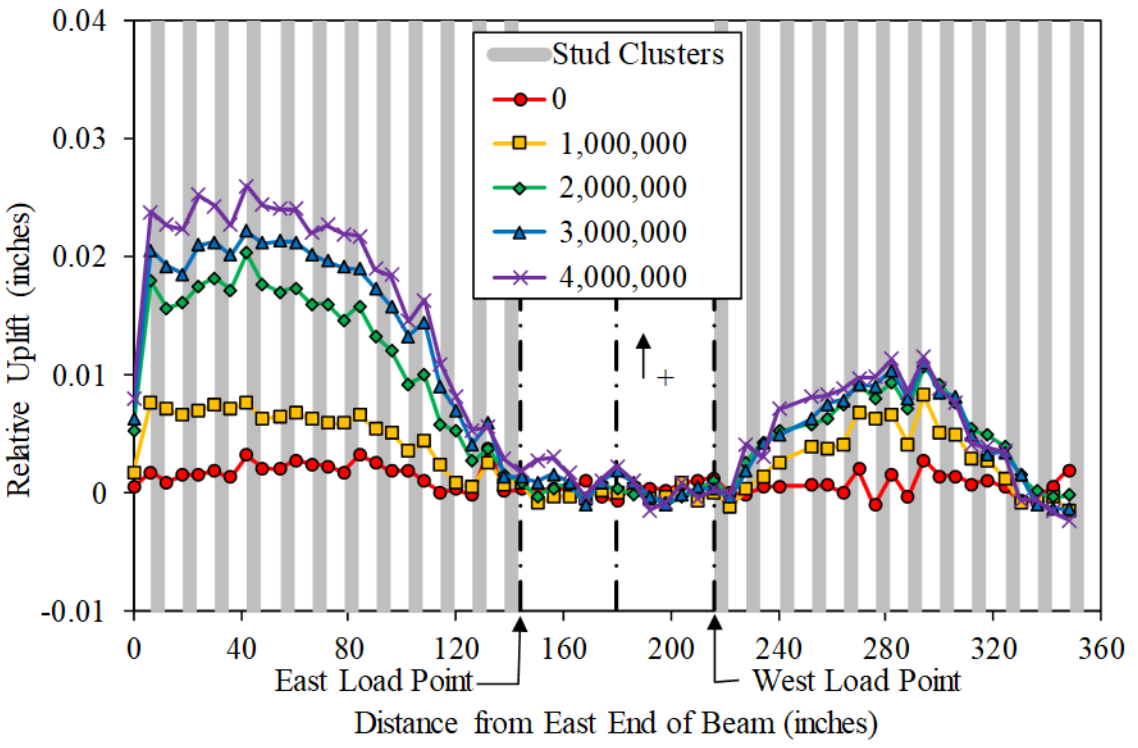

Source: FHWA.

Figure 182. Graph. Laser tracker uplift results for beam 1F3.

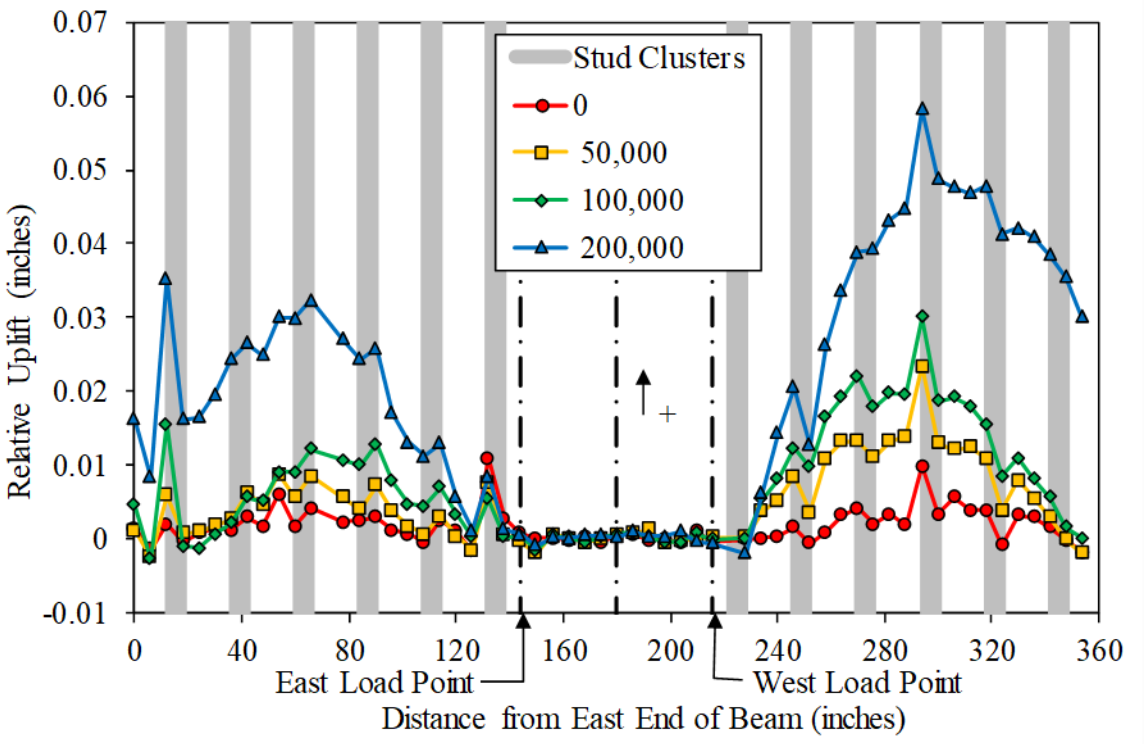

Source: FHWA.

Figure 183. Graph. Laser tracker uplift results for beam 2F1.

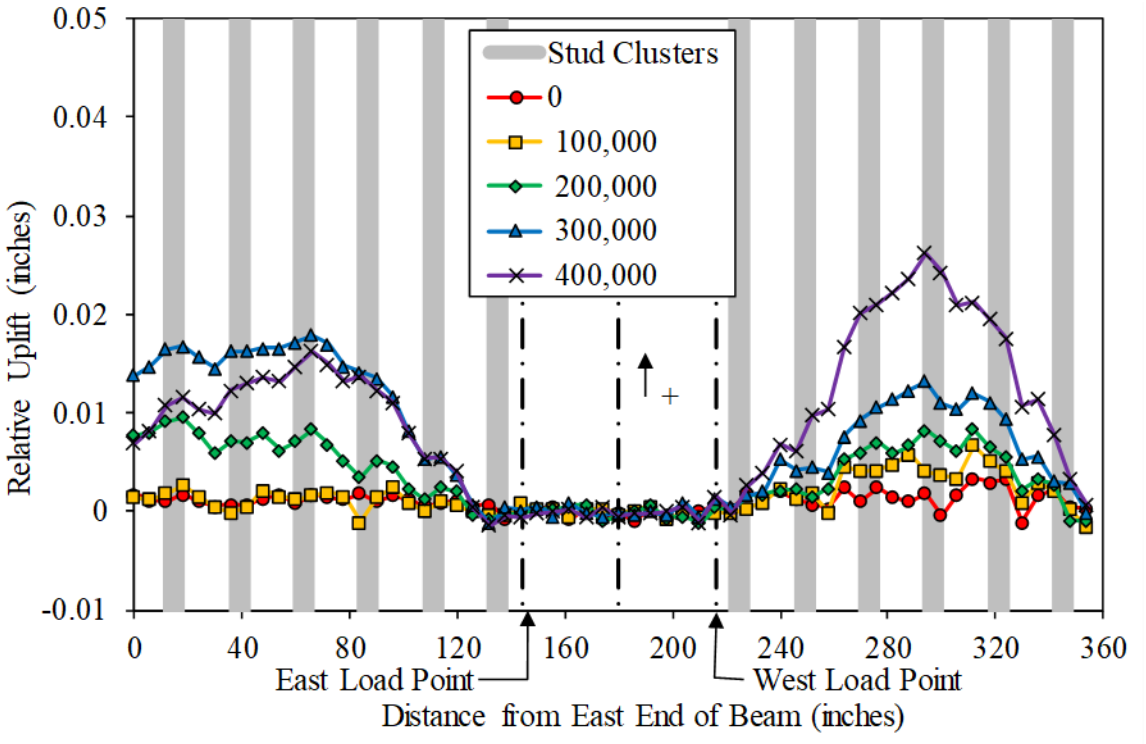

Source: FHWA.

Figure 184. Graph. Laser tracker uplift results for beam 2F2.

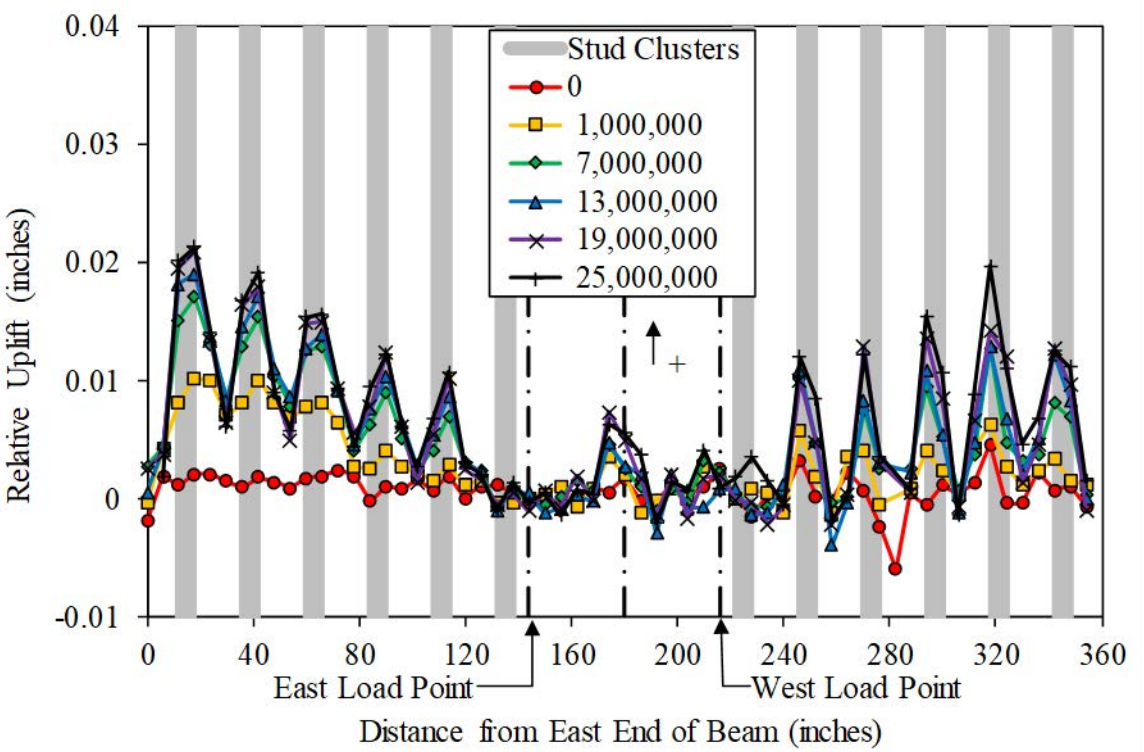

Source: FHWA.

Figure 185. Graph. Laser tracker uplift results for beam 2F3.

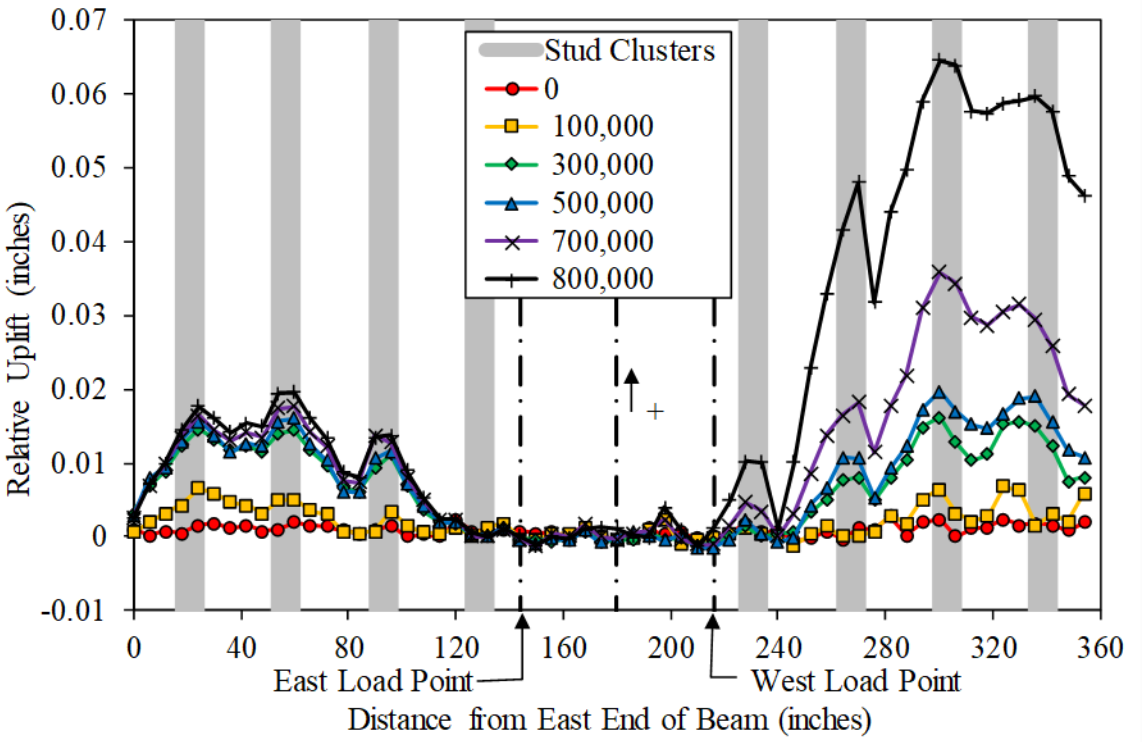

Source: FHWA.

Figure 186. Graph. Laser tracker uplift results for beam 3F1.

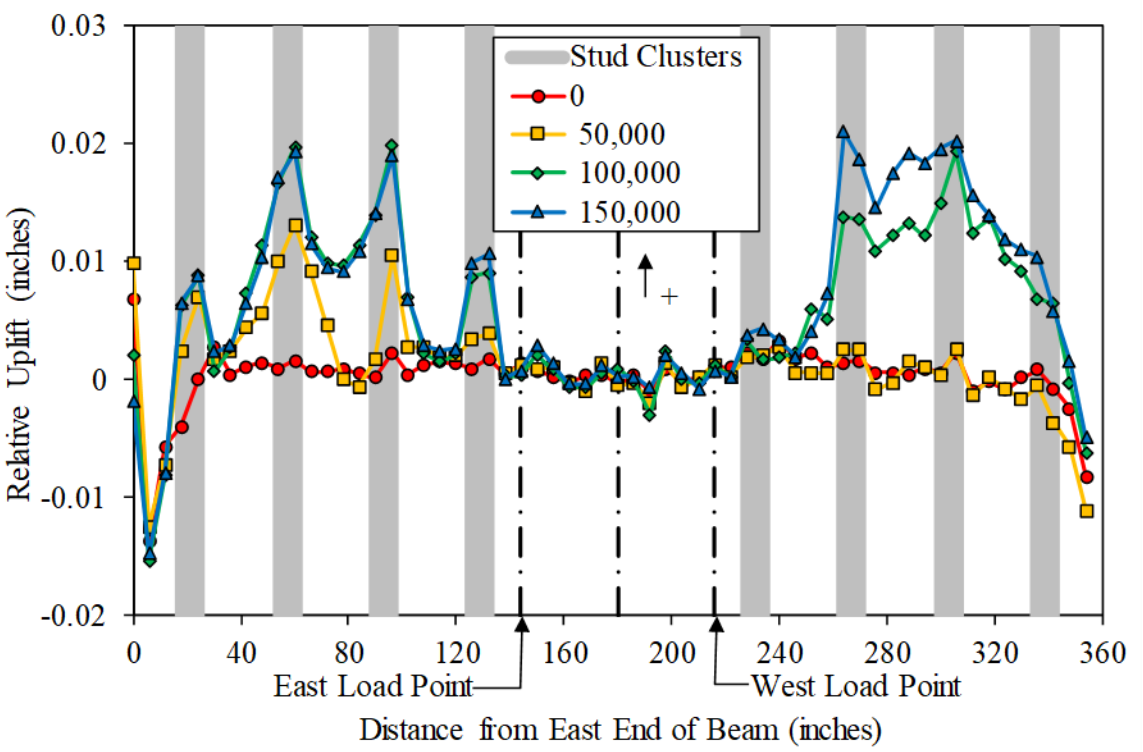

Source: FHWA.

Figure 187. Graph. Laser tracker uplift results for beam 3F2.

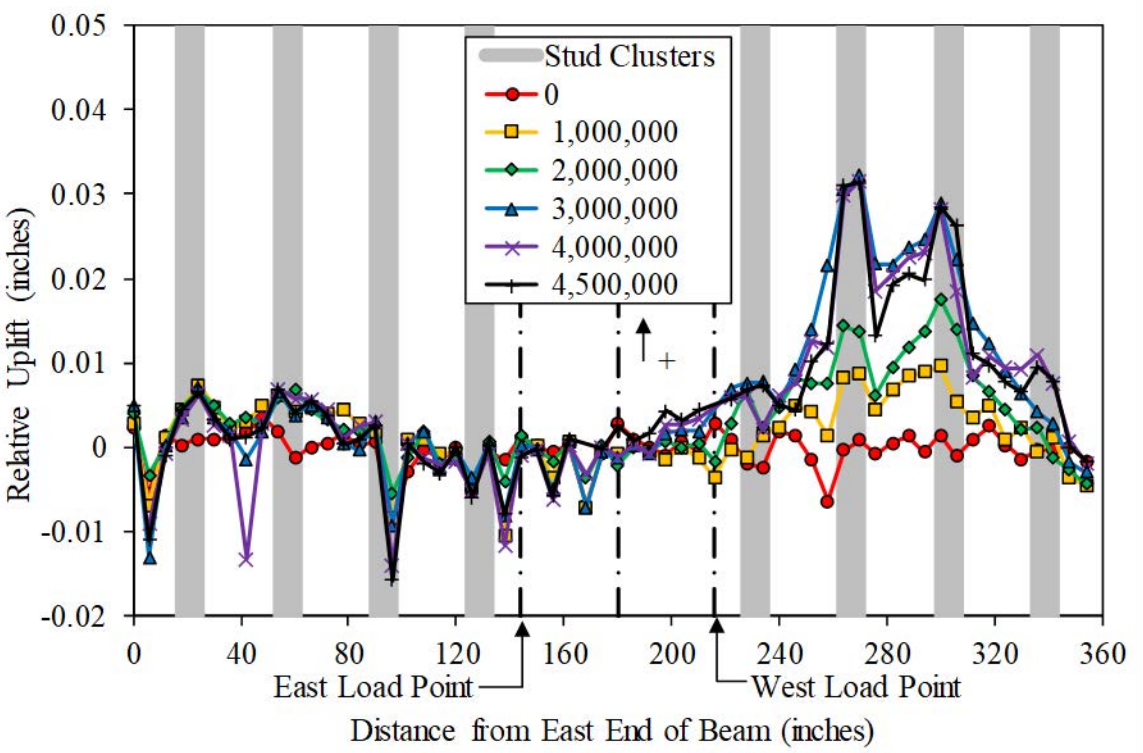

Source: FHWA.

Figure 188. Graph. Laser tracker uplift results for beam 3F3.

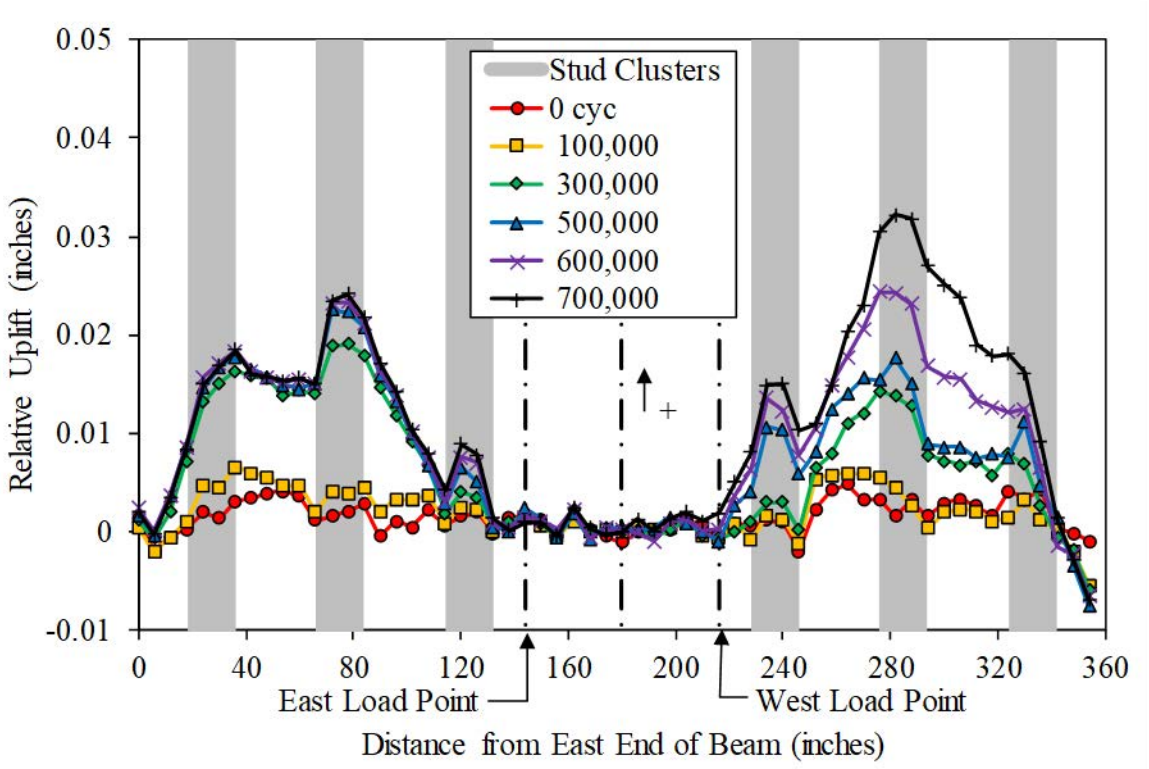

Source: FHWA.

Figure 189. Graph. Laser tracker uplift results for beam 4F2.

APPENDIX E. SHEAR STUD FORENSICS

This appendix contains forensic pictures of the crack pattern in the shear studs for the runout fatigue specimens. Researchers took two photos of each stud. The first is a downward-facing view of the beam's top flange with the fatigue crack in the flange exposed with magnetic particles. The second photo is a macroetch of the longitudinal section through the flange and stud, exposing the weld fusion line, weld heat affected zone, and the crack (if present). The macroetch was made by polishing the cross section and etching with a 2 percent solution of nitric acid in ethyl alcohol for 60 s.

SPECIMEN 2F3

Figure 190 through figure 237 show the photos corresponding to the 24 studs removed from the east and west shear spans of specimen 2F3. The studs were numbered sequentially from 1 at the end of the beam to 12 at the midspan.

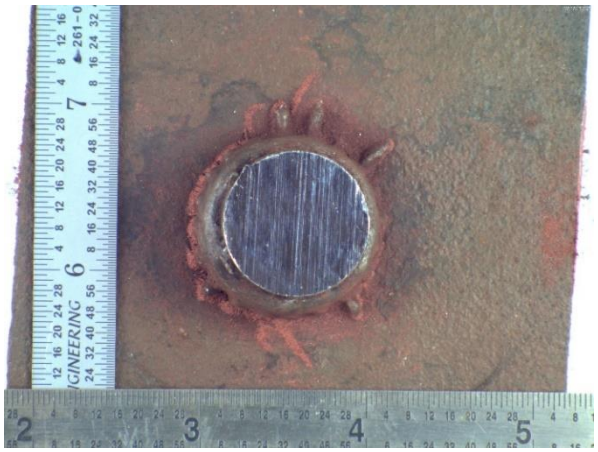

Source: FHWA.

Figure 190. Photo. 2F3_E1 plan view.

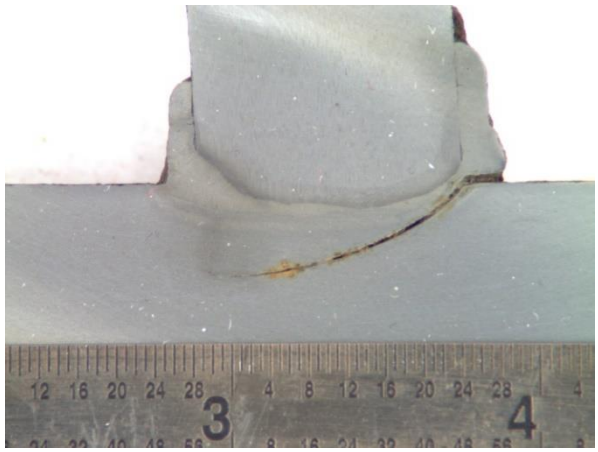

Source: FHWA.

Figure 191. Photo. 2F3_E1 cross section.

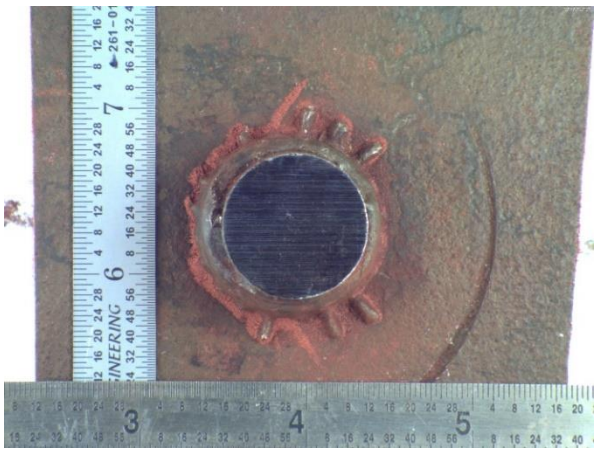

Source: FHWA.

Figure 192. Photo. 2F3_E2 plan view.

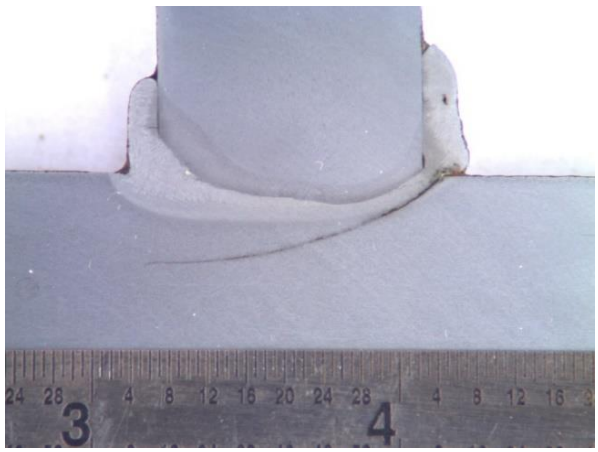

Source: FHWA.

Figure 193. Photo. 2F3_E2 cross section.

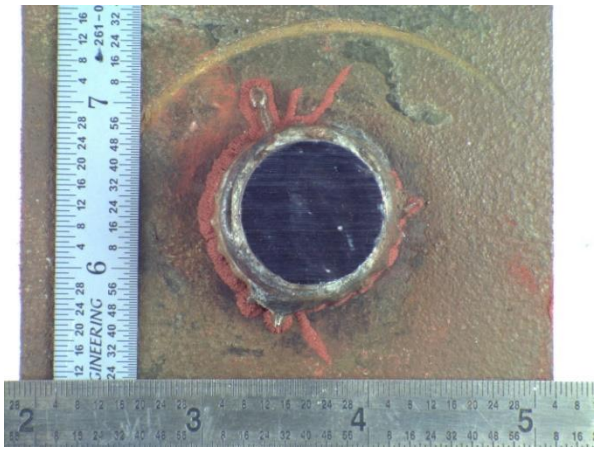

Source: FHWA.

Figure 194. Photo. 2F3_E3 plan view.

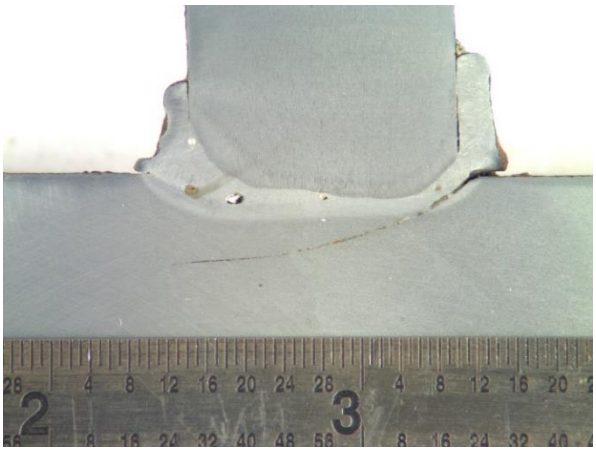

Source: FHWA.

Figure 195. Photo. 2F3_E3 cross section.

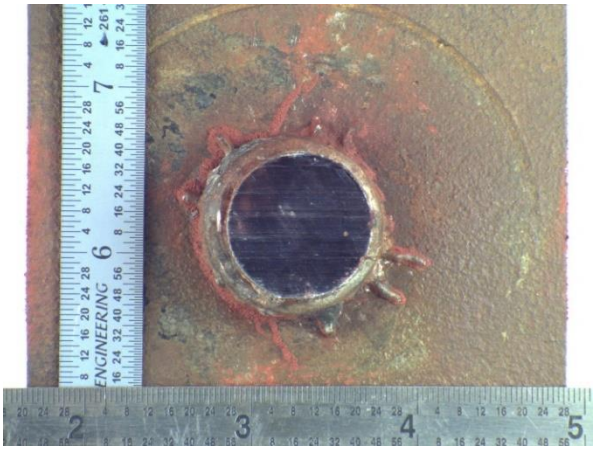

Source: FHWA.

Figure 196. Photo. 2F3_E4 plan view.

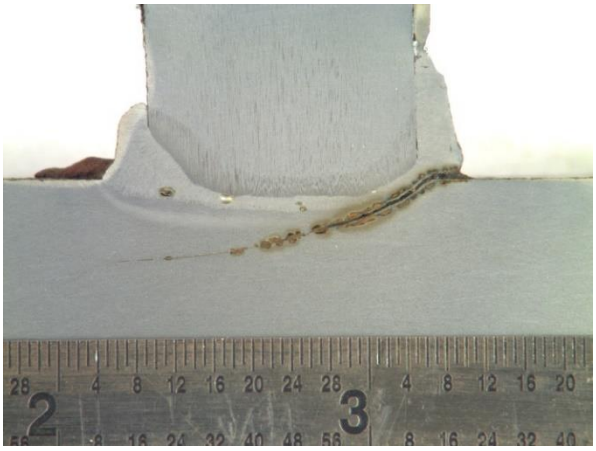

Source: FHWA.

Figure 197. Photo. 2F3_E4 cross section.

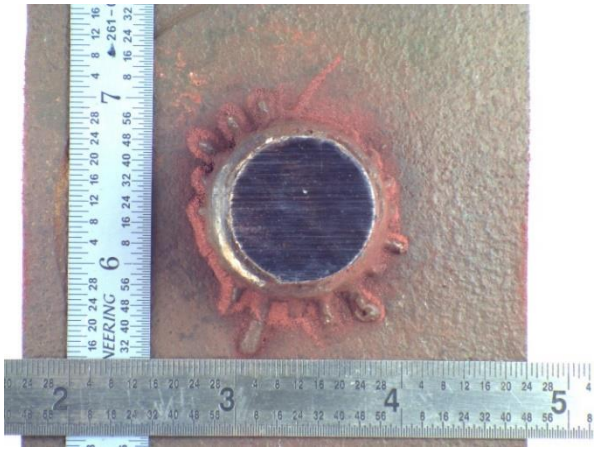

Source: FHWA.

Figure 198. Photo. 2F3_E5 plan view.

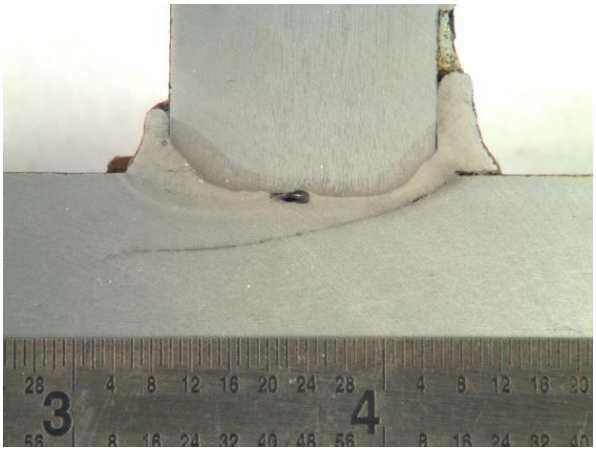

Source: FHWA.

Figure 199. Photo. 2F3_E5 cross section.

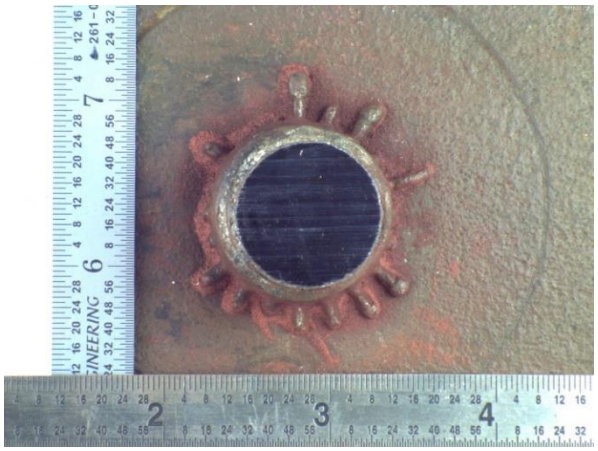

Source: FHWA.

Figure 200. Photo. 2F3_E6 plan view.

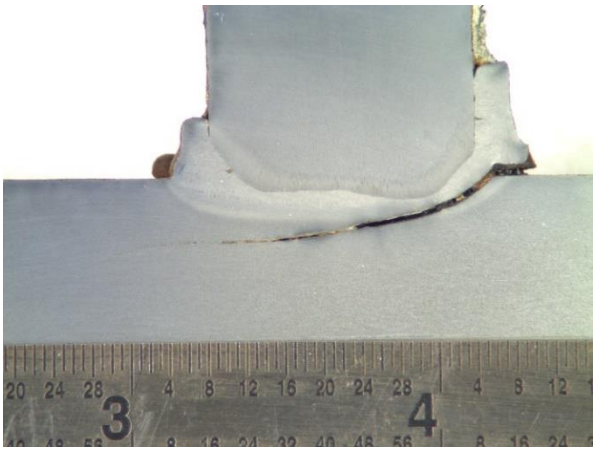

Source: FHWA.

Figure 201. Photo. 2F3_E6 cross section.

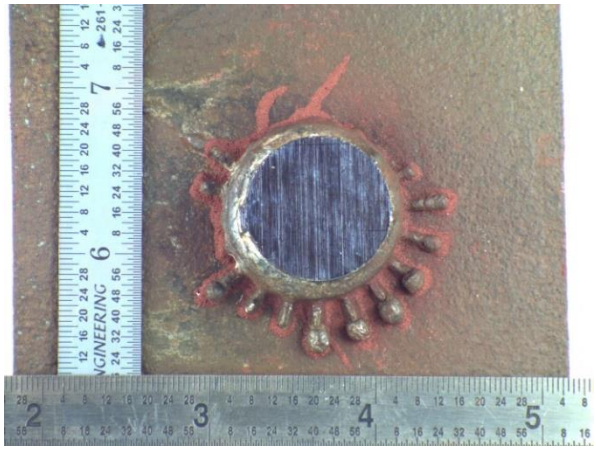

Source: FHWA.

Figure 202. Photo. 2F3_E7 plan view.

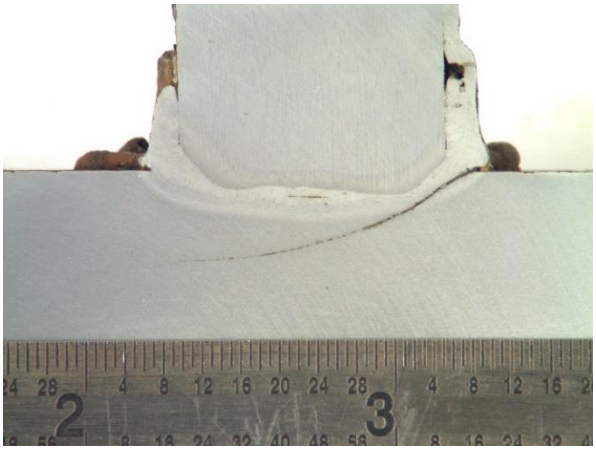

Source: FHWA.

Figure 203. Photo. 2F3_E7 cross section.

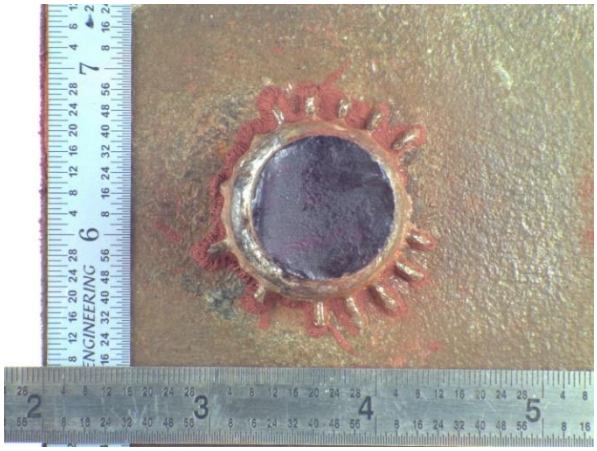

Source: FHWA.

Figure 204. Photo. 2F3_E8 plan view.

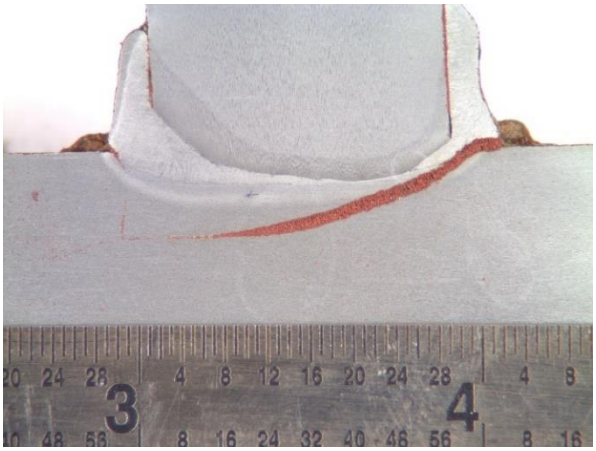

Source: FHWA.

Figure 205. Photo. 2F3_E8 cross section.

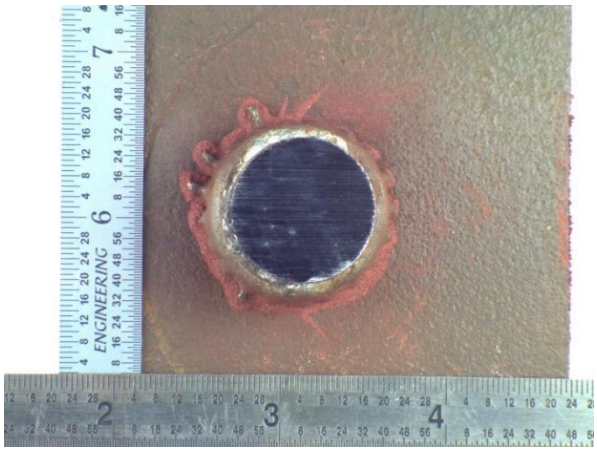

Source: FHWA.

Figure 206. Photo. 2F3_E9 plan view.

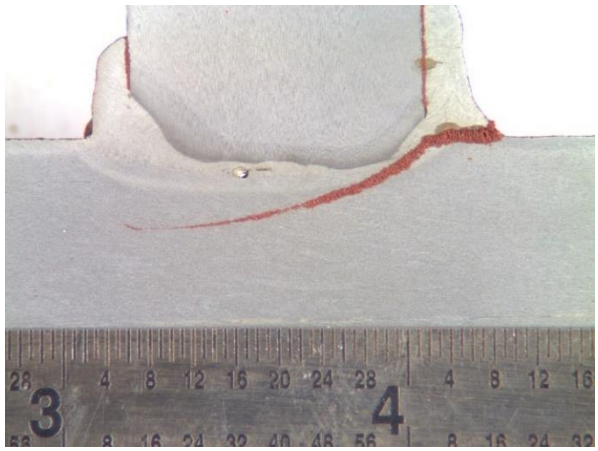

Source: FHWA.

Figure 207. Photo. 2F3_E9 cross section.

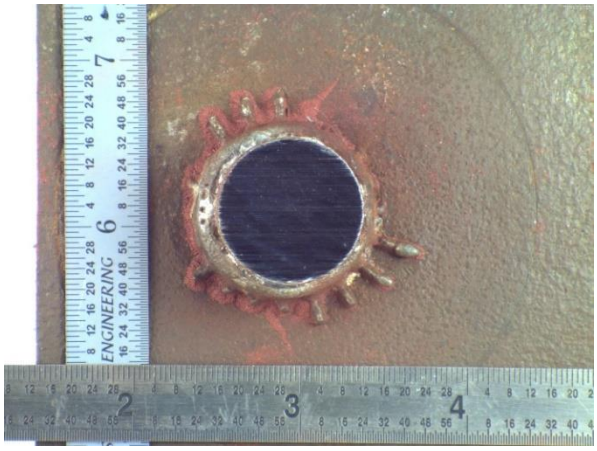

Source: FHWA.

Figure 208. Photo. 2F3_E10 plan view.

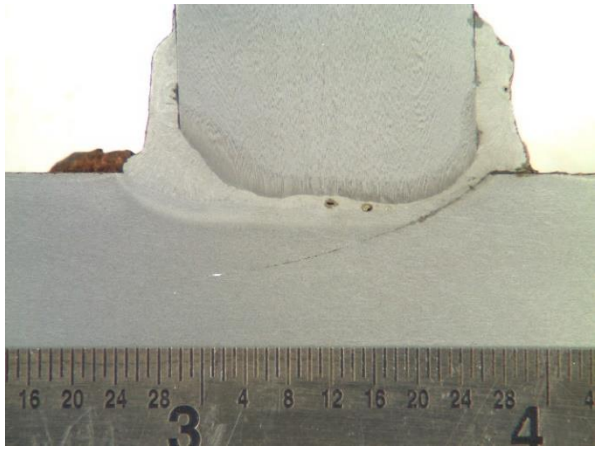

Source: FHWA.

Figure 209. Photo. 2F3_E10 cross section.

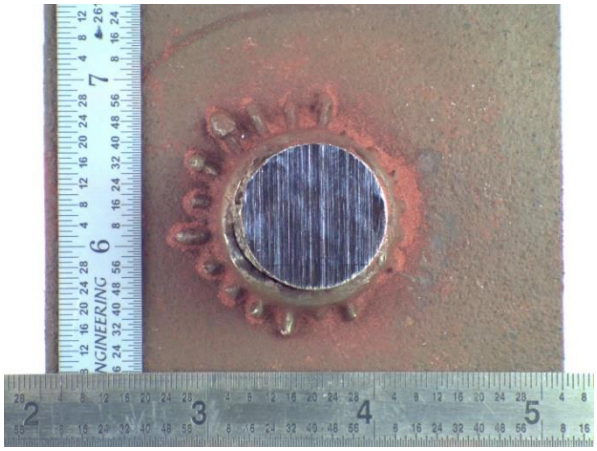

Source: FHWA.

Figure 210. Photo. 2F3_E11 plan view.

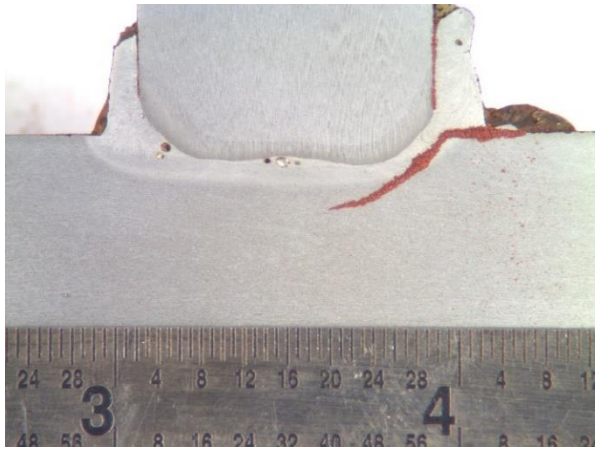

Source: FHWA.

Figure 211. Photo. 2F3_E11 cross section.

Source: FHWA.

Figure 212. Photo. 2F3_E12 plan view.

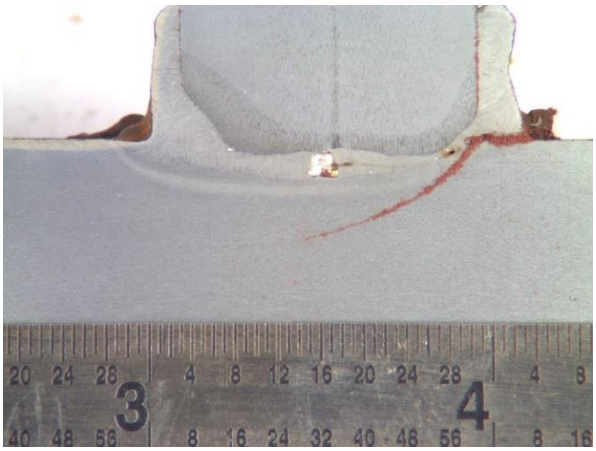

Source: FHWA.

Figure 213. Photo. 2F3_E12 cross section.

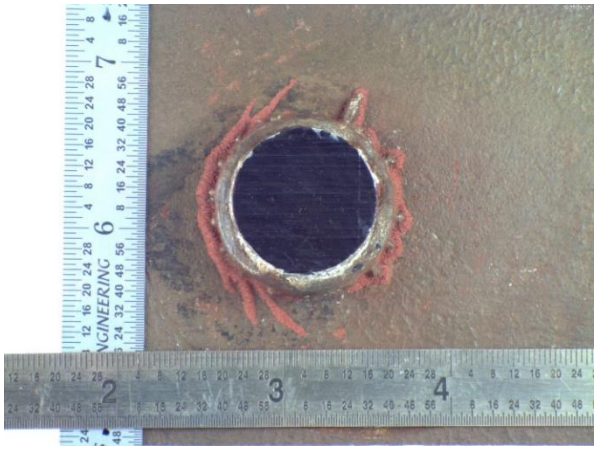

Source: FHWA.

Figure 214. Photo. 2F3_W1 plan view.

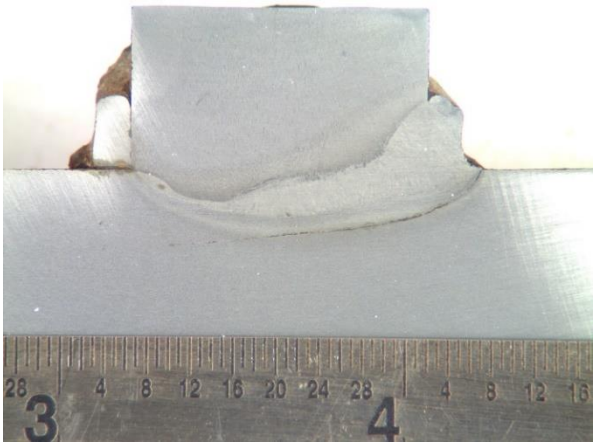

Source: FHWA.

Figure 215. Photo. 2F3_W1 cross section.

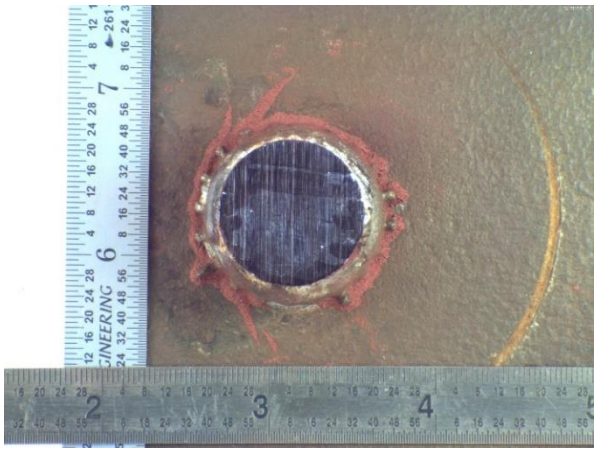

Source: FHWA.

Figure 216. Photo. 2F3_W2 plan view.

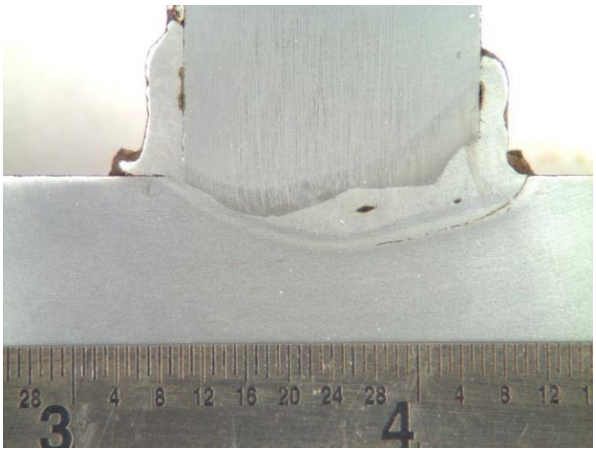

Source: FHWA.

Figure 217. Photo. 2F3_W2 cross section.

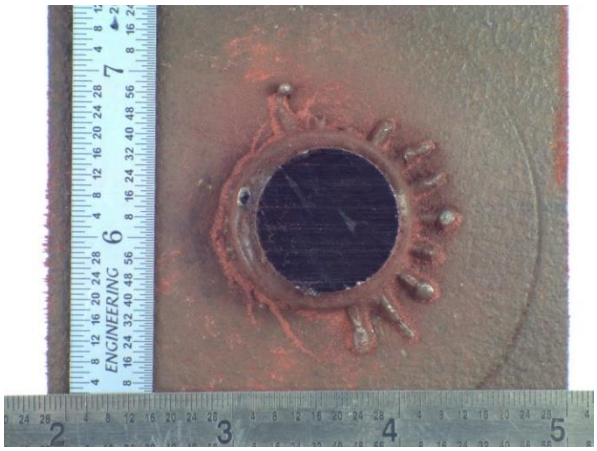

Source: FHWA.

Figure 218. Photo. 2F3_W3 plan view.

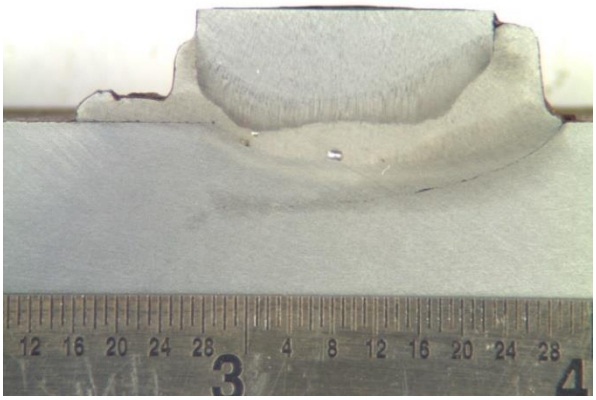

Source: FHWA.

Figure 219. Photo. 2F3_W3 cross section.

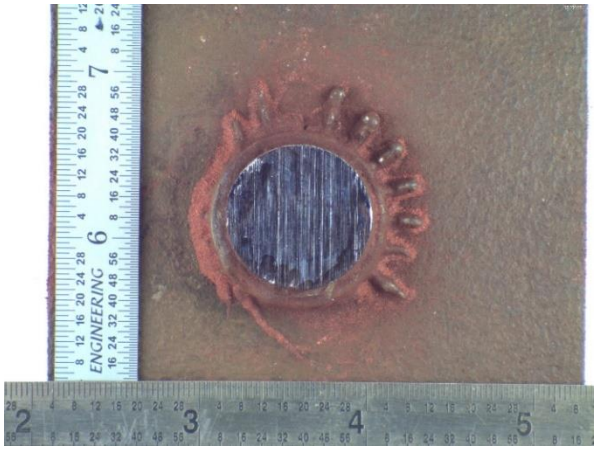

Source: FHWA.

Figure 220. Photo. 2F3_W4 plan view.

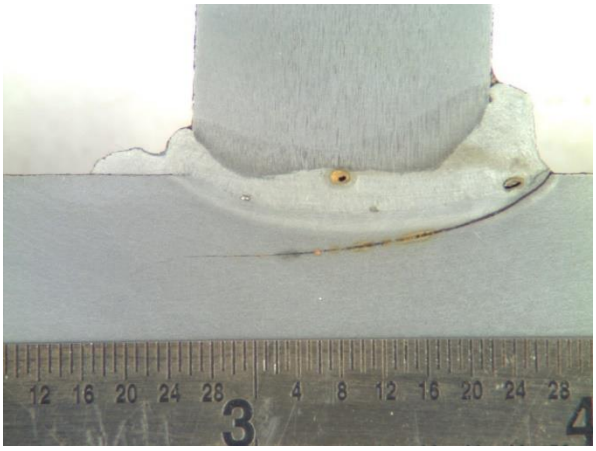

Source: FHWA.

Figure 221. Photo. 2F3_W4 cross section.

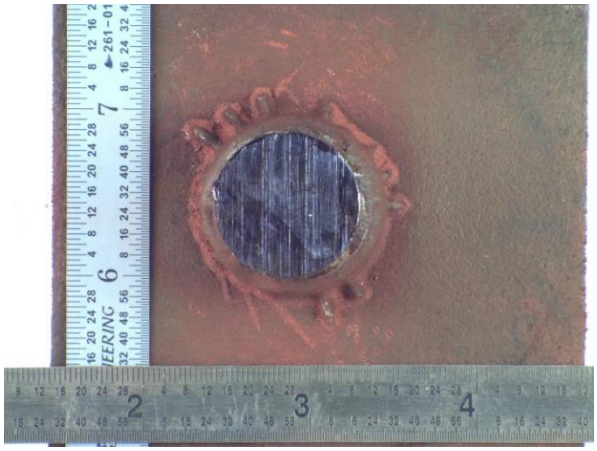

Source: FHWA.

Figure 222. Photo. 2F3_W5 plan view.

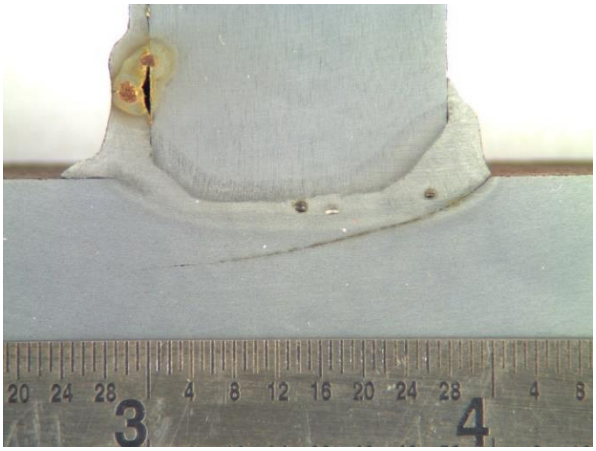

Source: FHWA.

Figure 223. Photo. 2F3_W5 cross section.

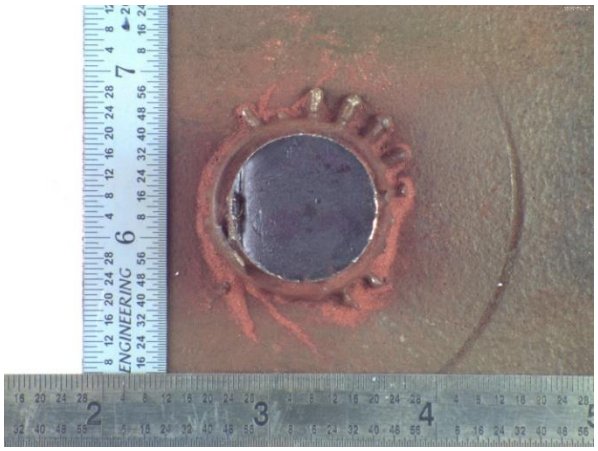

Source: FHWA.

Figure 224. Photo. 2F3_W6 plan view.

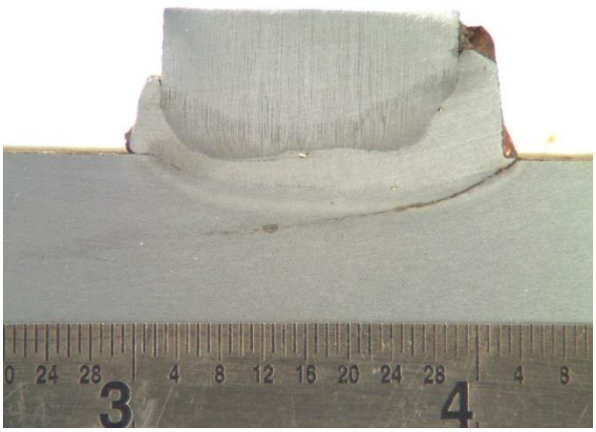

Source: FHWA.

Figure 225. Photo. 2F3_W6 cross section.

Source: FHWA.

Figure 226. Photo. 2F3_W7 plan view.

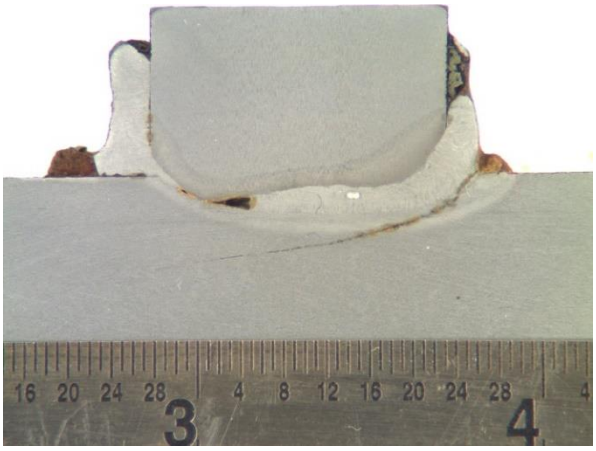

Source: FHWA.

Figure 227. Photo. 2F3_W7 cross section.

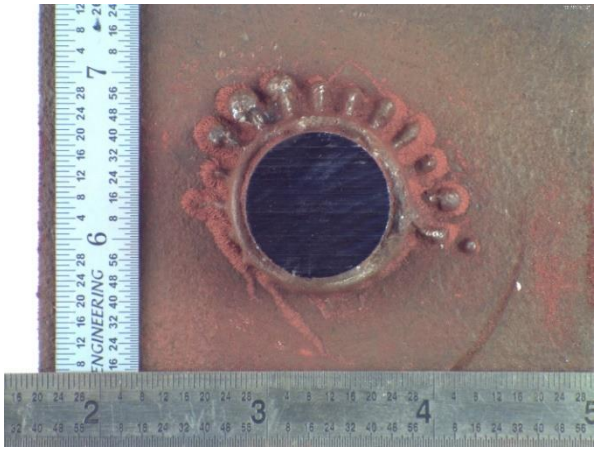

Source: FHWA.

Figure 228. Photo. 2F3_W8 plan view.

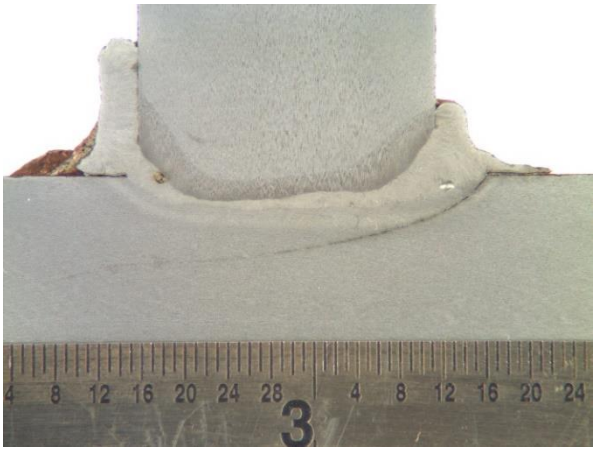

Source: FHWA.

Figure 229. Photo. 2F3_W8 cross section.

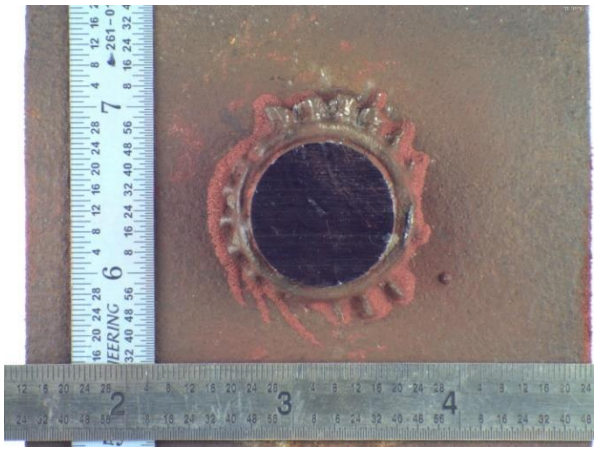

Source: FHWA.

Figure 230. Photo. 2F3_W9 plan view.

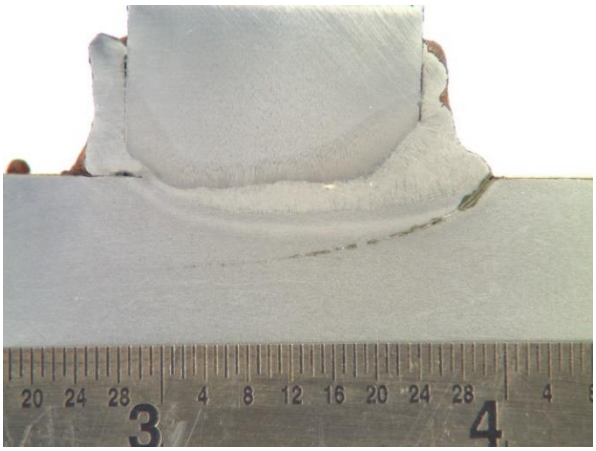

Source: FHWA.

Figure 231. Photo. 2F3_W9 cross section.

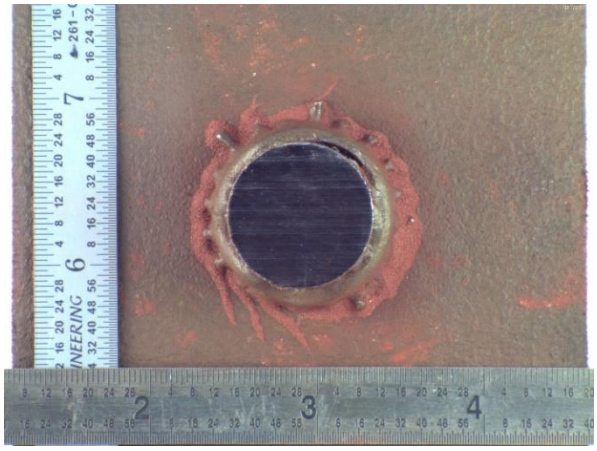

Source: FHWA.

Figure 232. Photo. 2F3_W10 plan view.

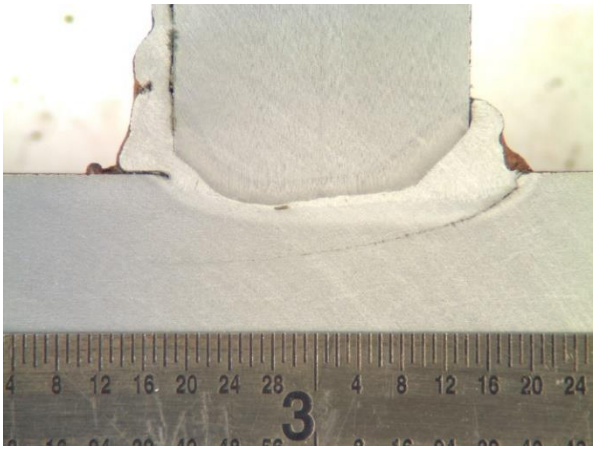

Source: FHWA.

Figure 233. Photo. 2F3_W10 cross section.

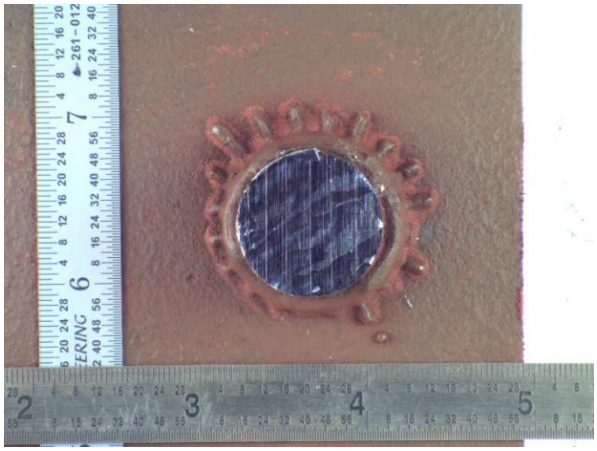

Source: FHWA.

Figure 234. Photo. 2F3_W11 plan view.

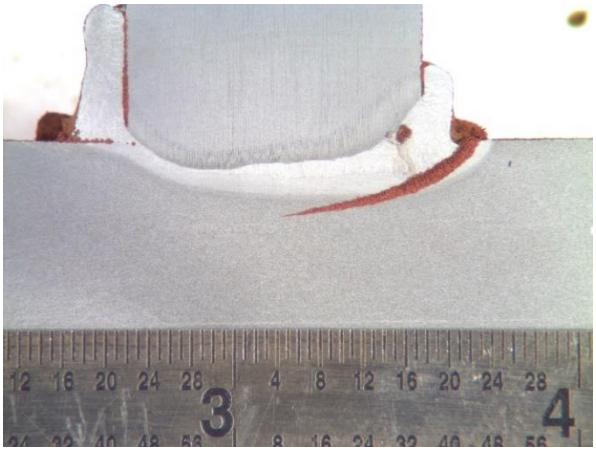

Source: FHWA.

Figure 235. Photo. 2F3_W11 cross section.

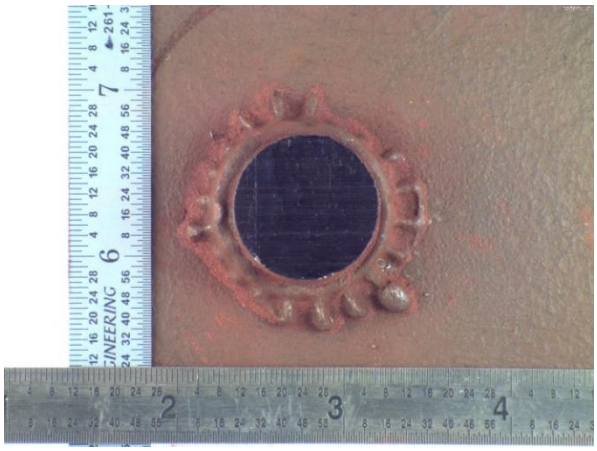

Source: FHWA.

Figure 236. Photo. 2F3_W12 plan view.

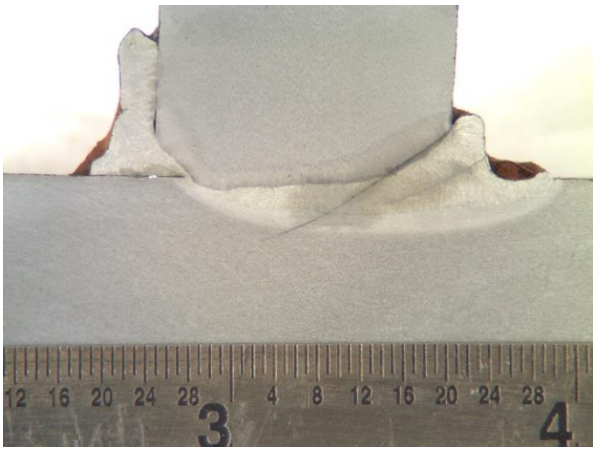

Source: FHWA.

Figure 237. Photo. 2F3_W12 cross section.

SPECIMEN 4F3

Figure 238 through figure 285 show photos corresponding to the 24 studs removed from the east and west shear spans of specimen 4F3. The studs were numbered sequentially from 1 at the end of the beam to 12 at the midspan.

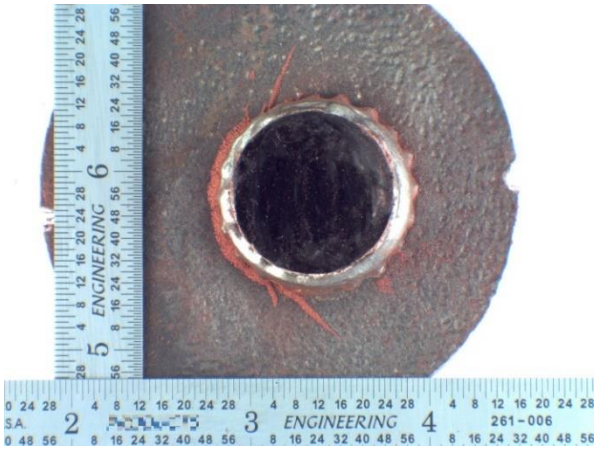

Source: FHWA.

Figure 238. Photo. 4F3_E1 plan view.

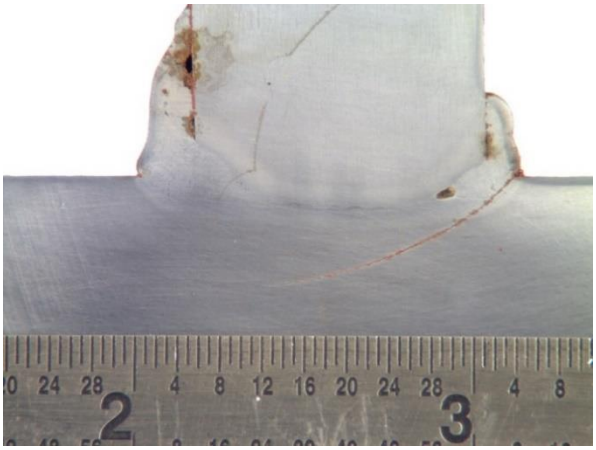

Source: FHWA.

Figure 239. Photo. 4F3_E1 cross section.

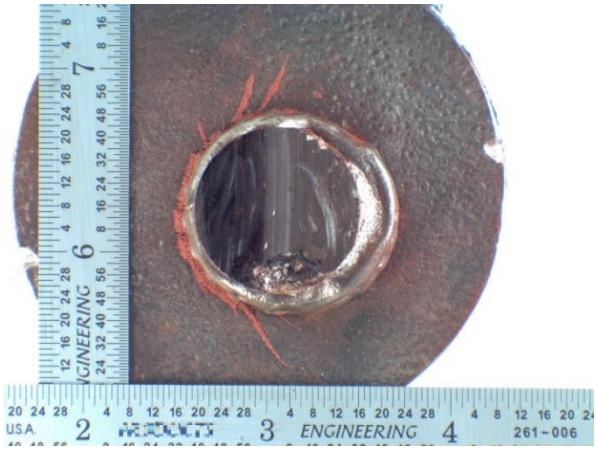

Source: FHWA.

Figure 240. Photo. 4F3_E2 plan view.

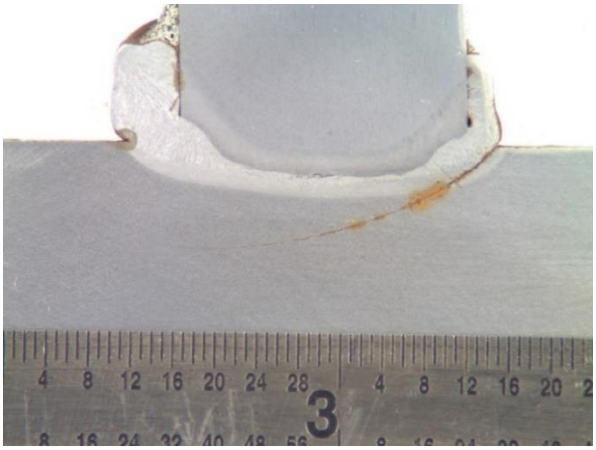

Source: FHWA.

Figure 241. Photo. 4F3_E2 cross section.

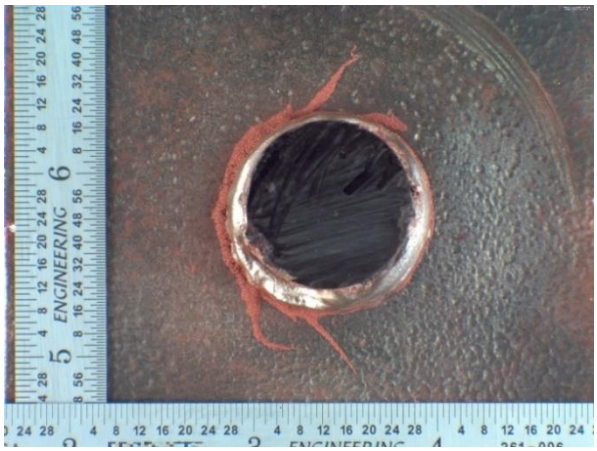

Source: FHWA.

Figure 242. Photo. 4F3_E3 plan view.

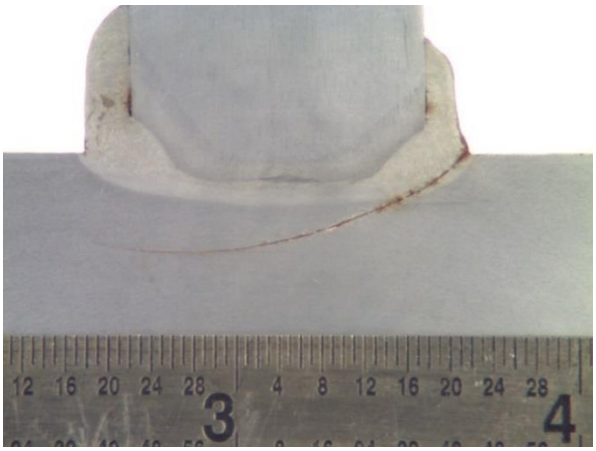

Source: FHWA.

Figure 243. Photo. 4F3_E3 cross section.

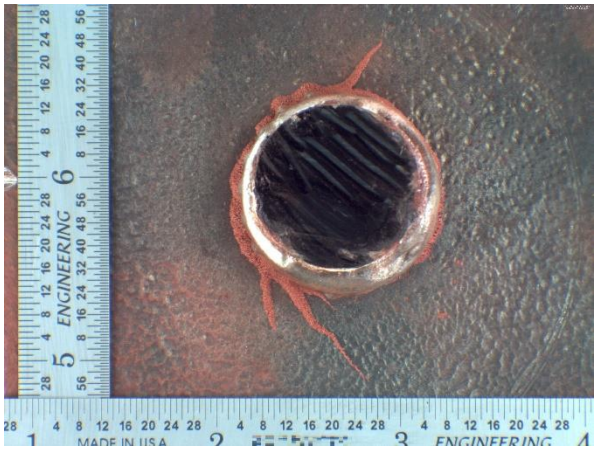

Source: FHWA.

Figure 244. Photo. 4F3_E4 plan view.

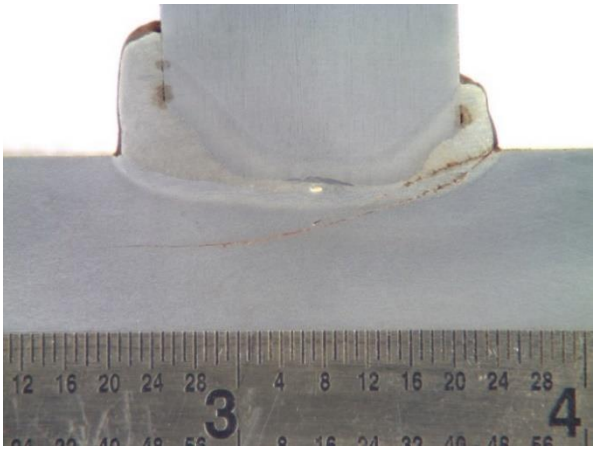

Source: FHWA.

Figure 245. Photo. 4F3_E4 cross section.

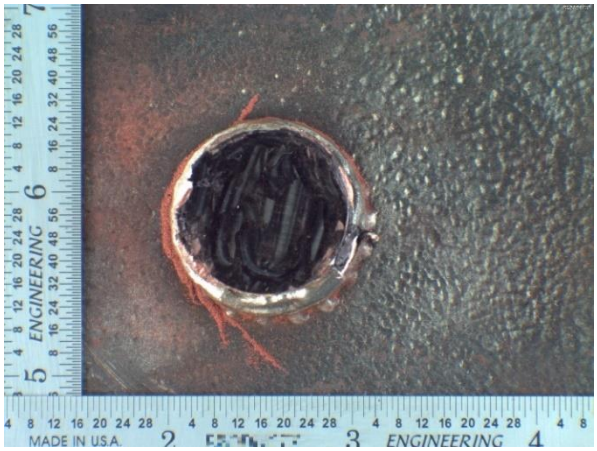

Source: FHWA.

Figure 246. Photo. 4F3_E5 plan view.

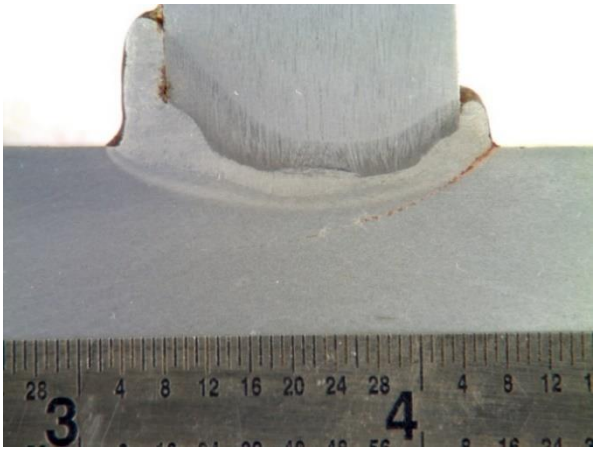

Source: FHWA.

Figure 247. Photo. 4F3_E5 cross section.

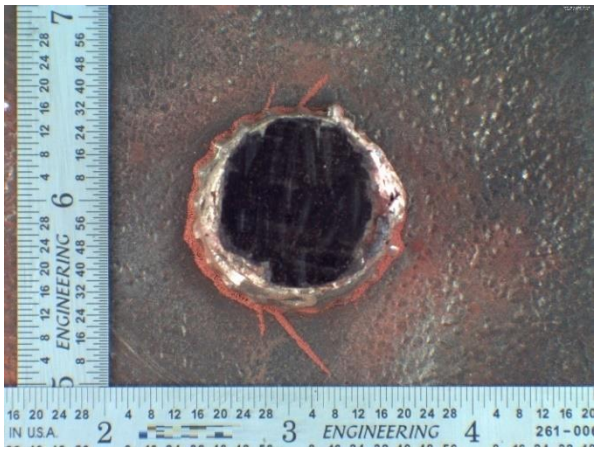

Source: FHWA.

Figure 248. Photo. 4F3_E6 plan view.

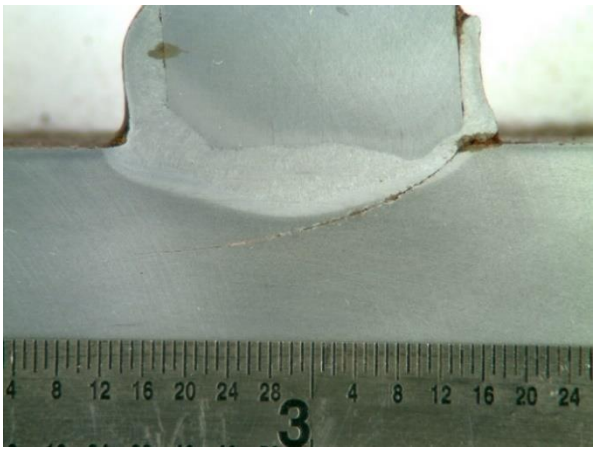

Source: FHWA.

Figure 249. Photo. 4F3_E6 cross section.

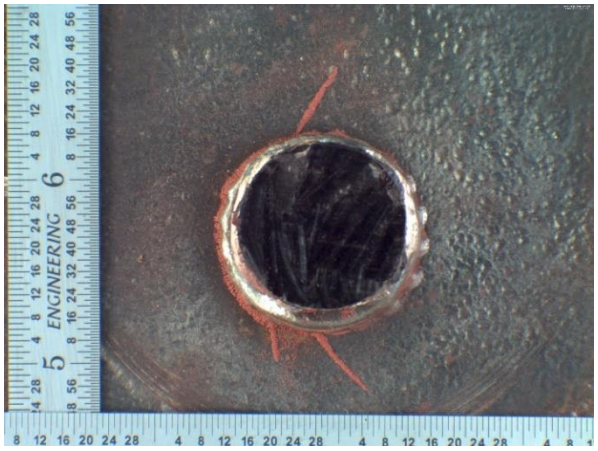

Source: FHWA.

Figure 250. Photo. 4F3_E7 plan view.

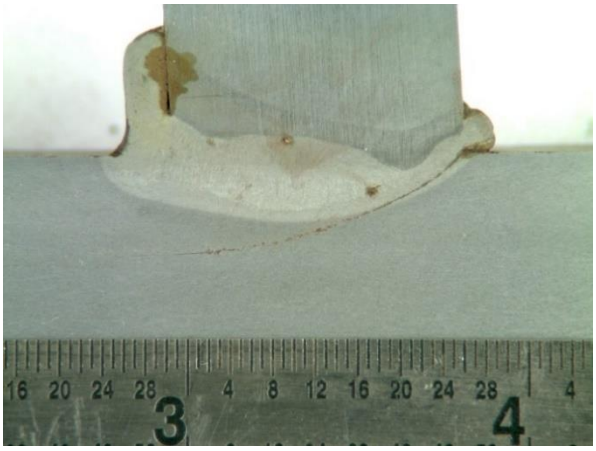

Source: FHWA.

Figure 251. Photo. 4F3_E7 cross section.

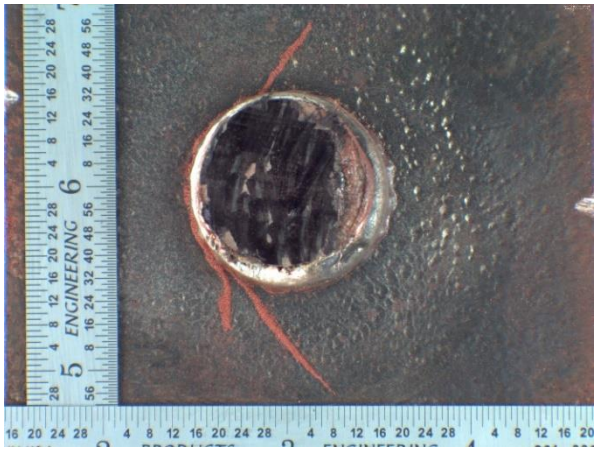

Source: FHWA.

Figure 252. Photo. 4F3_E8 plan view.

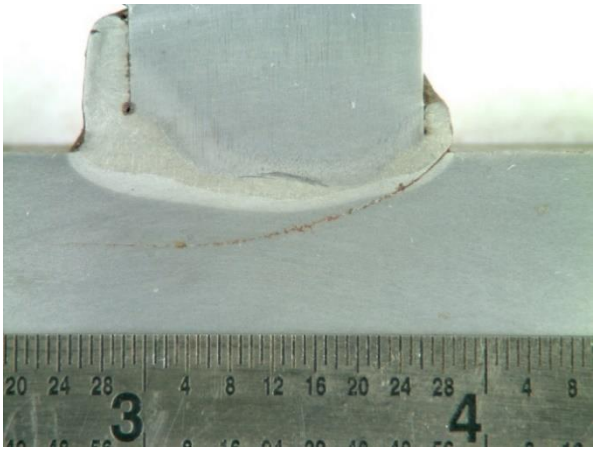

Source: FHWA.

Figure 253. Photo. 4F3_E8 cross section.

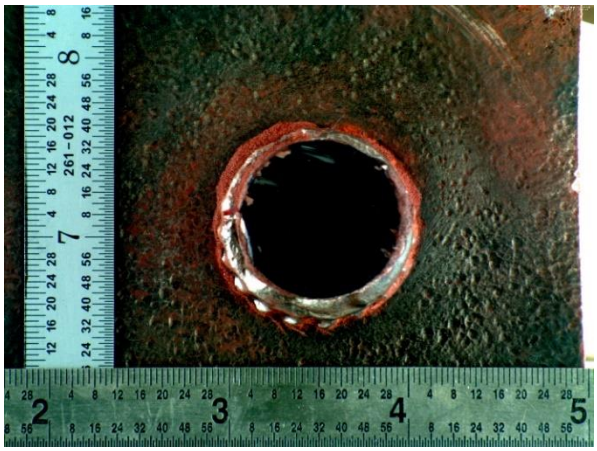

Source: FHWA.

Figure 254. Photo. 4F3_E9 plan view.

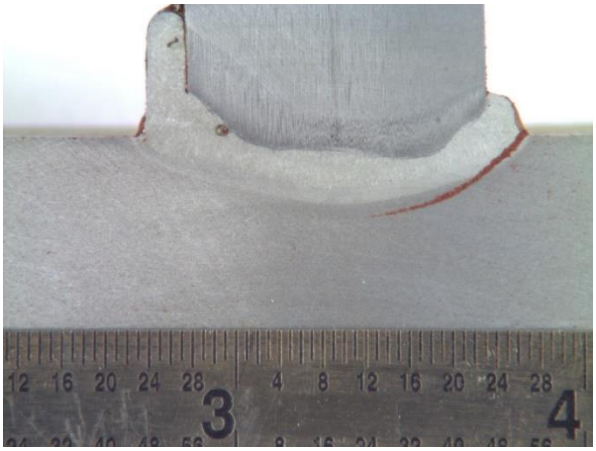

Source: FHWA.

Figure 255. Photo. 4F3_E9 cross section.

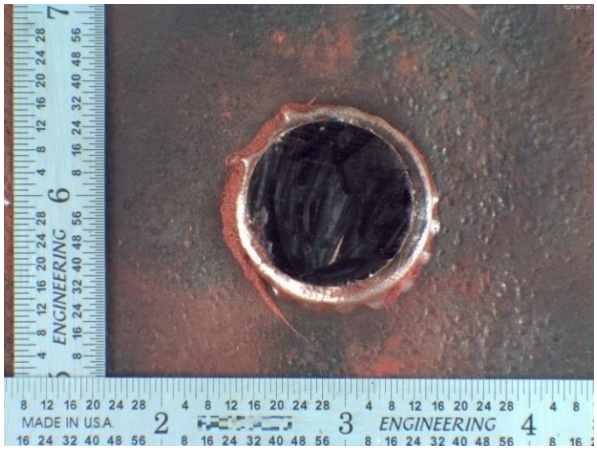

Source: FHWA.

Figure 256. Photo. 4F3_E10 plan view.

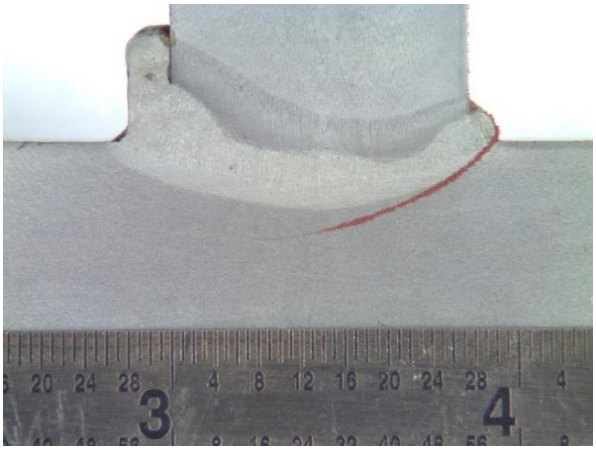

Source: FHWA.

Figure 257. Photo. 4F3_E10 cross section.

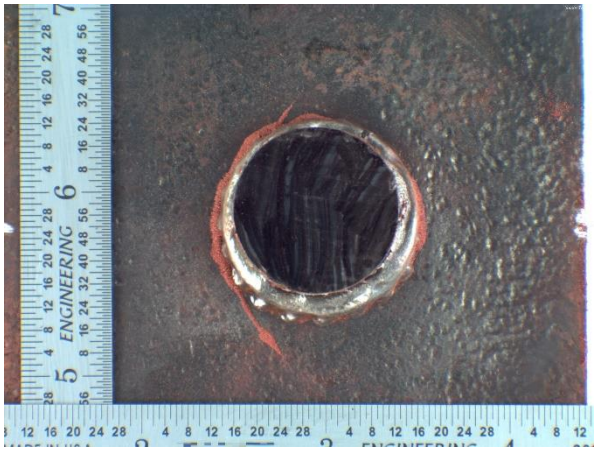

Source: FHWA.

Figure 258. Photo. 4F3_E11 plan view.

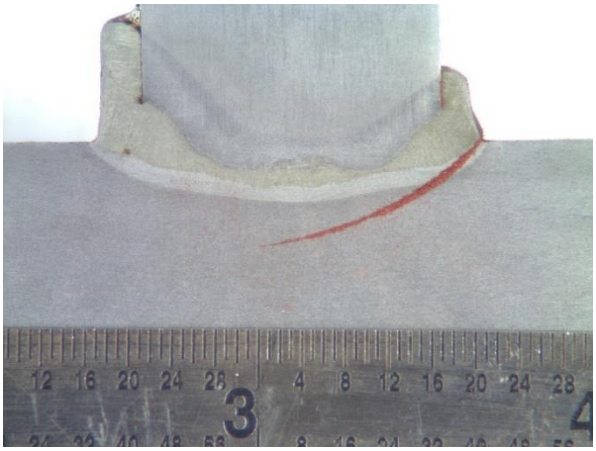

Source: FHWA.

Figure 259. Photo. 4F3_E11 cross section.

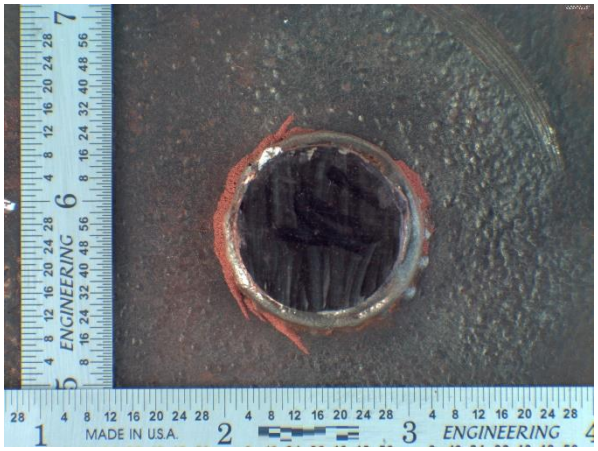

Source: FHWA.

Figure 260. Photo. 4F3_E12 plan view.

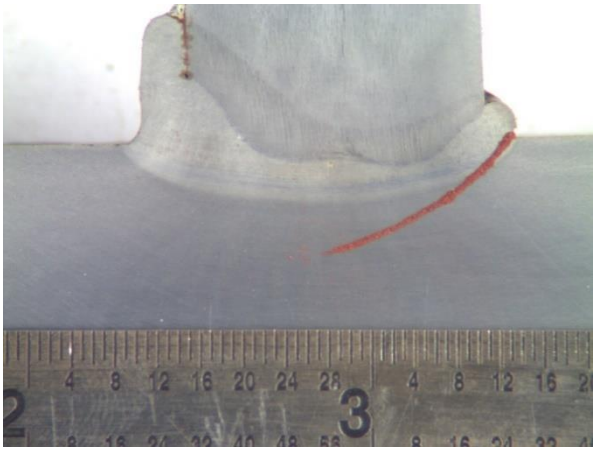

Source: FHWA.

Figure 261. Photo. 4F3_E12 cross section.

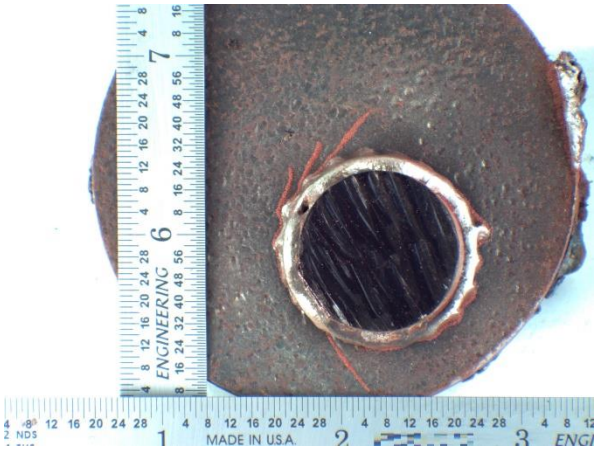

Source: FHWA.

Figure 262. Photo. 4F3_W1 plan view.

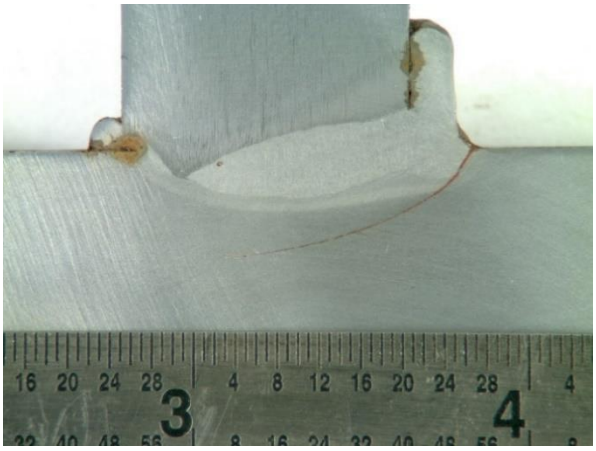

Source: FHWA.

Figure 263. Photo. 4F3_W1 cross section.

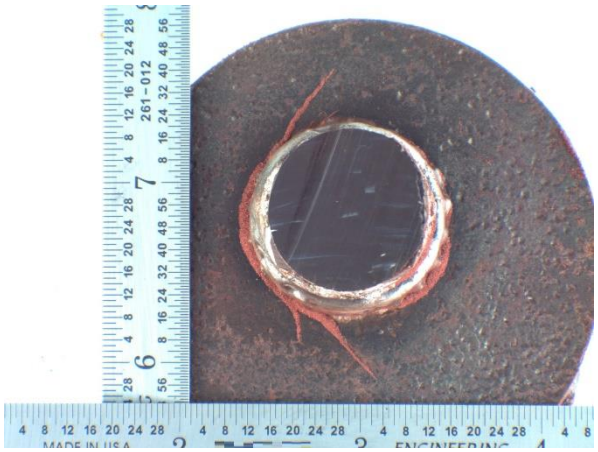

Source: FHWA.

Figure 264. Photo. 4F3_W2 plan view.

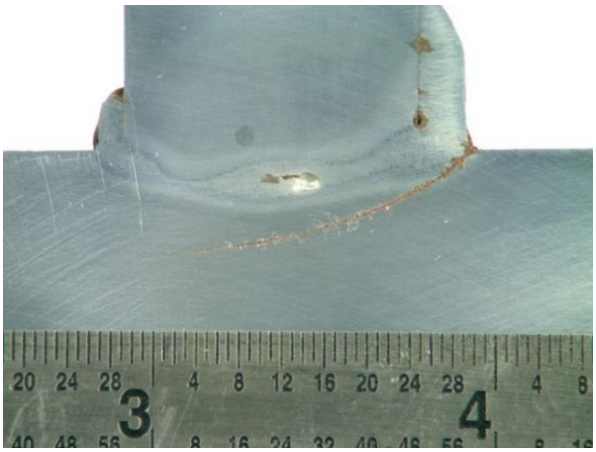

Source: FHWA.

Figure 265. Photo. 4F3_W2 cross section.

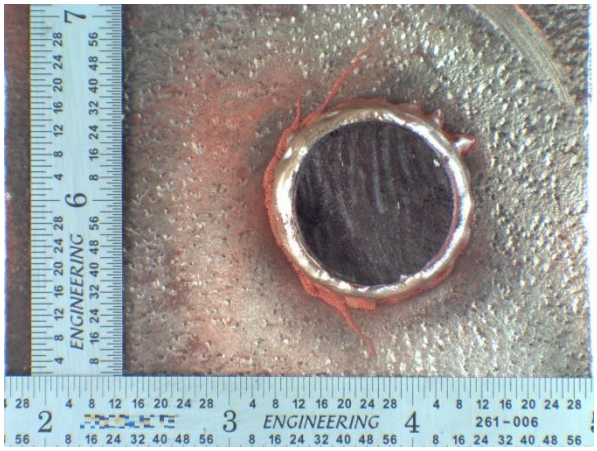

Source: FHWA.

Figure 266. Photo. 4F3_W3 plan view.

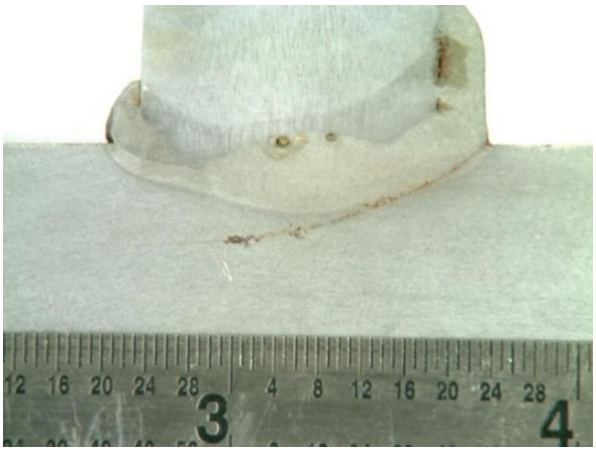

Source: FHWA.

Figure 267. Photo. 4F3_W3 cross section.

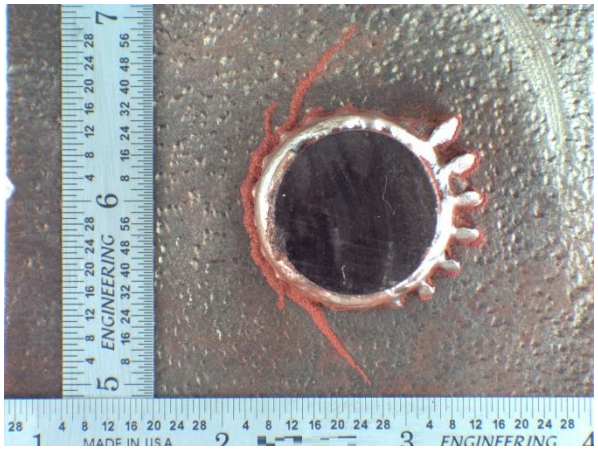

Source: FHWA.

Figure 268. Photo. 4F3_W4 plan view.

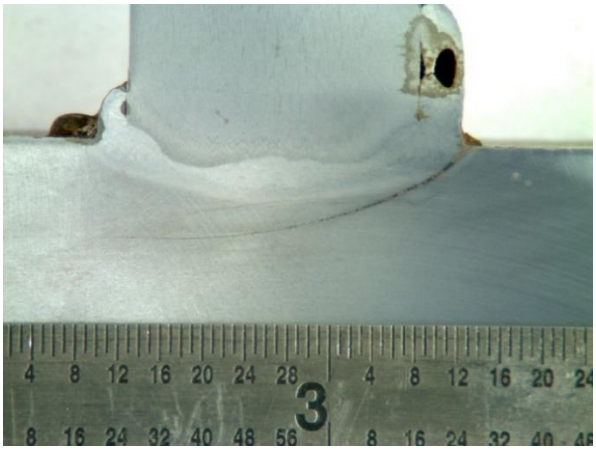

Source: FHWA.

Figure 269. Photo. 4F3_W4 cross section.

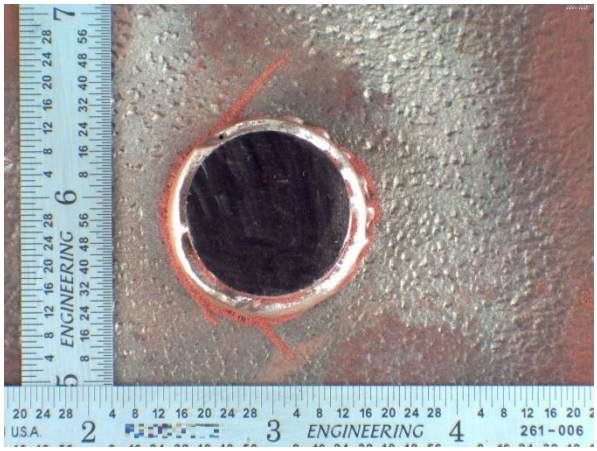

Source: FHWA.

Figure 270. Photo. 4F3_W5 plan view.

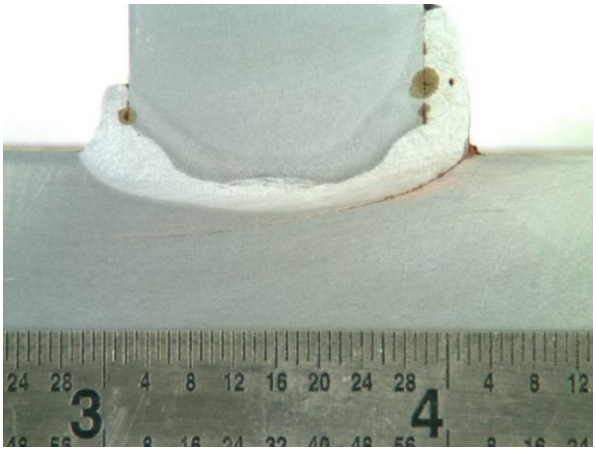

Source: FHWA.

Figure 271. Photo. 4F3_W5 cross section.

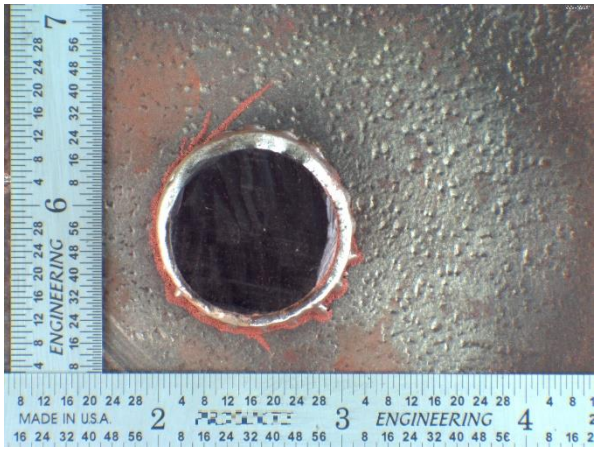

Source: FHWA.

Figure 272. Photo. 4F3_W6 plan view.

Source: FHWA.

Figure 273. Photo. 4F3_W6 cross section.

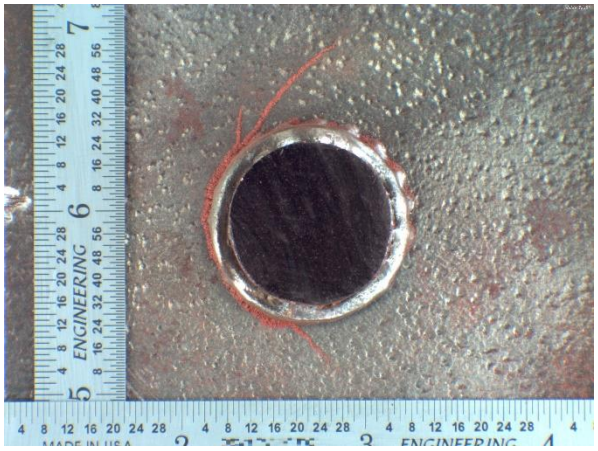

Source: FHWA.

Figure 274. Photo. 4F3_W7 plan view.

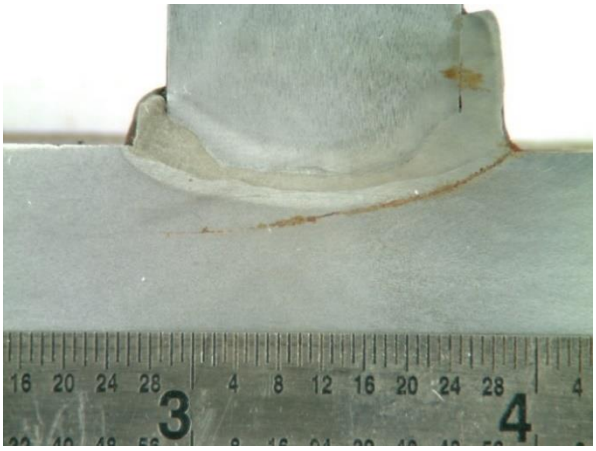

Source: FHWA.

Figure 275. Photo. 4F3_W7 cross section.

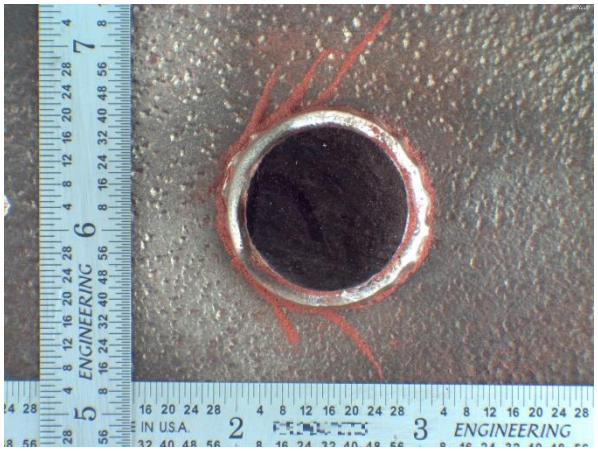

Source: FHWA.

Figure 276. Photo. 4F3_W8 plan view.

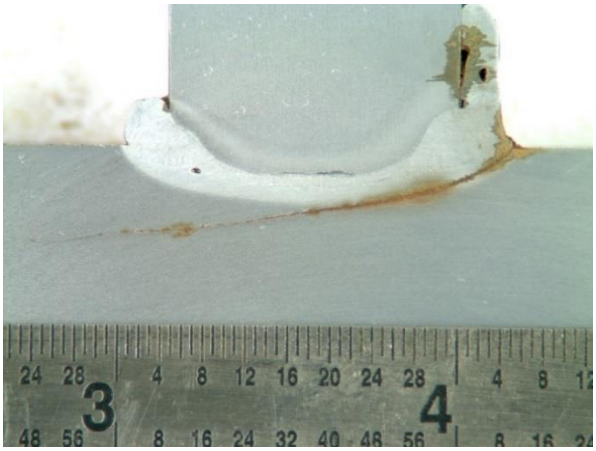

Source: FHWA.

Figure 277. Photo. 4F3_W8 cross section.

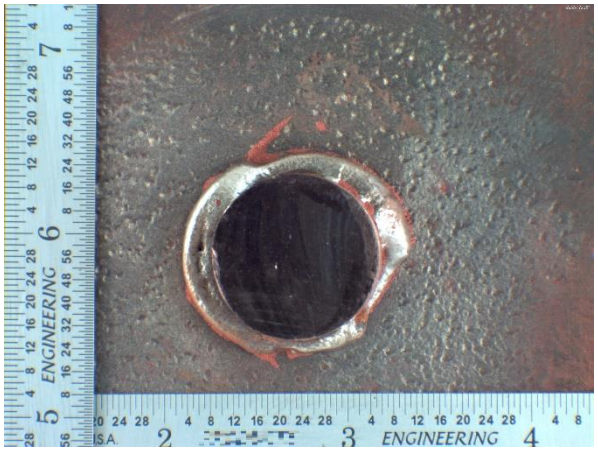

Source: FHWA.

Figure 278. Photo. 4F3_W9 plan view.

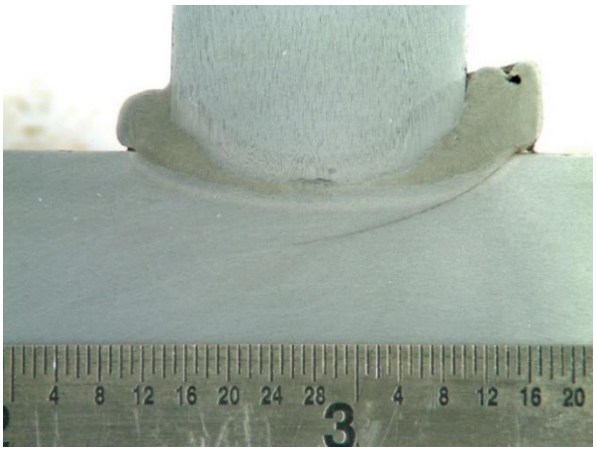

Source: FHWA.

Figure 279. Photo. 4F3_W9 cross section.

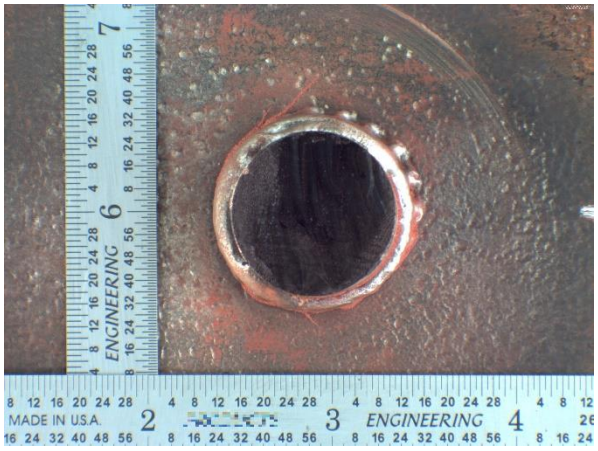

Source: FHWA.

Figure 280. Photo. 4F3_W10 plan view.

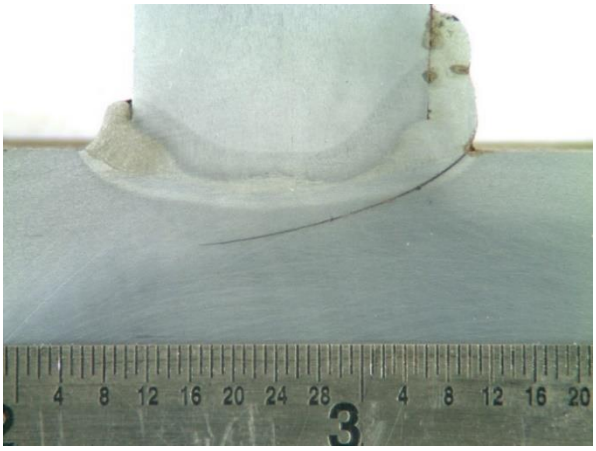

Source: FHWA.

Figure 281. Photo. 4F3_W10 cross section.

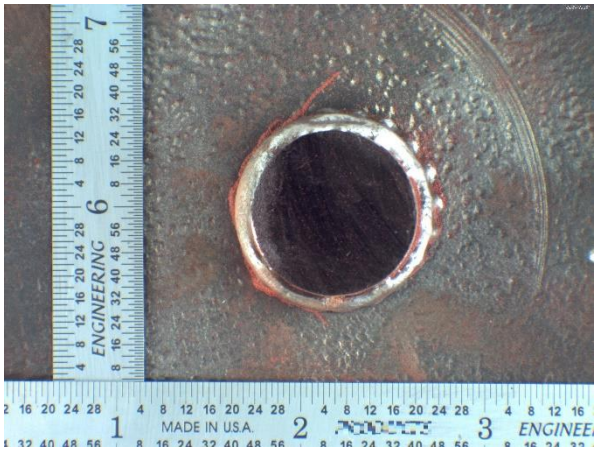

Source: FHWA.

Figure 282. Photo. 4F3_W11 plan view.

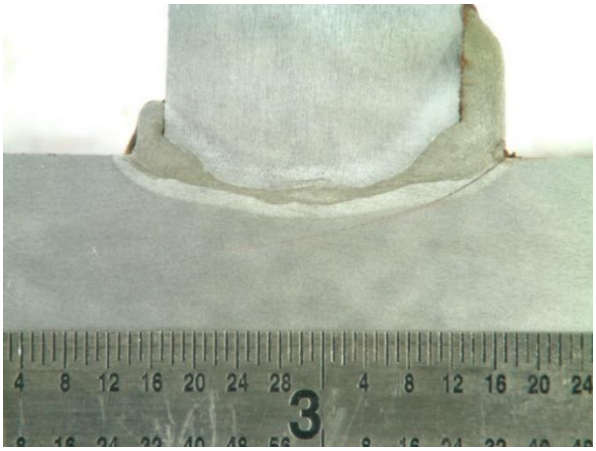

Source: FHWA.

Figure 283. Photo. 4F3_W11 cross section.

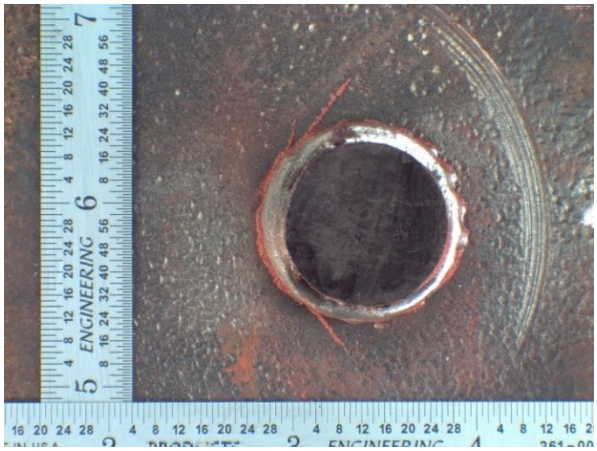

Source: FHWA.

Figure 284. Photo. 4F3_W12 plan view.

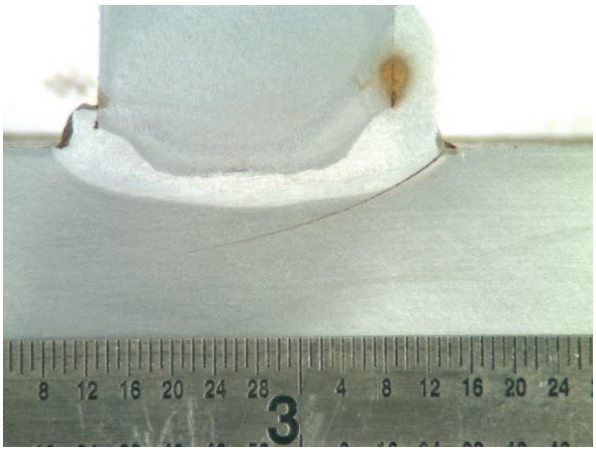

Source: FHWA.

Figure 285. Photo. 4F3_W12 cross section.

SPECIMEN PO-F1

Figure 286 through figure 289 show the photos of the fatigue specimen PO-F1. These specimens had only one stud welded to each side of the beam; the studs were numbered arbitrarily.

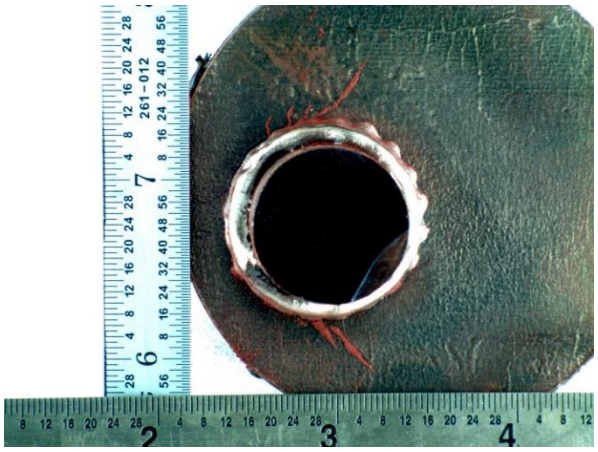

Source: FHWA.

Figure 286. Photo. POF1_1 plan view.

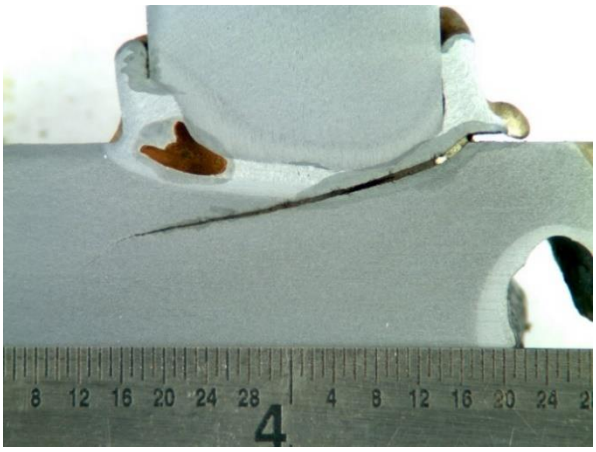

Source: FHWA.

Figure 287. Photo. POF1_1 cross section.

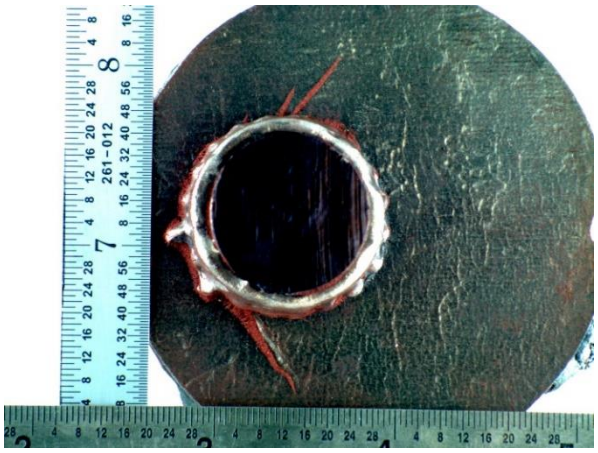

Source: FHWA.

Figure 288. Photo. POF1_2 plan view.

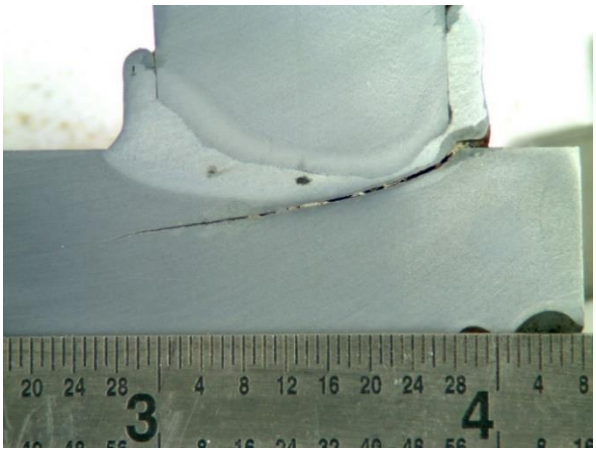

Source: FHWA.

Figure 289. Photo. POF1_2 cross section.

SPECIMEN PO-F6

Figure 290 through figure 293 show the photos of the fatigue specimen PO-F6. These specimens had only one stud welded to each side of the beam; the studs were numbered arbitrarily.

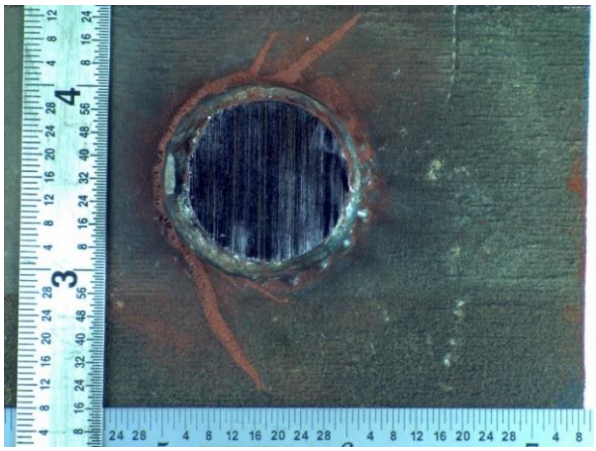

Source: FHWA.

Figure 290. Photo. POF6_1 plan view.

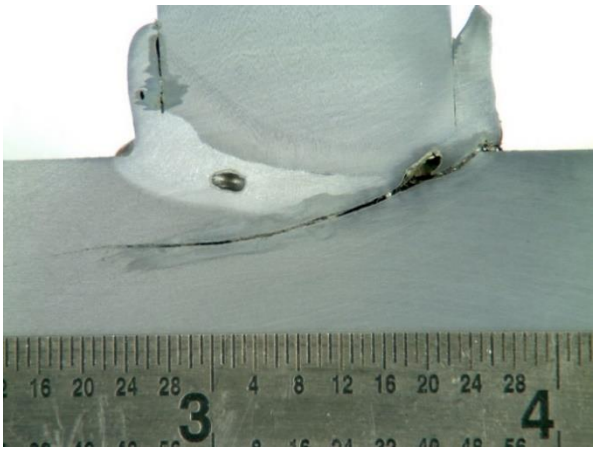

Source: FHWA.

Figure 291. Photo. POF6_1 cross section.

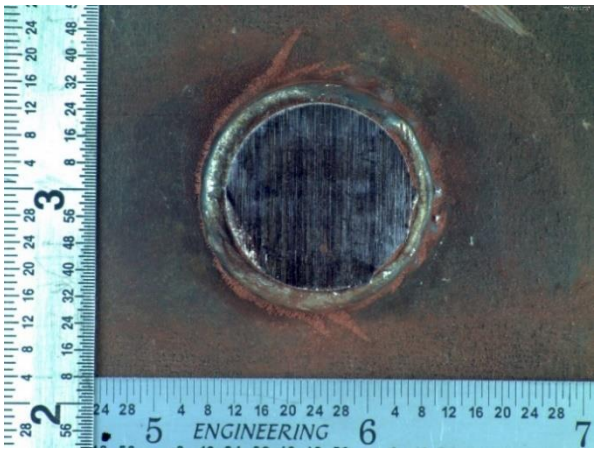

Source: FHWA.

Figure 292. Photo. POF6_2 plan view.

Source: FHWA.

Figure 293. Photo. POF6_2 cross section.

SPECIMEN PO-F11

Figure 294 through figure 297 show the photos of the fatigue specimen PO-F11. These specimens had only one stud welded to each side of the beam; the studs were numbered arbitrarily.

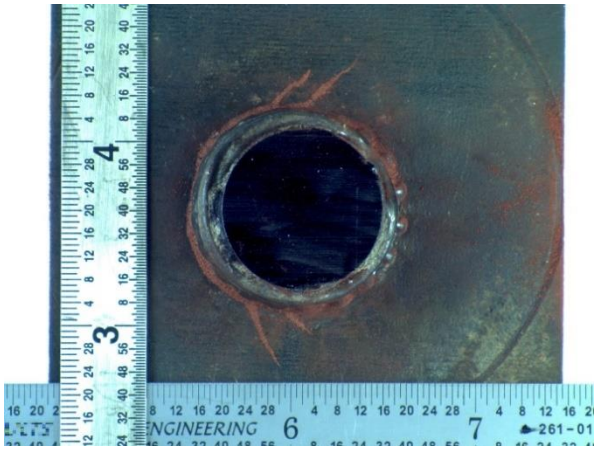

Source: FHWA.

Figure 294. Photo. POF11_1 plan view.

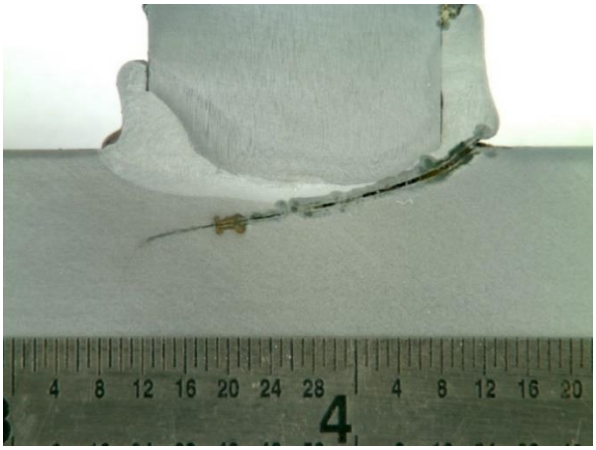

Source: FHWA.

Figure 295. Photo. POF11_1 cross section.

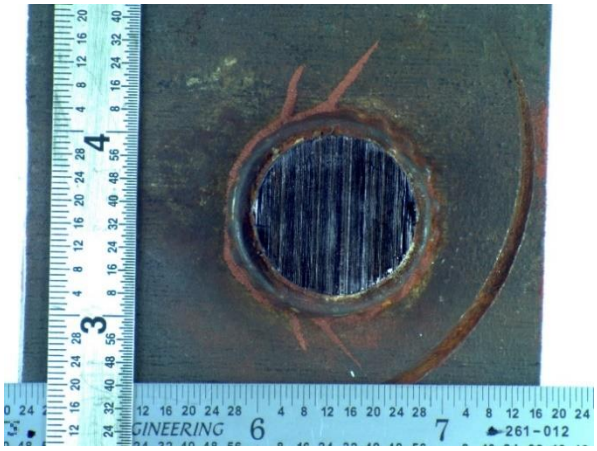

Source: FHWA.

Figure 296. Photo. POF11_2 plan view.

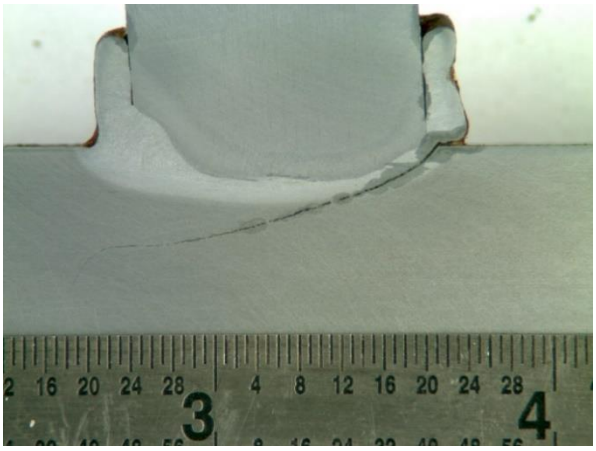

Source: FHWA.

Figure 297. Photo. POF11_2 cross section.

SPECIMEN PO-F12

Figure 298 through figure 301 show the photos of the fatigue specimen PO-F12. These specimens only had one stud welded to each side of the beam; the studs were numbered arbitrarily.

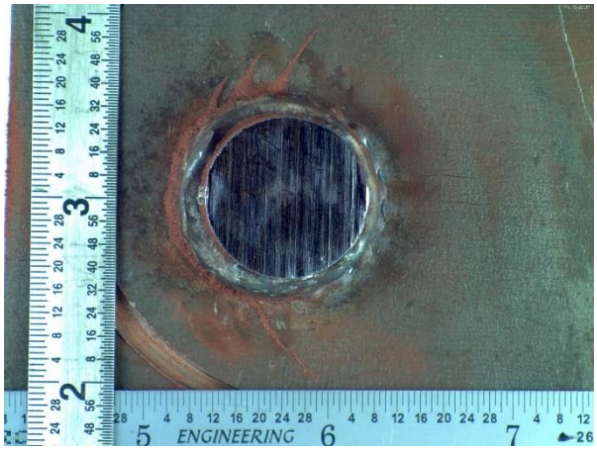

Source: FHWA.

Figure 298. Photo. POF12_1 plan view.

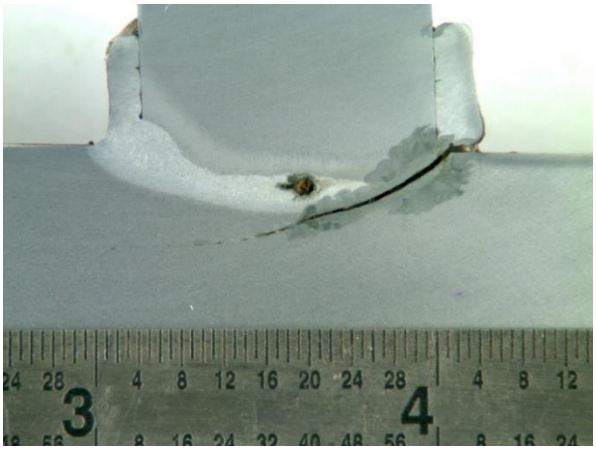

Source: FHWA.

Figure 299. Photo. POF12_1 cross section.

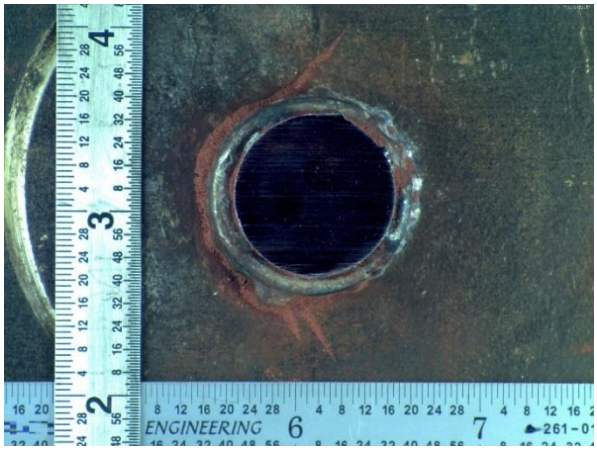

Source: FHWA.

Figure 300. Photo. POF12_2 plan view.

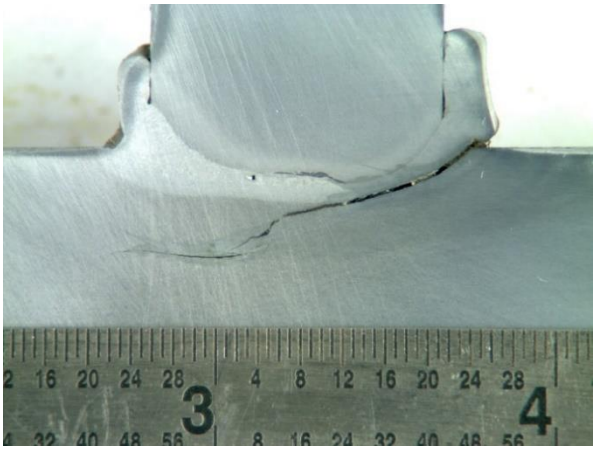

Source: FHWA.

Figure 301. Photo. POF12_2 cross section.

APPENDIX F. LARGE-SCALE STATIC TEST LVDT DATA

This appendix contains the LVDT data—both slip and uplift—for three of the large-scale static tests that were not presented in the report. Data are presented in the same order for each of the three beams. First the slip data for the west shear span, then for the east shear span, and then the uplift data at the midspan of each shear span are presented.

SPECIMEN 1S2

Figure 302 through figure 304 show the LVDT results for specimen 1S2.

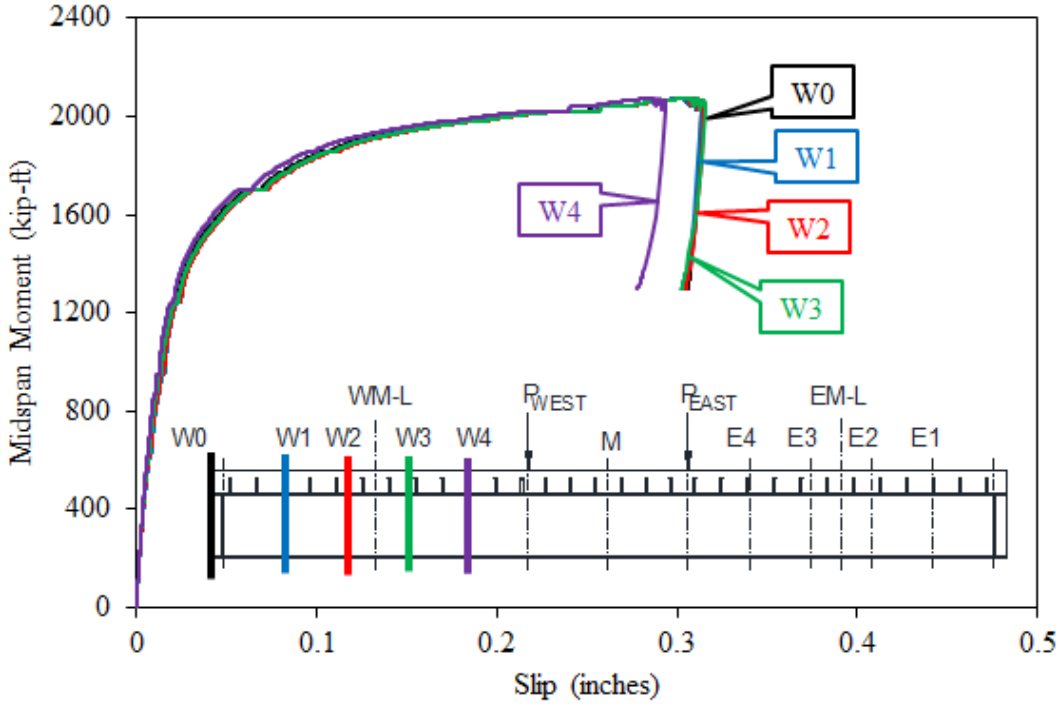

Source: FHWA.

Figure 302. Graph. LVDT results for slip in west shear span of beam 1S2.

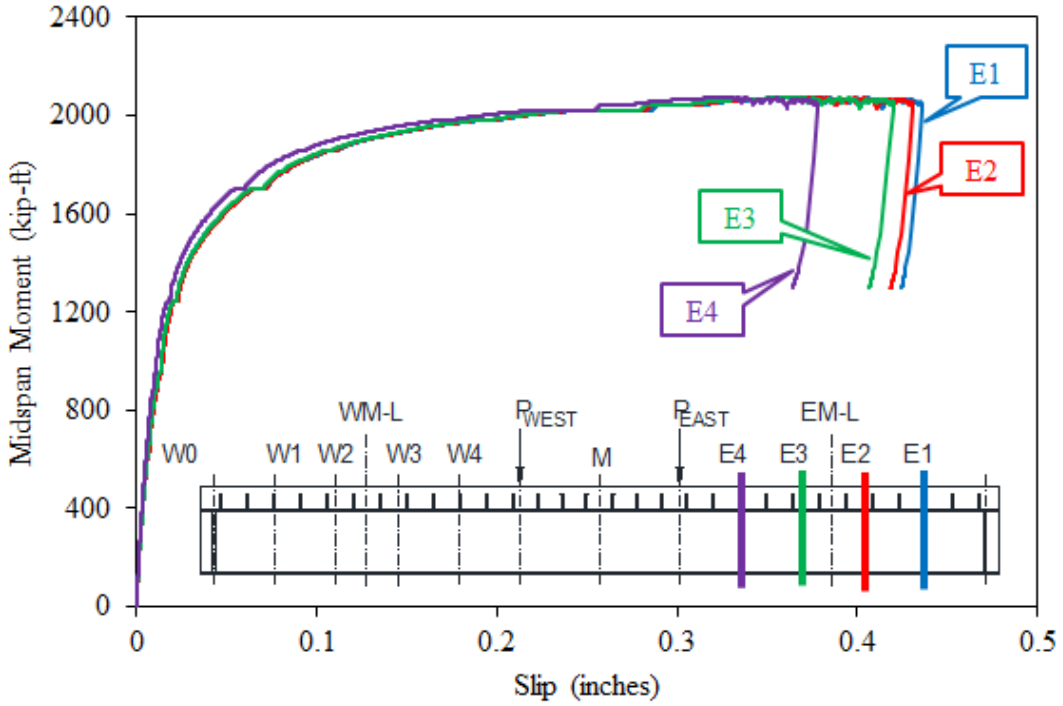

Source: FHWA.

Figure 303. Graph. LVDT results for slip in east shear span of beam 1S2.

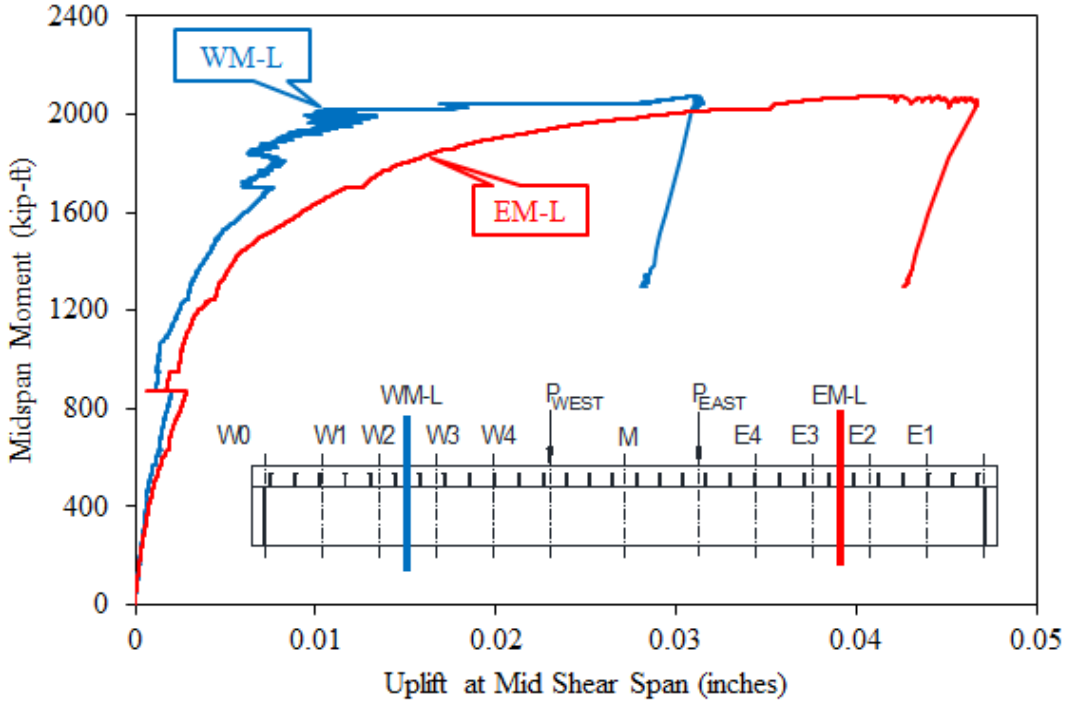

Source: FHWA.

Figure 304. Graph. LVDT results for uplift in both shear spans of beam 1S2.

SPECIMEN 2S1

Figure 305 through figure 307 show the LVDT results for specimen 2S1.

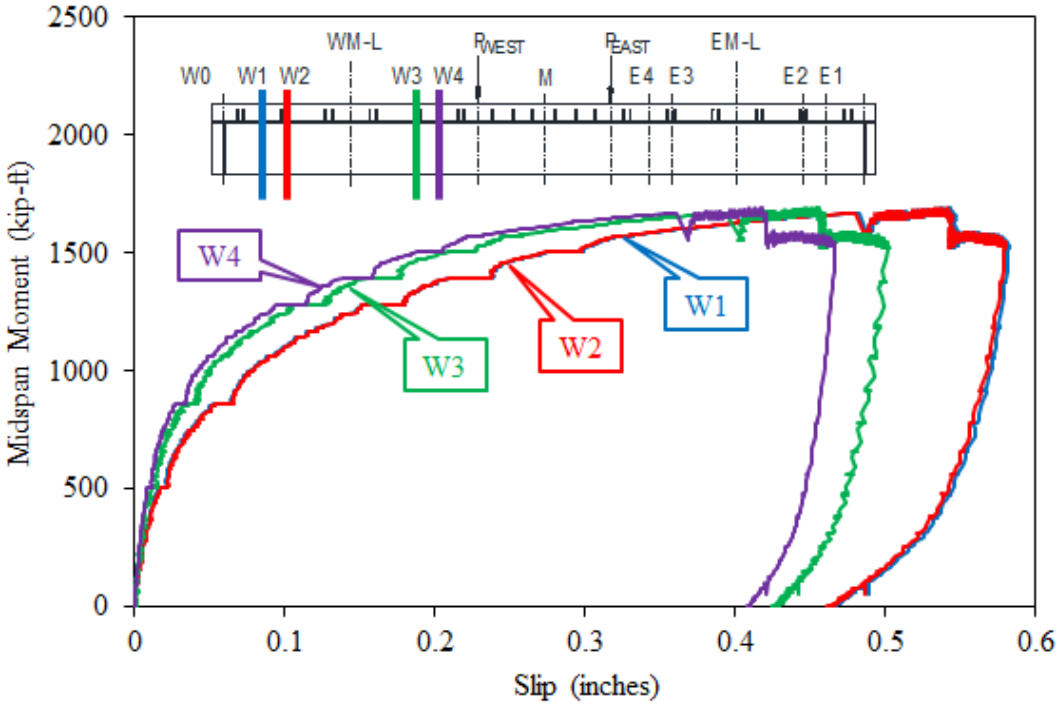

Source: FHWA.

Figure 305. Graph. LVDT results for slip in west shear span of beam 2S1.

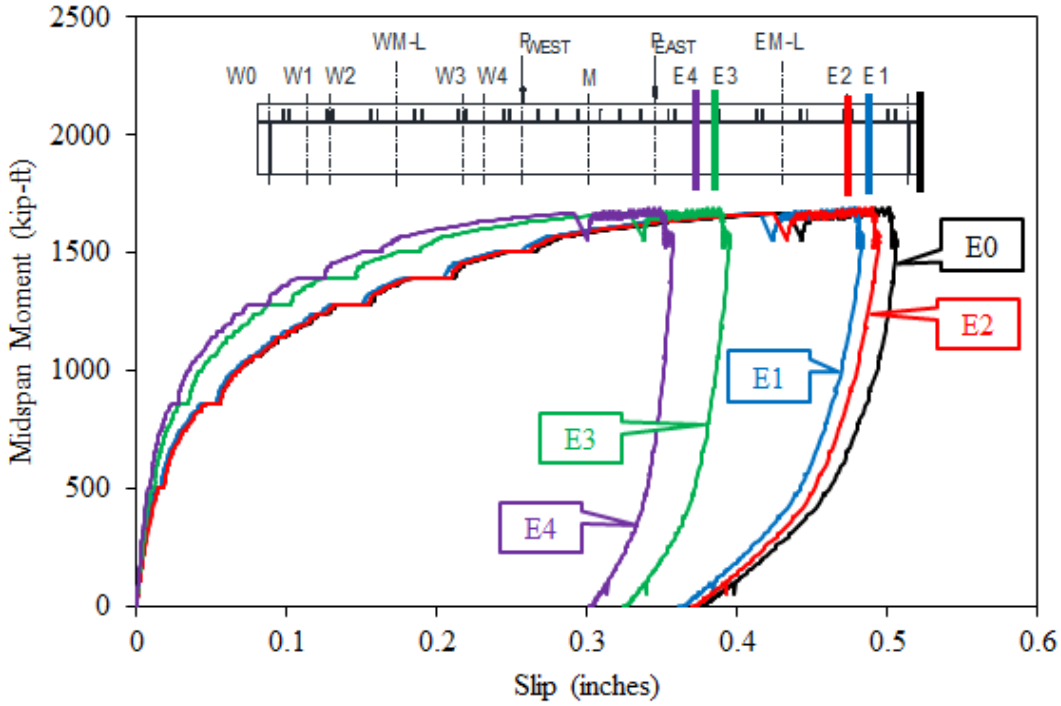

Source: FHWA.

Figure 306. Graph. LVDT results for slip in east shear span of beam 2S1.

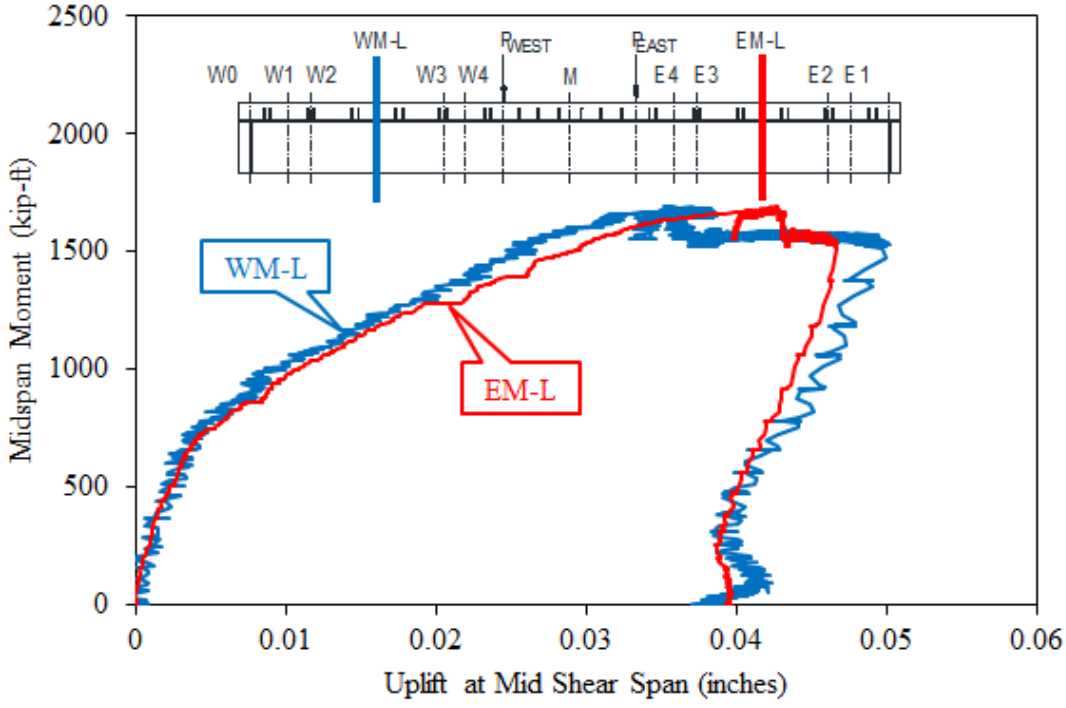

Source: FHWA.

Figure 307. Graph. LVDT results for uplift in both shear spans of beam 2S1.

SPECIMEN 3S1

Figure 308 through figure 310 show the LVDT results for specimen 3S1.

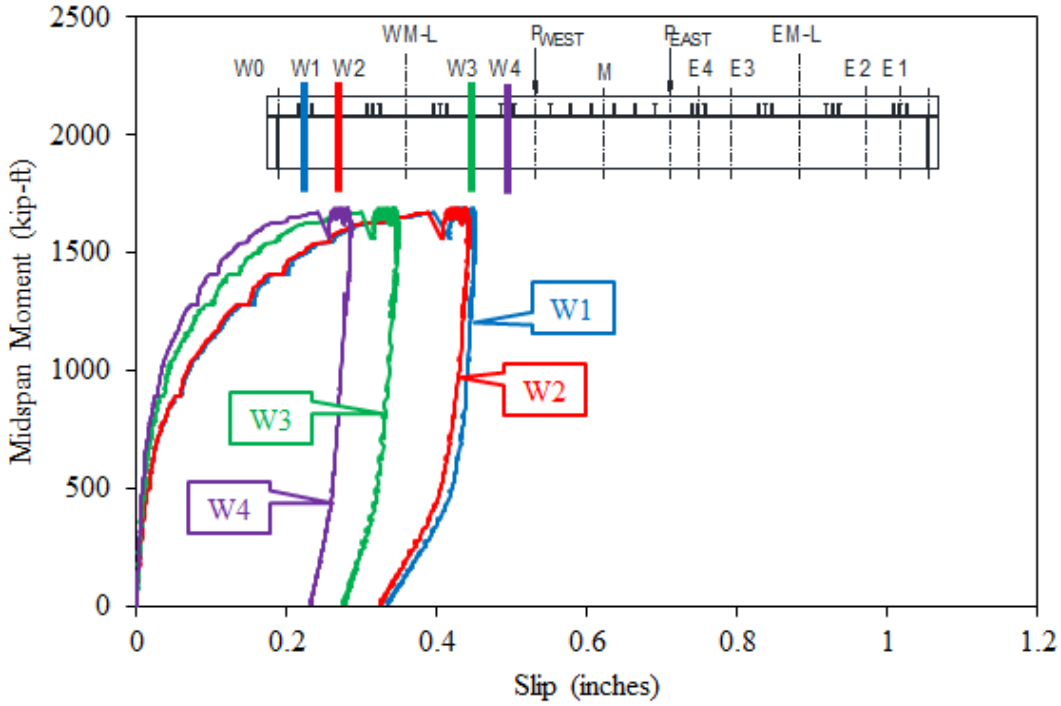

Source: FHWA.

Figure 308. Graph. LVDT results for slip in west shear span of beam 3S1.

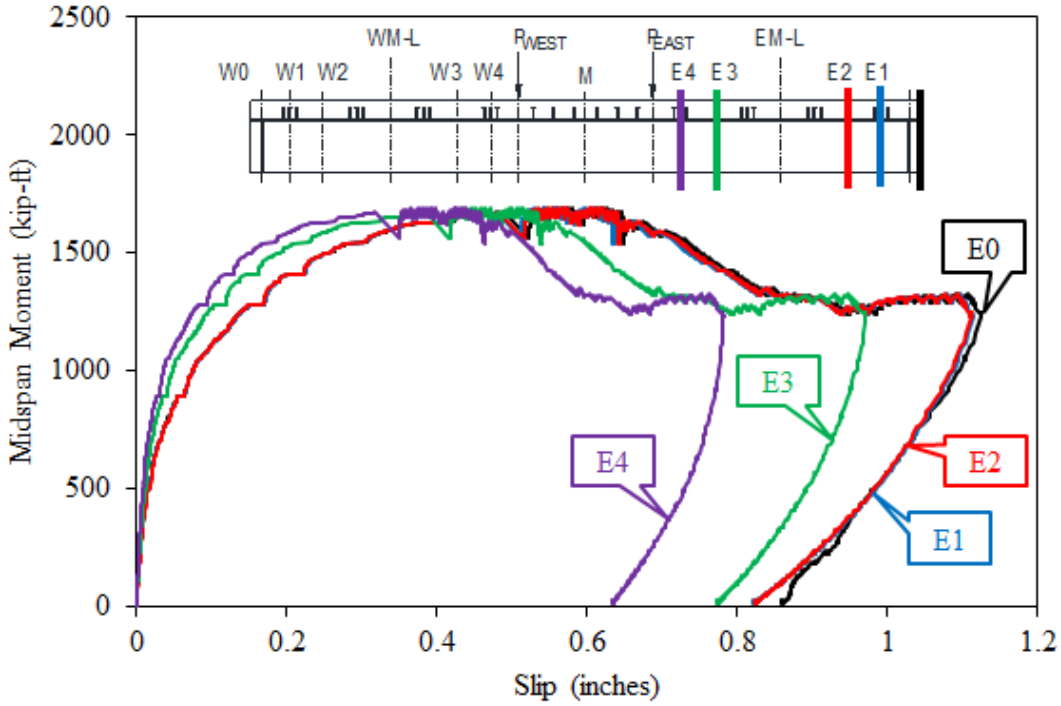

Source: FHWA.

Figure 309. Graph. LVDT results for slip in east shear span of beam 3S1.

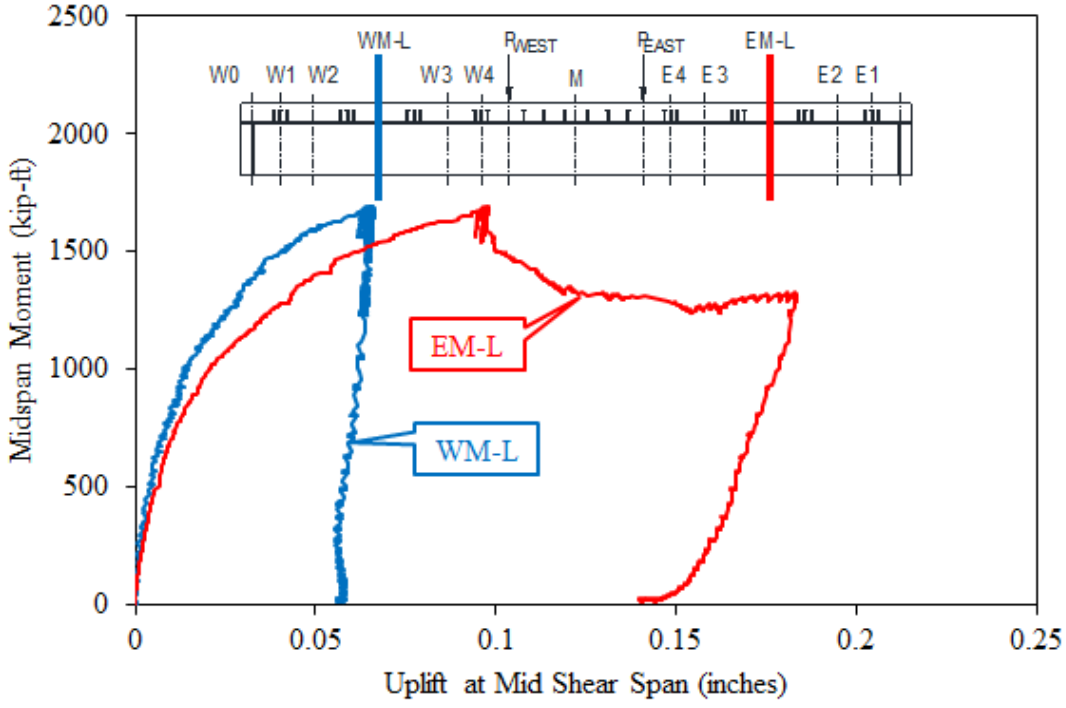

Source: FHWA.

Figure 310. Graph. LVDT results for uplift in both shear spans of beam 3S1.

APPENDIX G. SMALL-SCALE FATIGUE TEST LVDT DATA

This appendix contains the LVDT data from the small-scale fatigue tests. Figure 311 through figure 324 shows the relative slip range between the concrete decks and steel beam for each specimen. The LVDT data for each specimen are presented in the order in which the tests were conducted.

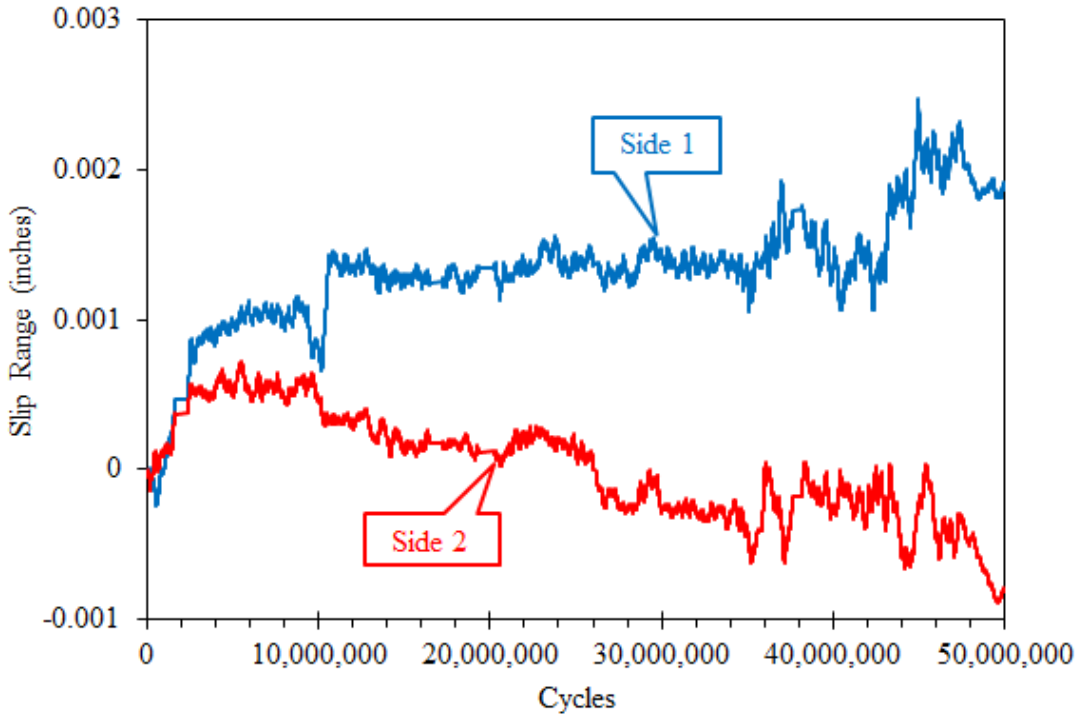

Source: FHWA.

Figure 311. Graph. LVDT slip range data for PO-F1.

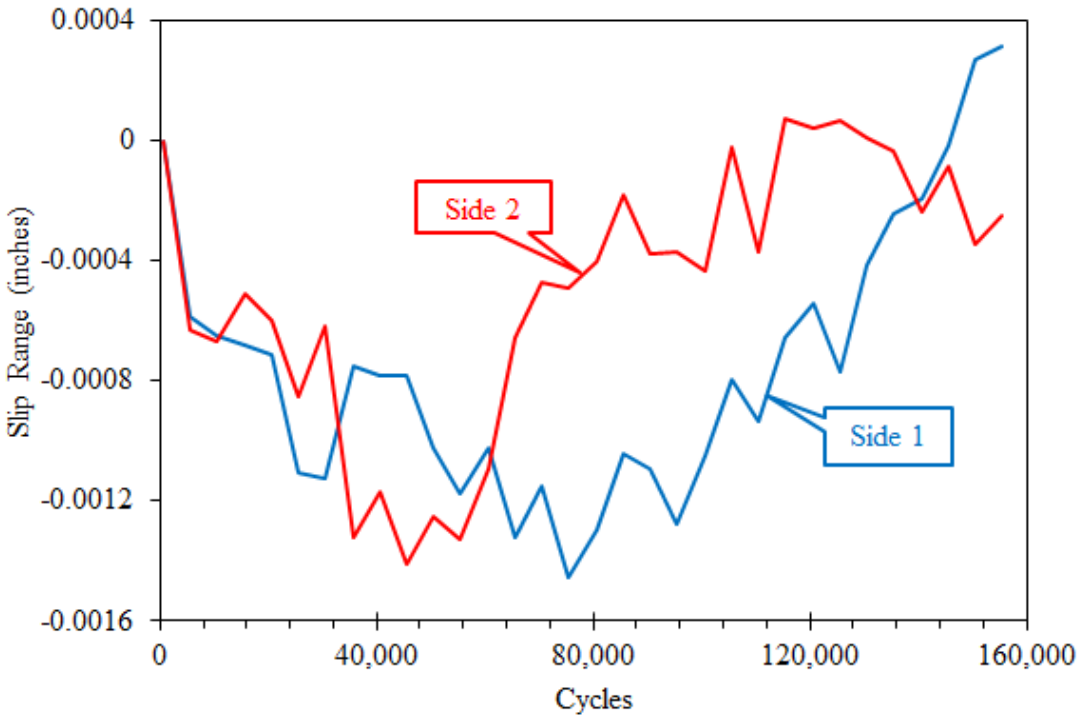

Source: FHWA.

Figure 312. Graph. LVDT slip range data for PO-F2.

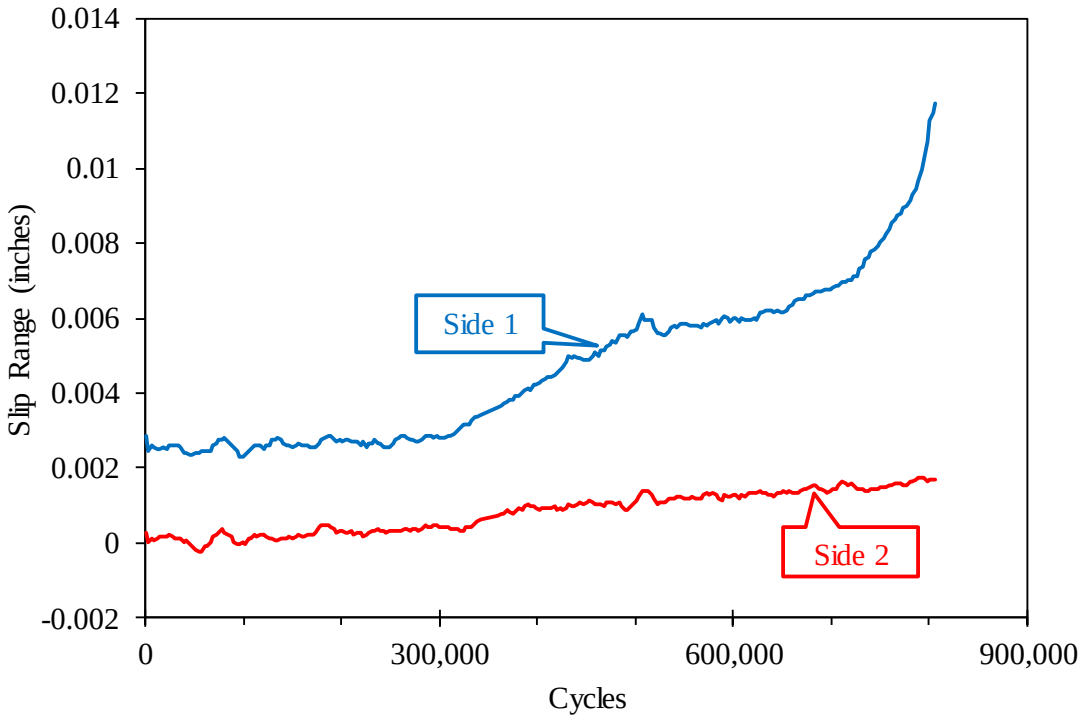

Source: FHWA.

Figure 313. Graph. LVDT slip range data for PO-F3.

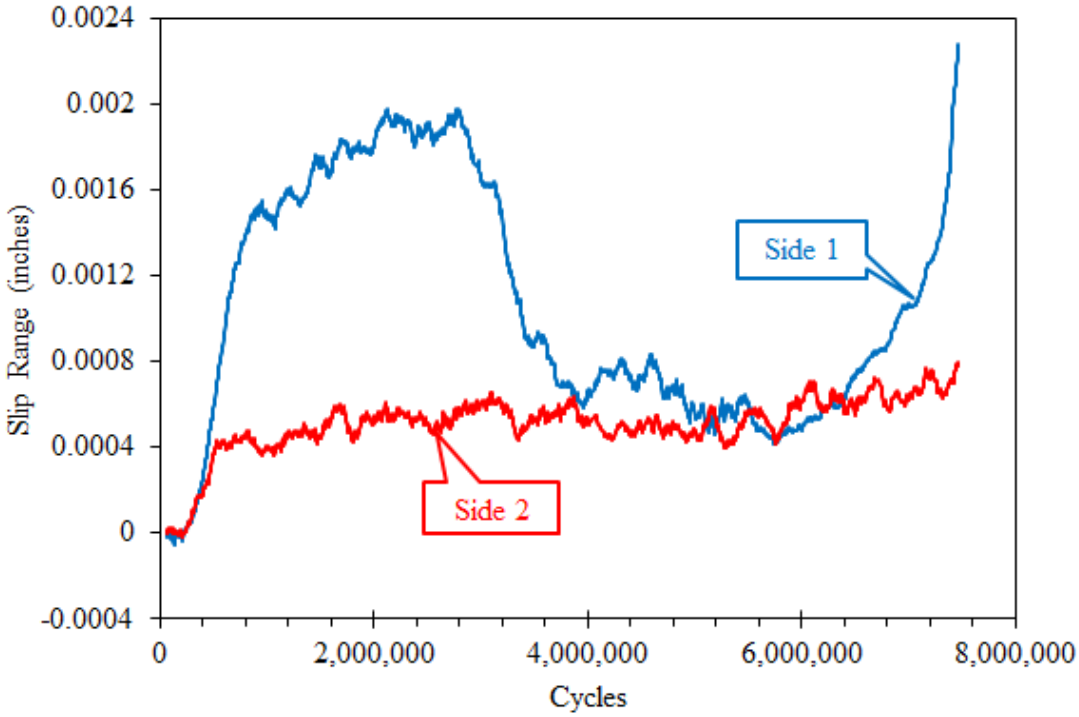

Source: FHWA.

Figure 314. Graph. LVDT slip range data for PO-F4.

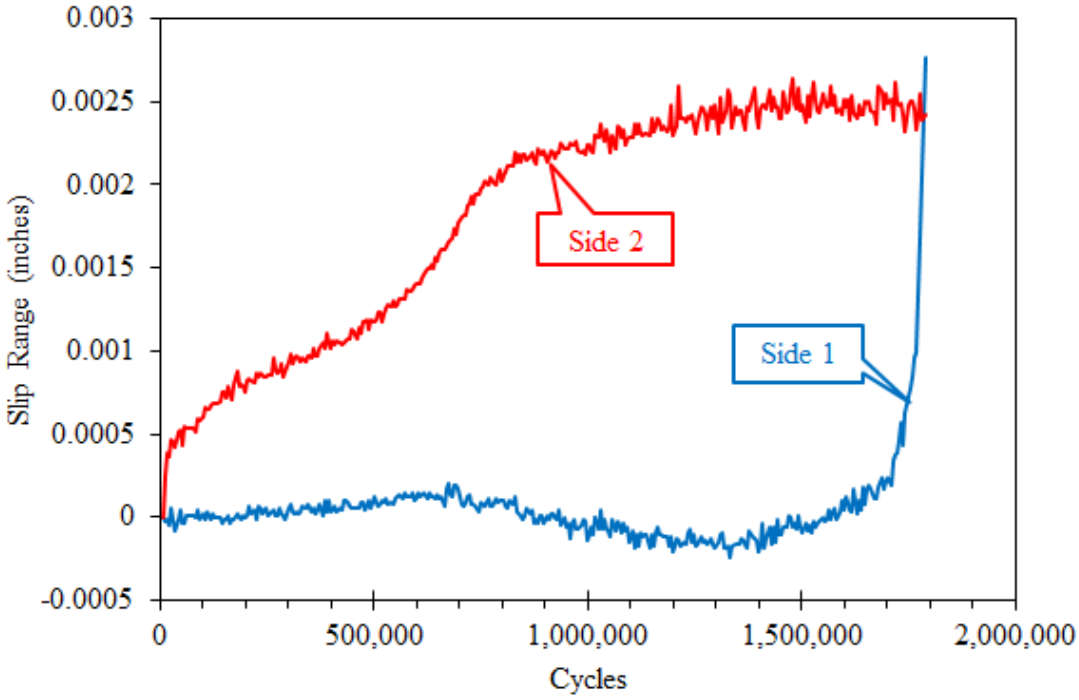

Source: FHWA.

Figure 315. Graph. LVDT slip range data for PO-F5.

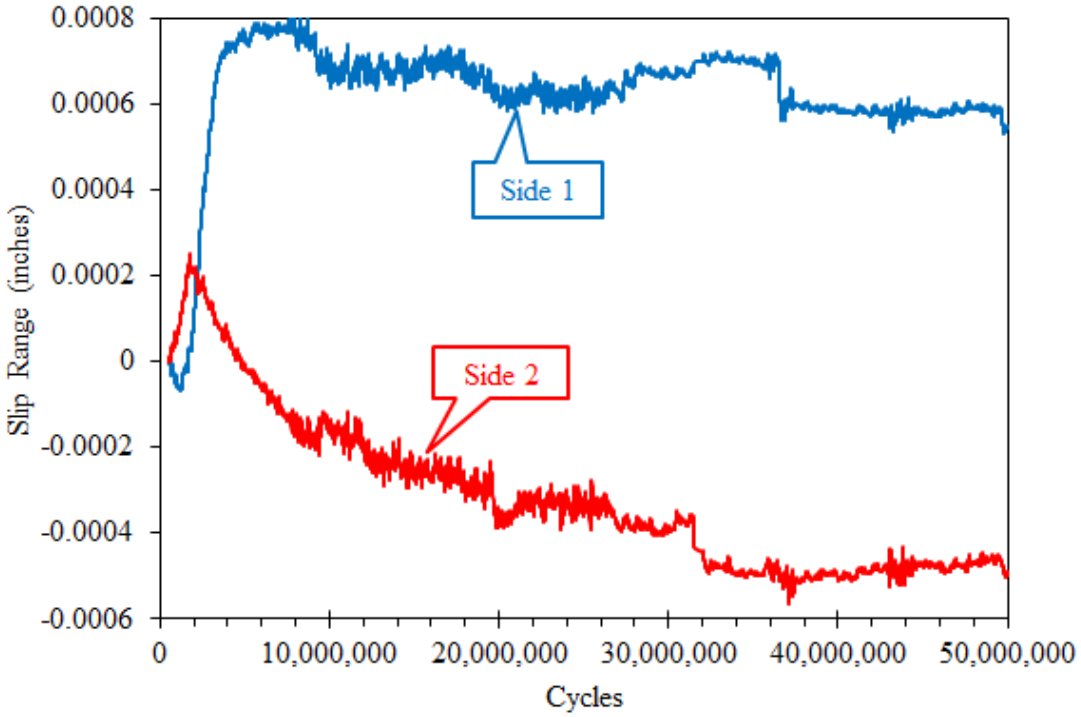

Source: FHWA.

Figure 316. Graph. LVDT slip range data for PO-F6.

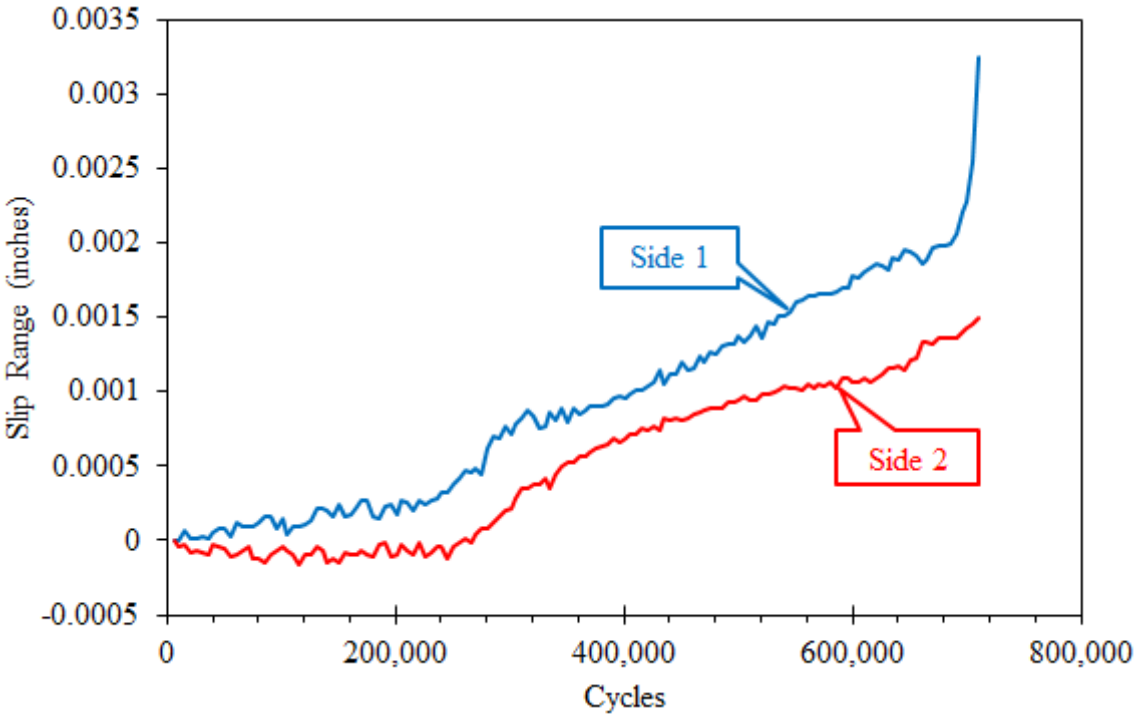

Source: FHWA.

Figure 317. Graph. LVDT slip range data for PO-F7.

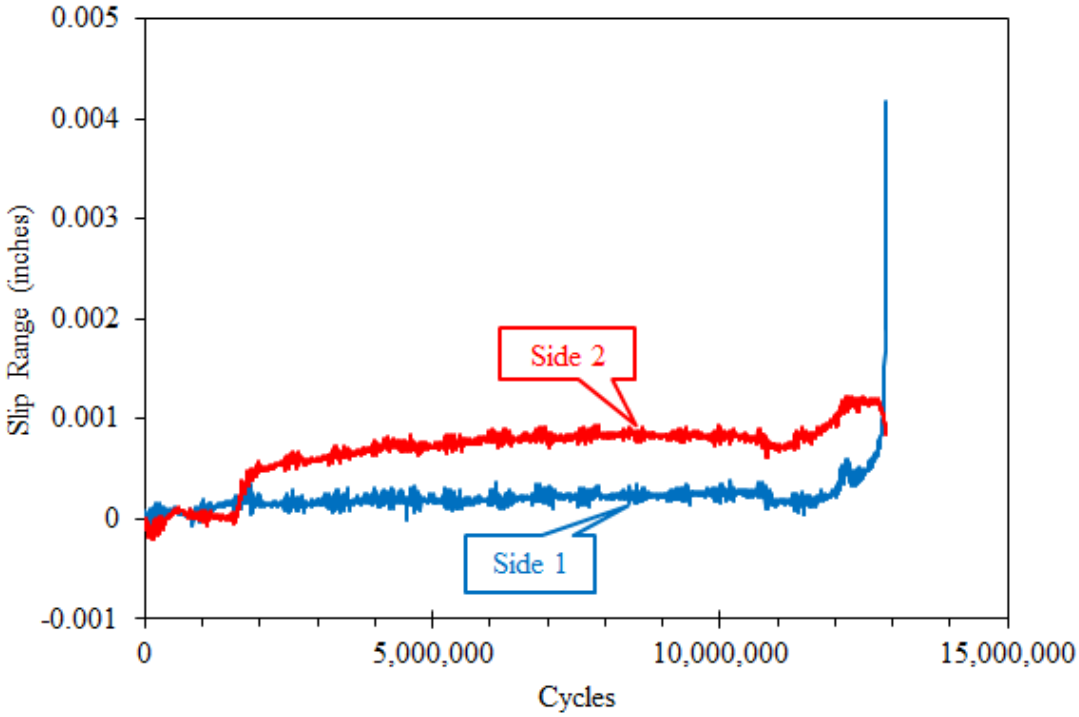

Source: FHWA.

Figure 318. Graph. LVDT slip range data for PO-F8.

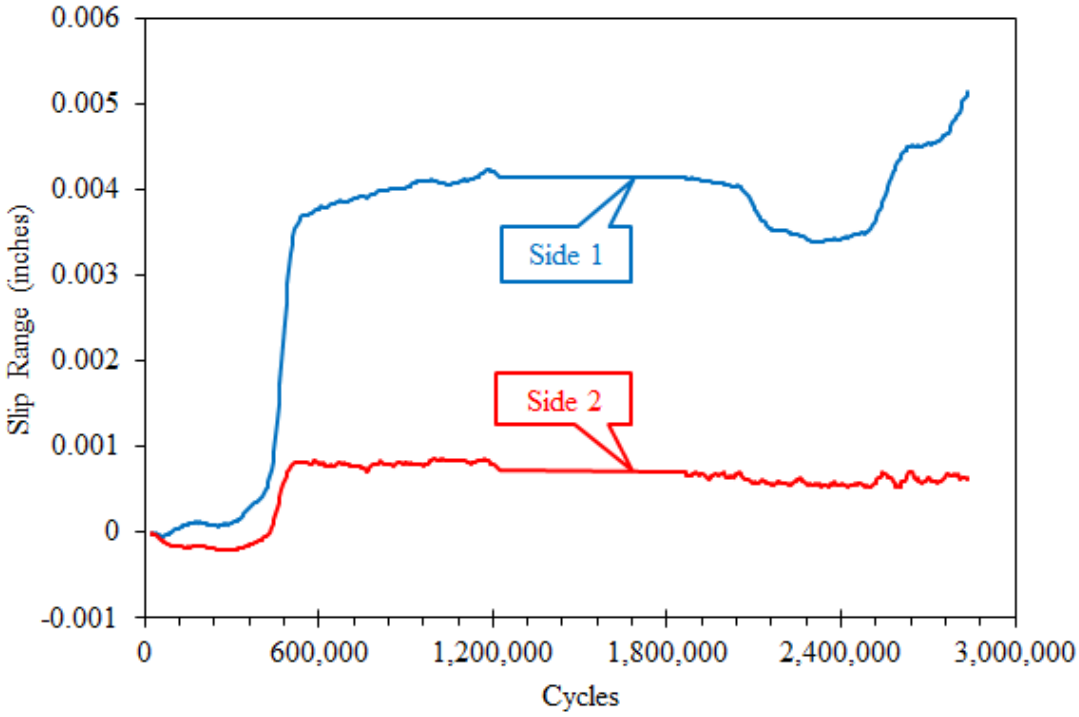

Source: FHWA.

Figure 319. Graph. LVDT slip range data for PO-F9.

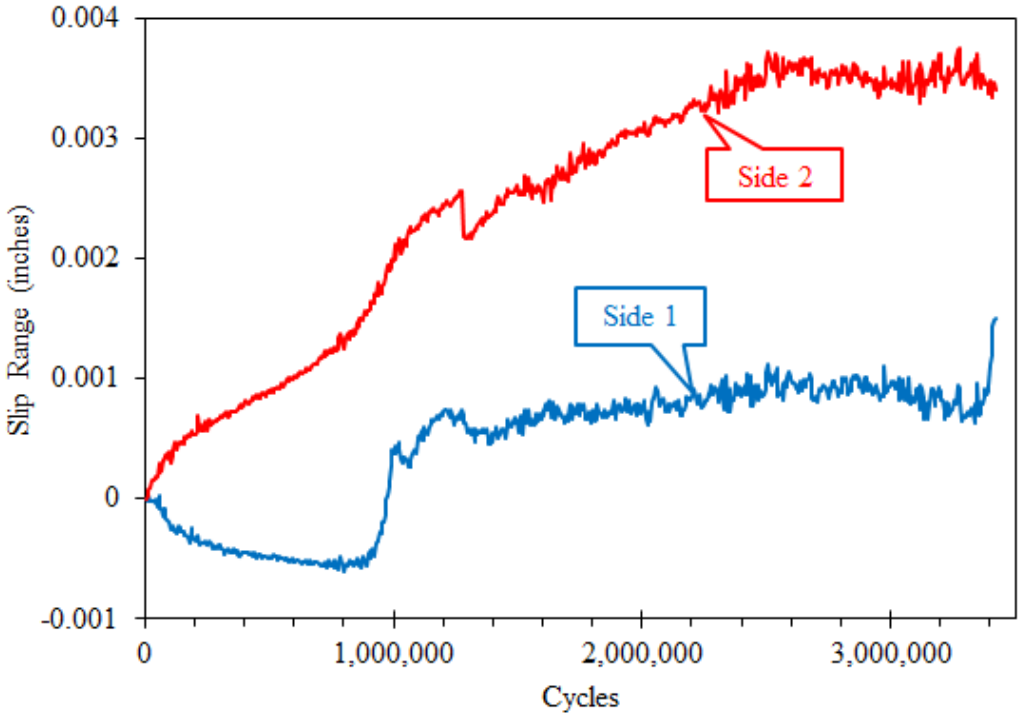

Source: FHWA.

Figure 320. Graph. LVDT slip range data for PO-F10.

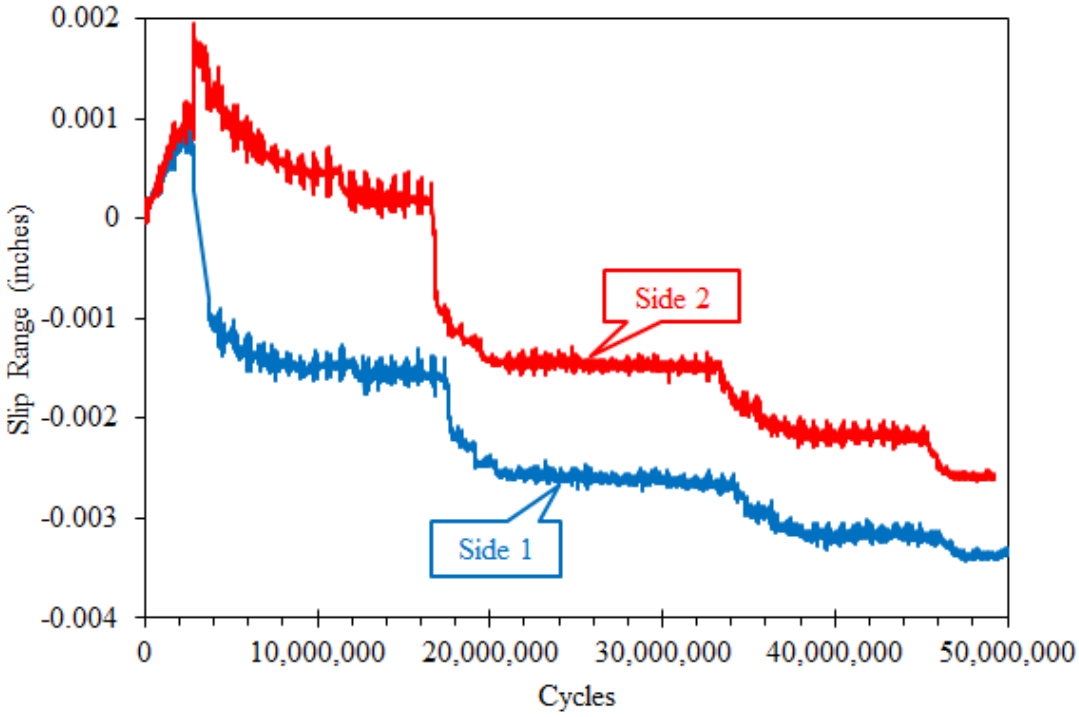

Source: FHWA.

Figure 321. Graph. LVDT slip range data for PO-F11.

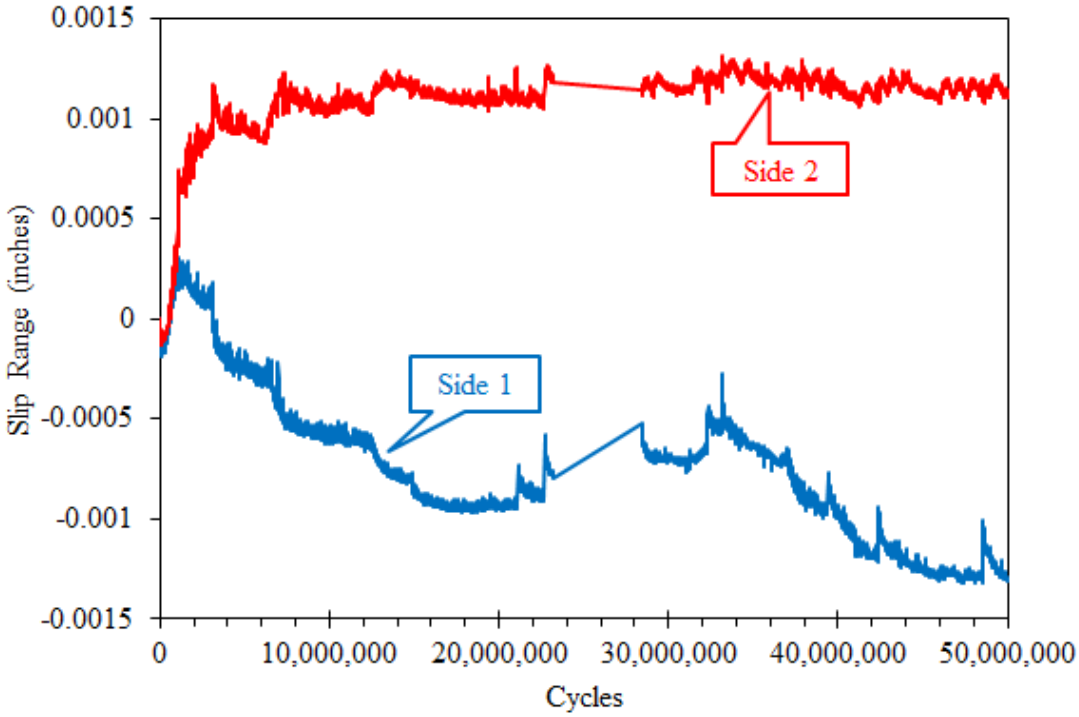

Source: FHWA.

Figure 322. Graph. LVDT slip range data for PO-F12.

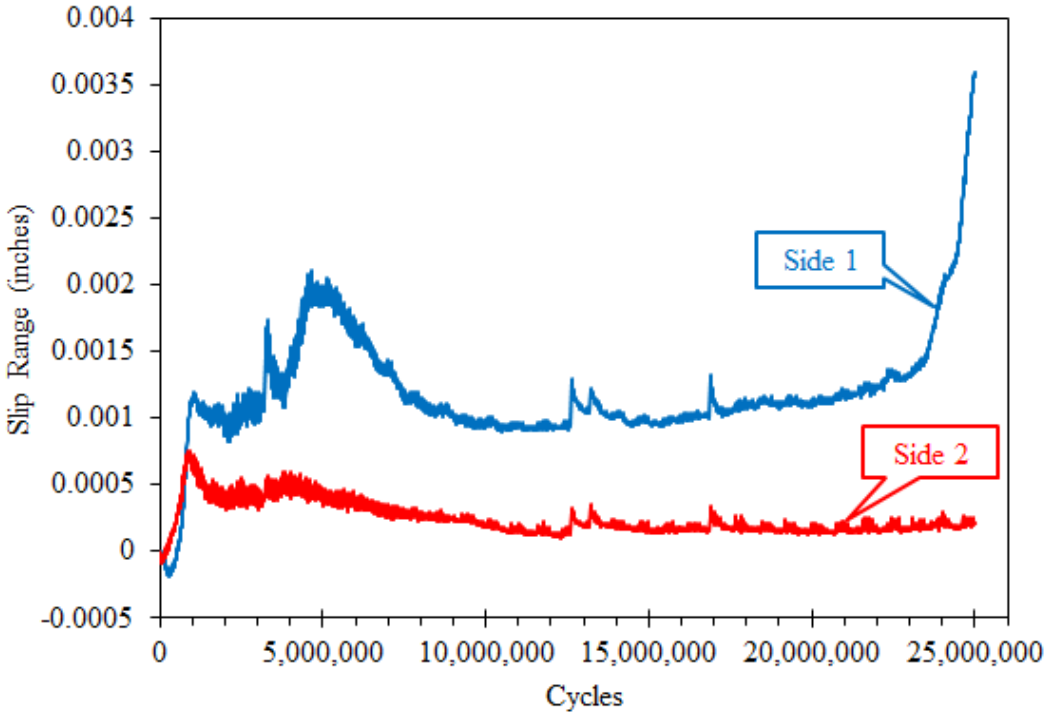

Source: FHWA.

Figure 323. Graph. LVDT slip range data for PO-F13.

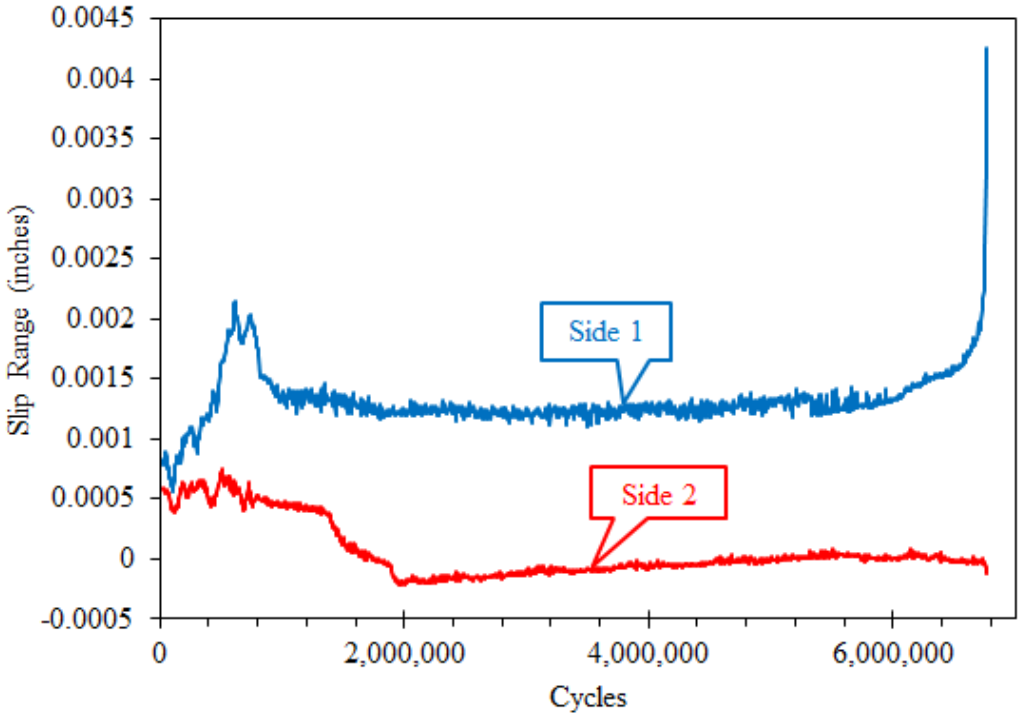

Source: FHWA.

Figure 324. Graph. LVDT slip range data for PO-F14.

APPENDIX H. HISTORICAL SHEAR STUD–FATIGUE DATA

Table 28 contains the historical shear stud S-N data used in the regression analysis of the large-scale fatigue tests. Table 29 shows the historical shear stud S-N data used in the regression analysis of the small-scale fatigue tests.

Table 28. Historical large-scale shear stud–fatigue data considered for regression analysis.[6]

Source	Stress Range (ksi)	Cycles to Failure
Toprac	16.5	105,000
Toprac	14.5	4,490,000
Toprac	17.8	260,000
Toprac	12.2	2,870,000
Toprac	10.5	2,282,000
Toprac	14.5	1,333,000
Toprac	17.8	120,000

Table 29. Historical small-scale shear stud–fatigue data considered for regression analysis.

Specimen Name	Stud Diameter (Inches)	Studs Per Side	Stress Range (ksi)	Cycles to Failure	Reference Number
PS1-1	0.75	2	13.9	1,303,669	43
PS2-1	0.75	2	13.3	823,970	43
PS2-2	0.75	2	13.3	845,000	43
PS3-1	0.75	2	13.3	652,300	43
PS3-2	0.75	2	13.3	652,300	43
PS4-1	0.75	2	24.2	52,801	43
PS4-2	0.75	2	24.2	52,836	43
PS5-1	0.75	2	24.2	58,630	43
PS5-2	0.75	2	24.2	67,877	43
PS6-1	0.75	2	13.7	3,170,000	43
PS6-2	0.75	2	13.7	3,554,000	43
PS7-1	0.75	2	13.7	5,140,000	43
PS7-2	0.75	2	13.7	6,096,000	43
PS8-1	0.75	2	11.1	21,391,000	43
PS8-2	0.75	2	11.1	20,965,000	43

Specimen Name	Stud Diameter (Inches)	Studs Per Side	Stress Range (ksi)	Cycles to Failure	Reference Number
PS9-1	0.75	2	11.1	24,305,000	43
PS9-2	0.75	2	11.1	35,000,000[a]	43
PS10-1	0.75	2	21.4	61,700	43
PS10-2	0.75	2	21.4	75,500	43
PS11-1	0.75	2	21.4	110,000	43
PS11-2	0.75	2	21.4	110,000	43
PS12-1	0.75	2	16.0	148,700	43
PS12-2	0.75	2	16.0	174,800	43
PS13-1	0.75	2	16.0	182,600	43
PS13-2	0.75	2	16.0	182,600	43
FT25-A1	0.98	4	14.5	2,133,970	44
FT25-A2	0.98	4	21.8	44,827	44
FT25-A3	0.98	4	24.7	60,000	44
FT25-B1	0.98	4	18.9	687,209	44
FT25-B2	0.98	4	21.8	61,063	44
FT25-B3	0.98	4	25.7	5,320	44
FT27-A1	1.06	4	18.6	142,641	44
FT27-A2	1.06	4	21.8	22,488	44
FT27-A3	1.06	4	24.7	13,766	44
FT30-A1	1.18	4	18.9	75,484	44
FT30-A2	1.18	4	21.8	10,436	44
FT30-A3	1.18	4	22.6	19,333	44
PS1	0.39	4	20.8	127,367	45
PS2	0.39	4	9.2	18,477,755	45
PS3	0.39	4	13.9	1,528,187	45
PS4	0.39	4	18.5	279,102	45
PS5	0.39	4	11.5	3,920,083	45
PS6	0.39	4	25.4	47,024	45
R1	0.75	2	20.3	616,000	46
R2	0.75	2	20.3	194,110	46
R3	0.75	2	20.3	190,460	46
R4	0.75	2	21.7	49,300	46
F1	0.50	4	15.5	572,000	47

Specimen Name	Stud Diameter (Inches)	Studs Per Side	Stress Range (ksi)	Cycles to Failure	Reference Number
F2	0.50	4	15.5	718,000	47
F3	0.50	4	15.5	1,088,000	47
F4	0.50	4	15.5	895,000	47
F5	0.50	4	15.5	1,251,000	47
F6	0.50	4	15.5	1,507,000	47
9	0.75	4	19.5	169,400	48
10	0.75	4	13.9	474,000	48
1	0.866	2	16.1	566,000	49
2	0.866	2	16.1	522,600	49
3	0.866	2	16.8	720,000	49
4	0.866	2	20.6	83,700	49
5	0.866	2	20.9	103,600	49
6	0.866	2	21.3	96,500	49
7	0.866	2	24.3	60,400	49
8	0.866	2	15.7	550,000	49
9	0.866	2	15.0	907,000	49
10	0.866	2	15.0	913,000	49
11	0.866	2	23.6	39,140	49
ST-F-A1	0.625	4	14.5	2,120,000	50
ST-F-A2	0.625	4	14.5	2,535,490	50
ST-F-A3	0.625	4	14.5	2,828,560	50
ST-F-B1	0.625	4	18.3	656,880	50
ST-F-B2	0.625	4	18.3	735,740	50
ST-F-B3	0.625	4	18.3	1,300,800	50
ST-F-C1	0.625	4	21.8	231,580	50
ST-F-C2	0.625	4	21.8	274,440	50
ST-F-C3	0.625	4	21.8	161,430	50
S1	0.866	4	15.64	6,200,000	51
S2	0.866	4	17.55	1,200,000	51
S3	0.866	4	19.17	5,100,000	51
S4	0.866	4	13.81	3,500,000	51
S5E	0.866	4	18.02	6,400,000	51
S-0.875-22-A	0.875	4	22	325,557	11

Specimen Name	Stud Diameter (Inches)	Studs Per Side	Stress Range (ksi)	Cycles to Failure	Reference Number
S-0.875-22-B	0.875	4	22	80,346	11
S-0.875-22-C	0.875	4	22	245,121	11
S-0.875-22-D	0.875	4	22	91,598	11
S-1.25-22-A	1.250	2	22	276,594	11
S-1.25-22-B	1.250	2	22	177,890	11
S-1.25-22-C	1.250	2	22	56,753	11
S-1.25-22-D	1.250	2	22	138,588	11
S-0.875-18-A	0.875	4	18	1,586,515	11
S-0.875-18-B	0.875	4	18	2,654,243	11
S-0.875-18-C	0.875	4	18	986,718	11
S-0.875-18-D	0.875	4	18	235,326	11
S-1.25-18-A	1.250	2	18	655,779	11
S-1.25-18-B	1.250	2	18	3,852,257	11
S-1.25-18-C	1.250	2	18	992,965	11
S-1.25-18-D	1.250	2	18	381,667	11
S-0.875-26-A	0.875	4	26	38,295	11
S-0.875-26-B	0.875	4	26	56,507	11
S-0.875-26-C	0.875	4	26	36,094	11
S-0.875-26-D	0.875	4	26	38,101	11
S-1.25-26-A	1.250	2	26	87,933	11
S-1.25-26-B	1.250	2	26	11,097	11
S-1.25-26-C	1.250	2	26	29,987	11
S-1.25-26-D	1.250	2	26	36,583	11
212	0.75	4	10	6,730,000[a]	52
616	0.75	4	10	5,810,000[a]	52
1020	0.75	4	10	6,711,000	52
214	0.75	4	12	2,960,000	52
618	0.75	4	12	2,223,000	52
216	0.75	4	14	305,000	52
620B	0.75	4	14	726,000	52
1024	0.75	4	14	390,000	52
218	0.75	4	16	292,000	52
622	0.75	4	16	435,700	52

Specimen Name	Stud Diameter (Inches)	Studs Per Side	Stress Range (ksi)	Cycles to Failure	Reference Number
220	0.75	4	18	100,000	52
624	0.75	4	18	142,680	52
1028	0.75	4	18	340,300	52
620	0.75	4	14	1,345,000	52
1	0.75	4	8.7	12,803,000	12
2	0.75	4	4.4	30,053,000[a]	12
3	0.75	4	5.8	12,251,908[a]	12
4	0.75	4	5.8	20,000,000[a]	12
5	0.75	4	7.3	31,401,000[a]	12
6	0.75	4	8.7	30,001,000[a]	12

[a]Test was a runout and did not produce a failure. These tests are shown in figure 99 but were not included in the regression analysis.

REFERENCES

1. AASHTO. (2014). *AASHTO LRFD Bridge Design Specifications*, Seventh Edition, American Association of State Highway and Transportation Officials, Washington, DC.

2. AASHTO. (2012). *AASHTO LRFD Bridge Design Specifications*, Sixth Edition, American Association of State Highway and Transportation Officials, Washington, DC.

3. AASHTO. (2017). *AASHTO LRFD Bridge Design Specifications*, Eighth Edition, American Association of State Highway and Transportation Officials, Washington, DC.

4. Slutter, R.G. and Fisher, J.W. (1966). "Fatigue Strength of Shear Connectors." *Highway Research Record No. 147*, pp. 65–88, National Research Council, Washington, DC.

5. King, D.C., Slutter, R.G., and Driscoll, G.C. (1965). "Fatigue Strength of ½-Inch Diameter Stud Shear Connectors." *Highway Research Record No. 103*, pp. 78–106, National Research Council, Washington, DC.

6. Toprac, A.A. (1965). "Fatigue Strength of ¾-Inch Stud Shear Connectors." *Highway Research Record No. 103*, pp. 53–77, National Research Council, Washington, DC.

7. AASHTO. (1977). *Interim Specifications for Highway Bridges*, American Association of State Highway and Transportation Officials, Washington, DC.

8. Eurocode 4. (2005). *Design of Composite Steel and Concrete Structures, Part 2: General Rules and Rules for Bridges*, EN 1994-2, European Committee for Standardization, Brussels, Belgium.

9. Council of Standards Australia. (2004). *Australian Standard: Bridge Design, Part 6: Steel and Composite Construction*, Council of Standards Australia, Sydney, Australia.

10. Japan Society of Civil Engineers. (2009). *Standard Specifications for Steel and Composite Structures*, First Edition, Japan Society of Civil Engineers, Tokyo, Japan.

11. Mundie, D.L. (2011). *Fatigue Testing and Design of Large Diameter Shear Studs Used in Highway Bridges*, Thesis, Auburn University, Auburn, AL.

12. Ovuoba, B. and Prinz, G.S. (2016). "Fatigue Capacity of Headed Shear Studs in Composite Bridge Girders." *Journal of Bridge Engineering*, *21*(12), American Society of Civil Engineers, Reston, VA.

13. Ollgaard, J.G., Slutter, R.G., and Fisher, J.W. (1971). "Shear Strength of Stud Connectors in Lightweight and Normal-Weight Concrete." *Engineering Journal*, *8*, pp. 55–64, American Institute of Steel Construction, Chicago, IL.

14. AASHTO. (1994). *AASHTO LRFD Bridge Design Specifications*, First Edition, American Association of State Highway and Transportation Officials, Washington, DC.

15. AASHTO. (2000). *Interim Revisions to the 16th Edition Standard Specifications for Highway Bridges*, American Association of State Highway and Transportation Officials, Washington, DC.

16. Abbas, H.H. (2012). "Static Strength of Stud-Type Shear Connectors." Robert Dexter Memorial Lecture, Presented at the Steel Market Development Institute, August 9, 2012, Chicago, IL.

17. Provines, J. and Ocel, J.M. (2014). "Strength and Fatigue Resistance of Shear Stud Connectors." *Proceedings of the 2014 National Accelerated Bridge Construction Conference*, Miami, FL.

18. Badie, S.S. and Tadros, M.K. (2008). *Full-Depth Precast Concrete Bridge Deck Panel Systems*, NCHRP Report 584, National Cooperative Highway Research Program, Washington, DC.

19. Newmark, N.M. and Siess, C.P. (1943). "Design of Slab and Stringer Highway Bridges." *Public Roads, 23*(1), pp. 157–165, Public Roads Administration, Washington, DC.

20. AASHO. (1941). *Standard Specifications for Highway Bridges*, Third Edition, American Association of State Highway Officials, Washington, DC.

21. AASHO. (1944). *Standard Specifications for Highway Bridges*, Fourth Edition, American Association of State Highway Officials, Washington, DC.

22. Viest, I.M. and Siess, C.P. (1954). "Design of Channel Shear Connectors for Composite I-Beam Bridges." *Public Roads*, *28*(1), pp. 9–15, Bureau of Public Roads, Washington, DC.

23. AASHTO. (1990). *Interim Specifications, Bridges, 1990*, American Association of State Highway and Transportation Officials, Washington, DC.

24. AASHTO. (1994). *Interim Specifications, Bridges, 1994*, American Association of State Highway and Transportation Officials, Washington, DC.

25. Okada, J., Yoda, T., and Lebet, J.P. (2006). "A Study of the Grouped Arrangement of Stud Connectors on the Shear Strength Behavior." *Structural Engineering/Earthquake Engineering, 23*(1), pp. 75–89, Japanese Society of Civil Engineers, Tokyo, Japan.

26. Shim, C.S., Lee, P.G., Kim, D.W., and Chung, C.H. (2008). *Effects of Group Arrangement on the Ultimate Strength of Stud Shear Connection*, International Conference on Composite Construction in Steel and Concrete, July 20–24, 2008, Tabernash, CO.

27. Issa, M.A., Patton, T.A., Abdalla, H.A., Youssif, A.A., and Issa, M.A. (2003). "Composite Behavior of Shear Connections in Full-Depth Precast Concrete Bridge Deck Panels on Steel Stringers." *PCI Journal*, *48*(5), September–October, pp. 76–89, Precast/Prestressed Concrete Institute, Chicago, IL.

28. AISC. (2005). *Steel Construction Manual,* 13th Edition, American Institute of Steel Construction, Inc., Chicago, IL.

29. Texas DOT. (2016). *Bridge Design Manual – LRFD*, 2015-1, Texas Department of Transportation, Austin, TX.

30. AASHTO/AWS (2010). *Bridge Welding Code*, Sixth Edition, AASHTO/AWS D1.5M/D1.5, American Welding Society, Miami, FL.

31. Lee, K.C., Abbas, H.H., and Ramey, G.E. (2010). "Review of Current AASHTO Fatigue Design Specifications for Stud Shear Connectors." *Structures Congress 2010 Proceedings*, pp. 310–321, American Society of Civil Engineers, Reston, VA.

32. Provines, J. and Ocel, J.M. (2014). "Strength and Fatigue Resistance of Clustered Shear Studs." *2014 World Steel Bridge Symposium Conference Proceedings*, Toronto, ON.

33. Provines, J. and Ocel, J.M. (2016). "Fatigue Resistance of Clustered Shear Studs." *2016 World Steel Bridge Symposium Conference Proceedings*, Orlando, FL.

34. Swenty, M.K. and Graybeal, B.A. (2013). *Material Characterization of Field-Cast Connection Grouts*, Report No. FHWA-HRT-13-041, Federal Highway Administration, McLean, VA.

35. Oliva, M.G., Bank, L.C., and Russell. J.S. (2007). *Full Depth Precast Concrete Highway Bridge Decks*, Innovative Bridge Research and Construction Contract No. 0607-48-01, University of Wisconsin, Madison, WI.

36. Mainstone, R.J. and Menzies, J.B. (1967). "Shear Connectors in Steel-Concrete Composite Beams for Bridges, Part I." *Concrete 1*(9), pp. 291–302, Concrete Society, London, United Kingdom.

37. Vecloth, J. (2013). "Experimental Evaluation of the Static Strength and Ductility of Large Diameter Shear Studs in Composite Bridge Construction." Thesis, University of Auburn, Auburn, AL.

38. Marvi, B. (2010). "Push-Off Tests on Full-Depth Precast Concrete Bridge Deck Panel to Steel Girder Connection." Thesis, Ryerson University, Toronto, ON.

39. ASTM A370. (2014). "Standard Test Methods and Definitions for Mechanical Testing of Steel Products." *ASTM Annual Book of Standards 01.03,* ASTM International, West Conshohocken, PA.

40. Galambos, T.V. (1988). *Guide to Stability Design Criteria for Metal Structures*, Fourth Edition, John Wiley & Sons, New York, NY.

41. ASTM C39. (2014). "Standard Test Method for Compressive Strength of Cylindrical Concrete Specimens." *ASTM Annual Book of Standards 04.02,* ASTM International, West Conshohocken, PA.

42. ASTM C109. (2013). “Standard Test Method for Compressive Strength of Hydraulic Cement Mortars.” *ASTM Annual Book of Standards 04.01*, ASTM International, West Conshohocken, PA.

43. Hallam, M.W. (1976). *The Behavior of Stud Shear Connectors under Repeated Loading*, Report No. R281, University of Sydney, School of Civil Engineering, Sydney, Australia.

44. Lee, P.G., Shim, C.S., and Chang, S.P. (2005). “Static and fatigue behavior of large stud shear connectors for steel-concrete composite bridges.” *Journal of Constructional Steel Research, 61*(9), 1270–1285, Elsevier Inc., Amsterdam, Netherlands.

45. Roberts, T. M. and Dogan, O. (1998). “Fatigue of Welded Stud Shear Connectors in Steel-Concrete-Steel Sandwich Beams.” *Journal of Constructional Steel Research, 45*(3), pp. 301–320, Elsevier Inc., Amsterdam, Netherlands.

46. Roderick, J.W. and Ansourian, P. (1976). *Repeated loading of composite beams*, Report No. R280, University of Sydney, School of Civil Engineering, Sydney, Australia.

47. Oehlers, D.J. (1990). “Deterioration in Strength of Stud Connectors in Composite Bridge Beams.” *Journal of Structural Engineering, 116*(12), American Society of Civil Engineers, Reston, VA.

48. Thurlimann, B. (1959). *Fatigue and static strength of steel shear connectors, Lehigh University, 1959 Reprint No. 144(59-8)*, Report No. 1253, Lehigh University, Lehigh, PA.

49. Faust, T., Leffer, A., and Mensinger, M. (2000). “LWAC in Composite Structures.” *Proceedings Second International Symposium on Structural Lightweight Aggregate Concrete*, Norwegian Concrete Association, Kristiansand, Norway.

50. Ahn, J.H., Kim, S.H., and Jeong, Y.J. (2007). “Fatigue experiment of stud welded on steel plate for a new bridge deck system.” *Steel and Composite Structures, 7*(5), pp. 391–404, Techno-Press, Daejeon, Korea.

51. Hanswell, G., Porsch, M., and Ustundag, C. (2007). “Resistance of headed studs subjected to fatigue loading – Part I: Experimental study.” *Journal of Constructional Steel Research, 63*(4), pp. 475–484, Elsevier Inc., Amsterdam, Netherlands.

52. Lehman, H.G., Lew, H.S., and Toprac, A.A. (1965). *Fatigue Strength of ¾ Inch Studs in Lightweight Concrete (Push-out Tests)*, Report No. 76-1F, University of Texas, Austin, TX.

HRDI-40/11-19(WEB)E